PROCEEDINGS OF THE ACADEMY OF SCIENCES OF THE USSR

Physical Chemistry Section

Volume 131, Numbers 1-6 March – April, 1960

CONTENTS

	PAGE	RUSS. ISSUE	RUSS. PAGE
The Radiolysis of KBr Solutions by 600 Mev Protons. S. A. Brusentseva and P. I. Dolin.	207	1	117
Critical Concentration Regions in Solutions of Soaps. P. A. Demchenko and A. V. Dumanskii.	211	1	120
The Macroscopic Stages in the Initiatory Reaction for the Bromination of Phenetole by N, N-Dibromo-5, 5'-Dimethylhydantoin in Dichlorethane. K. A. Kornev and G. A. Yangol'.	215	1	122
A. P. M.R. Study of the Energy Transfer Processes Occuring During the Radiolysis of Certain Frozen Hydrocarbons. Yu. N. Molin, I. I. Chkheidze, Al. A. Petrov, N. Ya. Buben, and V. V. Voevodskii.	219	1	125
New Data on the Effects of Radioactive Solids on Heterogeneous Isotopic Exchange. I. E. Mikhailenko and V. I. Spitsyn.	223	1	129
The Occlusion of Sulfur in Electroplated Metals. A. A. Sutyagina.	227	1	133
A Differential Capacity Study of the Adsorption of Surface-Active Ions on a Zinc Electrode. Chuan-sin' Tza, and Z. A. Iofa.	231	1	137
The Effects of Complexing with $TiCl_4$, $SnCl_4$, $AlCl_3$, and $AlBr_3$ on the Infrared Spectra of Certain Esters. D. S. Bystrov and V. N. Filimonov.	235	2	338
Relationship Between the Electrical Conductivity and The Work Function of Modified Zinc Oxide. V. I. Vladimirova, E. Kh. Enikeev, G. M. Zhabrova, and L. Ya. Margolis.	239	2	342
The Hyperfine Structure in the Paramagnetic Resonance Spectra of Benzophenone-K-Ketyl. V. M. Kazakova and Ya. K. Syrkin.	243	2	346
Some Peculiarities of Emulsification in Structurized Liquids. L. Ya. Kremnev and L. A. Borodina.	245	2	348
A Mechanism for the Decomposition of Hydroperoxide Intermediates in the Oxidation of Liquid n-Decane. Z. K. Maizus, and V. N. Yakovleva.	249	2	351
A Tracer Study of the Activation Mechanism of Chlorides. V. P. Maksimchuk and I. L. Rosenfel'd.	253	2	354
The Role of Chemical Reactions in Thermionic Emission. G. M. Panchenkov and A. M. Kolchin.	257	2	357
The Effects of External Radiation on the Isotopic Exchange of Sulfur in the K_2SO_4-SO_3 System at High Temperature. V. I. Spitsyn, I. E. Mikhailenko, I. V. Vereshchinskii and P. Ya. Glazunov.	261	2	360
The Mechanism of Predetonation Propagation of Flame in Rough Tubes. V. S. Babkin and L. S. Kozachenko.	265	3	591
Certain Features of the Kinetics of the Radiolysis of n-Heptane Over a Wide Range of Doses. V. G. Berezkin, I. M. Kustanovich, L. S. Polak, and N. Ya. Chernyak.	269	3	593
Surface Properties of Highly Dispersed Quartz. L. G. Ganichenko, M. M. Egorov, V. F. Kiselev, K. G. Krasil'nikov and G. S. Khodakov.	275	3	597

	PAGE	RUSS. ISSUE	RUSS. PAGE
The Kinetic Equation for Irreversible Reactions in Oscillographic Polarography. A. Ya. Gokhshtein and Ya. P. Gokhshtein.	279	3	601
An Infrared Investigation of the Hydrogen Exchange Between Acetone and DBr Vapors. B. A. Kuznetsov.	283	3	605
The Use of Very Fast Electrons for the Microdiffraction Study of the Structure of Soot Particles. N. M. Popov, V. I. Kasatochkin, and V. M. Luk'yanovich.	289	3	609
Adsorption Gas Radiography and Its Application to the Study of Promoted Catalysts for Ammonia Synthesis. Z. S. Roginskii and Yu. E. Sinyak.	293	3	612
Radiochemical Measurement of the Rate of Carbon Formation During the Decomposition of Ethyl Alcohol on a Dehydrogenating Catalyst. A. A. Balandin, G. V. Isagulyants, A. P. Rudenko and G. Stegner.	297	4	861
Molecular Sieves as Adsorbents of the 1st Structural Type. B. P. Bering, M. M. Dubinin, E. G. Zhukovskaya, and V. V. Serpinskii	303	4	865
Effect of Temperature and Concentration on the Frequency and Intensity of the Lines in the Raman Spectrum of Ketone-Chloroform Mixtures. Yu. G. Borod'ko and Ya. K. Syrkin.	307	4	868
The Equilibrium Between Strontium Molybdate and Hydrogen and the Thermodynamic Characteristics of SrMoO4. L. A. Zharkova, V. I. Lavrent'ev, T. N. Rezukhina and Yu. P. Simanov.	311	4	872
The Theory of Flame Propagation in Systems with Branched Chain Reactions. L. A. Lovachev.	317	4	876
The Mechanism of Chain Branching in the Oxidation of n-Decane. Z. K. Maizus, I. P. Skibida, and N. M. Emanuél'.	321	4	880
The Thermodynamics of the Extraction Equilibria for Strong Electrolytes Dissociated in the Organic Phase. A. M. Rozen, L. M. Gindin, and I. F. Kopp.	325	5	883
The Relation Between Activation Energy and Relative Adsorption Coefficient. A. E. Agronomov, Academician A. A. Balandin, and Yu. S. Mardashev	331	5	1120
The Differences Between the Times of Completion of Hydration and Attainment of Maximum Hardness of Crystal Structure in Plaster of Paris Suspensions. E. A. Amelina, E. E. Segalova and P. A. Rebinder.	335	5	1123
Work Function and Catalytic Activity of Iron Contacts in the Synthesis of Ammonia. E. Kh. Enikeev, A. V. Krylova, L. D. Kuznetsov, S. S. Lachinov, and S. Z. Roginskii.	339	5	1126
Equilibrium in the Reaction Between Lead Tungstate and Hydrogen, and the Thermodynamic Characteristics of $PbWO_4$. L. A. Zharkova, Ya. I. Gerasimov, T. N. Rezykhina, and Yu. P. Simanov.	343	5	1130
Statistical Theory of the Double Layer at the Metal-Solution Surface. V. G. Levich and V. A. Kir'yanov.	349	5	1134
The Plasticity of the High-Temperature Modifications of Polymorphic Metals. E. M. Savitskii and Ch. V. Kopetskii.	353	5	1137
The Reaction of the Isopropyl Radical with the Oxygen Molecule. L. I. Avramenko and R. V. Klesnikova.	357	6	1370
The Orientation of the π-Electron Oriental in the Cyclopropane Ring. V. T. Aleksanyan and Kh. E. Sterin.	361	6	1373
The Composition of the Products, and the Mechanism of Initiated Cracking of Gaseous Alkanes. E. M. Gamus-Chernyavskaya, S. Sh. Reznikova and A. D. Stepukhovich.	365	6	1376
Calculation of Product Yields in the Radiolysis of Alkanes. Yu. A. Kolbanovskii and B. A. Smirnov.	369	6	1380
Measurement of the Vapor Pressure of Solid Chromium by Means of Radioactive Indicators. An. N. Nesmeyanov and De Dyk Man.	373	6	1383
Magnetic Properties of $Cr_2O_3 - Al_2O_3$ Catalysts. A. M. Rubinshtein and A. A. Slinkin.	377	6	1386
The Time of Establishment of Sorption Equilibrium. D. P. Timofeev.	381	6	1390
A New Cavitation Method for Emulsion Polymerization. S. S. Urazovskii.	385	6	1393

THE RADIOLYSIS OF KBr SOLUTIONS BY 600 Mev PROTONS

S. A. Brusentseva and P. I. Dolin

(Presented by Academician A. N. Frumkin, November 20, 1959)
Translated from Doklady Akademii Nauk SSSR, Vol. 131, No. 1, pp. 117-119, March, 1960
Original article submitted November 10, 1959

Several papers have appeared in recent years in which the radiolysis of aqueous solutions by protons deuterons, and γ-particles of various energies was discussed [1-4]. It was proved that with increasing density of the ionization produced by the particle, or with increasing energy loss per unit path length $-dE/dX$, the yield of molecular water radiolysis products increased while that of free radical products decreased.

It seemed worth while to study heavy radiation of such a large energy that the value of $-dE/dX$ would approach the value characterizing light radiation. In such cases head-on collisions between the particles and the nuclei may produce effects distinguishing light from heavy irradiation. Direct collisions between fast electrons and the nuclei cannot produce any additional effects. In the case of high-energy protons (hundreds of Mev), direct collisions will result in the formation of multiply charged ions. These ions are produced when the nuclei knocked out of the molecules carry along the remainder of their electron cloud. Such multiply charged ions possess a high enough energy to induce ionization and excite the molecules in their path. Having a large charge and a relatively low velocity, the ions will produce a very high ionization density and thus influence the radiochemical psocesses. If the heavy particles do not have a very high energy, such an effect is not possible.

In this work protons accelerated to 600 Mev were used, and therefore effects due to head-on collisions were to be expected. In their value of $-dE/dX$ they were equivalent to 1 Mev electrons. The radiochemical processes induced by 1 Mev electrons are known to be identical with those induced by γ-radiation from Co^{60}. We therefore compared in our work the effects of 660 Mev protons on aqueous solutions with the effects induced by γ-radiation from Co^{60}.

The principal difficulty encountered in dealing with protons of such energies involves the determination of the energy absorbed by the solution. In order to determine this energy, we measured the flux of a full proton beam incident on a 1 cm^2 area. It is known that in water 660 Mev protons lose 2.1 Mev per 1 cm of their path length [5]. From this one can compute the dosage absorbed per 1 cm^3 of solution if the total flux is known. Two methods were used for the determination of the proton flux. One method involved placing a graphite plate of known dimensions in the path of the proton beam. The protons produce radioactive carbon C^{11}, which has a 20 min half-life. By measuring the activity of the graphite after irradiation with the help of a box counter, one can compute the total proton flux from the following equation $I = \frac{ne^{\lambda\tau}}{\sigma N_1 \eta (1 - e^{-\lambda t})}$, where n is the number of particles recorded on the counter per unit time, λ the decay constant of C^{11}, τ the interval between the end of irradiation and the beginning of counting, σ the reaction cross-section equal to 34 m barns, η the efficiency of positron recording, t the irradiation time, N_1 the number of carbon nuclei in a layer in which there is no self-absorption and which emits the same number of β-particles as would a layer of infinite thickness. For the plates used by us, $N_1 = 96 \times 10^{21}$ atoms.

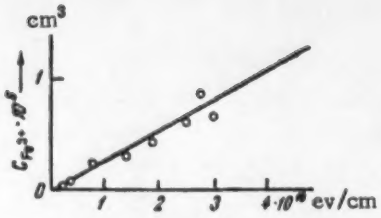

Fig. 1. The concentration of Fe^{+++} as a function of dosage.

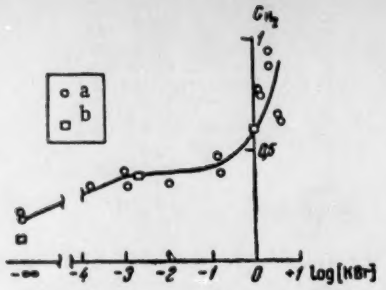

Fig. 2. The yield of hydrogen as a function of log [KBr]: a) 660 Mev protons; b) γ-rays from Co^{60}.

In the second method the proton flux was measured in an ionization chamber which was calibrated with a Faraday cylinder. The results obtained by different methods differed by 25-30%. Graphite plates were used for dosimetry, and the ionization chamber was used to verify the accuracy of the results. We used in our investigation $FeSO_4$ dosimetric solutions, air-free KBr solutions, and pure water. In $FeSO_4$ solutions the G (Fe^{+++}) was determined. The Fe^{+++} concentration was determined spectrophotometrically at the 304 mμ wave-length. The results obtained are presented in Fig. 1. The straight line represents the accumulation of trivalent iron with increasing dosage if we assume that the G(Fe^{+++}) for proton irradiation is the same as that for Co^{60} γ-radiation, namely 15.6. The circles represent experimental results, with the dosage determined from the activity of graphite plates. Fig. 1 shows that, within the range of experimental errors, both γ-rays and 660 Mev protons give the same G(Fe^{+++}). The average value of G(Fe^{+++}) in these experiments was 16.9. The slight increase in the G(Fe^{+++}), as compared to the value given for γ-radiation from Co^{60} can probably be attributed to the fact that the proton beam was inhomogeneous with a slightly higher intensity in the center. The $FeSO_4$ solutions were irradiated in glass bulbs of a diameter smaller than the graphite plate dimensions. Therefore, the mean proton flux on 1 cm^2 of the graphite plates used for dosage determination was lower than the actual flux on the bulb. We also investigated the hydrogen evolution from air-free KBr solutions. The amount was determined by burning the hydrogen over a platinum wire at 180-200°C in an analytical vacuum apparatus. The results are presented in Fig. 2. The curve plotted in this figure represents the yield of hydrogen as a function of log [KBr]. As the KBr concentration is increased to 10^{-3} M, G(H_2) increases, then remains constant in the 10^{-3}-10^{-2} M concentration range, and again begins to increase with increasing KBr concentration. γ-Radiation from Co^{60} gave a similar function of G(H_2) versus log [KBr] [6]. The slightly higher yields in the case of γ-radiation may be attributed to the different irradiation conditions. In the experiments with γ-radiation, the method of semipermeable cells was used so that a portion of the hydrogen evolved in the solution was transferred into the gas phase, whereas in the case of proton irradiation all the hydrogen remained in solution. In order to verify the correctness of this assumption, we carried out some experiments with γ-rays using the previously described method. The resulting values of G(H_2) coincided with the results obtained using 660 Mev protons (Fig. 2b).

Thus, by studying the radiolysis of aqueous $FeSO_4$ and KBr solutions, we showed that radiochemical processes depend exclusively on the energy loss per unit path length, -dE/dX.

However, the yield of hydrogen from pure air-free water was found to be quite different when protons were used instead of γ-radiation. The water used in these experiments was purified as follows. Twice-distilled water was irradiated by γ-rays from Co_{60} in order to destroy all organic impurities and then with ultraviolet light to destroy the H_2O_2 formed by γ-radiation. After that the water was redistilled in a quartz apparatus. The water thus purified had an electrical conductance of $0.7\text{-}0.6 \times 10^{-6}$ ohm^{-1} cm^{-1}. The yield of hydrogen from the water exposed to γ-radiation was 0.07 molecules per 100 ev. The H_2 concentration was $5\text{-}6 \cdot 10^{-9}$ moles/cm^3. But G(H_2) became 0.15-0.19 when 660 Mev protons were used. The difference between the two hydrogen yields can be explained in two ways. The difference may quite possibly be due to the effects of head-on collisions. The resulting multiply charged ions would produce the processes characterizing heavy radiation, which would make the hydrogen yield much higher than in the case of γ-radiation. However, the small difference may also be the result of trace impurities, to which the yield of hydrogen is very sensitive. One may therefore assume that 660 Mev protons and γ-rays from Co^{60} produce identical radiochemical effects.

LITERATURE CITED

[1] R. H. Schuler and A. O. Allen, J. Am. Chem. Soc. 79, 7, 1565 (1957).

[2] E. J. Hart, W. R. Rambler and S. R. Rochlin, Radiation Res. 4, 5, 379 (1956).

[3] H. A. Schwarz, J. M. Caffray, and G. Scholes, J. Am. Chem. Soc. 84, 8, 1801 (1959).

[4] N. F. Barr and R. H. Schuler, J. Phys. Chem. 63, 6, 808 (1959).

[5] E. Segre, Ed., Experimental Nuclear Physics, Vol. 1 [Russian translation] (IL, 1955) p. 163.

[6] S. A. Brusentseva and P. I. Dolin, Trans. 1st All-Union Confer. on Radiochemistry [in Russian] (Izd. AN SSR, 1958) p. 3.

[7] P. I. Dolin, Coll: Works on Radiochemistry [In Russian] (Izd. AN SSSR, 1959) p. 9.

CRITICAL CONCENTRATION REGIONS IN SOLUTIONS OF SOAPS

P. A. Demchenko and Corresponding Member of the Academy of Sciences of USSR A. V. Dumanskii

(Paper presented to the Colloid Chemistry Section of the 8th Mendeleev Congress in Moscow, March 23, 1959)
Translated from Doklady Akademii Nauk SSSR, Vol. 131, No. 1, pp. 120-121, March, 1960
Original article submitted November 2, 1959

With an increase in the concentration of solutions of detergent materials, within a narrow concentration range known as the critical concentration of micelle formation (CCM) which is characteristic for each substance, the true solution goes over abruptly into a colloidal one, which is accompanied by changes in the bulk properties of the solutions of the detergent materials [1-3]. In addition to the critical micelle concentration, in solutions of different soaps, when the concentration is increased to 60-90 grams per liter, a second critical region is observed [2, 1]. Not long ago the view was expressed that there are also to be observed in soap solutions other concentration limits for association [4]. No systematic investigation in this region has yet been carried out. The study of the limits of concentration for association in solutions of surface-active materials is of considerable scientific and practical interest for the broadening of our ideas about the structure and colloid chemical properties of solutions of associated colloids. Very recently the critical micelle concentration has been employed as a characteristic of the hydrophilic-oleophilic balance of detergent materials and for the determination of their practical effectiveness [5].

In the present work we present the results of a study of the concentration limits of association in solutions of sodium laurate and potassium laurate by a method involving the determination of solubilization. The specimens for the investigation were prepared from pure lauric acid and purified caustic alkalis by a method which has been described earlier [6, 7]. For the entire series of experiments, solutions of the required concentration were prepared from dry, powdered sodium laurate and potassium laurate by heating until a homogeneous solution of the soap was obtained. The limiting quantity of the solubilized hydrocarbon in the soap solution was determined by the reduction in volume in the graduated tube of the apparatus described in [8]. The study of the effect of increase in soap concentration on the solubilizing effect has shown that the dissolution of the toluene in the soap solution becomes appreciable only when the concentration of the sodium laurate or the potassium laurate reaches the value C_1 (Fig. 1), or approximately 0.026 moles per liter. Lower concentrations of the solutions of the soaps used possess practically no powers of solubilization. Upon increasing the concentration of the solutions of sodium laurate and potassium laurate beyond the value C_1, the solubilization of the toluene increases irregularly, changing in the neighborhood, of the limiting concentrations C_2, C_3, and C_4, having, respectively, the approximate values 0.28, 0.60 and 0.90 moles per liter (Fig. 2). Within the critical concentration regions for the solubilization of toluene in the solutions of soap which have been examined, the change is practically linear and may be characterized by the angles of slope of the experimental curves (expressed as tangents). For the sections C_1C_2, C_2C_3 and C_3C_4 the tangent of the angle of slope for sodium laurate is, respectively, 0.47, 0.81, and 1.11, and for potassium laurate 0.42, 0.43,* and 1.00 (Fig. 2). It is interesting to note that the first critical

*This is obviously an error. From the figure it appears that the value might be 0.73—Translator.

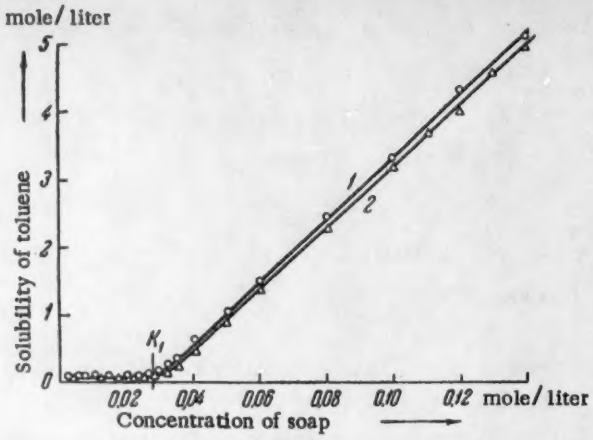

Fig. 1. The solubilization of toluene in dilute solutions of sodium laurate (1) and potassium laurate (2).

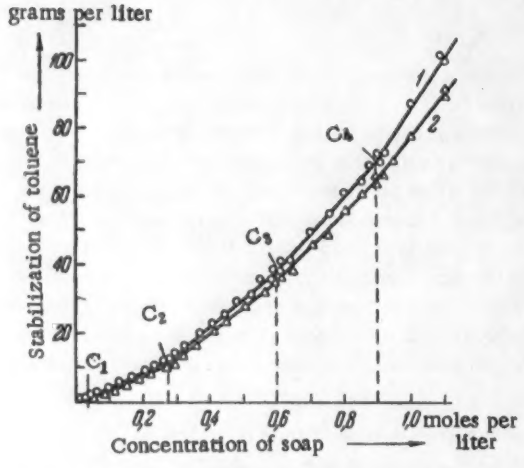

Fig. 2. Critical concentration regions in solutions of sodium laurate (1) and potassium laurate (2).

region C_1 has approximately the same value as the critical concentration for micelle formation in solutions of sodium and potassium laurates, as determined by other, independent methods [3, 5]. Consequently, the critical concentration for micelle formation of detergent substances may be determined with sufficient accuracy by the solubilization method.

In the concentration interval between the critical concentration for micelle formation and the second critical region, the solubilizing powers of solutions of sodium laurate and potassium laurate are practically identical. With further increase in the concentration of the soaps beyond C_2 in the solution, the solubilizing power of the solutions of sodium laurate increases more rapidly than that for solutions of potassium laurate; that is, it is greater for sodium laurate than for potassium laurate of the same concentration. The critical concentration regions for potassium and sodium laurates are nearly identical and are represented by similar breaks in the curves (Fig. 2). In concentrated solutions of the soaps, there apparently exist other critical concentration regions as well, in which, on account of the stepwise nature of the association, the building up of the internal structure of the solution occurs discontinuously. By this means more oleophilic micelles are formed, capable of binding larger quantities of the hydrocarbon than can the micelle structure of the less concentrated solutions of the detergent material.

The phenomenon of solubilization may be used for the quantitative evaluation of the practical value of the solutions of detergent substances [5, 6], their oleophilic character and micelle structure, the critical concentrations for micelle formation, and other critical concentration regions.

LITERATURE CITED

[1] H. B. Klevens, Chem. Rev. 47, 1 (1950).

[2] Z. N. Markina, K. A. Pospelova, and P. A. Rebinder, Transactions of the Third All-Union Conference on Colloid Chemistry [in Russian] (Izd. Akad. Nauk. SSSR, 1954) p. 410.

[3] M. E. L. McBain and E. Hutchinson, Solubilization and Related Phenomena (N. Y., 1955).

[4] P. Ekwall, Koll. Zeits. 136, 37 (1954).

[5] P. A. Demchenko, Masloboino-zhirovaya promyshlennost', No. 7, 36 (1959).

[6] A. V. Dumanskii and P. A. Demchenko, Dokl. Akad. Nauk. SSSR 78, 277 (1951).

[7] P. A. Demchenko, A. V. Dumanskii, and L. G. Demchenko, Koll. Zhurn. 14, 164 (1952).

[8] P. A. Demchenko, Masloboino-zhirovaya promyshlennost', No. 10, 22 (1959); Ukr. khim. zhurn. 24, 746 (1958).

THE MACROSCOPIC STAGES IN THE INITIATORY REACTION FOR THE BROMINATION OF PHENETOLE BY N,N-DIBROMO-5,5'-DIMETHYLHYDANTOIN IN DICHLORETHANE

K. A. Kornev and G. A. Yangol'

Institute of Polymer and Monomer Chemistry, Academy of Sciences of the Ukrainian SSR

(Presented by Academician V. N. Kondrat'ev, September 4, 1959)
Translated from Doklady Akademii Nauk SSSR, Vol. 131, No. 1, pp. 122-124,
March, 1960
Original article submitted June 29, 1959

N. M. Émanuél' [1] has directed attention to the great frequency with which the phenomenon of macroscopic initiation occurs in chain reactions. The real chain process, especially in complex chemical systems, does not reveal itself as a simple realization of this or that successive elementary stage from the commencement of the reaction to the complete using up of a substance, but rather in the form of complex reactions with distinct changes in mechanism as it proceeds. In its most significant form, this change in the mechanism of the course of a chain reaction has been observed in oxidation reactions. But we have succeeded in demonstrating the existence of macroscopic stages also in such chain reactions as the bromination of phenetole, initiated by diazoaminobenzene (DAAB), where the brominating agent used is N,N-dibromo-5,5'-dimethylhydantoin (DBDMH).

In earlier publications [2, 3] we have shown that the process of chlorinating phenetole in the presence of DAAB develops by means of a chain mechanism with the participation of free radicals; moreover, in the chlorination reaction, only one atom of chlorine takes part, forming, apparently, monochloramin-N-chlorobenzenesulfonamide. The clear distinction in the nature of the process of chlorinating phenetole, which we have observed while using N,N-dichlorobenzenesulfonamide and N-chlorobenzenesulfonamide, has been explained by us from the point of view of their chlorinating activity. When, instead of N,N-dichlorobenzenesulfonamide, N,N-dibromo-5,5'-dimethylhydantoin is used for this reaction, it has been shown that, in spite of the insignificant difference in the activity of the bromine atoms (as they appear in position 1 and position 3), there is, in this case, too, observed a clear demonstration of the nature of the utilization of the one and the other bromine atoms. Fig. 1 shows the kinetic curves for the using up of the halogenating agent for the initiation by DAAB of the bromination reaction of phenetole by means of N,N-dibromo-5,5'-dimethylhydantoin, according to the scheme:

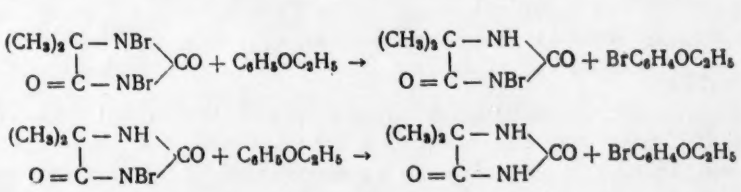

As we can see, the kinetic curves for the consumption of the halogenating agent present clear evidence of a two-stage process. Having commenced with the relatively rapid stage in the bromination of phenetole, after the using up of one of the bromine atoms, this is replaced by the slower stage of the reaction, corresponding to the formation in the bromination process of monobromamino-N-brom-5,5'-dimethylhydantoin (BDMB).

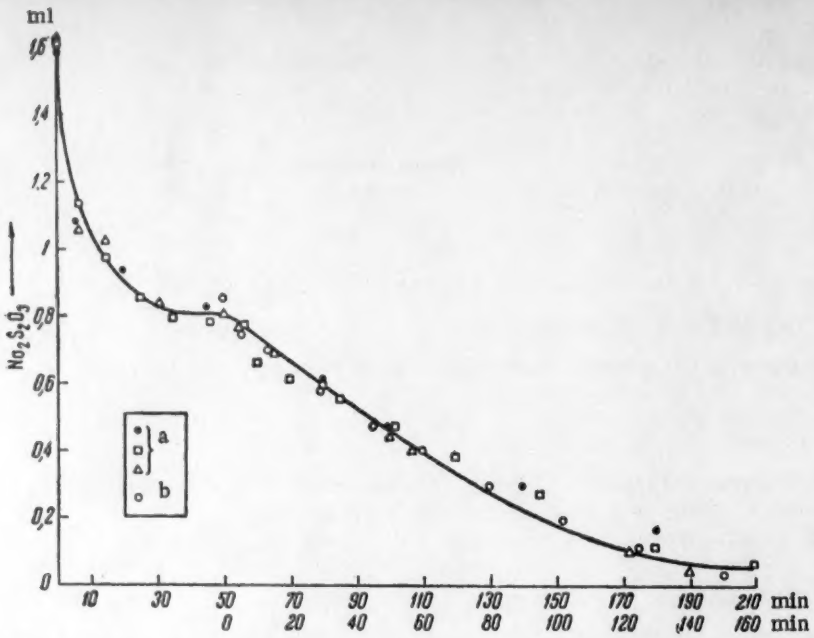

Bromination of phenetole by DBDMH and BDMH in dichlorethane. a) Phenetole 0.04 mole, DBDMH 0.02 mole, DAAB 0.0003 mole, hydroquinone 0.0004 mole. b) phenetole 0.04 mole, BDMH 0.04 mole, DAAB 0.0003 mole, hydroquinone 0.0004 mole.

The formation of the monobromamine (BDMH) and the nature of its brominating influence with respect to phenetole has been demonstrated by us in separate kinetic experiments with a definitely known preparation of BDMH, obtained by the direct bromination of dimethylhydantoin under the conditions described in the literature [4].

Kinetic experiments with BDMH have been carried out under just the same conditions as for DBDMH itself, and it has been clearly established that, when BDMH is used as the halogenating agent, twice the quantity of this is introduced, compared with the portion of bromine from DBDMH in experiments with this.

In addition to this, phenetole to the extent of 0.04 moles was introduced into an experiment in double portions: the second portion of phenetole to the extent of 0.02 moles was added after the using up of one bromine atom.

Under the conditions of these experiments, it was possible to reproduce completely the state of the reaction mixture in terms of its composition, and also in the experiments with DBDMH. As in the case of the latter, so also in the experiments with BDMH, at the point of the reaction of the second bromine atom in the reaction mixture there were present: the substance being halogenated, or phenetole; the product of bromination-bromophenetole; the halogenating agent - BDMH; the inductor and the antioxidant. The results of the kinetic experiments under discussion are shown in Fig. 1 (the kinetic curve is signified by the open circles). It is easy to satisfy oneself that this is completely in harmony with the kinetic curves corresponding to the monobromamine, obtained in the experiments with DBDMH.

Thus, the brominating effect of DBDMH in its reaction with phenetole proceeds through two clearly distinguished macrostages. During the bromination reaction, the substance BDMH is obtained, which enters into the reaction with phenetole only after the point of complete consumption of the first bromine atom of DBDMH. The consumption of both the first and the second bromine atom of DBDMH can be expressed by the unimolecular law:

$$(\Delta X)_\infty - \Delta X = (\Delta X)_\infty \cdot e^{-kt},$$

where ΔX is the quantity of halogenating agent used up at the time instant t, and ΔX_∞ is the same at the end of the reaction for each atom of bromine. The difference $(\Delta X)_\infty$-ΔX represents the actual quantity of the halogenating agent at each instant of time.

The semilogarithmic transformation of the kinetic curves of DBDMH and BDMH produces straight lines. It is possible to calculate from these the rate constants of the reactions. The are 6×10^{-2} min^{-1}, and 1.6×10^{-2} min^{-1}, respectively.

This phenomenon may be explained on the basis of the following assumptions. Evidently DBDMH and BDMH take part in the reaction under the influence of the inductor and are transformed according to the scheme:

$$DBDMH = Br^{\cdot} + BDMH^{\cdot}$$

$$BDMH = Br^{\cdot} + DMH^{\cdot}$$

$$k_1 = (Br^{\cdot})(BDMH^{\cdot})/(DBDMH) > k_2 = (Br^{\cdot})(DMH^{\cdot})/(BDMH)$$

We will postulate that k_1 is much greater than k_2. Hence, the concentration of bromine atoms will depend on the concentration of DBDMH, and the dissociation of BDMH will be suppressed. It therefore follows that the dissociation of BDMH into atomic bromine and a radical will be minimal so long as there is present in the solution the substance DBDMH in sufficient quantity to hold the concentration of $DMH^{\cdot}$ at so low a value that this radical will not take part in the development of the chain reaction of bromination. This assumption is confirmed by experiments in which DMH is added to the reaction mixture. In the case of bromination reaction by means of DBDMH, addition of DMH diminishes the velocity of the bromination reaction, which is presumably to be explained by the reaction of the DMH with the DBDMH to form BDMH. After the consumption of all the DBDMH, the influence of DMH disappears, and the DMH, as the experiments have shown, exerts no influence on the course of the bromination reaction using BDMH.

In view of the fact that the inductor and the antioxidant, under the conditions of the experiment, were brominated by DBDMH, the phenetole was introduced after the elimination of these by bromination and the determination of the zero point of the brominating agent.

LITERATURE CITED

[1] N. M. Émanuél', Problems of Chemical Kinetics, Catalysis, and Reactivity, [in Russian] (Izd. Akad. Nauk SSSR, 1955) pg. 117.

[2] K. A. Kornev, Dokl. Akad. Nauk SSSR 100, 1091 (1955).

[3] K. A. Kornev, Dokl. Akad. Nauk SSSR 105, 720 (1955).

[4] Orfeo O. Orazi and J. Meseri, cited in Chem. Abs. 44, 1950, p. 4423.

A P.M.R. STUDY OF THE ENERGY TRANSFER PROCESSES OCCURRING DURING THE RADIOLYSIS OF CERTAIN FROZEN HYDROCARBONS

Yu. N. Molin, I. I. Chkheidze, Al. A. Petrov, N. Ya. Buben, and Corresponding Member Acad. Sci. USSR V. V. Voevodskii

Chemical Kinetics and Combustion Institute of the Siberian Section of the Acad. Sci. USSR, the Chemical Physics Institute, and the Institute of Geology and the Development of of Natural Fuels of the Academy of Sciences USSR

Translated from Doklady Akademii Nauk SSSR, Vol. 131, No. 1, pp. 125-128, March, 1960
Original article submitted November 4, 1959

The rupture of chemical bonds which accompanies the radiolysis of organic compounds in the solid state may be preceded by an intramolecular and intermolecular energy transfer across a considerable distance. A large amount of research has been devoted to the study of this problem; the extent of energy transfer was either deduced from the chemical analysis of the end products (see, for example, [1]), or from physical measurements such as spectroscopy [2]. The application of paramagnetic resonance (p.m.r.) opens essentially new possibilities for the study of energy transfer processes, since the technique makes it possible to record the first step in the rupture of chemical bonds and the formation of free radicals, without being encumbered by secondary chemical reactions.

Compound	G, rad/100 ev
I. 1,1-Dicyclohexyldodecane	4,9
II. 1,1-phenyldodecane	0,42
III. 1-Phenyl-1-cyclohexyldodecane	0,46
A mixture of I and II (1 : 1 by volume)	0,73
Cyclohexane	1,6
Benzene	0,16

In this work we investigated the energy transfer in radiolyzed compounds I-III, listed in Table 1. The energy transfer was studied in two ways. First, as the p.m.r. spectra of simple hydrocarbons, irradiated in the frozen state, have already been investigated very thoroughly (benzene [3], cyclohexane [4], normal paraffins [4-6]), it is possible to locate the bonds being broken in complex molecules I-III by studying the forms of their p.m.r. spectra and thus follow the transfer of energy. Second, an energy transfer to the aromatic ring should be reflected in a reduced over-all yield of radicals since the aromatic rings in complex molecules seem to provide radiation shielding [7].

With these considerations in mind, we recorded the p.m.r. spectra of compounds I-III, benzene, and cyclohexane, all irradiated at -120°C by fast electrons (1.6 Mev) and also studied the kinetics of radical accumulation. Besides the individual compounds we also studied a mixture of compounds I and II. The p.m.r. spectra were recorded on an instrument which permitted measurements while the compounds were bombarded by fast electrons [8]. The technique has previously been described in detail [9], while the physical and chemical properties of compounds I-III are listed in [10]. Chemically

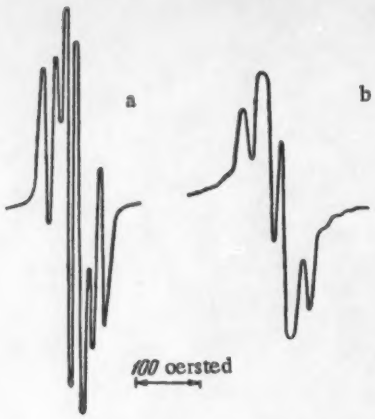

Fig. 1. The p.m.r. spectra of irradiated: a) Cyclohexane; b) compound I (120°).

Fig. 2. The p.m.r. spectra irradiated: a) Benzene; b) compound II; c) compound III; d) a 1 : 1 (by volume) mixture of compounds I and II (at -120°).

pure benzene and cyclohexane were used. The p.m.r. spectra of the investigated compounds were recorded at a frequency of ~9400 Mc/ sec and are plotted in Figs. 1 and 2 as the first derivative of the absorption curve.

The spectrum of compound I contains the same number of lines and is as even as the spectrum of irradiated cyclohexane, which is produced by the cyclohexyal radical, $C_6H_{11}^{\cdot}$ [4]. Thus, when compound I is irradiated, a large number of cyclohexyl-like radicals must be formed. The poorly resolved hyperfine structure (as compared to the resolution in the case of cyclohexane) in the p.m.r. spectrum may be attributed to a superposition of the spectra of various isomeric radicals with the general formula RC_6H_{10}. However, one should note that the spectrum of compound I contains additional lines (indicated by arrows) outside the range of the cyclohexyl radical spectrum which, it seems, should be attributed to the radicals formed when C-H bonds in the linear chain section of molecule I are ruptured. The p.m.r. spectra of radicals formed from linear hydrocarbons are known to have a spread of 150-160 oersteds [4-6]. Therefore, compound I yields radicals through the rupture of C-H bonds in the ring and in the linear portion of the molecular chain.

When compounds II and III were irradiated, they yielded spectra similar to those of irradiated benzene. This indicates that in the case of compounds II and III, as well as in the case of benzene [3], only two types of radicals are formed: one by the detachment of a hydrogen from the ring, another by the attachment of a hydrogen to the benzene ring. The lack of additional hyperfine structure in the spectra of compounds II and III and the fact that the components of the principal triplet are not as well resolved as in the case of benzene seems to be connected with the absence of internal rotation [3]. It is important to note that the spectra of these compounds (II and III) show no lines resulting from the rupture of C-H bonds in the linear chain or in the cyclohexyl ring. The mixture of compounds I and II gives p.m.r. spectra similar to those of compound II. The poor resolution and the presence of additional shoulders (indicated by arrows) can be attributed to some superposition of the spectrum of compound I. Therefore, when the mixture is exposed to radiation, most of the radicals are produced by compound II.

The spectra analyzed above indicate that the C-H bonds on the benzene ring are the first ones to break in compounds II and III. Consequently the energy received by various groups in the molecules II and III succeeds in redistributing itself before any chemical bonds are broken and is transferred into the benzene ring. In the case of the mixture, this intramolecular energy transfer is accompanied by a transfer of energy from compound I and II. The complex spectrum of compound I prevents any definitive conclusions as to whether there is a directed intramolecular energy transfer.

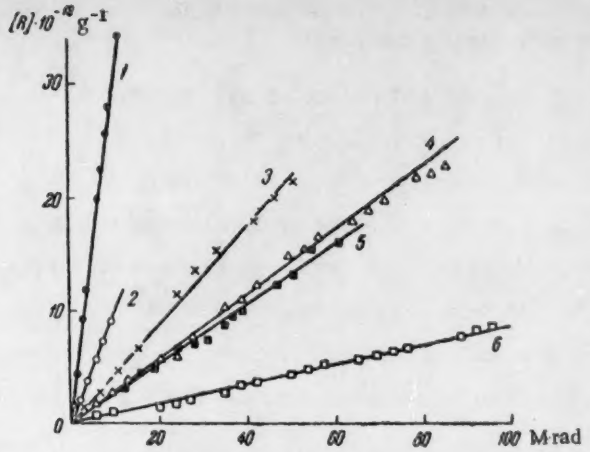

Fig. 3. Radical accumulation kinetics (-120°): 1) Compound I; 2) cyclohexane; 3) a 1 : 1 mixture (by volume) of compounds I and II; 4) compound III; 5) compound II; 6) benzene.

The initial portions of the radical accumulation curves are shown in Fig. 3. Compounds containing benzene rings exhibit no deviations from a straight line up to a dosage of 100 Mrad. The lines of compound I and cyclohexane do not remain straight past 10-30 Mrad. The radiation yields of radicals G_R computed from the initial portions of the accumulation curves are listed in the table. First of all, one should note that the yield of radicals from compounds II and III, which contain benzene rings, is smaller by one order of magnitude than the yield from compound I. This result provides additional evidence for the transfer of energy into the benzene ring which was previously deduced from the spectrum. If such a transfer did not occur and the radicals were to form freely on various parts of the molecule, compounds I, II, and III would all have had similar yields of radicals, since about 50 and 70%, respectively, of the electrons in compounds II and III are still constituents of saturated bonds. The transfer of energy into the benzene ring would explain why compounds II and III give almost identical yields of radicals. The energy received by these molecules becomes fully concentrated in the benzene ring, and the yield of radicals will depend entirely on the ring stability.

The low radiolysis yield observed in the case of the mixture (compounds I and II) provides additional evidence for the transfer of energy from compound I to II. If the mixture components had not interacted, the yield of radicals would have been $\gamma_I G_I + \gamma_{II} G_{II} \approx 2.5$, which is considerably higher than the experimentally observed one (γ_I and γ_{II} are the fractions of the electrons contributed by compound I and II, respectively, to the mixture). At the same time one should note that the yield of radiolysis products from the mixture was higher than from compound II. This result, together with the fact that the spectrum of the mixture is poorly resolved, indicates that not all the energy received by compound I succeeds in passing over to compound II before some of the bonds break. If we assume that the increased G_R for the mixture is entirely due to the formation of radicals from compound I, then we can show that about 10% of the molecules (I) fail to transfer their energy. This may possibly be connected with a relatively low efficiency of intermolecular energy transfer. There remains the possibility, however, that the frozen mixture of compounds I and II is not entirely homogeneous, which would also hinder the transfer of energy to compound II.

Let us note that compounds II and III yield almost three times as many radicals as irradiated benzene. The fact that the introduction of alkyl substituents on the benzene ring renders the molecules more unstable to radiation has been known for quite a while [11], but the reduced stability was usually attributed to the fact that bonds could now be ruptured in the side chain. Since the p.m.r. spectra seem to indicate that the radicals formed during radiolysis of compounds II and III are produced solely by the rupture of C-H bonds in the benzene ring, the indicated difference between the yields of radicals may be attributed to a decrease in the stability of the benzene ring produced by the introduction of the substituent.

In conclusion, the authors wish to thank G. K. Voronova for the assistance rendered in carrying out the experiments and in processing the experimental results.

LITERATURE CITED

[1] J. P. Manion and M. Burton, J. Phys. Chem. 56, 560 (1952).

[2] H. T. J. Chilton and G. Porter, J. Phys. Chem. 63, 904 (1959).

[3] I. I. Chkheidze, Yu. N. Molin, et al., Dokl. Akad. Nauk. SSSR 130, No. 6 (1960).*

[4] N. Ya. Chernyak, N. N. Bubnov, et al., Optika i Spektroskopiya 6, 564 (1959).

[5] B. Smaller and M S. Matheson, J. Chem. Phys. 28, 1169 (1958).

[6] R. S. Alger, T. H. Anderson, and L. A. Webb, J. Chem. Phys. 30, 695 (1959).

[7] L. T. Bugaenko, T. S. Nikitina, et al., The Chemical Effects of Ionizing Radiation [in Russian] (Moscow, 1958).

[8] Yu. N. Molin, A. T. Koritskii, et al., Doklady Akad. Nauk SSSR 123, 882 (1958).**

[9] A. T. Koritskii, Yu. N. Molin, et al., Vysokomolek. Soed. 1, 1182 (1959).

[10] S. R. Sergeenko, L. N. Kvitkovskii, et al., Dokl. Akad. Nauk SSSR 120, 541 (1958).**

[11] M. Burton, S. Gordon, and R. R. Hentz, J. Chim. Phys. 48, 190 (1951).

*See C. B. translation.

**Original Russian pagination. See C. B. translation.

NEW DATA ON THE EFFECTS OF RADIOACTIVE SOLIDS ON HETEROGENEOUS ISOTOPIC EXCHANGE

I. E. Mikhailenko and Academician Victor I. Spitsyn

Physical Chemistry Institute, Academy of Sciences USSR

Translated from Doklady Akademii Nauk SSSR, Vol. 131, No. 1, pp. 129-132, March, 1960
Original article submitted December 10, 1959

In a previous communication [1] the authors of this paper showed that the isotopic exchange of sulfur at 840°C in the $K_2\overset{\times}{S}O_4-SO_3$ system depends essentially on the specific activity of $K_2\overset{\times}{S}O_4$. Within the investigated range of activities, from 0.02-0.03 to 16.2 mC/g, the maximum exchange rate was detected at the potassium sulfate activity of 2-2.3 mC/g.

In this work the investigation was extended to K_2SO_4 samples with an even higher specific activity (up to ~ 130 mC/g). The new data confirm the previous results and make it possible to clarify slightly the mechanism of the observed phenomena. The apparatus and the experimental technique were similar to those described in [1]. Some of the samples were prepared by adding small amounts of Na_2SO_4 rich in S^{35} to a solution of chemically pure K_2SO_4. We had previously established that traces of Na_2SO_4 have no effect on the isotopic sulfur exchange in the $K_2\overset{\times}{S}O_4-SO_3$ system. The $K_2\overset{\times}{S}O_4$ samples with the highest specific activity were prepared by neutralizing labeled $H_2\overset{\times}{S}O_4$ with chemically pure KOH. The experimental results are presented in Table 1 and Fig. 1.

The isotopic exchange rate remains constant in the $K_2\overset{\times}{S}O_4$ activity range from 0.02-0.03 mC/g. It begins to increase when the sample activity exceeds 0.05 mC/g and attains a maximum at 2-2.5 mC/g (about 60% exchange in 10 min). As the specific activity of potassium sulfate is increased from 3 mC/g to 35 mC/g, the exchange rate decreases to 25% per 10 min. Above 61 mC/g the rate begins to increase again, attaining the value of 85% per 10 min at a K_2SO_4 activity of 131 mC/g. It is possible that the increased isotopic exchange rate observed when one increases the specific activity of samples from a few hundredths to 2-3 mC/g is due to the creation of positive charges on the solid phase surface as a result of an uninterrupted bombardment by β-particles. The isotopic exchange of sulfur seems to proceed through a reaction between SO_3 and SO_4^{2-} ions on the potassium sulfate surface, with $S_2O_7^{2-}$ ions formed as an intermediate product. An increased number of positively charged active centers on the surface favors the formation of these ions. The reduced exchange rate on samples with activities from 3 to 35 mC/g may possibly be due to a partial neutralization of the positive charges by the overabundance of electrons from the β-radiation. In any case, the activation energy measurements (see below) confirm the theory that the mechanism for the isotopic exchange varies with the specific activity of the $K_2\overset{\times}{S}O_4$ samples.

The sharply increased exchange rate observed when the specific activity of $K_2\overset{\times}{S}O_4$ is raised above 35 mC/g probably proceeds by a mechanism different from that responsible for the first branch of the curve in Fig. 1. In this case, presumably, pure radiation effects assume the dominant role; these involve an increased activation of SO_4^{2-} ions and of individual atoms in the crystal lattice, as well as of SO_3 molecules, by the β-particles. In a forthcoming communication [2], where the effects of external β-radiation on the isotopic

TABLE 1

Isotopic Exchange in the $K_2SO_4 - SO_3$ System at 840°C

K_2SO_4 sample no.	Amt. of Na_2SO_4 added, in %	Observed spec. act., in counts/min · g	Abs. activity, in mC/g	No. of experiments	Percent exchange (average)
1	0,04	$6,44 \cdot 10^5$	$1,7 \cdot 10^{-3}$	5	11,7
2	0,1	$9,37 \cdot 10^5$	$2,6 \cdot 10^{-3}$	6	11,5
3	—	$5,50 \cdot 10^5$	$6,1 \cdot 10^{-3}$	5	14,2
4	0,1	$12,1 \cdot 10^5$	$3,4 \cdot 10^{-1}$	7	24,5
5	0,1	$12,5 \cdot 10^5$	$3,5 \cdot 10^{-1}$	4	26,7
6	0,4	$72,6 \cdot 10^5$	2,0	5	65,5
7	0,4	$80,4 \cdot 10^5$	2,3	5	66,9
8	0,5	$13,5 \cdot 10^7$	3,0	4	60,9
9	2,6	$28,2 \cdot 10^7$	7,8	5	33,3
10	3,0	$58,5 \cdot 10^7$	16,2	4	36,6
11	2,0	$96,4 \cdot 10^7$	27,1	4	31,4
12	1,8	$12,3 \cdot 10^8$	34,6	7	25,2
13	—	$55,1 \cdot 10^8$	61,1	4	31,5
14	—	$74,7 \cdot 10^8$	74,9	5	43,2
15	—	$17,6 \cdot 10^9$	98,8	4	52,8
16	—	$21,2 \cdot 10^9$	131,3	8	85,5

TABLE 2

Rate Constants for the Isotopic Exchange Between SO_3 Gas and $Na_2\overset{x}{S}O_4$ of Various Specific Activities

Na_2SO_4 sample no.	Abs. activity in mC/g	Temp., in °C	Percent exchange	Rate constant, $k \cdot 10^2$	$\frac{1}{T} \cdot 10^4$	$\ln (k \cdot 10^2)$	$E = A \cdot R$ in kcal/mole
1	$1,7 \cdot 10^{-3}$	700	14,7	1,590	10,27	0,4637	24±2
		750	24,9	2,864	9,77	1,051	
		800	38,1	4,894	9,32	1,587	
		840	49,2	6,772	8,98	1,914	
2	1,02	700	25,8	2,984	10,27	1,0824	23±2
		750	46,8	6,212	9,77	1,8251	
		800	64,7	10,41	9,32	2,3421	
		840	73,1	13,13	8,98	2,5754	
3	10,7	700	24,3	2,784	10,27	1,0300	19±2
		740	36,0	4,464	9,90	1,4960	
		800	56,0	8,210	9,32	2,1050	
		840	69,3	11,810	8,98	2,4469	
4	24,5	700	20,4	2,282	10,27	0,8252	18±2
		740	26,9	3,134	9,90	1,1400	
		790	34,7	4,263	9,41	1,451	
		830	56,9	8,418	9,07	2,125	

exchange in the $K_2\overset{x}{S}O_4 - SO_3$ system are described, we will show that in exactly the same region (at a $3 \cdot 10^{16}$ ev dosage, which is equivalent to a potassium sulfate sample with an activity of 32 mC/g) the effects of fast electrons on the investigated process become first noticeable.

Some of the factors influencing the isotopic exchange rate in the $K_2SO_4 - SO_3$ system are examined more thoroughly. One might have assumed that the chloride ions formed in the K_2SO_4 sample as a result of the S^{35} decay increase the exchange rate in the $K_2SO_4 - SO_3$ system. To verify this assumption, we studied potassium sulfate samples with a specific activity of about 0.06 mC/g, containing 0.12% KCl. The percent exchange was 11.6% (in 10 min) and thus turned out to be practically identical with that observed on pure samples.

While studying the isotopic exchange in the $K_2\overset{x}{S}O_4 - SO_3$ system, we were interested in finding out whether the exchange activation energy changes when the radioactive isotope content in the sulfate is increased. We could not use in this case K_2SO_4 since the kinetics would have to be investigated above 1000°C, and this might cause some thermal dissociation of the salt. The desired isotopic exchange kinetics were investigated in $Na_2\overset{x}{S}O_4 - SO_3$ systems using sodium sulfate samples of various activities. The results are presented in Table 2 and Fig. 2.

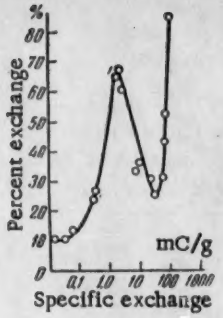

Fig. 1. The percent isotopic exchange as a function of the specific activity of $K_2\overset{\times}{S}O_4$.

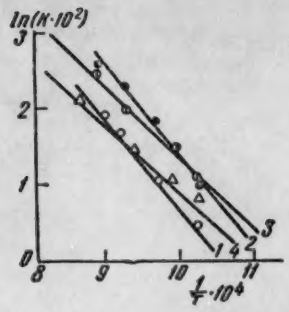

Fig. 2. Rate constant for the isotopic exchange in the $Na_2\overset{\times}{S}O_4-SO_3$ system as a function of 1/T.

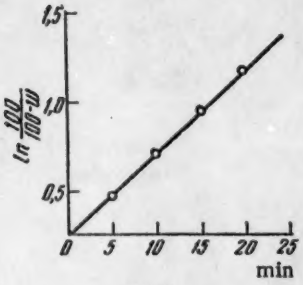

Fig. 3. $\ln \frac{100}{100-W}$ as a function of time in the isotopic exchange between $Na_2\overset{\times}{S}O_4$ and SO_3.

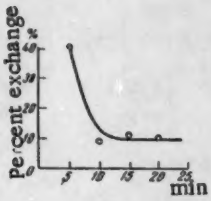

Fig. 4. Changes in the isotopic exchange rate in a $Na_2\overset{\times}{S}O_4-SO_3$ system.

The activation energy was determined from the Arrhenius equation $K = K_0 e^{-E/RT}$. The reaction rate constant was computed by using the equation $\ln \frac{100}{100-W} = kt$, where W is the percent exchange, t the duration of each experiment (10 min). This equation may only be used if the left side of the equation is a linear function of time (Fig. 3). The data presented above show that the mechanism for the isotopic exchange between $Na_2\overset{\times}{S}O_4$ and SO_3 changes when one increases the specific activity of samples from 0.02 and 1 mC/g to 11 and 25 mC/g. The specific activity of Na_2SO_4 and the isotopic exchange rate in the $Na_2\overset{\times}{S}O_4-SO_3$ system are interrelated in exactly the same manner as was observed in the case of the $K_2\overset{\times}{S}O_4-SO_3$ system. Chemically potassium potassium sulfate and sodium sulfate are very similar. On this basis one may conclude that the exchange mechanism in the $K_2\overset{\times}{S}O_4-SO_3$ system is the same.

The isotopic exchange of sulfur in the system studied by us is divided into two distinct phases: for a short period of time, about 5 min, the exchange rate is very rapid (attaining 40%), then rapidly declines. In this case the exchange evidently occurs inside a narrow surface layer of K_2SO_4. After that, the exchange rate in each subsequent 5 min period remains practically constant, at 10% below the value observed during the first 5 min (Fig. 4). In the second case the rate seems to be controlled by the diffusion of SO_4^{2-} in the solid phase.

We also investigated the isotopic exchange between radioactive sulfur trioxide and stable potassium sulfate (Table 3). We found that, after the sulfur trioxide was passed for 5 min over potassium sulfate, the activity of the latter decreased to a constant level. Undoubtedly the relatively high concentration of S^{35} which arises on the solid phase surface is responsible for the reduced exchange rate. The diffusion into the solid phase seems to be much slower than the reverse evolution of S^{35} atoms out of the solid into the gaseous phase, observed in the exchange between labeled K_2SO_4 and inert SO_3.

TABLE 3

Isotopic Exchange in the $K_2SO_4-\overset{x}{S}O_3$ System at 840°C. The Weight of K_2SO_4 = 0.28 g, the Initial Activity of SO_3 was 6.2 mC/g

Duration of $\overset{x}{S}O_3$ flow, in min.	Amount of $\overset{x}{S}O_3$, in g	Spec. activ. of K_2SO_4 after the expt., in mC/g (averaged from 4 expts.
5	0.2881	0.28
10	0.5762	0.20
15	0.8643	0.28
20	1.1524	0.27

TABLE 4

Isotopic Sulfur Exchange in the $K_2\overset{x}{S}O_4-SO_2$ System at Various Temperatures (the SO_2 weight was 0.6 g)

Temp., °C	K_2SO_4 wt., in g	Change in K_2SO_4 wt. after expt., in %	Initial activity, in counts/min	K_2SO_4 activity, in counts/min		Percent exchange	
				in counts/min	in % of initial		
600	0,3732	−0,1	$1784 \cdot 10^3$	$1805 \cdot 10^3$	100.9		
	0,3374	+0,1	$1614 \cdot 10^3$	$1665 \cdot 10^3$	103,0		
	0,3479	−0,2	$1663 \cdot 10^3$	$1640 \cdot 10^3$	101,0		
	0,3477	−0,1	$1663 \cdot 10^3$	$1648 \cdot 10^3$	99,1		
700	0,3295	−0,1	$1577 \cdot 10^3$	$1483 \cdot 10^3$	94,0	6,2	6,8
	0,2900	−0,2	$1388 \cdot 10^3$	$1307 \cdot 10^3$	94,2	6,9	
	0,3074	−0,1	$1471 \cdot 10^3$	$1422 \cdot 10^3$	93,3	6,8	
	0,2732	−0,1	$1308 \cdot 10^3$	$1237 \cdot 10^3$	94,6	7,5	
840	0,3147	—	$1582 \cdot 10^3$	$1393 \cdot 10^3$	88,0	14,4	13,6
	0,3373	−0,1	$1696 \cdot 10^3$	$1527 \cdot 10^3$	90,0	13,1	
	0,3532	−0,1	$1776 \cdot 10^3$	$1570 \cdot 10^3$	88,4	14,2	

At temperatures above 400° SO_3 begins to dissociate into SO_2 and oxygen. We therefore studied the isotopic exchange in the $K_2\overset{x}{S}O_4-SO_2$ system at various temperatures and at a constant activity of K_2SO_4 equal to $5.9 \times \times 10^{-2}$ mC/g. Sulfur dioxide was dried over $CaCl_2$ and conc. H_2SO_4, admitted into a quartz reaction tube at the rate of 13 liters/hr, and allowed to flow over a combustion vessel containing the labeled potassium sulfate. After that, the residual $K_2\overset{x}{S}O_4$ activity was measured and the percent exchange computed.

We have now established that sulfur undergoes exchange at 700° and above. The isotopic exchange rates at 840° in the $K_2\overset{x}{S}O_4-SO_3$ and the $K_2\overset{x}{S}O_4-SO_2$ systems are practically identical.

LITERATURE CITED

[1] V. I. Spitsyn and I. E. Mikhailenko, Dokl. Akad. Nauk SSSR, 121, 319 (1958).•

[2] V. I. Spitsyn, I. E. Mikhailenko, et al., Dokl. Akad. Nauk SSSR 131, No. 2 (1960).••

•Original Russian pagination. See C. B. translation.

••See C. B. translation.

THE OCCLUSION OF SULFUR IN ELECTROPLATED METALS

A. A. Sutyagina

Physical Chemistry Institute, Acad. Sci. USSR.

(Presented by Academician A. N. Frumkin, November 10, 1959)
Translated from Doklady Akademii Nauk SSSR, Vol. 131, No. 1, pp. 133-136, March, 1960
Original article submitted October 5, 1959

The literature devoted to the study of surface-active agents and their effects on the electrocrystallization of metals [1], particularly the work dealing with the role of specific agents in the formation of lustrous surfaces [2], contains many theories relating these effects to the physical adsorption of various compounds introduced into the solution or formed at the cathode. Accordingly, the amount of surface-active material occluded in the electroplate should depend on the adsorptivity of these materials (or of any products formed during electrolysis) and the surface charge of the electrode; it should be noted that the addition of surface-active agents to the electrolyte has many important practical applications in the preparation of useful electroplates.

Theories dealing with the adsorption of surface active agents on nickel have been discussed in several papers [3]. Certain workers have tried to connect the adsorptivity of these compounds, some of which contained sulfur, with their molecular structure, and especially with the presence of free electron pairs [4]. At the same time there has appeared some evidence in recent chemical literature that the adsorption may be accompanied by an irreversible molecular dissociation [5]. The fact that sulfur is occluded in the deposit when electroplating is carried out in a solution containing organic compounds was attributed by several workers [6] to the formation of metallic sulfides in the vicinity of the cathode. Thus the mechanism by which various impurities are incorporated into metal electroplates is still under discussion.

The results of our work on the effects of surface-active agents containing sulfur on the structure and properties of electroplated nickel, cobalt, zinc, and copper led us to the conclusion that the amount of impurities occluded and the occlusion mechanism both, depend to a large extent on the nature of the metal.

Our investigation of the electroplating in the presence of surface-active agents showed that the amount and form in which these impurities, particularly sulfur, were present in the metal depend mainly on the chemical forces operating between the surface of the freshly plated metal and the molecules (or ions) of the surface-active agent present in the immediate vicinity of the cathode. When the amounts of sulfur contained in plated nickel and zinc are compared, it becomes very obvious that the quantities are strikingly different. Thus, for example, when the thiourea concentration in the nickel electrolyte is increased from 0.1 to 0.4 g/liter (pH 2.5, D_k 1.3 amp/dm^2), the amount of sulfur in the plated metal increases from 0.8 to 5.26%, whereas a similar thiourea concentration change (from 0.2 to 0.4 g/liter) in the zinc electrolyte (pH 4, D_k 1 amp/dm^2) changes the sulfur content in electroplated zinc from 0.12 to 0.37%.

In Table 1 we have tabulated the total sulfur content in nickel and zinc electroplated from electrolytes containing: a) 160 g/liter $NiSO_4 \cdot 7H_2O$, 30 g/liter H_3BO_3, 10 g/liter NaCl, and b) 250 g/liter $ZnSO_4 \cdot 7H_2O$; into these electrolytes, surface-active agents such as thiourea, allyl thiourea, ß-thionaphthoic acid, thioacetic acid, etc., were successively introduced.

The Sulfur Content of Nickel and Zinc Electroplated in the Presence of Surface-Active Agents

Agent	Agent conc., g/liter	Electrolyte pH	Current density, amp/dm²	Total sulfur content, wt. %
		Nickel electroplate		
Thiourea	0.2	5.5	0.65	2.15
"	0.2	5.5	1.0	1.24
Allyl thiourea	0.2	5.5	1.0	0.75
β-thionaphthoic acid	1.0	3.7	0.6	0.084
Thioacetic acid	0.1	3.6	1.0	0.26
		Zinc electroplate		
Thiourea	3,0	4,7	0,6	0,27
"	3,0	4,7	1,4	0,19
Allyl thiourea	2,0	3,8	1,0	0,049

The data presented in the table demonstrated that occlusion in nickel is much more sensitive to the nature of the surface-active agent and to the electrolysis conditions. It was interesting to see if a reason could be found for this difference and if the sulfur-containing particles incorporated into electroplated nickel and zinc could be identified; these two metals were selected since, in the presence of surface-active agents, they crystallize in different ways.

We have also determined the total carbon content in electroplated zinc and nickel. Analysis indicated that the amount of carbon • present in nickel was considerably less than would be expected from the total sulfur content, if one had assumed that the surface-active compounds were adsorbed in their original form. Thus, while the numerical sulfur to copper ratio in thiourea is 2.66, the analytically determined ratio in electroplated nickel could be as high as 12.6 in certain experiments.

The above-discussed experimental results indicate that in the case of nickel and cobalt the surface-active agent is not just physically adsorbed in its original form but undergoes chemisorption, which is accompanied by the rupture of some of its bonds. This hypothesis was verified in two ways. The amount of sulfur present in the plated nickel as sulfide was determined from the amount of hydrogen sulfide evolved when the metal was dissolved in dilute hydrochloric acid.

To prove that the H_2S produced by the action of HCl results from the decomposition of sulfides occluded in the metal and not from a nickel-catalyzed decomposition (in the presence of hydrogen evolved when the metal dissolves) of the original surface-active agent (particularly thiourea), we conducted special experiments in which the sulfides were liberated from the metal by means of anodic solution. The latter were carried out in neutral solutions of sodium chloride and nickel chloride. In order to prevent the appearance of a zinc metal residue in the sulfide powder, we fastened the plated metals undergoing anodic solution to a magnet. The black sulfide powder which remained undissolved was chemically analyzed and studied by x-ray diffraction.

The chemical analysis of various powders thus obtained revealed that the sulfur: nickel ratio in these powders depends on the total sulfur content in the electroplated nickel. The sulfur: nickel ratio in these sulfides did not correspond to the stoichiometric ratio of these elements in known sulfides; in sulfides isolated from electroplates containing large amounts of sulfur, the sulfur: nickel ratio was occasionally as high as 2.5. The formation of sulfides saturated with sulfur has already been previously reported in the chemical literature [7]. Our investigation showed that a considerable portion of the sulfur present in the isolated sulfides was loosely bound

• The determination of carbon in nickel and zinc was carried out by V. S. Sedova by the combustion of powdered samples in a stream of oxygen. We take this opportunity to thank her for the assistance rendered to this work.

to the nickel; it could be removed by heating the powders at about 130°. Additional evidence to show that the sulfur is weakly bound was also obtained in experiments where the electroplated nickel was heated at 400-500°C. The sulfur: nickel ratio was only about 0.45 in powders left over from the anodic solution of preheated electroplates. This change in ratio, produced by preheating the plates, seems to be due to a solid-state reaction between nickel metal and the unstable nickel sulfides instead of being the result of a simple evaporation of sulfur, since the total sulfur content in electroplated nickel was not detectably changed after heating.

After comparing the amount of sulfur present as sulfide (determined by two methods) with the total sulfur content in the electroplated metals, we concluded that most of the occluded sulfur (over 90%) is present in the form of sulfide. The rest of the sulfur went into solution when the electroplated metal was chemically dissolved or decomposed by anodic electrolysis; the appearance of sulfur in these solutions may possibly be explained by assuming that some thiourea is occluded in the metal without decomposition and is then dissolved together with the metal. The carbon analyses seem to confirm this explanation.

An examination of results obtained with zinc reveals that the mechanism by which surface-active agents containing sulfur become occluded in electroplated zinc is very different from the one described for nickel. Electroplated zinc contains very little sulfur in the form of sulfide. A large portion of the sulfur is not chemically bound to the zinc. Quantitative data on the carbon and "unbound" sulfur indicate that most of the sulfur occluded in zinc comes from the thiourea which is adsorbed unchanged. This confirms the hypothesis proposed earlier [8] to explain the effects of 2,6-2,7 dithionaphthanoic acid on the electrocrystallization of zinc.

There is ample evidence in the chemical literature that nickel, when prepared in a certain way and saturated with hydrogen (the so-called Raney nickel), can quantitatively strip sulfur from both organic and inorganic compounds [9]. One may therefore assume that the freshly electroplated nickel also contains some hydrogen; it would then have properties similar to those of Raney nickel and react similarly with the surface-active agents containing sulfur. The above-described nickel properties would certainly explain why the sulfur content was so much higher than in the case of zinc.

As our experiments have demonstrated, there is a number of different forms and ways in which the sulfur originally present in the surface-active agent added to the electrolyte can become incorporated into electroplated metals, and consequently one can hardly expect to be able to explain the effects of various surface-active agents on the electrocrystallization of various metals (particularly their role in the structure formation) by using the same approach.

LITERATURE CITED

[1] M. A. Loshkarev, Dissertation, Ivanovsk Chem. Tech. Inst. [in Russian], 1948; M A. Loshkarev, V. Sotnikova, and A. Kryukova, Zhur. Fiz. Khim. 21, 219 (1947); A. A. Kryukova and M. A. Loshkarev, Dokl. Akad. Nauk SSSR 81, 1097 (1951); A. T. Vagramyan and Z. A. Solev'eva, Zhur. Fiz. Khim. 24, 10, 1252 (1950); A. I. Levin, Trans. Confer. on the Effects of Surface-Active Agents on the Electroplating of Metals [in Russian] (Vilnius, 1957), p. 11.

[2] K. M. Gorbunova, T. V. Ivanovskaya, and N. A. Shishakov, Zhur. Fiz. Khim. 25, 981 (1951); T. V. Ivanovskaya, Dissertation, Mendeleev Moscow Chem. Tech. Inst. [in Russian], 1955; Yu. Yu. Matulis, Trans. Confer. on the Effects of Surface-Active Agents on the Electroplating of Metals [in Russian] (Vilnius, 1957), p. 135; Z. A. Solov'eva, Trans. Confer. on the Effects of Surface-Active Agents on the Electroplating of Metals [in Russian] (Vilnius, 1957), p. 39.

[3] T. P. Hoar, Trans. Inst. Metal Finish Advance Copy 11, 8 (1953); J. L. Dye, O. J. Klingenmaier, J. Electrochem. Soc. 104, 5, 275 (1958); G. E. Gardam, Proc. of the Third International Conference on Electrodeposition (London, 1948); S. Wernick, Electrolytic Polishing and Bright Plating of Metals (London, 1948); L. I. Antropov and S. Ya. Popov, Zhur. Priklad. Khim. 27, 206 (1954).*

[4] C. Mann, Trans. Am. Electrochem. Soc. 69, 115 (1936); B. Egeberg and N. E. Promisel, Trans. Am. Electrochem. Soc., 74, 211 (1938); C. Roth, and H. Leidheiser, J. Electrochem. Soc. 100, 12, 533 (1953); A. N. Frumkin, Ergebn. exp. Naturwiss. 7, 254, 270 (1928); E. Cherneva and A. Gorodetskaya, Zhur. Fiz. Khim. 13, 1117 (1939).

*Original Russian pagination. See C. B. Translation.

[5] A. N. Frumkin, Trans. Confer. on the Effects of Surface-Active Agents on the Electroplating of Metals [in Russian] (Vilnius, 1957).

[6] B. Egeberg and N. E. Promisel, Trans. Am. Electrochem. Soc. 74, 211 (1938); S. E. Eaton, K. W. Fabian, and E. H. Newton, Met. Finish 50, 12, 63 (1952); J. Elze, Metal, H. 3/4, 104 (1955); A. V. Pamfilov and A. E. Panchuk, Ukr. Khim. Zhur. 23, 3391 (1957); A. V. Pamfilov and D. M. Morgart, Ukr. Khimi Zhur. 28, 5, 684 (1957); V. S. Vyzgo and G. A. Tsyganov, Dokl. Uzbek SSR, No. 5, 23 (1955).

[7] W. Biltz, Zs. anorg. u. allgem. Che. 228, 275 (1936).

[8] N. T. Kudryavtsev and G. V. Érshler, Dokl. Akad. Nauk. SSSR 72, 363 (1950).

[9] Elgin, Ind. and. Eng. Chem. 22, 1290 (1930); O. B. J. Fraser, Trans. Electrochem. Soc. 71, 425 (1937); J. Aurby, Bull. Soc. Chem. 5, 1336 (1938); J. Bougault, E. Cattelain, and P. Chabrier, Bull. Soc. Chim. 7, 7 (1940); R. Mozingo, D. Wolf, S. Harris, and K. Folkers, J. Am. Chem. Soc. 65, 1013 (1943); New Methods in Synthetic Organic Chemistry [in Russian], Coll: ed. D. N. Kursanova (1950) p. 215.

A DIFFERENTIAL CAPACITY STUDY OF THE ADSORPTION OF SURFACE-ACTIVE IONS ON A ZINC ELECTRODE

Chuan-sin Tza and Z. A. Iofa

M. V. Lomonosov Moscow State University

(Presented by Academician A. N. Frumkin, November 17, 1959)
Translated from Doklady Akademii Nauk SSSR Vol. 131, No. 1, pp. 137-140, March, 1960
Original article submitted November 16, 1959

The differential capacity of the double layer was first used by T. I. Borisova, B. V. Érshler, and A. N. Frumkin [1] in determining the potential of zero charge $\varphi_{\epsilon=0}$ on electrodes and solid metals (Pb, Tl, Cd). They showed that the capacity vs potential curves for these metals were similar to the well-known C, φ curves for the mercury electrode. C, φ curves have been used for determining $\varphi_{\epsilon=0}$ values and for adsorption studies on Fe [2], PbO_2 [3], Zn [4], and on other metals [5].

On solid metals the capacity varies with the frequency of the applied alternating current (capacity dispersion). Based on the fact that capacity dispersion is less on a smooth metal surface, for example a molten metal [1] or a single crystal [6], it was suggested [2] that the numerous microcracks in the surface of a polycrystalline metal screen part of the surface as the frequency is increased. This decrease in effective surface of the electrode explains the decrease in capacity at high frequencies. On the other hand, Bockris and Conway [7] explain capacity dispersion as being due to slow relaxation of water molecules on the surface of a solid electrode.

The object of the present work was to study the structure of the double layer at the zinc electrode by measuring the differential capacity.

B. S. Krasikov and V. V. Sysoeva [4] measured the capacity at the zinc electrode to determine $\varphi_{\epsilon=0}$. However, we were unable to obtain a potential close to the value $\varphi_{\epsilon=0} = -0.63$ v found by these authors (the normal potential of the zinc electrode $\varphi^0_{Zn} = -0.76$ v) because, when the negative potential was decreased, dissolution of zinc occurred and an anodic current was observed even at -0.85 v. Therefore, the accuracy of $\varphi_{\epsilon=0}$ values for zinc are questionable where the measurements were made in aqueous solutions. Electrocapillary measurements on molten salts at high temperatures [8] offer an independent method of finding $\varphi_{\epsilon=0}$, assuming a constant potential difference between the maxima of the electrocapillary curves for a given metal in a melt and in an aqueous solution. For zinc this method gave $\varphi_{\epsilon=0} \approx -0.65$ v.

We used an ordinary impedance bridge to measure the capacity. The electrode was prepared by growing a single crystal of spectrally pure zinc in a hard glass tube (i.d. 0.4-0.5 mm) so that the plate of the base was parallel* to the axis of the resulting fine wire. The area of the electrode immersed in the solution was measured with a microscope.

Figure 1 (curves 1 and 2) shows that the variation of differential capacity at a zinc single crystal in 0.2-1.0 N KCl was only 5-8% over the frequency range 0.4-1.0 kc/sec. In dilute solutions the variation was much greater, but in this case it was due to a parasitic bridge to ground, because the capacity–frequency curve for 0.01 N KCl at $\varphi = -1.22$ v was completely compensated when a compensating capacitor was inserted into the bridge circuit, as described by B. B. Damaskin [9]. Such a correction, however, can only be applied when the

* As in the Russian original.

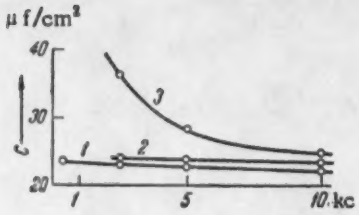

Fig. 1. Dependence of double-layer capacity on frequency at φ = - 1.22 v. 1) Zinc single crystal in 1.0 N KCl; 2) same in 0.2 N KCl; 3) polycrystalline zinc in 1.0 N KCl.

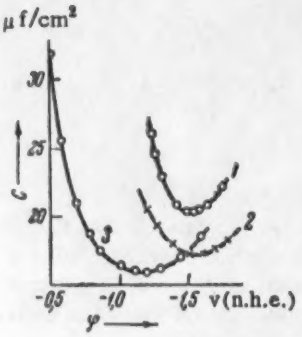

Fig. 2. Differential capacity of the double layer at different metals in 0.1 N KCl (frequency 10 kc/sec). 1) Zn; 2) Ga; 3) Hg.

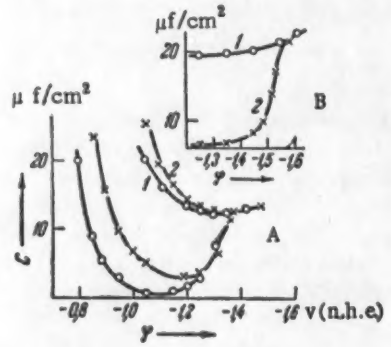

Fig. 3. Differential capacity at zinc single crystal (frequency 10 kc/sec). A: 1) 0.5 N KCl 2) 0.5 N KI; 3) 0.5 N KCl + 0.00024 N $N(C_4H_9)_4^+$; 4) 0.5 N KI + 0.00024 N $N(C_4H_9)_4^+$. B: 1) 1.0 N KCl; 2) 1.0 N KCl + 0.001 N $N(C_4H_9)_4^+$.

cell resistance is less than 100 ohms. In 0.001 N KCl (R = 5000 ohms) this method of compensation is not satisfactory. The effect of the state of the metal surface on capacity variation with frequency can be seen by comparing Curve 3 for polycrystalline zinc with Curve 1 (Fig. 1).

Figure 2, Curve 1 shows the variation of C with φ at a zinc single crystal in 0.1 N KCl. The curves for Hg and Ga in the same solution, based on the data of Grahame [10], are given for comparison. It is seen that the three curves are similar in form, especially if they are moved along the abscissa until the minima coincide. The branches of the curves rise more steeply from the minima, however, for Ga and Zn than for Hg. It was suggested that the rise of the C, φ curve for zinc when the cathodic potential was decreased might be due to pseudocapacity as the normal potential of the metal was approached. However, a simple calculation showed that pseudocapacity was insignificant in the region of the rise of the curve.* It is evident therefore that the positive branch of Curve 1 in Fig. 2 is due to adsorption of chlorine ions.

Figure 3A shows C, φ curves for the zinc electrode in solutions containing surface-active ions. The general form of these curves resembles that of the corresponding curves for mercury, which indicates a similar structure of the double layer on zinc and mercury. However, the difference between the C, φ curves 1 and 2 in Fig. 3A is much less than that between the corresponding curve on mercury [12], which is obviously related to the smaller adsorption of I^- on zinc. It should be noted that the instability constant of the halide complexes with mercury is much less than that for zinc, and also that the difference between these constants for Cl^- and I^- is much less in the case of zinc than for mercury [13].

$N(C_4H_9)_4^+$ ions are strongly adsorbed on zinc (Fig. 3 A). These ions are desorbed from the mercury electrode when the potential becomes sufficiently negative (φ = = - 1.58 v), but no desorption peak was observed in the zinc electrode curves (Fig. 3 B). This fact indicates that adsorption equilibrium is reached very slowly on zinc as compared with mercury. The desorption potential for $N(C_4H_9)_4^+$ ions on zinc in a solution of 1 N KCl + 0.001 N $N(C_4H_9)_4^+$ (Fig. 3 B) and the desorption peak for mercury in the same solution [14] are almost identical when

* The pseudocapacity was calculated using the formula [11] $C_p = \frac{n^2F^2D^{1/2}C}{RT\ \omega}$, assuming n = 2, F = 10^5 $\frac{\text{coulombs}}{\text{mole}}$ R = 8.3 $\frac{\text{joules}}{\text{mole}}$, D = 10^{-5} cm^2/sec, $\omega = 10000 \cdot 2\pi$. For E = - 0.76 v, c = 10^{-3} mole/cm^3, C = $2 \cdot 10^5$ $\mu f/cm^2$; for E = - 0.88 v, c = 10^{-7} mole/cm^3, C = 20 $\mu f/cm^2$; for E = -0.91 v, c = 10^{-8} mole/cm^3, C = 2 $\mu f/cm^2$. Since all the potentials were more negative than - 0.91 v, therefore the pseudocapacity in our experiments was less than 2 $\mu f/cm^2$.

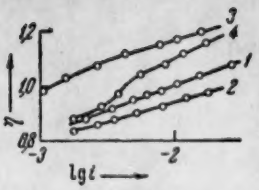

Fig. 4. Hydrogen overvoltage at zinc single crystal. 1) 0.5 N HCl + 0.5 N KCl; 2) 0.5 N HCl + 0.5 N KI; 3) 0.5 N HCl + 0.5 N KCl + 0.0004 N $N(C_4H_9)_4^+$; 4) 0.5 N HCl + + 0.5 N KI + 0.0004 N $N(C_4H_9)_4^+$.

referred to the $\varphi_{\epsilon=0}$ of the respective metals. Thus, the desorption peak for mercury in 1 N KCl + 0.001 N $N(C_4H_9)_4^+$ was observed at - 1.28 v, $\varphi_{\epsilon=0}$ = - 0.28 v, giving a difference of - 1.0 v. For zinc the potential of complete desorption was - 1.58 v, $\varphi_{\epsilon=0}$ = - 0.65 v, the difference being - 0.93 v.

Figure 4 shows the relationship between the hydrogen overvoltage at a zinc single crystal and the logarithm of the current density in a solution containing surface-active ions. These curves, like the capacity curves, resemble the corresponding ones for mercury. The adsorption of iodine ions lowered the overvoltage, but as in the case of the C, φ curves the effect was less at the zinc electrode than at the mercury electrode [15]. Lowering of the hydrogen overvoltage owing to adsorption of Cl^- and Br^- ions at a zinc amalgam electrode was observed by Ya. V. Durdin and E. G. Tsventarnyi [16]. The curves in Fig. 4 show that as in the case of mercury $N(C_4H_9)_4^+$ ions increased the hydrogen overvoltage at zinc considerably. Unfortunately, we did not reach the desorption potential for these ions while measuring the overvoltage. When the $N(C_4H_9)_4^+$ and I^- ions were present simultaneously the η, log i curves lay between Curves 2 and 3 in Fig. 4. As the negative potential is decreased, the adsorption of iodine ions increases, and the overvoltage decreases. This effect, which is due to a mutual increase in adsorption, was observed at the mercury cathode [15] but not at the zinc electrode over the potential range studied.

We thank Academician A. N. Frumkin for his interest and advice throughout this work.

LITERATURE CITED

[1] T. I. Borisova, B. V. Ershler, and A. N. Frumkin, Zhur. Fiz. Khim. 22, 925 (1948); 24, 337 (1950).

[2] É.O. Ayazyan, Doklady Akad. Nauk SSSR 100, 473 (1955); V. V. Losev, Doklady Akad. Nauk SSSR 88, 499 (1953).

[3] B. N. Kabanov, I. G. Kiseleva, and D. I. Leikis, Doklady Akad. Nauk SSSR 99, 808 (1954).

[4] B. S. Krasikov and V. V. Sysoeva, Doklady Akad. Nauk SSSR 114, 826 (1957).*

[5] V. L. Kheifets and B. S. Krasikov, Doklady Akad. Nauk SSSR 109, 586 (1956);* Zhur. Fiz. Khim. 31, 1992 (1957).

[6] D. I. Leikis and B. N. Kabanov, Transactions of the Institute of Physical Chemistry, Akad. Sci. USSR, 6 (1957).

[7] J. O' M. Bockris and B. E. Conway, J. Chem. Phys. 28, 707 (1958).

[8] S. Karpachev and A. Stromberg, Zhur. Fiz. Khim. 18, 47 (1944).

[9] B. B. Damaskin, Zhur. Fiz. Khim. 32, 2199 (1958).

[10] D. C. Grahame, Transactions of the Fourth Conference on Electrochemistry [in Russian] (Acad. Sci. USSR Press); Ann. Chem. 30, 1736 (1958).

[11] A. N. Frumkin, V. S. Bagotskii, and others, Kinetics of Electrode Processes [in Russian] (Moscow, 1952).

[12] A. N. Frumkin, B. B. Damaskin, and N. V. Nikolaeva-Fedorovich, Doklady Akad. Nauk SSSR 115, 751 (1957).*

[13] K. B. Yatsimirskii and V. P. Vasil'ev, Instability Constants of Complex Compounds [in Russian] (Acad. Sci. USSR Press, 1959).**

* Original Russian pagination. See C. B. Translation.

** English translation published by Consultants Bureau, New York, 1960.

[14] B. B. Damaskin, Dissertation [in Russian] (Moscow State University, 1959).

[15] Chuan-sin Tza and Z. A. Iofa, Doklady Akad. Nauk SSSR 125, 1065 (1959).*

[16] Ya. V. Durdin and E. G. Tsventarnyi, Vestn. Leningr. Univ. No. 10, 119.

* Original Russian pagination. See C. B. Translation.

THE EFFECTS OF COMPLEXING WITH $TiCl_4$, $SnCl_4$, $AlCl_3$, AND $AlBr_3$ ON THE INFRARED SPECTRA OF CERTAIN ESTERS

D. S. Bystrov and V. N. Filimonov

Physical Scientific Research Institute, A. A. Zhadanov Leningrad State University
(Presented by Academician A. N. Terenin, November 9, 1959)
Translated from Doklady Akademii Nauk SSSR, Vol. 131, No. 2, pp. 338-341, March, 1960
Original article submitted November 2, 1959

The study of adducts formed by esters with electron acceptors such as metal halides is of some importance due to the fact that $AlCl_3$ and several other metal halides are used as catalysts in the alkylation and acylation of aromatic compounds by esters [1]. In this work the interaction between esters and metal halides and the effects of this interaction on individual bonds in the ester were studied by examining the i. r. spectra of the complexes of $TiCl_4$, $SnCl_4$, $AlCl_3$, and $AlBr_3$ with methyl formate, isoamyl formate, ethyl acetate, and propyl acetate; using this method, it is also possible to determine the point at which the two components are linked.*

$TiCl_4$ and $SnCl_4$ form stable complexes with formate and acetate esters; these have the general composition $R_1COOR_2 \cdot TiCl_4$ and $2R_1COOR_2 \cdot SnCl_4$, and their properties have been studied in detail [3].

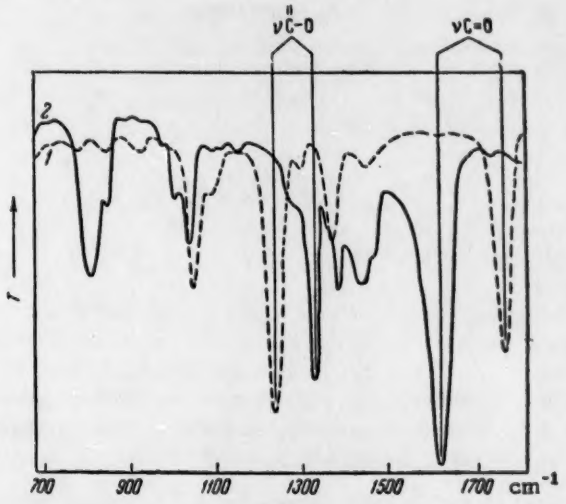

Fig. 1. Absorption spectra of ethyl acetate: 1) Gaseous ethyl acetate; 2) $CH_3COOC_2H_5 + TiCl_4$

*Preliminary data indicating that metal halides add to the carbonyl group of ethyl acetate were published by us in communication [2].

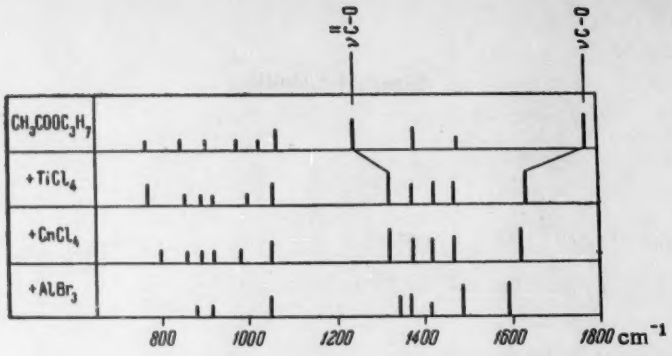

Fig. 2. Location of the absorption maxima of gaseous propyl acetate and of its adducts with $TiCl_4$, $SnCl_4$, and $AlBr_3$, respectively.

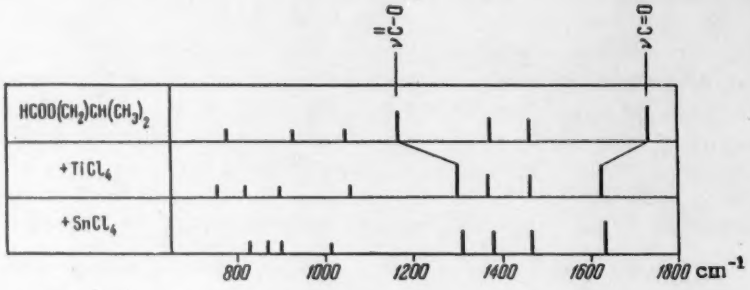

Fig. 3. Location of the absorption maxima of gaseous isoamyl formate and of its adducts with $TiCl_4$ and $SnCl_4$, respectively.

The complexes of $AlCl_3$ and $AlBr_3$ with formates and acetates have received much less attention. It is known, however, that, when ethyl is mixed with $AlCl_3$ [4] or $AlBr_3$ [5] at room temperature, the ester is not decomposed, even if excess aluminum halide is present, and can be recovered unchanged by treating the complex with ice-cold water.

The ester adducts of metal halides were studied in the solid state and were prepared as follows. Into an evacuated cell with NaCl windows, we placed a plane-parallel rock salt or fluorite plate which was used as a backing. The plate was cooled and coated with a thin layer of metal halide by the condensation of vapor ($TiCl_4$ and $SnCl_4$) or sublimation in vacuo ($AlCl_3$ and $AlBr_3$). After that, the cell was filled with the vapor of the investigated ester, which was allowed to react with the metal halide film. Prior to this the esters were dried over $CaCl_2$. After pumping out the excess free ester at room temperature, the plate was pushed into that section of the cell where the windows were, and the spectrum was recorded. This technique made it possible to prepare thin ($\approx$ 0.005 mm) layers which scattered little light without the need of exposing the adducts to air and dispersing them in a medium designed to reduce the scattering of light. At the same time, unfortunately, it was impossible to control rigidly the composition of the adducts formed.

The spectra were recorded on an IKS-14 spectrometer with NaCl and LiF prisms. A slit width of 15-20 cm^{-1} was generally used.

In Tables 1 and 2 we have compiled the absorption maxima for the adducts of ethyl acetate and methyl formate studied by us. For the sake of comparison, we have also included the vibrational frequencies of gaseous and liquid ethyl acetate and the fundamental frequencies of free methyl formate. In Fig. 1 we have plotted, as an example, the transmission curves of gaseous ethyl acetate and of the same ester after the formation of an

TABLE 1

Ethyl Acetate Frequencies (cm^{-1})

Literature data [6]	$CH_3COOC_2H_5$		$CH_3COOC_2H_5$			
	gas	liquid	+ $TiCl_4$	+ $SnCl_4$	+ $AlCl_3$	+ $AlBr_3$
$\nu C=O$	1770 s.	1745 s.	1625 s.	1633 s.	1620 s.	1610 s.
δCH_2, CH_3	1463 w.	1458 w.	1450 m.	1475 m. 1425 m.	1485 m. 1455 m.	1490 m. 1455 m.
δCH_3 acyl	1375 m.	1377 m.	1392 m.	1388 m.	1393 m.	1395 m.
$\nu C(=O)-O$	1245 s.	1250 s.	1335 s. 1160 w.	1325 s.	1345 m. 1163 w.	1348 m. 1165 w.
	1100 w.	1100 w.		1100 w.	1100 w.	1105 w.
	1058 m.	1050 m.	1045 m.	1045 m.	1045 m.	1045 m.
	930 w.	940 w. 918 w.	1010 m.	1008 m.	1007 m.	1010 m.
	852 w.	850 w.	850 m.	855 m.	840 m.	845 m.
	785 w.	785 w.	812 m.	815 w.	820 m.	810 w.

adduct with $TiCl_4$. Our spectra of propyl acetate and isoamyl formate adducts, and of the corresponding esters in the gas phase, are represented schematically in Fig. 2 and 3.

A comparison between the absorption spectra of pure esters and the spectra of corresponding adducts show that, in every case studied by us, the two most intense bands in the ester spectrum, at 1770-1750 and 1250-1200 cm^{-1}, disappeared when the adduct with metal halides was formed. The first band ($\nu C=O$) is generally assigned to the carbon-oxygen vibration of the carbonyl group, while the second one $\nu C(=O)$ is associated with the antisymetric bond vibration of the $C(=O)C$ = group in acetates or the $C(=O)-O$ group in formates [7, 8]. At the same time two new strong absorption bands, with maxima at 1635-1600 and 1360-1300 cm^{-1}, respectively, appear in the spectra of the adducts.

Such a change in the vibrational spectra cannot be explained by assuming that the metal halides are attached to the alkoxy oxygen of the ester. Indeed, if that were the case, one would only expect an insignificant change in $\nu C=O$ and a lowering in the vibrational frequency $\nu C(=O)-O$. On the other hand, the disappearance of absorption bands in the 1770-1750 cm^{-1} region and the appearance of new bands at considerably lower frequencies (120-160 cm^{-1} below) are in good agreement with the hypothesis that metal halides are attached to the carbonyl group of esters. The new absorption bands at 1635-1600 cm^{-1} can in this case be attributed to the vibration of a carbonyl group excited by the attachment of an electron acceptor. These bands are located very closely to the C = O band in the spectra of the $AlBr_3$ and $SnCl_4$ adducts of acetone (1635-1625 cm^{-1}) [9] and the $AlBr_3$ adduct of acetaldehyde (1660 cm^{-1}) [2]; the enumerated adducts are most certainly formed by the addition of the metal halide to the carbonyl group of the organic compound.

It should also be noted that the disappearance of the absorption bands at 1770-1750 cm^{-1} can also be explained in the case of ethyl acetate and propyl acetate by assuming that these esters change into the enol form when complexed with metal halides:

$$\begin{array}{l} H-O\ldots MetHal \\ H_3C=\overset{|}{C}-O-R \end{array}$$

The absorption bands at 1635-1600 cm^{-1} could then be attributed to the C = C stretching vibrations. This assumption, however, does not seem to be very plausible since formate adducts, which cannot change into an enol form, have absorption maxima at the same frequencies. Besides, the spectra of ethyl acetate adducts contains no characteristic frequencies for the C-H bond next to a double bond.

TABLE 2

Methyl Formate Frequencies (cm^{-1})

Literature data [7]	HCOOCH, (?)	HCOOCH, + $TiCl_4$	+ $SnCl_4$	+ $AlCl_3$	+ $AlBr_3$
$\nu C=O$	1754	1635 s.	1632 s.	1635 s.	1630 s.
δCH_3	1465 1454 1445	1435 m.	1440 m.	1442 m.	1437 m.
δCH	1375	1372 m.	1375 m.	1385 m.	1378 m.
$\nu C(=O)-O$	1207	1308 s.	1322 s.	1346 s.	1355 s.
δCH_3	1168	1180 w.	1170 w.	1175 w. 1100 w.	1100 w.
δCH	1032		1000 m.	978 w	
$\nu O-CH_3$	925	885 m.	883 m.	870 m.	865 w.
δOCO	767	811 m.	812 m.	828 m. 798 m.	830 w. 780 w.

The new intense absorption band at 1360-1300 cm^{-1} evidently has to be regarded as the $\nu C(=O)-O$ absorption displaced towards higher frequencies. The strong shift of this band seems to indicate that the $C(=O)-O$ bond is greatly strengthened at the expense of the weaker adjacent double bond. In the case of methyl formate one can also detect a shift in the vibrational frequency of the $O-CH_3$ bond from 925 to 885-865 cm^{-1}; the shift is very probably due to a weakening of this bond.

The increased frequency $\nu C(=O)-O$, as well as the lowered C = O vibrational bond frequency, indicates that the metal halides are attached to the carbonyl group. Thus, with the help of i.r. spectroscopy, it is possible to determine unequivocally the position at which the metal halide is attached to the ester.

As a rule $AlCl_3$ and $AlBr_3$ produce greater shifts in the absorption spectra of esters than $TiCl_4$ and $SnCl_4$ do, which is in line with the fact that aluminum halides are more active catalysts. A particularly large shift is observed when propylacetate forms an adduct with $AlBr_3$ (see Fig. 2).

The author feel deeply indebted to Acad. A. N. Terenin, under whose guidance this work was carried out.

LITERATURE CITED

[1] C. Thomas, Anhydrous Aluminum Chloride in Organic Chemistry [Russian translation] (IL, 1940).

[2] A. N. Terenin, V. N. Filimonov, and D. S. Bystrov, Izv. Akad. Nauk SSSR, Ser. Fiz., 22, 1100 (1958).

[3] N. S. Kurnakov and É. B. Shternin, Izv. Akad. Nauk SSSR, Otdel. Khim. Nauk 1936, 467; N. S. Kurnakov and N. K. Voskresenskaya, Izv. Akad. Nauk SSSR, Otdel. Khim. Nauk 1937, 797; Yu. A. Lysenko, O. A. Osipov, and E. K. Akopov, Zhur. Neorg. Khim. 1, 536 (1956); Yu. A. Lysenko and O. A. Osipov, Zhur. Obshchei Khim. 28, 1724 (1958).*

[4] D. N. Kursanov and R. R. Zel'vin, Zhur. Obshchei Khim. 9, 2173 (1939).

[5] Y. Takegami and U. Shingu, Bull. Inst. Chem. Research, Kyoto Univ. 24, 84 (1951); Chem. Abstr. 47, 12276 (1953).

[6] B. Nolin and R. N. Jones, Canad. J. Chem. 34, 1392 (1956).

[7] J. K. Wilmshurst, J. Mol. Spectr. 1, 201 (1957).

[8] S. A. Francis, J. Chem. Phys. 19, 942 (1951).

[9] V. N. Filomonov, D. S. Bystrov, and A. N. Terenin, Optika i Spektroskopiya 3, 480 (1957); A. N. Terenin, V. N. Filimonov, and D. S. Bystrov, Zs. Electrochem. 62, 180 (1958).

*Original Russian pagination. See C. B. translation.

RELATIONSHIP BETWEEN THE ELECTRICAL CONDUCTIVITY AND THE WORK FUNCTION OF MODIFIED ZINC OXIDE

V. I. Vladimirova, É. Kh. Enikeev, G. M. Zhabrova, and L. Ya. Margolis

Physical Chemistry Institute, Academy of Sciences USSR
(Presented by Academician M. M. Dubinin, November 4, 1959)
Translated from Doklady Akademii Nauk SSSR, Vol. 131, No. 2, pp. 342-345, March, 1960
Original article submitted October 30, 1959

The chemical literature contains a very large number of papers on the relationship between the electrical conductivity and the catalytic activity of semiconductors [1-4]. The most common technique for altering the electrical conductivity and its activation energy, a method used widely by many workers, involves the introduction into the oxide semiconductors of impurities which form solid solutions with it. The catalytic properties of such solid solutions, with regard to donor-acceptor reactions (CO oxidation, N_2O decomposition, H_2/D_2), can be varied extensively, which is directly connected with changes in the electrical conductivity and its activation energy.

In accordance with the electronic theories, several workers [5-7] have connected the activity of semiconductor catalysts with the position of the Fermi level relative to the surface. It should be noted that in several cases the experimental results are in conflict with the theoretical data. The discrepancies are probably due to the fact that the electrical conductivity of polycrystalline solids will not reflect any changes in the electron gas concentration near the surface. The position of the Fermi level can most precisely be established from the magnitude of the work function. In the present work we compared the electrical conductivity activation energy (E_σ) with the changes in work function (φ) produced by introducing impurities into ZnO.

To do this, we constructed an apparatus which made it possible to measure simultaneously the electrical conductivity and the contact potential difference on the same semiconductor sample and under identical conditions; this way any possible side-effects were eliminated. The investigation was carried out on zinc oxide with the impurities selected so that some of them increased the work function while others decreased it, as was established in a previous work [8]. The modified zinc oxide samples were prepared in various ways, so that the impurities could be introduced either at the surface or into the ZnO. Luminophorous zinc oxide was used as the starting material.

Lithium and sodium were introduced by saturating zinc oxide with the respective oxalates; this was followed by topochemical decomposition at relatively moderate temperatures: 450-500°C. Specified experiments proved that at the temperature and maintenance times used in this work, the oxalates were totally decomposed. In preparing ZnO samples containing lithium, one would expect the solid solutions to form even at 450°; in the case of ZnO and sodium, the formation of solid solutions was less likely, due to the large ionic radius of sodium. Thorium was introduced by treating zinc oxide with thorium nitrate solutions, which coated the surface with a layer of thorium hydroxide. [$Th(OH)_4$ normally precipitates at pH 3.5-4; in aqueous solution zinc hydroxide is formed on the zinc-oxide surface at pH = 8.4]. Firing at 450° resulted in the decomposition of the zinc hydroxide to zinc dioxide. Zinc sulfate was introduced through adsorption from a solution of the corresponding electrolyte. As has already been established [9], the adsorption of zinc sulfate on zinc oxide is irreversible and is accompanied

Expt. No.	Zinc oxide samples	E_a ev	$\Delta\varphi$ ev	$\Delta\varphi_{ZnO} - \Delta\varphi$ (ev)
1	ZnO	0,08	—0,7	0
2	ZnO + 8% Na_2O	0,32	+0,8	—1,5
3	ZnO + 8% Li_2O	0,5	—0,1	—0,6
4	ZnO + 8% Li_2O	0,25*	—0,03	—0,67
5	ZnO + 14,5% $ZnSO_4$	0,24	—1,3	+0,6
6	ZnO + 2% ThO_2	0,17	—0,9	+0,2

*Sample fired at 1100°C.

by the formation of basic zinc sulfates and a subsequent hydrolytic decomposition. Samples containing zinc sulfate were also fired at 450°C.

Zinc oxide samples containing different impurities were studied by means of x-ray diffraction and electron diffraction. The samples were compressed into pellets under a pressure of 200 kg/cm^2 and placed into a special cell which was connected with an apparatus for the simultaneous determination of electrical conductivity and contact potential difference. We used Miller's method [10] and a 300 cps frequency for the determination of electrical conductivity. The resistance measurements were accurate to within 15-20%. The contact potential difference between the investigated semiconductor and a gold reference electrode was determined by means of a vibrating-reed condenser [11]. The measured contact potential differences were accurate to within ± 0.01 v. The samples were conditioned at 300-400°C in vacuo (10^{-5} mm of Hg) or in a carbon monoxide atmosphere until the resistance became constant. On all our samples the electrical conductivity activation energy and the contact potential difference were determined as the samples were heated and while they were cooling.

The table lists the experimentally determined electrical conductivity activation energies (in ev), contact potential differences with references to gold, and the differences between the work functions of pure and modified ZnO.

The above-listed data show that the electrical conductivity activation energy of pure zinc oxide is very insignificant, which indicates also that the sample was almost entirely free of adsorbed oxygen. Our electrical conductivity activation energy was very close to the literature value for zinc oxide [12].

The introduction of chemically different impurities reduces the electrical conductivity and increases its activation energy. The electrical resistance at 350° decreased in the order:

$$\underset{\text{Sample No. 3}}{ZnO + Li_2O} > ZnO + Na_2O > ZnO + ZnSO_4 > ZnO + ThO_2 > ZnO.$$

Thus, if one were to rely solely on the electrical conductivity measurements, one would conclude that all of the impurities introduced by us into zinc oxide were electron acceptors, displacing the Fermi level downward towards the upper limit of the valence band.

However, work function measurements yielded somewhat different results. The data presented above show that lithium and sodium reduce the work function of pure zinc oxide, whereas zinc sulfate and thorium dioxide increase it. Consequently, on the basis of work function data, one may conclude that both lithium and sodium impurities are electron donors, displacing the Fermi level towards the conductance band, but that sodium has a more pronounced effect than does lithium.

Even when the firing temperature of a ZnO + 8% Li_2O sample was raised considerably, the effect of lithium ion and E_σ and $\Delta\varphi$ was in the same direction. The slight decrease in the magnitude of E_σ should probably be attributed to the recrystallization of zinc oxide at 1100°C.

The distribution of the impurities will depend on the preparatory conditions and on the chemical properties of both the solid and the impurities. Thus, the impurities may form solid substitution or inclusion solutions or become adsorbed on the surface. Changes in the electrical conductivity and work function of solids will depend on the location of impurities in the solid.

It should be noted that all the workers who had studied zinc oxide doped with lithium oxide had presumed that the lithium ions introduced into the zinc oxide lattice force zinc ions out into interstitial spaces (which should result in increased lattice parameters); yet the chemical literature contains practically no direct x-ray crystallographic evidence to indicate any formation of solid solutions in the ZnO + Li_2O system. Thus, for example, it was shown [13] that the lattice parameters of zinc oxide remained essentially unchanged after samples containing 0.12 and 0.32% lithium were fired at1000-1200°C, high above the temperature at which sintering occurs (Taman's temperature is 870°). The lattice constant of pure zinc oxide is 3.2432, while that of zinc oxide containing 0.12% Li_2O was 3.2431 [13].

The x-ray crystallographic measurements on modified zinc oxide were performed by N. A. Shushakov and co-workers and by M. Ya. Kushnerev, for which service the authors wish to thank them. According to our data, the lattice parameters remain unchanged when impurities are introduced into zinc oxide, and therefore we have no direct evidence for the formation of solid solutions.

Evidently, as all the above-mentioned results seem to suggest, when lithium oxide and sodium oxide are introduced into zinc oxide, their content at the surface and inside the solid is different.

Impurities located on the surface and those present in the layer adjacent to the surface, at a depth exceeding the screening length, have different effects on the electrical conductivity and the work function. Several observations clearly indicate that the work function changes as a result of surface charge and not because of any effects which could be directly attributed to the alkali ion (Na^+ or Li^+) dipole moment [5]. Impurities located deep inside have no effect on the work function and act as electron acceptors increasing E_σ, while these same impurities may act as electron donors on the grain surface and reduce the work function (φ). It is very likely that lithium dissolves in the zinc oxide layer next to the surface to form a solid inclusion solution, since the lithium oxide has a higher concentration on the surface than inside the solid. That is why the impurity affects the E_σ and $\Delta\varphi$ in different ways. Even electron diffraction could not detect any lithium oxide in samples of ZnO + 8% Li_2O fired at 450°.

Zinc sulfate is just adsorbed on the surface of ZnO. In such cases any changes in both the electrical conductivity and the work function will be determined by the displacement of the Fermi level from the surface, as was found to be true (see the table). The same applies to ZnO containing ThO_2.

Thus, in many cases changes in the electrical conductivity of modified catalysts can not be used as the sole criterion to locate the Fermi level at the surface. Therefore, any research devoted to the determination of quantitative relationships between the catalytic activity and the electrical conductivity of modified catalysts may lead to erroneous results if the distribution of the impurity between the inside and the surface of the solid is not examined in detail.

LITERATURE CITED

[1] G. M. Schwab and J. Block, Zs. Phys. Chem. N. F. 1, 42 (1954); Zs. Elektrochem. 58, 756 (1954).

[2] G. Parravano, J. Am. Chem. Soc. 75, 1452 (1953).

[3] N. P. Keier, S. Z. Roginskii, and I. S. Sazonova, Dokl. Akad. Nauk SSSR 105, 859 (1956).*

[4] A. Bielianski, I. Deren, and I. Haber, Bull. Polish Acad. Sci. [in Polish] 3, 3, 221 (1955); 4, 791 (1955).

[5] K. Hauffe, Advances in catalysis 7, 213 (1955).

[6] S. Z. Roginskii, Dokl. Akad. Nauk SSSR 126, 4, 817 (1959).*

[7] F. F. Vol'kenshtein, Uspekhi Khim. 27, 1304 (1958).

[8] É. Kh. Enikeev, L. Ya. Margolis, and S. Z. Roginskii, Dokl. Akad. Nauk SSSR 130, No. 4 (1950).

[9] G. M. Zhabrova and E. V. Egorov, Radiokhimiya No. 5, 538 (1959).

[10] P. H. Miller, Rev. Sci. Instr. 7, 298 (1952).

*Original Russian pagination. See C. B. Translation.

[11] V. F. Bogolyubov, Radiotekhnika i elektronika No. 3, 323 (1957).

[12] D. J. Bevan, J. P. Shelton, and J. S. Anderson, J. Chem. Soc. 1948, 1729.

[13] A.Cimino, M. Marezio, and A. Santoro, Naturwiss. 44, No. 11-12, 348 (1957).

THE HYPERFINE STRUCTURE IN THE PARAMAGNETIC RESONANCE SPECTRA OF BENZOPHENONE-K-KETYL

V. M. Kazakova and Corresponding Member Acad. Sci. USSR
Ya. K. Syrkin

M. V. Lomonosov, Moscow Institute of Fine Chemical Technology
Translated from Doklady Akademii Sci. USSR, Vol. 131, No. 2, pp. 346-347, March, 1960
Original article submitted November 4, 1959

In a previous communication [1] we reported that the paramagnetic resonance (p.m.r.) spectra of several ketyls (these result from the reaction between ketones and alkali metals) formed in a stream of an inert gas in the form of insoluble film on the surface of metal shavings. We were interested in examining the hyperfine structure (h.f.s.) in the p.m.r. spectra of ketyls since from the h.f.s. one can determine the distribution of the spin density of the unpaired electron throughout the molecule. Here, however, we encountered several difficulties, mainly due to the fact that most ketyls are insoluble in common organic solvents. Only the potassium ketyls of benzophenone and phenyldiphenyl ketone will dissolve in benzene. We studied the p.m.r. spectra of dilute solutions of benzophenone-K-ketyl and phenyldiphenyl-K-ketyl at room temperature in a radio frequency spectrometer using high-frequency magnetic field modulation and resonant-cavity stabilization of the clystron frequency [2]. The spectra were recorded on an automatic potentiometer in the form of the first derivative of the absorption curve. In the spectrum of benzophenone-K-ketyl, h.f.s. was detected. In addition to this, at first only seven peaks appear (Fig. 1), but, when the solution is diluted, the spectrum becomes more fully resolved (Fig. 2). The entire spectrum consists of 23 lines with a 2.1 gauss separation between the initial septet components and a 0.7 gauss splitting inside the septet. This type of spectrum can be explained in the following way. The seven components initially observed are due to an indirect interaction between the unpaired electron and the 4 ortho and 2 para ring protons. Further splitting arises from the interaction with 4 meta protons; at the same time, if the ratio of $a_1 : a_2 = 3 : 1$, one should only observe 23 of the 35 h.f.s. components, which was experimentally confirmed.

Fig. 1.

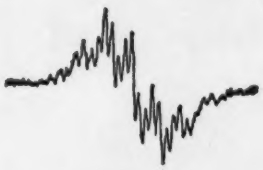

Fig. 2.

Using McConnell's empirical equation, $a = Q\rho$, where $Q = -22.5$, and our own experimental data, we were able to

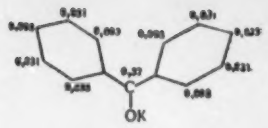

Fig. 3.

estimate the unpaired electron spin densities in ρ-π-orbitals of the phenyl ring carbons. The spin densities thus calculated were $|\rho|$ = = 0.093 in the ortho and para positions, and $|\rho|$ = 0.031 in the meta position (Fig. 3).

Using the molecular orbital treatment and the Hückel approximation, we calculated the distribution density of an unpaired electron in diphenylmethyl; for the ortho and para carbons ρ = 0.10, while on the methyl carbon ρ = 0.4, both of which are in good agreement with our experimental results. It is interesting to note that our results indicate equal spin densities in the ortho and para positions, whereas, in the case of triphenyl methyl Lupinski [3] considers the spin density in the para position to be negligibly small in comparison with the ortho and meta positions. Brovetto and Ferroni [4], who computed the values of ρ in triphenyl methyl using the LCAO treatment, report identical values for the ortho and para positions. Similar results are obtained when the spin densities are calculated by the molecular orbital method.

The hyperfine structure of phenyldiphenyl-K-ketyl in benzene could not be resolved. We are currently pursuing the investigation of the p.m.r. spectra of aromatic and aliphatic metal ketyls in solution.

LITERATURE CITED

[1] V. M. Kazakova and Ya. K. Syrkin, Izv. Akad. Nauk SSSR, Otdel. Khim. Nauk 1959, No. 4, 755.•

[2] A. G. Semenov and N. N. Bubnov, Pribory i tekhnika eksperimenta (1959), No. 1, 92.

[3] J. H. Lupinski, J. Chem. Phys. 26, No. 6, 1766 (1957); H. S. Jarrett, and G. I. Sloan, J. Chem. Phys. 22, 10, 1783 (1954).

[4] Brovetto and Ferroni, Nuovo Cimento, 5, 142 (1957); F. C. Adam and S. I. Weissman, J. Am. Chem. Soc. 80, 2057 (1958).

•Original Russian pagination. See C. B. Translation.

SOME PECULIARITIES OF EMULSIFICATION IN STRUCTURIZED LIQUIDS

L. Ya. Kremnev and L. A. Borodina

The All-Union Highways Scientific and Research Institute, Leningrad Branch
(Presented by Academician P. A. Rebinder, April 22, 1959)
Translated from Doklady Akademii Nauk SSSR, Vol. 131, No. 2, pp. 348-350, March, 1960
Original article submitted May 22, 1959

It is well known that the type of aggregated stable concentrated emulsion obtained from two ideal liquids with low Newtonian viscosity (such as water and benzene) is essentially determined by the molecular surface properties of the emulsifier used in preparing it: the emulsifier forms on the surface of the droplets a structural and mechanical barrier which prevents them from coalescing [1]. Upon this basis hydrophilic emulsifiers make it possible to obtain direct emulsions (that is, the "oil in water" (O/W) type), while oleophilic emulsifiers stabilize inverted emulsions (that is, the "water in oil" (W/O) type).

On the other hand, liquids possessing a steric structure and having a high effective (structural) viscosity, show their own specific behaviour on emulsification. To this group belong, for example, bitumens and tars of viscous types at temperatures above 40° [2] and less viscous types at ordinary temperature. In the presence of hydrophilic surface-active emulsifiers, which in considerable concentration of the agent impart structure to the water, these are able to form with the water not only direct but also inverted emulsions.

When the bitumen or tar is added gradually to the aqueous solution of the emulsifier (concentration C), as we should expect, there is formed a direct emulsion, and the concentration of the bitumen in it may be increased to large values, until the formation of a limiting concentration of the emulsion ("limiting emulsion") (Fig. 1, 1). In the converse case, when the bitumen or tar is treated by stepwise addition of the aqueous solution of the same emulsifier, an inverted emulsion (water in oil type) is always formed, the concentration of which may be increased up to a definite limit Q, depending on the concentration C of the emulsifier in the water (Fig. 1, 2). Q denotes the weight concentration of the disperse phase in the limiting emulsion.

As an example, there are displayed in Fig. 1 the emulsification isotherms obtained with the bituminous material B-5, which at ordinary temperatures behaves like a highly structural system, and with aqueous solutions of a cation active emulsifier (the emulsifying agent A-20), namely, the benzoylsulfonate of methyldiethyl-2,5-dioctylphenoxyeicosaethyleneoxymethylammonia:

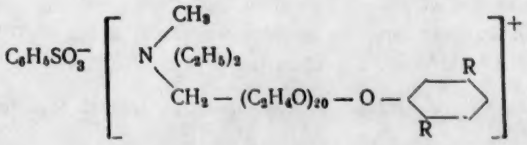

where R = C_8H_{17}.

The results of emulsification are determined, certainly, not only by the introduction of the hydrophilic emulsifier and its concentration, but also by the content of oleophilic surface-active substances in the bitumens

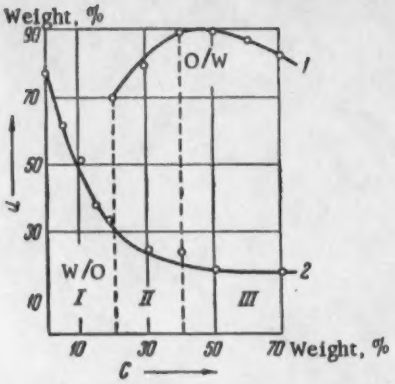

and tars, and further by the thixotropic structure characteristics of this system. In the course of the curves, there can be distinguished three regions of concentration of the hydrophilic emulsifier C, according to their effect on the emulsification.

In region I there is stabilized only inverted emulsions, the water in oil type. It is characteristic that, in the emulsification of pure water, the weight concentration in the emulsion Q is a maximum, but, with increase in the concentration of the emulsifier in the water, Q is slowly reduced from 77.8% to 20%. This effect is produced by the antagonistic interaction between the oleophilic emulsifiers of the bitumen and the hydrophilic emulsifier in the water solution; each of these tends to destroy the emulsification of both the aqueous solution and the bitumen, respectively, as a consequence of which mutually cancelling quantities of both the stabilizers are eliminated from the emulsification processes [3]. In region I there is present no excess of the hydrophilic emulsifier; therefore, necessarily, it is impossible to stabilize the direct emulsion (oil in water type).

In region II is developed the direct emulsion of bitumen in water (the oil in water type); this is initially coarse, since the excess of hydrophilic emulsifier is not yet sufficient to stabilize highly disperse emulsions; but, with increase in the concentration of the hydrophilic emulsifier, the dispersion of the emulsification increases. In the same region there takes place some reduction in the value of Q in the inverted emulsion, which may be attributed to a change in the structural and mechanical properties of the bitumen under the influence of the emulsifier A-20.

In the region III, similarly, there are easily obtained both types of highly disperse emulsions in proportion to the quantity of emulsifier introduced into the liquids. Some reduction of Q in the direct emulsion is determined by the continuing increase in the degree of dispersion of the globules of the bitumen. As to the inverted emulsion, in this region the concentration of the hydrophilic emulsifier is the result of emulsification which, as in region II also, wholly depends on the structural and mechanical properties of the bitumen. Stabilization of the globules of water and aqueous solutions in region I is accomplished both by the oleophilic emulsifiers of the bitumen and, to a considerable extent, by the incorporation of the globules in the steric network of the bitumen, thixotropically reestablished after their partial destruction in the course of dispersion. However, in the regions II and III the emulsifying properties of the oleophilic emulsifiers of the bitumen are reduced because of their antagonistic interaction with the hydrophilic emulsifier. Consequently the only factor in producing the aggregative stability here of the inverted emulsion, is the structural and mechanical properties of the bitumen.

In full agreement with the ideas of P. A. Rebinder [1], the universal structural and mechanical factor in the stabilizing of the disperse systems in our conditions is the manner in which this can predominate over the hydrophilic properties of the emulsifier even when the latter is present in very high concentrations in the aqueous solution, so that even then stable emulsions of the water in oil type can be maintained.

A similar effect of powerful stabilization of direct emulsions by hydrophobic metallic soaps, through the formation of a structural and mechanical barrier, has been discovered earlier by A. B. Taubman and A. F. Koretskii [4], during the formation of oil emulsions with the help of solid emulsifiers.

The same results as with the bitumen of type B-5 have also been obtained by us with anion active hydrophilic emulsifiers, both with bitumens of viscous types and with tars, the emulsions possessing at ordinary temperatures solid-like properties [2]. In these cases the bitumen was heated up to 60-70° (that is, until it attained the conditions of a highly structured liquid and then submitted to emulsification.

The authors are most grateful to Academician P. A. Rebinder for his valuable comments, especially during the reading of the manuscript.

LITERATURE CITED

[1] P. A. Rebinder, Koll. Zhurn. 20, 527 (1958);• Koll. Zhurn. 8, 157 (1956).

•Original Russian pagination. See C. B. Translation.

[2] N. V. Mikhailov and S. Ya. Shalyt, Koll. Zhurn. 18, 609 (1956).•

[3] L. Ya. Kremnev, Koll. Zhurn. 20, 546 (1958).•

[4] A. B. Taubman and A. F. Koretskii, Dokl. Akad. Nauk SSSR 120, No. 1, 126 (1958);• Koll. Zhurn. 20, 676 (1958).•

•Original Russian pagination. See C. B. Translation.

A MECHANISM FOR THE DECOMPOSITION OF HYDROPEROXIDE INTERMEDIATES IN THE OXIDATION OF LIQUID n-DECANE

Z. K. Maizus, Corresponding Member Akad. Sci. USSR
N. M. Émanuél, and V. N. Yakovleva

Chemical Physics Institute, Academy of Sciences USSR
Translated from Doklady Akademii Nauk SSSR, Vol. 131, No. 2, pp. 351-353, March, 1960
Original article submitted December 14, 1959

While studying the oxidation of n-decane, we proved that the over-all decomposition rate of hydroperoxide intermediates practically coincides with the formation rate of oxidation products [1]. This indicates that hydroperoxides constitute the sole primary intermediates in the liquid-phase oxidation of n-decane. Now that the first step in the complex oxidation of saturated hydrocarbons has been elucidated, the mechanism of hydroperoxide decomposition and the formation of final oxidation products have to be investigated.

While studying the decomposition of hydroperoxides in the absence of oxygen (i.e., under conditions where fresh hydroperoxides could not be formed), we made several observations which attested to the complexity of this reaction. On the basis of these observations, one could safely conclude that the free radicals formed when the O-O bonds in hydroperoxides are broken induce a chain decomposition of hydroperoxides [2-4]. The experimentally measured decomposition rate of hydroperoxides was regarded as representing the over-all rate of two reactions: a monomolecular and a chain reaction.

In order to prove that the n-decyl hydroperoxides formed from n-decane do indeed undergo a chain decomposition and to get a quantitative relationship between the molecular and chain decomposition routes, we used the method whereby induced hydroperoxide decomposition is suppressed by the addition of inhibitors. This technique has been widely used in studying the relationship between the decomposition rate and the structure of substituted benzoyl peroxides [5], in the oxidation of cyclohexane [6], etc.

The inhibitor, in our case α-naphthol, was introduced into n-decane while the latter was undergoing oxidation in a stream of oxygen at 130°. The inhibitor was introduced at various stages of the reaction. The kinetic curve for the formation of hydroperoxides (Fig. 1, 1) shows a sharp break when α-naphthol is introduced, which is due to the fact that the inhibitor breaks the chain in the formation of hydroperoxides. After the inhibitor is introduced, the concentration of hydroperoxides does not remain constant, as would have been the case if the decomposition proceeded solely by a chain route; instead, appreciable decline in the concentration of hydroperoxides is observed. Consequently, the decomposition of hydroperoxides proceeds partially without involving free radicals, namely by a non-chain route. The specific rate of the non-chain reaction does not depend on the intial concentration of hydroperoxides and is also independent of any other oxidation products present in the system. In fact, regardless of the time at which α-naphthol was introduced, the resulting decomposition rate constant remained the same, $k = 1.7 \times 10^{-3}$ min^{-1} (see Fig. 1, curves 2, 3, and 4). Consequently the specific rate of the non-chain decomposition of hydroperoxides, measured by the inhibitor method, represents the specific rate of the first step in the decomposition of hydroperoxides to radicals.

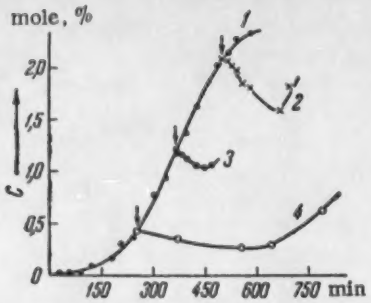

Fig. 1. Kinetic curves for the oxidation of n-decane at 130°; the concentration of hydroperoxides: 1) In the absence of inhibitors; 2, 3, and 4) in the presence of α-naphthol. Arrows indicate the time at which α-naphthol was introduced

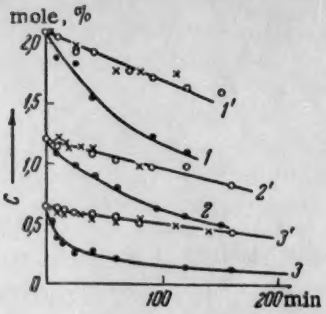

Fig. 2. Decomposition kinetics of n-decyl hydroperoxides in n-decane at 130° (under nitrogen): 1, 2, and 3) with no inhibitor present; 1', 2', and 3') in the presence of α-naphthol. The crosses on curves 1', 2', and 3' denote concentrations of hydroperoxides in experiments where the decomposition was studied in an atmosphere of O_2 (in the presence of α-naphthol).

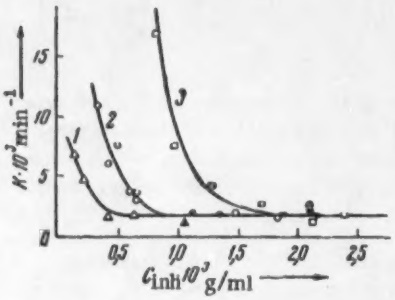

Fig. 3. The specific decomposition rate of n-decyl hydroperoxides in n-decane at 130° under nitrogen as a function of inhibitor concentration. The concentration of hydroperoxides: 1) 0.63%; 2) 1.21%; 3) 2.1%. The cross-hatched points represent similar experiments under O_2.

Since the absolute rate constant of a non-chain decomposition of hydroperoxides is much smaller than the over-all specific decomposition rate determined before [1], it is imperative to compare the decomposition of hydroperoxides in the presence of inhibitors with decomposition under conditions where there is no interference with the chain reaction.

To do this, we carried out two parallel experiments by stopping the flow of oxygen at the same initial concentration of hydroperoxides and measuring the rate of hydroperoxide decomposition (in an atmosphere of nitrogen), in the presence of inhibitors in one case and without inhibitors in another. The kinetic curves plotted in Fig. 2, show that the addition of inhibitors retards the decomposition of hydroperoxides, hence, under the ordinary conditions of n-hexane decomposition, some of the decomposition of hydroperoxides must be induced by free radicals.

On the basis of these data, a mechanism can be postulated for the inhibition. In studying the inhibition of oxidation reactions, it is customary to assume that the naphthols react with RO_2 radicals, which in this case propagate the chain reaction. However, when hydroperoxides undergo decomposition in a nitrogen atmosphere there are no RO_2 radicals produced. Consequently, α-naphthol does not react exclusively with RO_2 radicals but also with other free radicals, such as RO radicals, formed in the decomposition of hydroperoxides.

The ratio between the chain and non-chain decomposition rates of n-decyl hydroperoxides does not remain constant during the oxidation of n-decane. Instead it changes with the over-all rate of hydroperoxide decomposition and the extent of oxidation. The chain length in the decomposition of hydroperoxides provides a quantitative measure of this ratio; by starting from the same initial concentration of hydroperoxides and comparing the specific rates of inhibited (in the presence of α-naphthol) and uninhibited decompositions, we can in turn compute the chain length. Using this method we found that the chain length in the decomposition of n-decyl hydroperoxides (at 130° in n-decane) changes from 20 members at the start of the reaction (hydroperoxide concentration 0.6%) to 3 members when the concentration of hydroperoxides reaches 2.1%. In Fig. 2 we have also presented

the results obtained from similar non-chain decompositions of n-decyl hydroperoxides (in n-decane) but carried out in the presence of oxygen; these results fully coincide with those obtained under nitrogen. This indicates that the presence of oxygen has no effect on the non-chain decomposition of hydroperoxides. The measured rate constants for the decomposition of n-decyl hydroperoxides are plotted in Fig. 3 as a function of the inhibitor concentration. When the α-naphthol concentration is increased, the specific decomposition rate of hydroperoxides (under nitrogen) at first decreases sharply, then above a certain concentration of the inhibitor becomes constant. The lower the initial concentration of the hydroperoxides, the sooner the curve levels off. The specific rate in the presence of excess inhibitor measures only the non-chain decomposition of hydroperoxides and should therefore be independent of experimental conditions. Similar experiments done under oxygen (black dots in Fig. 3) yield the same limiting rate constant for the decomposition of hydroperoxides.

The absolute rate constant for the non-chain decomposition of hydroperoxides varied from 1.7 to 1.9 × × 10^{-3} min^{-1} in different experiments and was close to the rate constant for the chain branching in the oxidation of n-decane, $k = 1.1 \times 10^{-3}$ [7].

The slight difference between the two constants could indicate that the non-chain decomposition of hydroperoxides to radicals is accompanied by a molecular decomposition to give ketones and water. To verify this hypothesis, we conducted special experiments in which the n-decyl hydroperoxides were isolated from oxidized n-decane (for the method see [8]) and their decomposition in the presence of α-naphthol investigated. No ketones were found among the products of this reaction. It seems that the slightly smaller specific rate of chain branching may be attributed to the so-called "cage effect". It is very probable that a small portion of the R radicals, formed from a reaction between RO radicals, formed from a reaction between RO radicals and the solvent, react with the OH radical without leaving the "cage"

That the RO radicals are formed in the non-chain decomposition of hydroperoxides was also confirmed in experiments where the decomposition of n-decyl hydroperoxides was inhibited by phenol (8.5×10^{-8} moles/liter) and the concentration of alcohols among the reaction products was measured. Under these conditions the kinetic curves for the consumption of hydroperoxides and the formation of alcohol were in complete agreement, or in other words all of the alcohol was formed from the hydroperoxides through subsequent reactions of the RO radicals, as can be seen below:

Time from the start of experiment, min:	45	70	110	200	260
Amount of hydroperoxide decomposed, mole %	0.1	0.24	0.40	0.61	0.96
Amount of alcohol formed, mole, %	0.1	0.26	0.38	0.64	0.94

Thus one may safely conclude that the chain-branching in the oxidation of n-decane represents a non-chain decomposition of n-decyl hydroperoxides into free radicals, one of which is RO.

LITERATURE CITED

[1] L. S. Vartanyan, Z. K. Maizus, and N. M. Émanuél, Zhur. Fiz. Khim. 30, 856 (1956).

[2] J. W. L. Fordham and H. L. Williams, Canad. J. Res. 27B, 943 (1949).

[3] G. H. Twigg, Disc. Farad. Soc. 14, 240 (1953).

[4] V. Stannett and R. B. Mesrobian, J. Am. Chem. Soc. 72, 4125 (1950).

[5] C. G. Swain, W. H. Stockmayer, and J. T. Clarke, J. Am. Chem. Soc. 72, 5426 (1950).

[6] E. T. Denisov, Zhur. Fiz. Khim. 33, 1198 (1958).

[7] D. G. Knorre, Z. K. Maizus, and N. M. Émanuél, Dokl. Akad. Nauk SSSR 123, 123 (1958).•

[8] Z. K. Maizus, L. G. Privalova, and N. M. Émanuél, Coll. Liquid-Phase Oxidation of Hydrocarbons [in Russian] (Izd. AN SSSR, 1959).

• Original Russian pagination. See C. B. Translation.

A TRACER STUDY OF THE ACTIVATION MECHANISM OF CHLORIDES

V. P. Maksimchuk and I. L. Rosenfel'd

Physical Chemistry Institute, Academy of Sciences USSR
(Presented by Academician A. N. Frumkin November 21, 1959)
Translated from Doklady Akademii Nauk SSSR, Vol. 131, No. 2, pp. 354-356, March, 1960
Original article submitted November 5, 1959

The chloride ion is one of the most active anions and is capable of reactivating a great number of passive metals. The activation mechanism has not as yet been concretely established, but two theories are currently available: the film theory [1, 2] and the adsorption theory [3-5].

In one of our papers [6] we established that the activation of stainless steel by chloride ions can be entirely suppressed not only with typical oxidizing agents, but also with sulfate ions. Attempts to interpret these results from the standpoint of the film theory ran into considerable difficulties, and we therefore suggested that the processes taking place on the surface of alloys in the presence of anions may involve adsorption. The passivity of the alloy surface should then depend on the predominantly adsorbed anions.

To confirm this interpretation, we determined the adsorption of chloride ions by using a radioactive tracer (Cl^{36}) with a half-life of 4×10^5 years and a specific activity of 0.058 mC/g. The amount of NaCl adsorbed was determined by measuring the activity change in a 0.01 N NaCl solution, removing aliquots before and after adsorption. To make the changes of NaCl concentration large, we utilized a porous electrode with a large surface (about 10^4 cm^2) made of compressed chromium powder [7]. We were able to use a chromium electrode instead of one made of stainless steel because, as was previously demonstrated, the passivation of stainless steel by $SO_4^{=}$ ions depends chiefly on the chromium content of the steel. The adsorption was expressed in terms of the amount of chloride extracted by a sample from solution. The cathode and the anode compartments of the electrolytic cell were separated by a sintered disc to prevent any diffusion of the cathode reaction products to the anode.

The anode compartment was filled with 15 cc of a nonradioactive 0.01 N NaCl solution, into which we inserted a chromium electrode; the cathodic polarization was carried out for 30 min at -1.2 v. After that the nonradioactive solution was replaced by a radioactive NaCl solution of the same concentration. Equilibrium was established by keeping the unpolarized chromium electrode in the radioactive solution for one hour. At the end of this time the reversible electrode potential became - 0.14 v. A sample of the solution was removed, the electrode potential displaced by 100 mv in the positive direction and maintained there for 30 min; another aliquot was removed, the electrode potential increased by another 100 mv, and so on.

In Fig. 1 we have plotted the amount of chloride adsorbed as a function of the electrode potential; any one electrode was used only for four successive measurements. Before each measurement, the electrode was subjected to cathodic polarization in a nonradioactive 0.01 N NaCl solution (time 30 min, potential - 1.2 v).

It is a characteristic feature of these phenomena that, though all the experiments were carried out under identical conditions, the amounts of chloride adsorbed were different. In the first experiment, carried out on a fresh electrode (after the above-described preliminary treatment), we found that the chloride ions could only be adsorbed at large positive potentials (Fig. 1, 1), above + 1.3 v. But when after this experiment the electrode

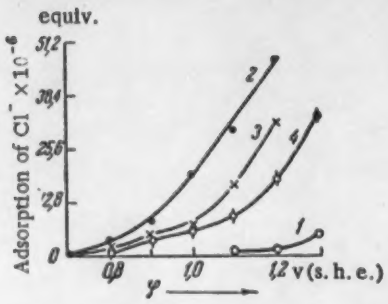

Fig. 1. The adsorption of Cl^- ion on one and the same chromium electrode. 1) During the first measurement; 2) during the second measurement; 3 and 4) during the third and fourth measurements.

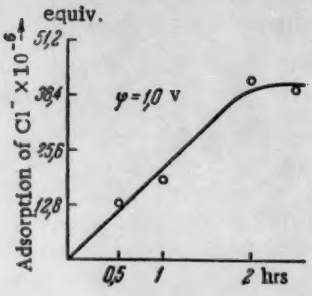

Fig. 2. The adsorption of chloride from a 0.01 N NaCl solution as a function of time, at $\varphi = 1.0$ v.

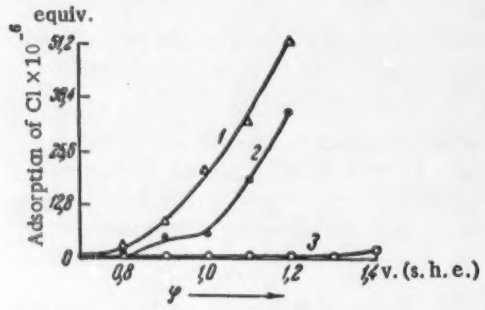

Fig. 3. The adsorption of chloride on chromium: 1) From a 0.01 N NaCl solution; 2) from a solution of 0.01 N NaCl + 0.01 N Na_2SO_4; 3) from a solution of 0.01 N NaCl + 0.1 N Na_2SO_4.

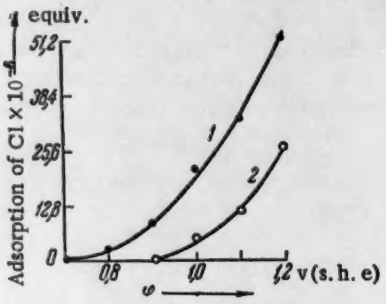

Fig. 4. The adsorption of chloride on chromium: 1) From 0.01 N NaCl; 2) from a solution of 0.01N NaCl + 0.002N NaOh. A) Adsorption of $Cl^- \times 10^{-6}$.

was subjected anew to cathodic polarization and the experiment repeated in a fresh radioactive NaCl solution, the adsorption of Cl^- ions was greatly increased and became measurable at + 0.8 v instead of at + 1.3 v. Thus during the first measurement the surface seems to undergo a type of "activation", as if some type of a barrier hindering the adsorption of chloride ions on chromium is lowered. The adsorptions observed in the second experiment are the maximum values for all potentials. During subsequent experiments (Fig. 1, Curves 3 and 4) the amount of chloride adsorbed declined. This decline may be explained by the fact that the chloride ions irreversibly adsorbed during preceding measurements interfere with any further adsorption of Cl^-.

That the chloride ions are adsorbed irreversibly on chromium is directly apparent from the fact that no desorption can be achieved even after prolonged cathodic polarization at - 1.2 v. The fact that successive data obtained on any one electrode were inconsistent forced us to use a fresh electrode for each measurement; every electrode was first "activated" at + 1.3 v for 20 min in a 0.01 N solution of nonradioactive NaCl, then subjected to cathodic polarization and the rest of the treatment already described.

In Fig. 2 we have shown the change in chloride adsorption with time at a constant potential of 1.0 v. One can see that the number of anions adsorbed increases steadily for the first 2 hours, then saturation ensues and the curve practically levels off.

Figure 3 shows the amount of chloride ion adsorbed from NaCl solutions containing various concentrations of Na_2SO_4 as a function of the chromium electrode potential. Curve 1 represents the adsorption of Cl^- from pure 0.01 N NaCl and coincides with Curve 2 in Fig. 1. Much less chloride is adsorbed from a solution of 0.01 N

NaCl + 0.01 N Na_2SO_4 (Fig. 3 Curve 2) than from pure 0.01 N NaCl. Besides, the potential at which chloride adsorption becomes noticeable is somewhat displaced in the positive direction.

When enough Na_2SO_4 is added to satisfy the condition $C_{Na_2SO_4} : C_{NaCl} \geq 10$, there is no measurable chloride adsorption even at high positive potentials (Fig. 3, 3).

Figure 4 shows the effects of hydroxyl ions on the adsorption of Cl^- ions from NaCl solutions. It should be noted that OH^- ions interfere much more effectively with the adsorption of Cl^- ions than do sulfate ions. Thus both $SO_4^=$ and OH^- ions can prevent the adsorption of chloride on chromium. At the same time both of these ions are known to inhibit the pitting of stainless steel containing alloyed chromium. The obvious conclusion is that the above-mentioned anions hinder the adsorption of chloride ions on the surface of chromium or solid Fe + Cr solutions and by the same token suppress the pitting of stainless steel.

One can therefore conclude that the chemisorption of Cl^- on the metal surface constitutes the first step in the activation process. If the chemisorption of chloride ions is prevented by adding sufficient amounts of extraneous ions, such as $SO_4^=$ or OH^-, to the NaCl solution, the activating effect of Cl^- will be suppressed, and consequently the cause of corrosion will be eliminated.

The irreversible adsorption of chloride ions, demonstrated in our experiments, raises some doubts as to the correctness of the hypothesis proposed by certain workers [2] to explain the reactivation of passive metals by chloride ions.

The data presented above are not in variance with the adsorption theory of chloride activity [3, 4].

LITERATURE CITED

[1] U. R. Evans, Corrosion, Passivity, and Protection of Metals [Russian translation] (1941) p. 99.

[2] T. P. Hoar and U. R. Evans, J. Chem. Soc. 1932, 2476.

[3] B. V. Ershler, Zhur. Fiz. Khim. 18, 131 (1944); Trans. 2nd Confer. on Metal Corrosion [in Russian] (1943) p. 52.

[4] L. V. Vanyukova and B. N. Kabanov, Zhur. Fiz. Khim. 28, 1025 (1954).

[5] H. H. Uhlig, J. Electrochem. Soc. 97, 11, 215 (1950).

[6] I. L. Rozenfel'd and V. P. Maksimchuk, Dokl. Akad. Nauk SSSR 119, 986 (1958).*

[7] S. V. Trachuk and N. N. Voronin, Zhur. Fiz. Khim. 32, 201 (1958).

*Original Russian pagination. See C. B. Translation.

THE ROLE OF CHEMICAL REACTIONS IN THERMIONIC EMISSION

G. M. Panchenkov and A M. Kolchin

M. V. Lomonosov Moscow State University

(Presented by Academician A. V. Topchiev November 21, 1959)
Translated from Doklady Akademii Nauk SSSR, Vol. 131, No. 2, pp. 375 -359,
March, 1960
Original article submitted November 4, 1959

Natural and synthetic ion emitters are used frequently in mass spectrometry as sources of ionic beams, and yet the phenomena accompanying emission are not, as yet, fully understood. It seems that M. A. Eremeev and co-workers were the first [1, 2] to attempt an investigation of the thermionic emission mechanism. While studying the effects of electrical fields on the emission of alkali ions from aluminosilicates, they found that the emitting power did not correspond to the ionic mobility.

Subsequently we reported [3] on the role of diffusion processes in the emission of cesium ions from aluminosilicates. We showed that in thin emitter layers (less than 0.1 mm thick), at relatively low temperatures (500-800°) and high concentrations, diffusion does not constitute the rate-determining process. In the present communication we are presenting the results of some additional work on the mechanism of thermionic emission; we studied the interaction between the emitter and the metallic backing (the heater). An aluminosilicate ion-exchanger of the composition $Al_2O_3 \cdot 4SiO_2 \cdot XH_2O$ treated with a cesium chloride solution was used as emitter. The work was done in a MS-4 model mass spectrometer. We discovered that the emitter failed to emit any ions when placed on a platinum backing, whereas the use of tantalum backing resulted in a considerable ionic current of Cs^+. When however, the platinum backing was used with an emitter to which some tantalum powder had previously been added, an ionic current was detected of the same order of magnitude as that obtained with a tantalum backing.

We therefore set up a series of experiments to study the relationship between the ionic current and the chemical activity of the powdered metal added to the emitter. Our backing consisted of a platinum ribbon which had been washed with ethyl alcohol and water, then baked out in the mass spectrometer until all the alkali metal impurities present in platinum were "boiled out". The temperature was measured by welding a 0.1 mm platinum–platinum-rhodium thermocouple to the heater. The emitter was mixed with the metal powder and deposited on the central portion of the backing. The appearance of a cesium ion current was observed at about 500°C. In all of the experiments, the work function was checked by the temperature dependence of the emission current. The "activation energies" for the emission of Cs^+ turned out to be identical (2.70 ± 0.06 ev), within the limits of experimental errors. The effects of copper, tungsten, tantalum, zirconium, and aluminum powders, and of powdered graphite, on the emission of Cs^+ were studied. It turned out that the ion-current increased with increasing metal activity. The addition of powdered graphite to an aluminosilicate emitter yielded an emission current of the same magnitude as that obtained with tantalum.

Apparently the emitter and the metal react to give cesium atoms, which are then ionized and emitted. The possibility of such a reaction was already pointed out by Kunsman [4].

It should be noted that certain platinum samples which had seen previous use (for example, such as have been exposed to the flame of a gas burner) contain some impurities (most frequently carbon) which may react

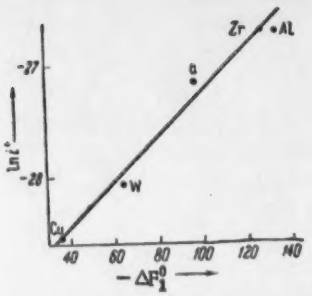

Fig. 1. The logarithm of the Cs^+ ionic current as a function of ΔF_1° at 655°C.

with the emitter and yield an appreciable ionic current. We also observed some carburization of platinum while working with graphite powder.

It was very interesting to see how the emitter would behave at high temperatures when mounted on a platinum heater to which no metal powders were added. Brief heating at 1500°C yielded an intense Cs^+ current. When the temperature was lowered to the normally used value (~ 600°C), the ionic current became equal in magnitude to the Cs^+ current previously obtained with a tantalum backing. There is no doubt that the emission observed at lower temperatures after such an activation comes from the products formed by a thermal dissociation of the emitter.

It was also interesting to study the effects of oxidizing agents on emission. We used for this purpose a tantalum heater (backing) to which a platinum–platinum-rhodium thermocouple was welded. We first deposited on the backing an emitter which, when heated, emitted Cs^+ ions (a 1.5×10^{-11} amp ionic current). After this control experiment the old emitter was removed from the backing and replaced by a new one to which manganese dioxide (MnO_2) had been added. When heated to the same temperature, the new emitter yielded an ionic current of Cs^+, which was only one fortieth the previous current (4×10^{-13} amp) but gradually increased by a factor of 2.5 (to 10^{-12} amp) after 20 min. This experiment provides additional evidence that chemical reactions occur during emission; the oxidizing agent shifts the reduction equilibrium in the reverse direction, decreasing the concentration of cesium ions. The subsequent increase of current seems to be connected with a loss of manganese dioxide from the emitting layer.

To correlate all of our data, it was necessary to compute the free energy for the reaction $CsOR + \frac{x}{y} Me \rightleftharpoons Cs + \frac{1}{y} Me_xO_y + R$, where R is the aluminosilicate lattice. Due to the lack of thermodynamic constants for CsOR and R, we failed to obtain a complete set of such calculations. However, for reactions which differ only in the chemical nature of Me and Me_xO_y, it is possible to compute ΔF_t° with a fair degree of accuracy and avoid these difficulties.

If ΔF_t° is represented as:

$$\Delta F_t^0 = \Delta F_{Cs}^0 + \Delta F_R^0 + \frac{1}{y} \Delta F_{Me_xO_y}^0 - \Delta F_{CsOR}^0 - \frac{x}{y} \Delta F_{Me}^0,$$

then in all of the examined reactions

$$\Delta F_{Cs}^0 + \Delta F_R^0 - \Delta F_{CsOR}^0 = \Delta F_2^0$$

is a constant.

In this manner the problem is substantially simplified and is reduced to the determination of

$$\Delta F_1^0 = \frac{1}{y} \Delta F_{Me_xO_y}^0 - \frac{x}{y} \Delta F_{Me}^0.$$

The ΔF_1° was calculated for the following reactions:

$$Cu \rightarrow Cu_2O; \quad W \rightarrow WO_2; \quad Ta \rightarrow Ta_2O_5; \quad Al \rightarrow Al_2O_3; \quad Zr \rightarrow ZrO_2.$$

We used in our calculations the thermodynamic constants listed in [5].

In Fig. 1 we have plotted the logarithm of the ionic current observed by us at 655° as a function of ΔF_1°. It is quite clear that the logarithm is a linear function of ΔF_1°; consequently, the ionic current must be a linear function of the equilibrium constant for the corresponding reaction, which proves that the indicated reactions really take place.

Thus, on the basis of the experimental data presented above, one can assert that at relatively low temperatures, high cesium concentrations, and thin emitter layers, the emission is primarily controlled by the formation of cesium atoms in a chemical reaction with the backing and their subsequent ionization from the surface.

The authors wish to express their deep gratitude to Z. F. Kolchina for the assistance rendered during this work.

LITERATURE CITED

[1] M. A. Eremeev and L. Kh. Ash, Zhur. Teoret. Fiz. 23, 435 (1953).

[2] M. A. Eremeev and A. Yur'eva, Zhur. Teoret. Fiz. 23, 430 (1953).

[3] G. M. Panchenkov, A. M. Kolchin, and P. A. Akishin, Fiz. Tverd. Tela 1, 918 (1959).•

[4] C. H. Kunsman, Proc. Nat. Acad. Sci. USA, 12, 659 (1926); Science, 62, 269 (1925); J. Frankl. Inst. 203, 635 (1927).

[5] O. Kubashewsky and E. Evans, Metallurgical Thermochemistry [Russian translation] (IL, 1954).

•Original Russian pagination. See English translation.

THE EFFECTS OF EXTERNAL RADIATION ON THE ISOTOPIC EXCHANGE OF SULFUR IN THE $K_2\overset{\times}{S}O_4 - SO_3$ SYSTEM AT HIGH TEMPERATURE

Academician Vic. I. Spitsyn, I. E. Mikhailenko, I. V. Vereshchinskii, and P. Ya. Glazunov

Physical Chemistry Institute, Academy of Sciences USSR
Translated from Doklady Akademii Nauk, Vol. 131, No. 2, pp. 360-363, March, 1960
Original article submitted December 10, 1959

V. I. Spitsyn and I. E. Mikhailenko already proved [1, 2] that the specific radioactivity of potassium sulfate containing S^{35} greatly influences the isotopic exchange of sulfur in the $K_2\overset{\times}{S}O_{4(s)}-SO_{3(g)}$ system at 840°C. It was therefore important to find out what role radiation effects induced in the gas phase on the surface of the exchanging salt by β-radiation play in the exchange. With this in mind, we studied the isotopic exchange at a low potassium sulfate activity but under conditions where the labelled K_2SO_4 sample and the SO_3 vapor were exposed to external radiation in the form of an electron beam from a betatron, which was so designed as to permit the bombardment of an outside target by the electrons [3]. A schematic representation of the apparatus used by us is shown in Fig. 1.

The apparatus was set up on a movable stand and placed, together with the betatron, in an insulated compartment which had concrete walls to provide radiation shielding. A special panel was used for the remote control of all instruments. The required amount of SO_3 was distilled out of 60% oleum into a calibrated test tube before the experiment. The current of dry air circulating through the apparatus and later used to carry SO_3 vapor was turned on before beginning the experiment. The sulfur trioxide was evaporated evenly and at a fixed rate by sliding a movable heater automatically down the calibrated test tube. The working tube and the dish used for weighing the $K_2\overset{\times}{S}O_4$ were both made of quartz. The heating element in the oven consisted of a thin nichrome tape wrapped around the quartz reaction tube. Using a remote automatic control system [4], we maintained the experimental temperature constant to within ± 3°C. Through the mantle and the asbestos thermal insulator around the oven, we cut a narrow slit (9 × 70 mm) which exposed the quartz tube and the dish inside to a 5 Mev electron beam. The stability of the betraton beam was controlled by means of an ionization chamber–recorder. The experiment was followed visually on a television attachment.

The $K_2\overset{\times}{S}O_4$ sample used for the investigation of isotopic exchange had a specific activity of 4.6×10^{-2} mC/g. The experimental conditions were similar to those described before [1]. Two modifications of electron bombardment were used: 1) the $K_2\overset{\times}{S}O_4$ and the surrounding gas irradiated simultaneously, and 2) only the gas irradiated before entering the oven (18 cm long working quartz tube). In the latter case the slit was covered with a lead shield.

The radiation dosage received by the potassium sulfate was determined by means of ferrous sulfate dosimetry. We used a 2.3×10^{-3} M solution of Mohr salt in 0.8 N H_2SO_4; the Fe^{+++} concentration was determined spectrophotometrically from the absorption at 304 mμ. The volume of the dosimetric solution poured into the quartz dish was close to that occupied by potassium sulfate.

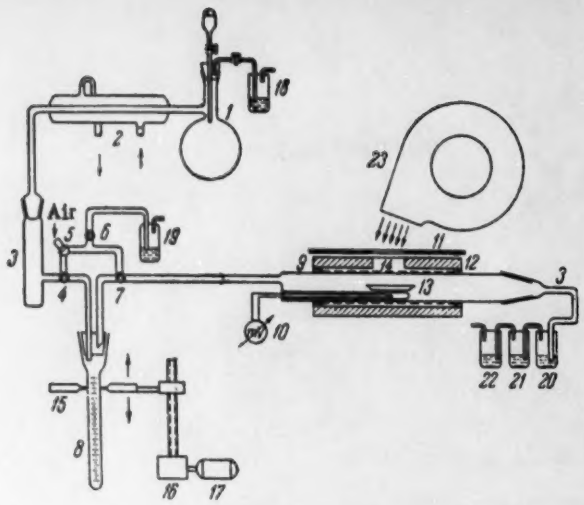

Fig. 1. Schematic representation of the apparatus used for the study of the high temperature isotopic exchange under electron bombardment. 1) Round-bottom flask containing the oleum; 2) condenser; 3) receiver for SO_3; 4, 5, and 7) three-way stopcocks; 6) two-way stopcock; 8) calibrated test tube; 9) quartz reaction tube; 10) millivolt meter with a platinum–platinum-rhodium thermocouple; 11) lead shield; 12) asbestos thermal insulator; 13) quartz dish; 14) oven slit; 15) heating element; 16) reducing gear; 17) Warren motor; 18, 19, 20, 21, and 22) wash bottles containing concentrated H_2SO_4; 23) betatron chamber.

TABLE 1

Calculated Examples of Electron Radiation Dosages Absorbed by Potassium Sulfate and the Gas Involved in Exchange (a mixture of air and SO_3 vapor, $P_{SO_3} = 19$ mm).

The dosage received by the ferrous sulfate solution in 10 min, ev/ml	Material investigated				Dosage received in 10 min, ev.		
	irradiated compound	density g/cm³	$\frac{D_e}{D_e\ (H_2O)}$	irradiated volume, ml	by a K_2SO_4 sample	SO_3	
						stationary	in an air-stream
$8{,}0\cdot10^{17}$	K_2SO_4	1,13	8,6	0,35	$2{,}8\cdot10^{16}$	$4{,}7\cdot10^{15}$	$1{,}1\cdot10^{15}$
$2{,}3\cdot10^{16}$	SO_3	$3{,}6\cdot10^{-3}$	4	14			

The dosage absorbed by the gas was determined by replacing the working tube with a special cell in which the experimental conditions were reproduced. In our calculations we assumed that the scattering and secondary adsorption of electrons by the dosimetric solution were no different from the same phenomena in the case of solid potassium sulfate or gaseous SO_3, and we also neglected any possible energy exchange between air and SO_3. In determining the integral dosage absorbed by the irradiated samples, we allowed for their specific gravities and volumes, as well as for the ratios of their electron densities to that of water $D_e/D_e(H_2O)$. The calculated dosages are presented in Table 1.

The isotopic exchange was studied at various dose intensities with 4 to 12 experiments per dosage. In no case was any radiochemical decomposition of potassium sulfate detected.

TABLE 2

Changes in the Activity of K_2SO_4 Observed During the Investigation of the Isotopic Sulfur Exchange in the $K_2SO_4-SO_3$ System Exposed to Electron Bombardment (0.58 g of SO_3 passed through)

Dosage received in 10 min, ev	Material irradiated	Weight of K_2SO_4, g	K_2SO_4 wt. after expt., g	Weight difference		Initial activity, counts/min	K_2SO_4 activity after the expt.		Percent exchange	
				g	%		counts/min	in % of initial	%	average
$1,1 \cdot 10^{17}$	Salt and vapor	0.3506	0.3513	+0.0007	+0.2	$1043 \cdot 10^3$	$7610 \cdot 10^2$	72.9	34.6	
		0.3950	0.3959	+0.0009	+0.2	$1176 \cdot 10^3$	$8628 \cdot 10^2$	73.4	33.2	33,6
		0.3474	0.3470	—0.0004	—0.1	$1034 \cdot 10^3$	$7518 \cdot 10^2$	72.7	32.7	
		0.3575	0.3582	+0.0007	+0.2	$1064 \cdot 10^3$	$7839 \cdot 10^2$	73.7	33.8	
$1,06 \cdot 10^{18}$	Vapor	0.3845	0.3849	+0.0004	+0.1	$1481 \cdot 10^3$	$1277 \cdot 10^3$	86.3	18.0	
		0.4326	0.4330	+0.0004	+0.1	$1668 \cdot 10^3$	$1407 \cdot 10^3$	84.3	21.0	
		0.4503	0.4508	+0.0005	+0.1	$1736 \cdot 10^3$	$1447 \cdot 10^3$	83.4	22.6	20,5
		0.3724	0.3728	+0.0004	+0.1	$1437 \cdot 10^3$	$1208 \cdot 10^3$	84.2	20.5	

TABLE 3

The Effects of Electron Bombardment on the Percent Isotopic Exchange in the $K_2\overset{x}{S}O_4-SO_3$ System (temperature 840°, length of experiment 10 min, $K_2\overset{x}{S}O_4$ weights 0.35-0.45, SO_3 0.58 g, gas stream velocity 37 liters/hr, P_{SO_3} 19 mm)

Expt. series	Dose intensity recorded by the $FeSO_4$ solution, ev/ml, sec	Dosage received in 10 min, ev	Materials investigated	No. of expts.	Percent exchange, average
1	Without bombardment	—	—	4	14,4
2	$1,8 \cdot 10^{13}$	$3,4 \cdot 10^{15}$	Salt and vapor	4	14 7
3	$1,3 \cdot 10^{14}$	$2,8 \cdot 10^{16}$	Salt and vapor	12	28,7
4	$5,1 \cdot 10^{14}$	$1,1 \cdot 10^{17}$	Salt and vapor	10	33,7
5	$3,9 \cdot 10^{13}$	$1,1 \cdot 10^{18}$	Vapor	4	20,5
6	$7,4 \cdot 10^{13}$	$2,1 \cdot 10^{18}$	Vapor	8	20,3

In Table 2 we have presented some examples of potassium sulfate activity changes observed during the investigation of isotopic exchange under bombardment. The averaged results of all the experiments are compiled in Table 3.

The data presented above indicate that the bombardment of the solid phase in the $K_2SO_4-SO_3$ system by electrons has practically no effect on the exchange rate when the dosage is of the order of 10^{15} ev/10 min. When the radiation dosage is increased to 10^{16}-10^{17} ev, the percent exchange increases and becomes directly proportional to the logarithm of the dosage (Fig. 2).

It should be noted that the equivalent β-radiation from the samples of radioactive K_2SO_4 has a much greater effect on the exchange rate. For example, an electron radiation dosage of 3.4×10^{15} ev/10 min received by solid potassium sulfate (Table 3, 2nd set of experiments) would correspond to a specific radioactivity of 2.3 mC/g (in these calculations we considered the number of β-particles emitted by the sample during 10 min; effects accumulated before the start of the experiment [5] were not considered). The above-mentioned radioactive sample underwent a 66.9% exchange [2] and was exchanging 2.5-3 times faster than $K_2\overset{x}{S}O_4$ of low activity. Under similar conditions no such effect was observed when an equivalent external radiation source was used.

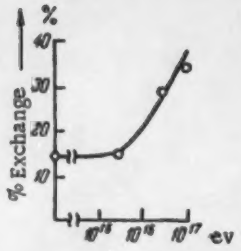

Fig. 2. The percent exchange of sulfur in the $K_2\overset{x}{S}O_{4(s)}-SO_{3(g)}$ system as a function of the integral dosage received from the electron beam (within 10 min).

It seems that the electrons bombarding the surface of the labelled potassium sulfate excite the $SO_4^{=}$ ions and individual atoms in the existing active exchange centers.

SO_3 vapor also becomes activated by electron radiation (Table 3, 5th and 6th set of experiments). Here evidently SO_3 and SO_2 ions of different charges are formed. However, these effects are relatively weak: the exchange is increased by bombardment by about 40%, but, within the range of radiation dosages $1\text{-}2 \times 10^{13}$ ev/10 min, it remains practically constant.

LITERATURE CITED

[1] Vic. I. Spitsyn and I. E. Mikhailenko, Dokl. Akad. Nauk SSSR 121, 319 (1958).•

[2] I. E. Mikhailenko and Vic. I. Spitsyn, Dokl. Akad. Nauk SSSR 131, 1 (1960).•

[3] B. A. Kononov, Izv. Tomsk. Politekh. inst. im. S. M. Krylova 87, 322 (1957).

[4] A. P. Rudenko, Remote Automatic Temperature Control Systems for Electric Ovens [in Russian] (Moscow, 1958).

[5] Vic. I. Spitsyn, Izv. Akad. Nauk SSSR, Otdel Khim. Nauk 11,1296 (1958).

•Original Russian pagination. See C. B. Translation.

THE MECHANISM OF PREDETONATION PROPAGATION OF FLAME IN ROUGH TUBES

V. S. Babkin and L. S. Kozachenko

Chemical Kinetics and Combustion Institute, Siberian Section, Academy of Sciences, USSR
(Presented by Academician S. A. Khristianovich, November 27, 1959)
Translated from Doklady Akademii Nauk SSSR, Vol. 131, No. 3, pp. 591-592,
March, 1960
Original article submitted November 16, 1959

A large number of papers have been devoted to the problem of the initiation of detonation in rough tubes [1-5]. These works have examined problems regarding the reasons for flame acceleration, the specific mechanism of the acceleration, and the influence of various factors (the degree of roughness, composition of the mixture, and initial pressure) on the initiation of detonation.

The aim of the present work was to study the mechanism of combustion and to examine the structure of accelerating flames in the predetonation period in rough tube conditions, in which the mechanism of detonation propagation involves adiabatic ignition of the gas from compression in the detonation wave.

In our experiments we used a half-closed tube of length 900 mm, with hydraulic resistance $\lambda = 0.08$. The roughness was produced by sticking brass turnings, of average size $2 \times 1.5 \times 0.5$ mm, to two opposite sides of the 20×20 mm square channel. The two other sides of the channel consisted of the smooth surfaces of optical glasses, through which half-shadow still photographs were taken on a moving film to produce a relative section of the moving flames and shock waves. The combustion mixture (H_2 + air, normal and enriched with oxygen up to 28.7%) was fed into the closed end of the tube and ignited there by means of a weak electric spark.

The experiments gave a picture of the development of combustion in the predetonation period and showed that it is possible to distinguish three successive stages in this process.

The first stage is the short-lived propagation of the laminar flame after ignition of the mixture. In the second stage the combustion takes place in a turbulent stream, and the flame front is greatly distorted and drawn slightly forward. The source of ignition of the mixture in this case is provided by the flame centers which move furthest forward. In these stages the flames are analogous to the flames in smooth tubes: photographs of the latter may be found in many works, for example in [6, 7]. The third stage of predetonation combustion begins when the shock wave (Fig. 1) formed in front of the accelerating turbulent flame reaches a definite intensity. In this stage combustion proceeds in a complex formed by the shock wave and the turbulent flame. Ignition of the mixture now takes place at the rough walls close to the wave front. The flame is propagated from the walls to the center of the tube, producing a conical forward surface behind which lies the turbulent combustion zone in the form of a burning coil.*

Figure 2 gives nine stills showing the propagation of combustion on going from the second stage to the third. The first four stills from the left show the propagation of the turbulent wave, with a slight hemispherical

*An analogous combustion mechanism has been considered for the case of detonation in rough tubes by Ya. B. Zel'dovich [8] and for smooth tubes by M. A. Rivin [9].

Fig. 1. Shock wave in front of the turbulent wave front in a rough tube.

Fig. 2. The production of a combustion mechanism involving ignition at the tube walls in a mixture of 25% H_2 + 21.5% O_2 + 53.5% N_2.

surface following the shock wave. The fifth and subsequent stills show the combustion in the third stage in the form of the complex, with ignition at the rough walls.

The further development of the complex is characterized by an increase in its velocity and an increase in the length of the burning coil, which in some cases exceeds the tube diameter by a factor of 5 or more.

The combustion of the compressed gas takes place under conditions of a turbulent boundary layer and a system of waves reflected from the roughness on the walls. Under these conditions the long coil of the complex is unstable and undergoes a marked rotational and vibrational motion: when the complex exists for a prolonged period, this motion leads to breakdown of the coil into sections and to a decrease in the length of the complex to 1.5-2 times the diameter of the tube. Acceleration and development of the complex is completed by initiation of detonation of the front of the shock wave. The mixture in the complex gradually burns up behind its front.

Measurements were made of the velocity of the shock wave at which the complex is formed in mixtures of different composition. The results of the measurements are given in the table.

The formation of the complex takes place after not more than 30-50 μ sec. At this moment the flame is situated at a distance of 0.5-3 tube diameters from the wave front. No significant part appears to be played,

Mixture			D, m/sec	Mixture			D, m/sec
H_2, %	O_2, %	N_2, %		H_2, %	O_2, %	N_2, %	
21,75	22,45	55,8	890	40	17,2	42,8	1065
22,7	22,2	55,1	925	44,25	16	39,75	1066
24,25	21,73	54,02	930	45,85	15,53	38,62	1090
25	21,5	53,5	935	50,6	14,18	35,22	1152
30,8	19,88	49,32	990	54,15	13,15	32,7	1380

however, by the diffusion and thermal effect of the flame on the ignition of the mixture. This is confirmed by experiments in which a complex analogous to that in the predetonation period is produced when an artificial shock wave of the appropriate intensity passes from a smooth tube to a rough tube.

In conclusion it should be noted that the mechanism of predetonation propagation of flame under consideration is typical of tubes with a wide range of degrees of roughness, although each case has its own characteristic features.

LITERATURE CITED

[1] K. I. Shchelkin, Zhur. Éksper. Teor. Fiz. 10, No. 7, 823 (1940).

[2] V. Ditsent and K. I. Shchelkin, Zhur. Fiz. Khim. 19, Nos. 4-5, 221 (1945).

[3] K. I. Shchelkin, Zhur. Tekh. Fiz. 17, No. 5, 613 (1947).

[4] Ya. B. Zel'dovich, Zhur. Tekh. Fiz. 17, No. 1, 3 (1947).

[5] A. S. Sokolik, Zhur. Éksper. Teor. Fiz. 21, No. 10, 1164 (1951).

[6] U. Neubert, Zs. f. techn. Phys. 24, 8, 179 (1943).

[7] E. Schmidt, H. Steinicke, and U. Neubert, Fourth Symposium (International) on Combustion (Baltimore, 1953).

[8] Ya. B. Zel'dovich, The Theory of Combustion and Detonation of Gases [in Russian] (Moscow–Leningrad, 1944).

[9] M. A. Rivin, Dokl. Akad. Nauk SSSR, 67, 5, 875 (1949).

CERTAIN FEATURES OF THE KINETICS OF THE RADIOLYSIS OF n-HEPTANE OVER A WIDE RANGE OF DOSES

V. G. Berezkin, I. M. Kustanovich, L. S. Polak, and N. Ya. Chernyak

Oil Chemical Synthesis Institute, Academy of Sciences, USSR
(Presented by Academician A. V. Topchiev, November 18, 1959)
Translated from Doklady Akademii Nauk SSSR, Vol. 131, No. 3, pp. 593-596, March, 1960
Original article submitted November 18, 1959

A large number of studies have been devoted to the radiolysis of normal hydrocarbons [1-3]. The literature does not, however, contain any systematic examination of the yields of different radiolysis products over a wide dose range. The present work deals with this question. The radiation sources used, the method of filling and closing the ampoules with the hydrocarbon to be irradiated, the purification and degree of purity of the test substance (heptane), and the dosimetry have been described earlier [1]. The present study was carried out at a temperature of 300° K in the dose range $0.25\text{-}28 \cdot 10^{21}$ ev.

Figure 1 shows the yields of hydrogen, methane, and C_2-C_5 fraction; the yields of H_2 and CH_4 were determined by the method described earlier [1], and the method for the determination of the C_2-C_5 yields is described below. In order to reveal the nonlinearity range more clearly, the initial linear sections of the curves have been produced (dotted lines). The deviation from linearity for H_2 and CH_4 starts close to a dose of $10\text{-}12 \cdot 10^{21}$ ev.

The composition of the C_2-C_5 fraction in the products of heptane radiolysis was studied by gas–liquid chromatography. In order to increase the sensitivity and resolving power of the chromatograph for the analysis of the products of hydrocarbon radiolysis, we did not use the methods employed by other authors [3-5] but employed a stepwise arrangement involving the use of two chromatographic assemblies. In the first apparatus (stationary liquid phase–a methylphenylpolysiloxane oil), the C_2-C_5 fraction was separated from the higher radiolysis products and unreacted heptane. A detailed analysis of this fraction was carried out on the second apparatus, by the method described in [5], at 0°. The stepwise arrangement enables a detailed chromatographic analysis of the products of hydrocarbon radiolysis to be carried out after irradiation by relatively small doses. The sensitivity of the apparatus is $\sim 1 \cdot 10^{-3}$ ml gas (carrier gas–helium). The reproducibility of the measurements is ± 5%. The calibration constant for quantitative analysis was determined with an error of ± 10%.

Since all the available literature data [2, 3] on the composition of the gaseous products of hydrocarbon radiolysis were obtained by removing a sample of the irradiated product for subsequent analysis by one of various methods, and since this introduces the possibility of errors in the determination of the composition of the gas, as a result of the actual sampling process, as has already been shown [6], we carried out our experiments by irradiating the heptane in special small ampoules, the entire contents of which were then transferred to the gas–liquid chromatography apparatus by breaking the ampoules in a special inlet arrangement on the chromatograph. The data obtained are given in the table and are free from any errors associated with the removal of samples. These data relate to comparatively small integral radiation doses. In the other experiments the C_2-C_5 fraction was removed by the method described in [6].

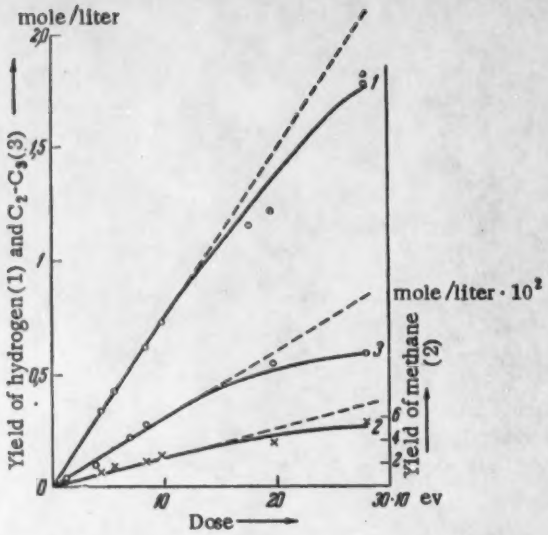

Fig. 1. Relationship between the yield of hydrogen (1), methane (2) and C_2-C_5 hydrocarbons (3) and the absorbed energy.

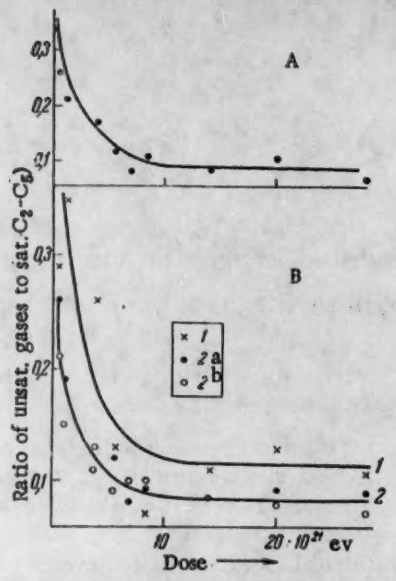

Fig. 2. A) The relationship between the ratio of unsaturated gases to saturated gases in the C_2-C_5 fraction and the absorbed energy. B) the relationship between the ratio of unsaturated hydrocarbons to the "complementary" saturated hydrocarbons and the energy absorbed: 1) C_2H_4/C_2H_{12}; 2a) C_3H_6/C_4H_{10}; 2b) α-C_4H_8/C_5H_{12}.

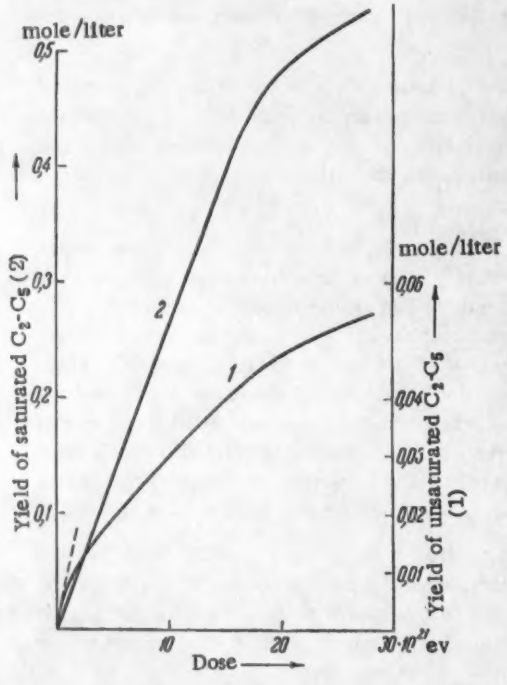

Fig. 3. Relationship between the yield of unsaturated (1) and saturated (2) C_2-C_5 hydrocarbons and the absorbed energy.

Figure 1, Curve 3, shows the yield kinetics for the products of the C_2-C_5 fraction. The deviation from linearity takes place at doses of the same order of magnitude as in the case of H_2. Examination of the ratio of unsaturated and saturated hydrocarbons in the C_2-C_5 fraction (Fig. 2) shows that, in the dose range $0.25\text{-}10 \cdot 10^{21}$ ev, the percentage of unsaturated hydrocarbons falls from ~ 35% to ~ 8%; this takes place as a result of the marked nonlinearity of the yield of unsaturated gases, which starts even at very low doses (Fig. 3).

It may be assumed that the formation of light hydrocarbons takes place by breakdown of the molecule of the original hydrocarbon to form two radicals, according to reaction (1), with the subsequent formation of saturated hydrocarbons from these radicals by recombination with H atoms or with other radicals, or by breakdown of the molecule into saturated and unsaturated fragments according to reaction (2):

$$R_{n+m}H_{2n+2m+2} \rightarrow \dot{R}_nH_{2n+1} + \dot{R}_mH_{2m+1}, \quad (1)$$

$$R_{n+m}H_{2n+2m+2} \rightarrow R_nH_{2n+2} + R_mH_{2m}. \quad (2)$$

Dose	Dose $0.5 \cdot 10^{21}$ ev/ml				Dose $1.18 \cdot 10^{21}$ ev/ml			
	yield, 10^{-4} mole/liter	quantity in C_2-C_5 fraction, %	difference $[C_nH_{2n+2}] - [C_mH_{2m}]$, $n+m=7$, %		yield, 10^{-4} mole/liter	quantity in C_2-C_5 fraction, %	difference $[C_nH_{2n+2}] - [C_mH_{2m}]$, $n+m=7$, %	
Ethane	2,12	15,9	11,3		5,98	17,1	14,4	
Pentene	0,61	4,6			0,94	2,7		
Pertane	3,10	23,3	16,2		7,75	22,2	15,3	
Ethylene	0,94	7,1		Average 14,3	2,41	6,9		Average 16,8
Propane	2,54	19,1	15,0		7,87	22,5	19,3	
Butylene	0,55	4,1			1,12	3,2		
Butane	2,70	20,3	14,7		7,49	21,4	17,4	
Propylene	0,75	5,6			1,40	4,0		
Total	13,31	100,0			34,96	100,0		

The formation of unsaturated gases at room temperature can obviously only take place according to Equation (2); the other suggested mechanism for their formation, by breakdown of alkyl radicals or their disproportionation, is less probable, since these reactions have a high activation barrier. Judging from the fact that at low doses, when the secondary processes play a smaller part, the ratio of unsaturated gases to saturated gases amounts to 0.35 (and is probably even higher at still smaller doses), it may be assumed that rupture of the C-C bond in the original hydrocarbon according to reaction (2) is at any rate not less probable than rupture according to reaction (1). If the probability of radicals produced according to reaction (1) recombining with other radicals is dependent only on their concentration, then the "complementary" saturated hydrocarbons formed in the process (C_2 and C_5, C_3 and C_4) should be obtained in equivalent quantities. Consequently, since reaction (2) also produces saturated hydrocarbons in quantities equivalent to the complementary unsaturated hydrocarbons, we should observe the following relationship:

$$[C_2H_6] - [C_5H_{10}] = [C_5H_{12}] - [C_2H_4]; \quad [C_3H_8] - [C_4H_8] = [C_4H_{10}] - [C_3H_6]. \tag{3}$$

The corresponding differences are given in Table 1. Analysis of the data in Table 1 shows that relationship (3) applies, and this provides significant confirmation for the suggested scheme. The nonlinearity of the yield of unsaturated hydrocarbons even at low doses may be explained by the fact that, since the concentration of unsaturated compounds very quickly starts to become equal to and even greater than the stationary concentration of radicals, the following reaction with H (or other radicals) becomes possible.

$$C_nH_{2n} + H \rightarrow C_nH_{2n+1}, \tag{4}$$

since the unsaturated gases still make up the greater part of the gases dissolved in the liquid phase. This reaction competes with the reaction involving recombination of H atoms with one another and with the radicals. The consumption of atomic hydrogen according to Equation (4) should lead to a breakdown of linearity in the yield of molecular hydrogen, but, since the absolute quantities of unsaturated compounds is much less than the quantity of H, in practice we observed linearity for the yield of hydrogen up to $1 \cdot 10^{22}$ ev, although, strictly speaking, nonlinearity (i.e. the existence of secondary reactions) for all products should obviously start almost from the start of the irradiation. The observed region of nonlinearity for the yields is approximate, is determined by the sensitivity of the analytical methods, and is significant only for the estimation of the dose range in which it is possible to make a reasonable determination of the radiation–chemical yields of the radiolysis products; the observed nonlinearity of the curves in Fig. 1 probably results from the protective action of the unsaturated compounds.

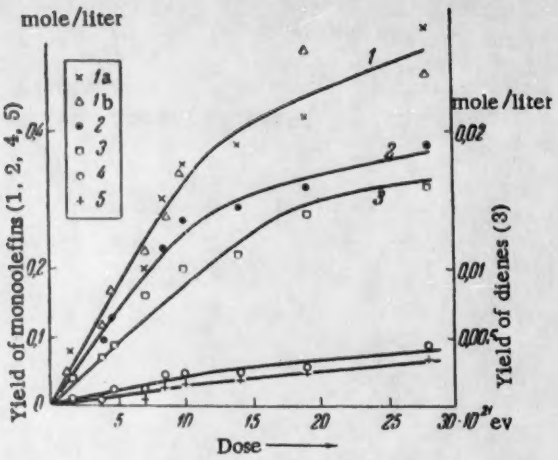

Fig. 4. Relationship between the yield of liquid unsaturated hydrocarbons and the absorbed energy: 1) olefins (total) from infrared spectral data (1a) and from the bromine numbers (1b); 2)trans-olefins; 3) dienes; 4) α-olefins; 5) vinylidene structures.

The radiation yields calculated from the linear sections of the curves for the radiolysis of heptane are (in molecules/100 ev): H_2 4.5, CH_4 0.2, saturated C_2-C_5 hydrocarbons 1.6, unsaturated C_2-C_5 hydrocarbons (calculated from the slope of the tangent at the start of the curve) ~ 0.4, and liquid unsaturated compounds 2.0.

Figure 4 shows how the yield of various liquid olefins and dienes varies with the dose. The different structures of the olefins were identified and the amounts determined from the infrared absorption spectra, using an IKS-14 spectrophotometer with NaCl prism. The spectra were recorded for a layer thickness of 0.1 mm. The greatest yield is shown by trans-olefins (ν = 865 cm^{-1}, E = 105), and much lower yields are shown by α-olefins (ν = 0.912 cm^{-1}, E = 125) and vinylidene structures (ν = 889 cm^{-1}, E = 140). The relative error in the determination of the olefins of each structure does not exceed ± 8%. The olefin content obtained by taking the sum of the concentrations of these structures shows good agreement with data obtained in the determination of the olefins by the bromine method. The concentration of dienes was determined from the absorption spectra with an ISP-28 spectrograph using a photographic method in the 2300 A range. The molar extinction coefficient was determined using heptadiene and found to be equal to 10^3. The deviation from linearity for the formation of olefins takes place at doses of 10-12 · 10^{21} ev (Fig. 4), as on the curve for H_2.

It is interesting to note that ~ 20% of the liquid unsaturated compounds (even at doses of only ~ 1 · 10^{21} ev) consists of heavy unsaturated compounds (with more than 10 carbon atoms) [7].

LITERATURE CITED

[1] L. S. Polak, A. V. Topchiev, and N. Ya. Chernyak, Dokl. Akad. Nauk SSSR 119, 2, 307 (1958);* Proceedings of the Second International Conference on the Peaceful Uses of Atomic Energy, Geneva, 1958 [in Russian] 4, 254 (Moscow, 1959).

[2] H. A. Dewhurst, J. Phys. Chem., 61, 11, 1466 (1957); 62, 1, 15 (1958).

[3] H. A. Dewhurst and E. H. Winslow, J. Chem. Phys. 26, No. 4, 969 (1957).

[4] J. M. Caffrey and A. O. Allen, J. Phys. Chem. 62, No. 1, 33 (1958).

*Original Russian pagination. See C. B. Translation.

[5] G. G. Devyatykh, A. D. Zorin, and A. E. Ezheleva, Nauchn. Doklady Vyssh. Shk., Ser. Khim. i Khim. Tekhnol., No. 4, 724 (1958).

[6] A. M. Brodskii, Yu. A. Kolbanovskii, et al., Dokl. Akad. Nauk SSSR, 122, 1035 (1958).•

[7] V. G. Berezkin, I. M. Kustanovich, L. S. Polak, A. V. Topchiev, and N. Ya. Chernyak, Dokl. Akad. Nauk SSSR, 129, No. 5, 1042 (1959).•

• Original Russian pagination. See C. B. Translation.

SURFACE PROPERTIES OF HIGHLY DISPERSED QUARTZ

L. G. Ganichenko, M. M. Egorov, V. F. Kiselev, K. G. Krasil'nikov and G. S. Khodakov

M. V. Lomonosov, Moscow State University, and the Scientific Research Institute of New Construction Materials

(Presented by Academician M. M. Dubinin, December 8, 1959)
Translated from Doklady Akademii Nauk SSSR, Vol. 131, No. 3, pp. 597-600, March, 1960
Original article submitted November 20, 1959

As is well known, the adsorption and energy relationships on surface elements of silica depend considerable on the degree of hydration, which in turn depends on the chemical and structural crystal surface properties. In most cases where adsorption on the surface of quartz was studied, the nature and structure of the surface as well as its effect on adsorption have not been examined very closely. The available literature data show large discrepancies between the reported degree of hydration and individual adsorption isotherms; these differences were either attributed to the presence of clay impurities [1] or to the existence of submicroscopic cracks in individual quartz crystals [2]. It was also shown [3] that a possible cause for these discrepancies might be found in the aggregation of quartz particles after dry milling. The fact that all of the papers dealing with the adsorption and degree of hydration of quartz surfaces fail to describe the milling procedure used (which applies to [2] also) and also fail to take into account any possible effects of particle aggregation, renders the interpretation and comparison of the available experimental data extremely difficult. The relationship between the degree of hydration and the structural characteristics of the surface layer in highly dispersed quartz still constitutes only a partially solved problem.

In the present work we undertook a thorough investigation of water vapor adsorption (since the adsorption of water is very sensitive to surface conditions [4]) and the degree of surface hydration in quartz powders of various grain sizes, all prepared by milling the same original sample. To eliminate any aggregation effects [3], we prepared all our powders by milling clear crystalline quartz in a steel vibration mill in the presence of excess water. The sample with the coarsest grain (Q-6) was prepared by grinding the quartz in a mortar, also in the presence of a large amount of water. The powders obtained under various milling conditions were rendered free of iron impurities in the manner already described [3]. The adsorption of water vapor and nitrogen as well as the determination of structural water were carried out in an analytical-gas apparatus. The experimental data we presented in Table 1 and Fig. 1.

As can be seen in Fig. 1, the initial isotherms of all the samples fired at 200°C begin high above the corresponding reversible isotherms, which were obtained after a prolonged exposure of all the samples to water vapor at 20° and at $p/p_s = 1$. This is probably due to the fact that the reversible adsorption of water vapor gives off much less energy on such samples than fresh ones fired at 200°C [5]. When the vapor is pumped off at low temperatures, the large number of silanol groups present on the surface give rise to hydrogen bonding between neighboring groups and decrease the adsorption energy [5].* The reversible adsorption on quartz (Table 1) is much

*Besides, when silica is processed at low temperatures, some water of crystallization may remain on the surface [6].

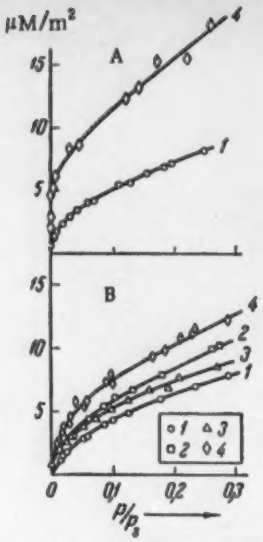

Fig. 1. The initial (A) and reversible (B) adsorption isotherms of water vapor on quartz: 1) Q-3; 2) Q-5; 3) Q-4; 4) Q-6.

greater than on silica gels which had been fired at the same temperatures [4]. Table 1 and Fig. 1 show that various samples, though processed in the same way, still exhibited various degrees of surface hydration and different specific adsorption, particularly in the initial portions of their isotherms. The difference between the degrees of hydration and the specific adsorptions can not in this case be attributed to different origins of the various samples or to any possible aggregation effects (as was done in [1,2]) but seems to be connected with differences in the surface structures of the samples under investigation.

A detailed determination of the degree of surface hydration has previously been made from an analysis of the crystallographic planes in single quartz crystals [7]. It was also pointed out [7] that these calculations could not be extended readily to quartz powder since the distribution of surfaces among the crystallographic planes was not known. The results would only provide the upper and lower limits (in the absence of thermal treatment) for the degree of surface hydration on powdered quartz. Attempts to improve these data [1, 8] by assuming a certain probable distribution of particle surfaces among the crystallographic planes yielded a certain limiting degree of hydration, which according to [8] was valid, not only for quartz surfaces, but also the surfaces of other silica modifications, such as silica gel. Similarly, the degree of hydration and consequently the structure of the surface were assumed to be entirely independent of several factors determined by the "past history" of a sample.

According to current ideas [9] a crystal surface cannot, even in principle, be regarded as a static structure. By starting from conditions which would provide the optimum screening for the Si^{++++} ion, Weyl [9, 10] showed that one of the ways in which a crystal might decrease its surface energy involves a breakup of its lattice so as to improve the cation screening; in the case of silica, the SiO_4 tetrahedra present at the surface would rearrange in such a manner that only oxygen atoms would be exposed at the surface. The mechanical agitation accompanying the pulverization of quartz crystals gives rise to an amorphous layer at the surface resembling Beilby's layers.* The existence of such a layer at the surface of pulverized quartz was confirmed by several methods, including: x-ray and electron diffraction, differential thermal analysis, infrared spectroscopy, and solubility measurements [12-14]. The milling of quartz changes the packing of the SiO_4 tetrahedra at the surface. The polymorphic transitions observed in crystalline silica at relatively low temperatures, 117-250° ($\gamma \rightleftharpoons \beta$ tridymite, $\alpha \rightleftharpoons \beta$-crystobalite), provide some indication of the relatively large mobility of the SiO_4 tetrahedra in the solid phase. One may assume that the rearrangement of the SiO_4 tetrahedra at the

Adsorption and Structural Characteristics of the Samples

Sample	Firing temp., °C	Specific surface, m^2/g	Particle diameter, mμ	Degree of surface hydration, $\mu M/m^2$	Amorphous phase content, %	Amorphous layer width, Å	Irreversible adsorption, $\mu M/m^2$
Q-3	200 300	50,8	44	5,8 5,3	50	45	0,7
Q-4	200 300	53,0	43	6,7 5,4	45	39	0,9
Q-5	200 300	31,7	72	9,9 7,4	28	40	1,7
Q-6	200 300	2,4	960	12,4 8,2	10	190	—

*In 1921 Beilby [11] detected some disintegration of crystals during the polishing of metallic surfaces.

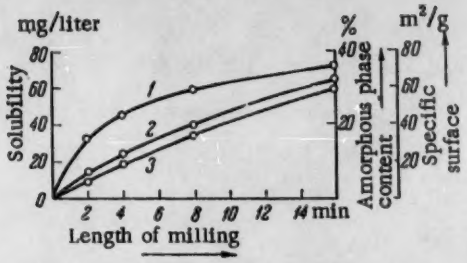

Fig. 2. Solubility (1), amorphous phase content (2), and the specific surface (3) of quartz as a function of the milling time in the vibrational mill.

surface will be facilitated by the fact that the tetrahedra are only linked by a single bond to the interior of the solid. Our observations failed to detect any crystalline modifications of SiO_2 in the surface layers of milled quartz; the same fact was noted in [12]. The amorphous layer has a density lower than that of crystalline α-quartz but higher than that of fused quartz.

The amorphous layer fraction in the quartz samples studied by us was determined by means of a differential thermal analysis [12]; from the heat of transition $\alpha \rightleftharpoons \beta$, we calculated the percentage of crystalline quartz capable of undergoing this transition. The experimental data and the calculated widths of the amorphous layer are presented in Table 1. To elucidate the factors responsible for the formation of amorphous layers of quartz, we set up special experiments. Fig. 2 shows that the amorphous phase content and the specific surface of quartz increase on prolonged milling. At the same time the width of the amorphous layer changes very little. Prolonged grinding in a mortar yielded sample Q-6 (Table 1) which had a small specific surface but a thick amorphous layer (apparently in this case most of the mechanical work went not into cleaving the crystals but into deforming them). The disorganization of a lattice increases its free energy. A study of the equilibrium solubility (Fig. 2) shows that the concentration of SiO_2 in solution increases when the milling time and the amorphous phase content are increased.

The degree of surface hydration depends on the number of free corners presented by the SiO_4 tetrahedra at the surface and consequently on the ionic packing. It is therefore obvious that even under identical preparatory conditions the degrees of hydration on various silica surfaces can not be the same but will be determined essentially by the structures of these surfaces. According to Table 1, samples with smaller specific surfaces exhibit greater surface hydration. Consequently the adsorptivity per unit of surface slightly increases when the grain size of silica is increased. Since, according to the data given in [15], the surface energy of a siloxane surface is 259 ergs/cm^2 while that of a silanol surface 129 ergs/cm^2, the specific surface energy of a partially hydrated silica should increase when the degree of surface hydration is decreased. Table 1 and the data obtained on silica gels [16] indicate that specific surface energy tends to increase with decreasing grain-size and consequently with decreasing degree of surface hydration. These data confirm Weyl's theory [9, 10], according to which very small crystals should exhibit increased specific surface energy. In the case of semiconductors, it was conclusively proved [17] that adsorption properties depend on the degree of dispersion of the adsorbent.

Previous results [2, 18] which indicated that silica gel and crystalline quartz have identical adsorption properties and exhibit the same maximum hydration are in conflict with our results. S. P. Zhdanov [2] based his earlier conclusions on the fact that the "absolute" adsorption isotherms of water vapor on quartz and silica gel coincide. In his calculations the author used specific surfaces calculated from the same isotherms for which he later constructed the "absolute" isotherm. It was later shown [19] that the BET treatment will not distinguish isotherms with similar values of C since any fine differences between the surfaces are automatically compensated by the value of C. When the "absolute" isotherms on hydrated and methylated silica gels are calculated by this method, the curves coincide since the distinction between these surfaces is very fine [20]. Therefore, the earlier data [2, 18] cannot be used as evidence for the theory that the surfaces of different silica samples are hydrated to the same extent and are consequently in the same physical state.

LITERATURE CITED

[1] W. Stöber, Koll. Zs. 145, 117 (1956).

[2] S. P. Zhdanov, Dokl. Akad. Nauk SSSR 120, 103 (1958).•

[3] V. F. Kiselev, K. G. Krasil'nikov, and G. S. Khodakov, Dokl. Akad. Nauk SSSR 130, 6 (1960).••

[4] M. M. Egorov and T. S. Egrova, Zhur. Fiz. Khim. 32, 2624 (1958).

[5] M. M. Egorov, K. G. Krasil'nikov, et al., Zhur. Fiz. Khim. 33, 65 (1959).

[6] E. A. Hayser and W. A. Weyl, Koll. Zs. 124, 72 (1951).

[7] H. Seifert, R. Buhl, and K. F. Seifert, Koll. Zs. 141, 146 (1955).

[8] S. P. Zhdanov and A. V. Kiselev, Zhur. Fiz. Khim. 31, 2213 (1957).

[9] W. A. Weyl and E. C. Marboe, Some Mechanical Properties of Glasses and Crystals as Affected by Changes in Chemical Binding Forces (Munich, 1959).

[10] W. A. Weyl, Structure and Properties of Solid Surfaces (Chicago, 1953), p. 147.

[11] G. T. Beilby, Aggregation and Flow in Solids (N. Y., 1921).

[12] P. B. Dempster and P. D. Ritchie, J. Appl. Chem. 3, 182 (1953).

[13] M. Cignitti and A. Uva, Ricerca scient. 28, 1915 (1958).

[14] G. S. Khodakov and É. R. Plutsis, Dokl. Akad. Nauk SSSR 123, 725 (1958).•

[15] S. Brunauer, D. L. Kantro, and C. H. Weise, Canad. J. Chem. 34, 1483 (1956).

[16] M. M. Egorov, K. G. Krasil'nikov, and V. F. Kiselev, Zhur. Fiz. Khim. 32, 2448 (1958).

[17] Sh. M. Kogan, Problems in Kinetics and Catalysis [in Russian] (1960).

[18] A. V. Kiselev and G. G. Muttik, Kolloid. Zhur. 19, 562 (1957).•

[19] V. F. Kiselev and K. G. Krasil'nikov, Zhur. Fiz. Khim. 33, 2621 (1959).

[20] L. G. Ganichenko, M. M. Dubinin, E. D. Zaverina, V. F. Kiselev, and K. G. Krasil'nikov, Izvest. Akad. Nauk SSSR, Otdel Khim. Nauk. No. 3 (1960).••

•Original Russian pagination. See C. B. Translation.

••See C. B. Translation.

THE KINETIC EQUATION FOR IRREVERSIBLE REACTIONS IN OSCILLOGRAPHIC POLAROGRAPHY

A. Ya. Gokhshtein and Ya. P. Gokhshtein

Electrochemistry Institute, Academy of Sciences, USSR
(Presented by Academician A. N. Frumkin, December 18, 1959)
Translated from Doklady Akademii Nauk SSSR, Vol. 131, No. 3, pp. 601-604, March, 1960
Original article submitted December 16, 1959

The equation for the maximum current of an irreversible polarographic wave given by Delahay [1],

$$I_p = 3{,}01 \cdot 10^5 n (\alpha n)^{1/2} S D^{1/2} C_0 v^{1/2},$$

reflects the fact that the current is a diffusion current. It relates the current to the diffusion coefficient D and the rate of change of potential v. Here and subsequently the following symbols are used: C_0 is the concentration of original substance in the bulk of the solution (mole/ml); C(0, t) is the concentration close to the electrode at time t after the start of electrolysis; E is the potential of the electrode relative to the normal hydrogen electrode (v); E_p is the potential of the peak; I is the current of the electrochemical reaction (amp); I_p is the current of the peak; k_0 is the rate constant related to the potential of the normal hydrogen electrode (cm/sec); m, μ and ψ are auxiliary variables, n is the number of electrons in the reaction; q = vnF/RT; S is the electrode area (cm^2); x is the distance from the electrode (cm); F is the Faraday; R is the gas constant; T is the temperature (°K); α is the barrier coefficient; αn corresponds to the rate-determining state; δ is the arbitrary unit of measurement of the quantity m; and $\varphi(t) = \partial C(0, t)/\partial x$.

Below we derive a simple equation expressing the maximum current in terms of the rate constant and the potential of the peak, which is always known from the oscillogram. At the same time the equation will not contain the rate of change of the potential or the diffusion coefficient, which are often unknown. The derivation is based on the statement that the ratio of the concentration of reacting substance in the layer next to the electrode, to its concentration in the mass of the solution is constant for the point of the peak and equal to 0.230. It is independent of D, v and the other quantities. In order to show this, it is convenient to convert the integral relationship between the concentration and its gradient at the electrode boundary [2]

$$C(0, t) = C_0 - \sqrt{\frac{D}{\pi}} \int_0^t \frac{\varphi(\tau)\, d\tau}{\sqrt{t - \tau}} \qquad (1)$$

to the dimensionless form. Substituting

$$\varphi = C_0 \sqrt{\pi q / D}\, \phi, \quad t = \delta m / q, \quad \tau = \delta \mu / q \qquad (2)$$

and then dividing by C_0, we have

$$\frac{C(0,\ t)}{C_0} = 1 - \sqrt{\delta}\int_0^m \frac{\psi(\delta\mu)\,d\mu}{\sqrt{m-\mu}}. \tag{3}$$

If the substance is supplied to the electrode by diffusion alone, then for the irreversible reaction

$$\frac{I}{nFS} = D\varphi(t) = C(0,\ t)\,k_0 \exp\left[-\alpha\frac{nF}{RT}E\right]. \tag{4}$$

Obtaining from this an expression for C(0, t) and substituting it in (1), we obtain an expression for φ (t)

$$D\varphi(t) = k_0 \exp\left(-\alpha\frac{nF}{RT}E\right)\left[C_0 - \sqrt{\frac{D}{\pi}}\int_0^t \frac{\varphi(\tau)\,d\tau}{\sqrt{t-\tau}}\right]. \tag{5}$$

Substitution from (2) converts it into an equation for ψ (δ m)

$$\psi(\delta m) = \frac{k_0}{\sqrt{D\pi q}} \exp\left(-\alpha\frac{nF}{RT}E\right)\left[1 - \sqrt{\delta}\int_0^m \frac{\psi(\delta\mu)\,d\mu}{\sqrt{m-\mu}}\right]. \tag{6}$$

For a potential changing linearly with time, E = $\bar{E}$ - vt, the factor in front of the square brackets in (6) is converted to the form exp (δ m - σ), where

$$\sigma = \alpha nF\bar{E}/RT + {}^1/_2 \ln D\pi q - \ln k_0. \tag{7}$$

With these symbols

$$\psi(\delta m) = \exp(\delta m - \sigma)\left[1 - \sqrt{\delta}\int_0^m \frac{\psi(\delta\mu)\,d\mu}{\sqrt{m-\mu}}\right]. \tag{8}$$

At the start (t = 0, m = 0), the current and the quantity ψ proportional to it are practically equal to zero. From (8) it follows that

$$\psi(+0) = e^{-\sigma} - o(e^{-\sigma}), \tag{9}$$

i.e., ψ (+ 0) differs from $e^{-\sigma}$ by a small quantity one order of magnitude higher than $e^{-\sigma}$, and thus, for small values of $e^{-\sigma}$, they may be taken as equal. The possibility of choosing σ according to (9) avoids the necessity of calculating it according to Formula (7). In the calculations it is possible to define σ in such a way that ψ (+ 0) is equal to a given small quantity, for example 10^{-3}. The latter is chosen to be commensurable with the permissible error. The arbitrariness in the choice of σ within the limits indicated does not change the function ψ (δ m) significantly and only changes the distance between the start of the reading of the amplitude and the value of it at which the maximum of the function is reached.

Thus ψ (δ m) and consequently the integral

$$\tilde{I} = \sqrt{\delta}\int_0^m \frac{\psi(\delta\mu)\,d\mu}{\sqrt{m-\mu}} \tag{10}$$

are independent of the experimental parameters and the substance. Now, however, the concentration ratio

m	$\frac{C(0,t)}{C_0}$	$\tilde{I}$	ψ	m	$\frac{C(0,t)}{C_0}$	$\tilde{I}$	ψ
0	1,0000	0,0000	0,0000	18	0,9329	0,0671	0,0371
1	0,9995	0,0005	0,0008	19	0,9165	0,0835	0,0459
2	0,9989	0,0011	0,0010	20	0,8977	0,1023	0,0566
3	0,9984	0,0016	0,0013	21	0,8720	0,1280	0,0693
4	0,9978	0,0022	0,0016	22	0,8427	0,1573	0,0843
5	0,9970	0,0030	0,0020	23	0,8078	0,1922	0,1017
6	0,9960	0,0040	0,0025	24	0,7667	0,2333	0,1215
7	0,9949	0,0051	0,0031	25	0,7192	0,2808	0,1435
8	0,9934	0,0066	0,0040	26	0,6654	0,3346	0,1671
9	0,9916	0,0084	0,0050	27	0,6057	0,3943	0,1915
10	0,9893	0,0107	0,0062	28	0,5412	0,4588	0,2155
11	0,9864	0,0136	0,0078	29	0,4738	0,5262	0,2375
12	0,9828	0,0172	0,0098	30	0,4057	0,5943	0,2560
13	0,9783	0,0217	0,0123	31	0,3394	0,6606	0,2697
14	0,9727	0,0273	0,0154	32	0,2777	0,7223	0,2777
15	0,9657	0,0343	0,0192	33	0,2223	0,7777	0,2800
16	0,9570	0,0430	0,0240	34	0,1747	0,8253	0,2771
17	0,9462	0,0538	0,0299	35	0,1364	0,8636	0,2723

•The arbitrary unit of the argument $\Delta E = 0.2303 \frac{RT}{nF} \frac{1}{\alpha} v$. At 25°, $\Delta E = 0.00591/\alpha n$.

defined by the expression (3) should also be independent of these factors. Since the current of the electrochemical reaction and the function ψ (δ m) pass through a maximum simultaneously, the maximum value of the current always corresponds to the same concentration ratio.

For its determination, the integral (10) was represented according to the formula described earlier [3]. Equations (8), (10) and (3) were then used in turn to determine the values of ψ (δ m), $\tilde{I}$ (m) and $C(0, m)/C_0$ for m = 1, 2, ..., 35. The values taken for σ and δ were in $10^{3.2}$ and 0.23026, respectively. The results are given in Table 1.

By means of interpolation with polynomials of seventh degree, we can find the value of m_p at which ψ is a maximum, and the ratio $C(0, t)/C_0$ at this point:

$$m_p = 32{,}86; \quad C(0,\ t_p)/C_0 = C\left(0, \frac{\delta m_p}{q}\right)\Big/ C_0 = 0{,}2297. \tag{11}$$

The relations (11) and (4) lead finally to the formula for the maximum current of the irreversible reaction,

$$I_p = 0{,}230 nFSC_0 k_0 \exp\left[-\alpha \frac{nF}{RT} E_p\right]. \tag{12}$$

One application of this formula is the determination of the rate constant k_0 from the known current and potential at the maximum point

$$k_0 = 4{,}35 \frac{I_p}{nFSC_0} \exp\left[\alpha \frac{nF}{RT} E_p\right]. \tag{13}$$

at 25°

$$I_p = 2{,}22 \cdot 10^4 nSC_0 k_0 10^{-16.91 \alpha n E_p}; \tag{12*}$$

$$k_0 = 0{,}450 \cdot 10^{-4} \frac{I_p}{nSC_0} 10^{16.91 \alpha n E_p}. \tag{13*}$$

Since here the potential of the peak appears in the index of the power with a high coefficient, it should be determined with the highest possible accuracy. When Ep changes by 1 mv, k_0 acquires the factor 1.04. A method for the accurate determination of the potential of the peak has been developed by Favero and Vianello [4] [4]. If account is taken of the current created by the background, the error in the determination of the potential of the peak is further reduced [5]. A large excess of indifferent electrolyte, by decreasing the loss of potential in the diffusion layer, also helps to increase the accuracy [6].

As an example we have calculated k_0 for the reduction of Nb^{5+} in 0.1 M Trilon B solution at 25°. For the first, irreversible wave n = 1, E_p = -0.616 relative to the saturated hydrogen electrode, $I_p = 14.28 \cdot 10^{-6}$ amp, $C_0 = 2.152 \cdot 10^{-6}$ mole/ml, $S = 1.529 \cdot 10^{-2}$ cm^2, v = 2.45 v/sec (v does not come into the calculations), and $\alpha n = 0.34$. From (13 •), $k_0 = 0.56 \cdot 10^{-5}$ cm/sec.

The quantity αn appears in (12) and (13). Its value may be obtained by comparing the current at the maximum with the current of the descending branch of the polarographic oscillogram. From the equation for the descending branch [7], it follows, for example, that $I_p/I_{0.3} = 3.18 \sqrt{\alpha n}$, where $I_{0.3}$ is the value of the current at a potential 0.3 v more negative than the potential of the peak.

LITERATURE CITED

[1] P. Delahay, J. Am. Chem. Soc. 75, 1190 (1953).

[2] Y. P. Gokhshtein and A. Y. Gokhshtein, Proc. 2-nd International Congress of Polarography (Cambridge, August, 1959).

[3] Ya. P. Gokhshtein and A. Ya. Gokhshtein, Dokl. Akad. Nauk SSSR 128, 985 (1959).•

[4] P. Favero and E. Vianello, Rend. Accad. Nazl. Lincei 21, 313 (1956).

[5] A. Ya. Gokhshtein, Zhur. Anal. Khim. 14, 485 (1959).••

[6] A. N. Frumkin, V. S. Bagotskii, Z. A. Iofa, and B. N. Kabanov, The Kinetics of Electrode Processes [in Russian] (Moscow, 1952), p. 76.

[7] Ya. P. Gokhshtein and A. Ya. Gokhshtein, Report to the Polarography Conference [in Russian] (Kishinev, 1959).

•Original Russian pagination. See C. B. Translation.

••See C. B. Translation.

AN INFRARED INVESTIGATION OF THE HYDROGEN EXCHANGE BETWEEN ACETONE AND DBr VAPORS

B. A. Kuznetsov

M. V. Lomonosov Moscow State University

(Presented by Academician N. N. Semenov, November 13, 1959)
Translated from Doklady Akademii Nauk SSSR Vol. 131, No. 3, pp. 605-608, March, 1960
Original article submitted November 13, 1959

The use of isotopes for the study of exchange reactions, which serve as models for many common chemical reactions, has been very successful especially from the kinetic standpoint. However, the success was primarily achieved in liquid-phase reactions. Gas-phase exchange, particularly exchange of hydrogen, constitutes at the present time a relatively neglected field, and there is no doubt that this particular fact may be chiefly responsible for the relative lag in other studies involving applications of hydrogen isotopes.

It is a well-known fact that compounds in which the hydrogen is attached to an atom containing a free electron pair (compounds of the type ROH, HHal, RNH_2) undergo a very rapid hydrogen exchange in the vapor phase [1, 2]. In the present work we decided to study pairs of compounds where one component has the free electron pair (HBr, H_2O) while the other has an active hydrogen (acetone).

The exchange between acetone and DBR was studied in a vacuum apparatus, represented schematically in Fig. 1. The reaction was carried out in molybdenum and quartz vessels, which were placed in an oven. After the reaction the mixture was transferred into cell 1 where each component was analyzed for deuterium. The vessel and the cell were both maintained at constant temperatures. Special experiments were carried out to demonstrate that any exchange which might have taken place in the cell during the analysis could be neglected. The extent of exchange was determined from the band intensities in the following regions: 2400 cm^{-1} (HBr), 1872 cm^{-1} (DBr), 3000 cm^{-1} (CH), and 2100 cm^{-1} (CD). The deuterium contents obtained from various measurements were averaged.

The instrument was calibrated with respect to DBr and HBr and corrected for the effects of total pressure on the band intensity and with regards to acetone by using a sample of known deuterium content. Acetone samples containing from 5 to 90% of deuterium (in steps of 5-10%) were prepared by means of exchange between acetone and heavy water (93.6% D) containing some NaOD (pH = 12).

A preliminary determination of the deuterium content was carried out by using an equation derived from the expression for the isotopic equilibrium constant. The equilibrium constant was taken as 0.85 [3, 4]. The isotopic composition of deuterated acetones was also verified by analyzing the samples in a model MS-4 mass spectrometer. The analyses were in good agreement with the theoretically predicted results. Eight-fold exchange yielded fully deuterated acetone. Each exchange operation required 10 days. The acetone was separated from water by distillation. Specially prepared Al_2O_3 was used as a drying agent [5]. After the sample was dried, it was redistilled. Trace amounts of water were detected with the help of the potassium iodide–lead iodide double salt.

DBr was prepared by decomposing PBr_5 with heavy water in vacuo. Excess PBr_5 was also used as a drying agent. The purity of the resulting DBr was determined from the vapor pressure at its melting point. The

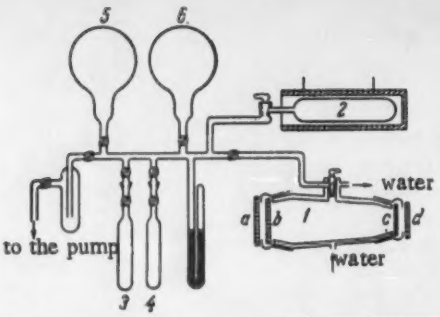

Fig. 1. A schematic representation of the apparatus used in the exchange investigation. 1) Gas cell; 2) reaction vessel; 3, 4, 5, 6,) storage vessels.

deuterium content of all the products was determined mass-spectroscopically from the heavy hydrogen line, while a special method was used to get the hydrogen from the compounds [6]. The exchange was calculated with the help of an equation which we derived by discounting the effects of the initial isotopic content.

If we use the notation accepted by S. Z. Roginskii [7], where R denotes the exchange rate of nonisotopic molecules, which proceeds undetected, and an additional isotopic effect is introduced by using Rf_1 to denote the initial exchange rate,

$$AX_n + B\dot{X}_m \rightleftarrows AX_{n-1}\dot{X} + B\dot{X}_{m-1}X,$$

and Rf_2 the initial rate for the reverse exchange,

$$A\dot{X}_n + BX_m \rightleftarrows A\dot{X}_{n-1}X + BX_{m-1}\dot{X},$$

then we can write the following differential equation for the rate at which the heavy isotope AX_n is accumulated, taking into account the fraction which the isotopic exchange rate constitutes of the over-all exchange rate,

$$\tilde{d}\dot{A}/dt = Rf_1(1-\rho_a)\rho_b - Rf_2(1-\rho_b)\rho_a,$$

where $\dot{A}$ and $\dot{B}$ are the amounts of isotope $\dot{X}$ in AX_n and BX_m respectively; $\rho_a = \dot{A}/nA$; $\rho_b = \dot{B}/mB$; A and B the concentrations of AX_n and BX_m, respectively.

A general solution of this equation gives the formula:

$$Rf_1 = -\frac{mnAB}{tq(\rho_{a_2}-\rho_{a_1})(nA+mB)}\ln\left(\frac{(\rho_{a_1}-\rho_{a_2})(\rho_{a_0}-\rho_{a_1})}{(\rho_a-\rho_{a_1})(\rho_{a_0}-\rho_{a_2})}\right)$$

where

$$\rho_{a_{1,2}} = p/2q \pm \sqrt{(p/2q)^2 + \rho/q}; \quad q = (k-1)nA/(nA+mB);$$
$$p = (k-1)(\bar{\rho} - mB/(nA+mB)) - 1;$$

$k = f_2/f_1$ is the isotopic equilibrium constant; m and n give the number of equivalent atoms undergoing exchange in molecules AX_n and BX_m; $\bar{\rho}$ is the deuterium content of the entire system; ρ_{a_0} the initial deuterium content of component AX_n. The Rf_1 obtained from this equation remains constant with a fair degree of accuracy regardless of the extent of exchange.

To calculate the reaction rate by the use of our equation, we have to know the equilibrium constant. The equilibrium constant k obtained by us at 218° was 2.3 ± 0.1. The experimental data are presented in Table 1. The equilibrium constant 2.3 was close to the value calculated theoretically from the vibrational frequencies of acetone-d_6,• namely 1.98. The calculated ratio of the partition functions $(Q_2/Q_1)^{1/6}_{ac} = 4.168$; the experimental value is 4.6 if we take $(Q_2/Q_1)_{HBr} = 2.01$ [8].

To establish the reaction mechanism, we determined the reaction order with respect to each component at 218°C in quartz and molybdenum vessels. • The kinetic curves are plotted in Fig. 2. Fig. 3 also shows that the reaction is first order with respect to acetone and DBr.

Next we studied the relationship between the reaction rate and the ratio s/v. The reaction rate in the stoppered vessel was directly proportional to s/v. (When $s/v = 0.9\ cm^{-1}$ we got Rf_1 = 21 mm of Hg while for $s/v = 5.9\ cm^{-1}$ Rf_1 = 125 mm, both at t = 218°C, P_{ac} = 70 mm, P_{DBr} = 420 mm.

• These determinations were done with the help of N. D. Elkina.

The Equilibrium Constant k for Acetone + DBr and for Acetone-d_6 + HBr at 218°•

$(I_0 - I)/I_0$ from the CH band	D, % from the CH band	D, % from the CD band	D, % average	k	Exchange t, min	Direction of reaction
0,260	53,9	53,9	53,9	2,42	66	Forward exchange
0,221	62,0	48,0••	53,9	2,42	180	Ditto
0,232	60,4	48,6	53,0	2,42	120	Ditto
0,246	57,1	53,5	55,6	2,42	150	Reverse
0,236	56,4	56,4	56,4	2,28	255	Ditto
0,213	60,5	48,7	53,1	2,24	120	Ditto
				2,3±0,1		

•Total deuterium content in forward exchange was 0.432, in reverse exchange 0.465.
••The high D% indicated by the CH band and the low % given by the CD band result from a partial condensation of acetone on the walls. Our results make it possible to account for this effect.

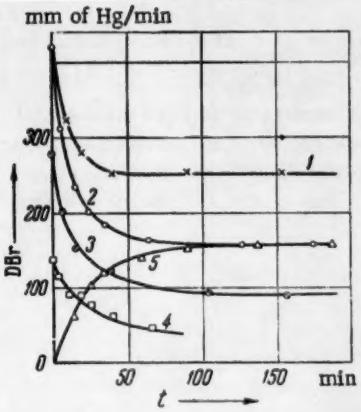

Fig. 2. Kinetic curves for the exchange between acetone and DBr (1-4) and between acetone-d_6 and HBr (5) at 218°C. 1) P_{ac} = 35 mm, P_{DBr} = 420 mm; 2) P_{ac} = 70 mm, P_{DBr} = 420 mm; 3) P_{ac} = 70 mm, P_{DBr} = 280 mm; 4) P_{ac} = 70 mm, P_{DBr} = 140 mm; 5) $P_{ac\text{-}d_6}$ = 70 mm, P_{HBr} = 420 mm.

We also determined the temperature dependence of the exchange rate. Fig. 4 shows that between 32 and 218°C the line obeys Arrhenius' equation. For s/v = 0.9 cm^{-1}, the exchange rate can be expressed by the equation

$$Rf_1 = 1.3 \cdot 10^{-19} e^{-5300/RT} \text{ [Acetone] [DBr] moles/sec.}$$

One would have to assume that the reaction occurs between the molecules of acetone adsorbed on the wall and the DBr molecules colliding with the wall. When the heat of adsorption and the fraction of wall surface covered with acetone were estimated, the above-made assumption led to a calculated frequency factor of 10^{-19}.

As a matter of fact, if we take the exchange rate on the surface and the gas-phase exchange rate calculated from the equation, we will get

$$\frac{s}{v}\frac{n_1\bar{v}}{4}\theta e^{-E_{true}/RT} = k_0 n_1 n_2 e^{-E_{eff}/RT};$$

where s/v is the surface to volume ratio in cm^{-1}; $\bar{v}$ the velocity of DBr molecules in cm/sec; θ the fraction of the surface covered up; n_1 and n_2 the respective concentrations of DBr and acetone in the vapor phase; Q the adsorption heat of acetone.

It follows from the equation that

$$k_0 = \frac{s}{v}\frac{\bar{v}}{4n_2}\theta e^{-Q/RT} \simeq 10^{-15} e^{-Q/RT},$$

since $\theta \sim e^{Q/RT}$ and $E_{eff} = E_{true} - Q$. If we take Q = 9 kcal/mole, which can be estimated roughly from the increased adsorption heat for two CH_3 groups [9], then the frequency factor at t = 218°C is 10^{-9} while E_{true} = = 14 kcal/mole.

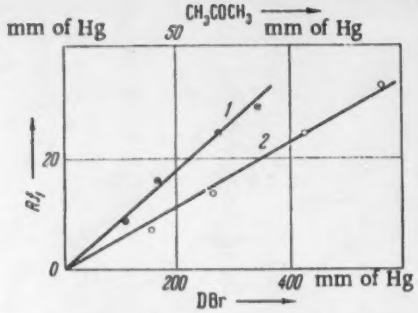

Fig. 3. The exchange rate as a function of acetone pressure at t = 218°, P_{DBr} = 420 mm (1) and as a function of DBr pressure at t = 219°, P_{ac} = 70 mm (2).

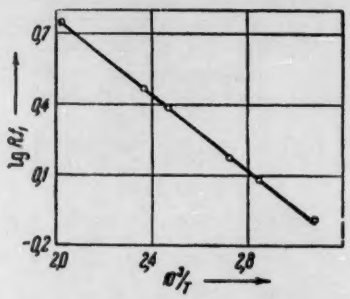

Fig. 4. Temperature dependence of the exchange rate, s/v = 0.7 cm^{-1}, P_{ac} = 45 mm, P_{DBr} = 270 mm.

There are by 1-2 orders of magnitude fewer collisions between DBr molecules adsorbed on the wall and the acetone vapor than the number observed in the earlier discussed mechanism. Accordingly such collisions will contribute very little to the over-all exchange. Since reactions in the adsorbed layer would have a frequency factor of 10^{-27}, they were entirely neglected [10].

Under our conditions the value of P/P_s for acetone was changed from 0.001 to 0.1 and the corresponding fraction of surface covered changed from 0.01 to 0.5, which indicates that we were not operating under conditions allowing the formation of a surface film where the reaction would follow liquid-phase laws [11].

We have to assume that the proton transfer which leads to exchange occurs only during a bimolecular collision and is therefore facilitated on the walls. The observed reaction has to be classified as an acid-base reaction, since HBr acts as a proton donor. That the reaction can not proceed through the formation of ions on the surface can be deduced from the work done by N. M. Chirkov [11], who studied the electrical surface conductance at low P/P_s ratios of hydrogen bromide.

Therefore, the reaction scheme on the wall can be represented by the equations:

$$CH_3\overset{\overset{O}{\|}}{C}CH_3 + DBr \xrightarrow{s} CH_3C(OD)=CH_2 + HBr$$

$$CH_3C(OD)=CH_2 + DBr \xrightarrow{f} CH_3\overset{\overset{O}{\|}}{C}CH_2D + DBr$$

Our work also indicates that the wall reaction is much facter than the vapor-phase enolization of ketones.

LITERATURE CITED

[1] A. I. Brodskii, Izvest. Akad. Nauk SSSR, Otdel Khim. Nauk, No. 1, 3 (1949).

[2] H. Kwart, L. P. Kuhn, and E. L. Bannister, J. Am. Chem. Soc. 76, 5998 (1954).

[3] A. I. Brodskii, Zhur. Fiz. Khim. 9, 75 (1937).

[4] R. Klar, Zs. Phys. Chem. B26, 335 (1934).

[5] F. M. Y. Jonson, J. Am. Chem. Soc. 34, 94 (1912).

[6] R. Viallard, et al. Chim. Analyt. 36, 4, 102 (1954),

[7] S. Z. Roginskii, Theoretical Foundations for the Use of Isotopic Techniques in the Study of Chemical Reactions [in Russian] (Moscow, 1956) p. 133.

[8] H. S. Urey, J. Chem. Soc. 562, (1947).

[9] A. A. Isirikyan, A. V. Kiselev, and B. A. Frolov, Zhur. Fiz. Khim. 33, 2, 389 (1959).

[10] S. Glasstone, K. Laidler, and H. Eyring, The Theory of Absolute Reaction Rates [Russian translation] Moscow, 1948) p. 365.

[11] N. M. Chirkov, Doctoral Dissertation (Chemical Physics Institute, Academy of Sciences USSR, 1956).

THE USE OF VERY FAST ELECTRONS FOR THE MICRODIFFRACTION STUDY OF THE STRUCTURE OF SOOT PARTICLES

N. M. Popov, V. I. Kasatochkin, and V. M. Luk'yanovich

(Presented by Academician M. M. Dubinin, November 21, 1959)
Translated from Doklady Akademii Nauk SSSR, Vol. 131, No. 3, pp. 609-611, March, 1960
Original article submitted November 20, 1959

The procedure by which an optical electron image and an electron diffraction spectrum are obtained from an extremely small section of the same object, referred to as microdiffraction [1], greatly extends the possible applications of electron diffraction and electron microscopy. The electron microscopes being produced at present, with accelerating voltage not more than 100 kv, do not permit a decrease in the diameter of the area of the object from which a diffraction pattern can be obtained to a value of less than 1 μ, as a result of the insufficient clarity of the diffraction picture. This limitation can be overcome by increasing the velocity of the electrons, which makes it possible to increase the clarity of the image of the diffraction spectrum without increasing the thermal load on the object. Increase in the velocity of the electrons also increases the permissible thickness of the object under study and increases the resolution of the diffraction picture (as a result of the decrease in the aberration of the lenses).

The present study was carried out on an electron microscope with an accelerating voltage of 400 kv [2] (relativistic velocity 557 kev, wavelength 0.0165 A, resolving power at the image 20 A), on which the diameter of the microdiffraction area could be reduced to 500 A.

Figure 1 illustrates diagramatically the arrangement of lenses forming the image in this instrument. The upper focal plane of the objective contains the object, while a movable aperture diaphragm is set up in the lower focal plane. A movable selector diaphragm is placed close to the intermediate "diffraction" lens, in the image plane of the first stage. When working "on image," the image of the first stage of the diffraction lens is transferred to the focal plane of the projection lens, and an image of the object appears on the screen or photographic plate. By an appropriate decrease in the ampere-turns of the diffraction lens, the diffraction spectrum, whose primary image lies in the lower focal plane of the objective lens, is transferred to the screen. The selector diaphragm introduced into the plane of the primary image (with the aperture diaphragm removed) cuts out on the image a section of the object whose diameter is less than that of the diaphragm by a factor equal to the magnification of the objective lens. When the diffraction lens goes over to "diffraction working," the diffraction picture obtained on the end screen corresponds exactly to that section of the object which was limited by the image of the selector diaphragm. By introduction of the aperture diaphragm, it is possible to isolate on the screen any reflection of the diffraction spectrum. If we then go over to the image, we obtain a particular dark-field image of the object in which the bright regions correspond to the favorably orientated atomic planes of the lattice with the indices of the reflection.

The objects studied were particles of thermal soot, before and after isothermal ignition in an inert atmosphere at 3200° for 20 minutes. X-ray diffraction data showed that the ignited soot had a comparatively high degree of homogeneous graphitization (γ = 0.78) [4, 5].

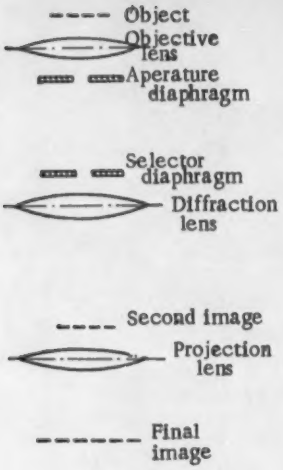

Fig. 1.

Figure 2 (a) gives the light-field image (negative) of a particle of ignited thermal soot, in which the small circles show the images of a selector diaphragm of diameter 600 A, together with the diffraction spectra (b, c, d, e, f) of the corresponding sections of the particle (indicated by arrows). The layer lines formed on the electron diffraction diagrams for the separate sections are arranged in the direction of the radii of the particle. The zero layer line contains a number of bright reflections representing the nodes of the reciprocal lattice of graphite with indices 001 (basal reflections). The nature of the diffraction pictures indicates that they are produced by separate crystalline blocks of the graphitized soot particle. The radial orientation of the lines of the basal reflections on the electron diffraction diagrams of the sections of the particle correspond to the radial direction of the normals of the basal planes of the graphitized blocks of which the particle is made up. In those cases where the selector diaphragm cuts out an area at the edges of two adjacent graphite blocks (Fig. 2 f), two series of basal reflections are produced, and the angle between them characterizes the mutual orientation of the blocks. This can be observed particularly clearly when the angle between the directions of the basal planes of the adjacent blocks is large. The intense hoops and rings which are then produced indicate the presence of layers of nongraphitized carbonaceous material between the blocks. The amorphous nature of the material in these layers is confirmed by the absence of diffraction rings with indices hkl, h0l and 0kl on the electron diffraction diagram. The shape and size of the graphitized blocks and amorphous layers can be observed directly on the image of the particles. Each graphitized block can be picked out very clearly on the particular dark-field image of the particle (Fig. 2 g), obtained by the electron beam of the basal reflection indicated by the arrow in Fig. 2 f (the position of the image of the aperture diaphragm is shown in Fig. 2 f, by a small circle).

The length of the largest block is $\sim$ 1500 A, and the average layer thickness is 200-300 A. The electron diffraction diagrams of the graphitized blocks show the characteristic drawn-out appearance of the reflections with indices 100, 101, 102, 110, 112, etc., along an equator, with the formation of layer lines. This indicates the incomplete azimuthal orientation of the basal planes of the graphite crystal lattice, in accordance with x-ray diffraction data [4]. A detailed study of the azimuthal order and defects in the crystal lattice of the graphitized blocks requires further quantitative examination of the positions, shapes, and intensities of the reflections on the electron diffraction diagrams.

The electron diffraction diagram for the whole of a particle of graphitized thermal soot, obtained for a microdiffraction area diameter of 0.5 μ, results from the superposition of the diffraction pictures of all the graphitized blocks and amorphous layers. In addition to the diffraction rings, point basal reflections are produced, whose position on the electron diffraction diagram reflects the symmetry of the growth of the graphitized blocks in the soot particle during the isothermal ignition.

Fig. 3 (a) gives a light-field (negative) image of a particle of the original thermal soot, together with the diffraction spectra (b, c, d, e, f) of separate sections of diameter 600 A, indicated by the small circles. The diffraction pictures are characterized by the presence of a series of basal reflections whose sharpness indicates the comparatively high degree of order of the basal planes of the carbon in the direction of the normals to these planes. In this case the layer lines formed on the electron diffraction diagrams do not break down to separate point reflections (in contrast to the case of the graphitized particles). The curvature of the layer lines, together with the slight tangential broadening of the basal reflections, indicates the spherical orientation of the basal planes, whose normals are radially arranged. The absence of reflections with indices khl, h0l, and 0kl indicates the complete azimuthal disorientation of the basal planes of the carbon. The nature of the electron diffraction diagrams, in accordance with the x-ray diffraction data [6], confirms the suggestion regarding the amorphous nature of the carbonaceous material in the original particles. The normals of the basal planes are situated fairly uniformly in the direction of the radii of the spherical soot particles, as is indicated by the radial arrangement of the series of basal reflections in the electron diffraction diagrams of the separate sections of the particle.

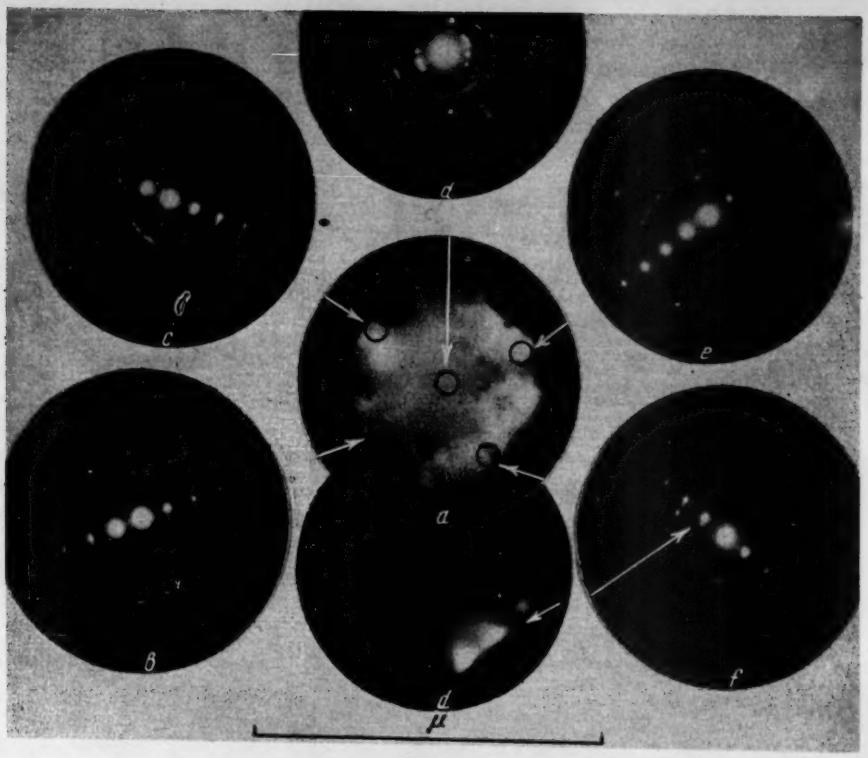

Fig. 2.

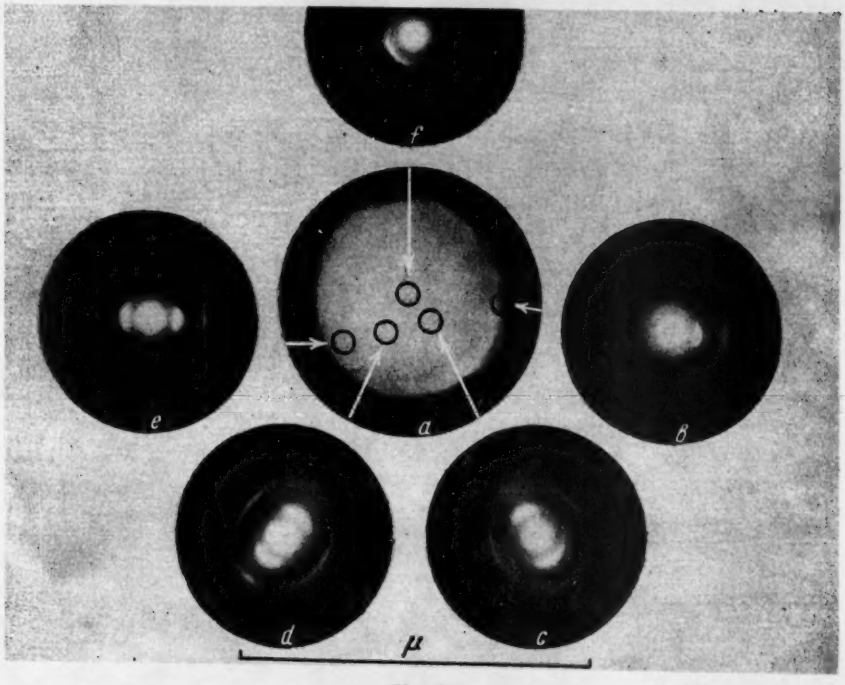

Fig. 3.

Figure 3 shows extremely clearly that the angular disorientation of the arc-shaped reflections on the electron diffraction diagram is greater, the closer the macrodiffraction area studied lies to the center of the spherical particle. This is quite natural since the curvature of the spherical layers of carbon increases on going towards the center of the particle. From this example we see how it is possible to break down the "spherical" texture, which cannot be detected by ordinary "macrodiffraction," into a series of sloping-layer textures by the microdiffraction method.

The data obtained in the study of the structure of soot particles are in good agreement with the theory of the probable mechanism of their growth [7], according to which the aromatic synthetic products of pyrolysis of the gas condense in orientated fashion on the particle surface, probably in the form of flat, atomic, nucleation networks of aromatic carbon with side radicals. The growth of the carbon network takes place in the solid phase as a result of processes involving thermal destruction and synthesis in the side radicals. These processes can be assumed to lead to the formation of soot particles consisting of a carbonaceous substance of polymeric structure in the form of an accumulation of orientated aromatic carbon networks linked together in three dimensions via the side radicals. The spherical shape of the soot particles results from the regular deposition of carbonaceous material from the gas phase over the whole surface of the particle. The atomic–molecular structure of the soot particle is similar to that of bright carbon, which differs only in the symmetry of packing of the planar carbon networks [7]. It has already been pointed out [8] that bright carbon deposited on the walls of a reaction vessel shows planar packing of the carbon networks under the influence of the planar support.

Microdiffraction of high-speed electrons thus reveals new possibilities for the detailed study of the atomic structure of carbon. The high penetrating power of very fast electrons makes it possible to obtain images and diffraction pictures from relatively large carbon particles, and the decrease in the microdiffraction area, which is also associated with the increase in the velocity of the electrons, makes it possible to use the diffraction method to study not only isolated particles, but also their internal mosaic.

LITERATURE CITED

[1] M. E. Haine, K. S. Page, and R. J. Garfett, J. Appl. Phys. 21, 173 (1950).

[2] N. M. Popov, Izv. Akad. Nauk SSSR Ser. Fiz. 23, No. 4, 436 (1959); 23, No. 4, 494 (1959); N. M. Popov and B. B. Zvyagin, Kristallografiya 3, No. 6 (1958); N. M. Popov and B. B. Zvyagin, Izv. Akad. Nauk SSSR, Ser. Fiz. 23, No. 6 (1959).

[3] E. A. Leont'ev, V. M. Luk'yanovich, and B. S. Mil'man, Dokl. Akad. Nauk SSSR 112, 461 (1957).•

[4] V. I. Kasatochkin and A. T. Kaverov, Dokl. Akad. Nauk SSSR 117, No. 5 (1957).••

[5] V. I. Kasatochkin and A. T. Kaverov, Dokl. Akad. Nauk SSSR 120, No. 5 (1958).••

[6] J. Biscow and B. E. Warren, J. Appl. Phys. 13, 364 (1942).

[7] V. I. Kasatochkin, Izv. Akad. Nauk SSSR, Otd. Khim. Nauk 1953, No. 10, 28 (1953).•

[8] G. Ruess, Monatsh. Chem., 76, 253 (1957).

•Original Russian pagination. See C. B. Translation.

••See C. B. Translation.

ADSORPTION GAS RADIOGRAPHY AND ITS APPLICATION TO THE STUDY OF PROMOTED CATALYSTS FOR AMMONIA SYNTHESIS

Corresponding Member Acad. Sci. USSR Z. S. Roginskii
and Yu. E. Sinyak

Physical Chemistry Institute, Academy of Sciences, USSR
Translated from Doklady Akademii Nauk SSSR, Vol. 131, No. 3, pp. 612-615, March, 1960
Original article submitted December 31, 1959

Radiography has found extensive application in various scientific fields [1-4], but, as far as we are aware, this clear and direct method has not yet been applied to work on catalysis.

The present communication reports briefly the data obtained in a radiographic study of the catalyst used for the industrial synthesis of ammonia. The use of ordinary radiography is made difficult in this case by the absence of convenient radioactive isotopes of the chemical elements used as promoters or forming the catalyst. Thus Al^{29} is not readily available and its half-life is too short ($\tau_{1/2}$ = 6.5 min); K^{40}, with $\tau_{1/2} = 1.3 \cdot 10^9$ yr, is also unsuitable. Since the preparation of promoted catalysts is a long process, K^{42} ($\tau_{1/2}$ = 12.4 hr, E_β = 1.1 Mev) is also inconvenient. The radiation from Fe^{55} or Fe^{59}, which consists of electrons, internal conversion, and γ-rays with energy 1.2 Mev, is difficult to apply for radiographic purposes, because of the considerable volume distortion of the γ-radiation. Of the components of the reaction involved in the synthesis of ammonia, N_2 has no isotope convenient for radiographic measurements. We have, therefore, developed the new method* of adsorption gas radiography. In this method the radiograms are obtained by means of photography, using the radiation from radioactive isotopes taken as the simple elements or in the form of chemical compounds and absorbed on the surface of the solid under study. When more than one phase, or pores and zones with very different adsorptive properties are present, these features can be observed on the images.

An advantage of adsorption gas radiography is the possibility of studying the topography of elements which have no radioactive isotopes. At the same time it is possible to vary, over wide limits, the size and physicochemical properties of the molecules used as radiation source and to eliminate completely the volume effects. The material for autoradiographic examination is introduced to the prepared specimen either with the latter isolated or during a particular process. The time required to introduce the isotopic tracer is less than in ordinary radiography, which is particularly important when using short-lived isotopes. Experiments can very readily be repeated with the same specimen and different radioactive adsorbed materials.

In catalysis, gas adsorption radiography appears promising for the study of the nature of the distribution of added promoting agents, for the study of the topography of the poisoning of catalytic and adsorption processes, the topography of catalytically active centers, etc.

The chief requirement of adsorption gas radiography in the study of the distribution of promoters in a catalyst is a radioactive gas which is preferentially adsorbed on the added promoter under study.

*The theory of the method will be described elsewhere.

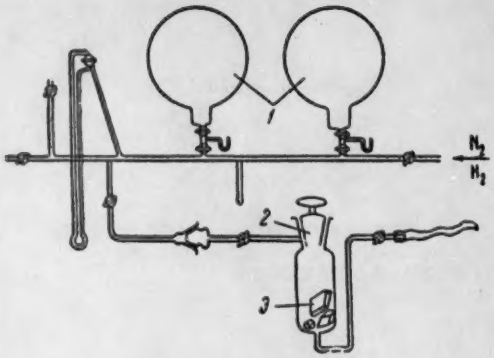

Fig. 1. Diagram of the vacuum apparatus for adsorption gas radiography. 1) Containers for $C^{14}O_2$; 2) reaction vessel for catalyst sections 3.

In catalysts for the synthesis of ammonia, the chief promoter is potassium oxide, added to cast iron. Any acidic gas may be used as indicator for the study of the distribution of an alkaline promoter; we used $C^{14}O_2$. An advantage of the radioactive isotope chosen is the softness of the β radiation of C^{14}, while a disadvantage is the long half-life ($\tau_{1/2}$ = 5570 yr).

EXPERIMENTAL

The nature of the distribution of the alkaline promoter in the ammonia catalyst was studied using an industrial specimen containing 2% K_2O and 5% Al_2O_3. The catalyst was studied in the reduced and nonreduced states. The previously prepared sections were placed in the reaction vessel of the vacuum apparatus (Fig. 1), in which the chemisorption of the CO_2 labeled with C^{14} took place.

It was known from data obtained earlier that CO_2 is chemisorbed exclusively by the sections of the alkaline promoter [7], and is not desorbed in an atmosphere of nitrogen, argon or hydrogen at room temperature [8]. All the operations involved in unloading and exposing the sections were therefore carried out in an atmosphere of purified nitrogen. In order to prevent side interaction between the photographic plate and the section during the exposure, the latter was covered with a thin layer of collodion and placed in a desiccator. Since the half-life period is long, the time of exposure amounted to several days. It may be reduced by using special photographic plates.•

The results obtained for nonreduced Fe_3O_4 with additives are shown in Fig. 2 (a), which shows optical reflection photomicrographs, Fig. 2 (b) shows a radiogram of the same specimen, and Fig. 2 (c) shows a radiogram of another specimen at similar magnification. In photographs 2b and 2c the white regions correspond to alkali, and the dark regions, to the surface of iron or alumina. Particularly noticeable features are the sharp difference between the optical and radiographic photographs of the same specimen (Fig. 2, a and b) and the nonuniform distribution of the alkaline promoter over the catalyst grains. The radiograms show clearly zones where there is no alkali at all and regions characterized by a considerable concentration of the alkaline additive. It is possible that the potassium oxide reacts to produce a compound which forms a separate phase.

Fig. 3 shows a photomicrograph (a) and radiogram (b) of a reduced specimen. It can be clearly seen that the optical photograph 3 a differs less from 3 b than 2 a does from 2 b. This shows that during reduction a significant change has taken place in the topography of the distribution of the alkali in the specimen. The adsorption gas radiography method can also be used to determine the distribution of the Al_2O_3 and the structure of the Fe.

•Up to the present "Spectrographic, Type 1" plates have been used.

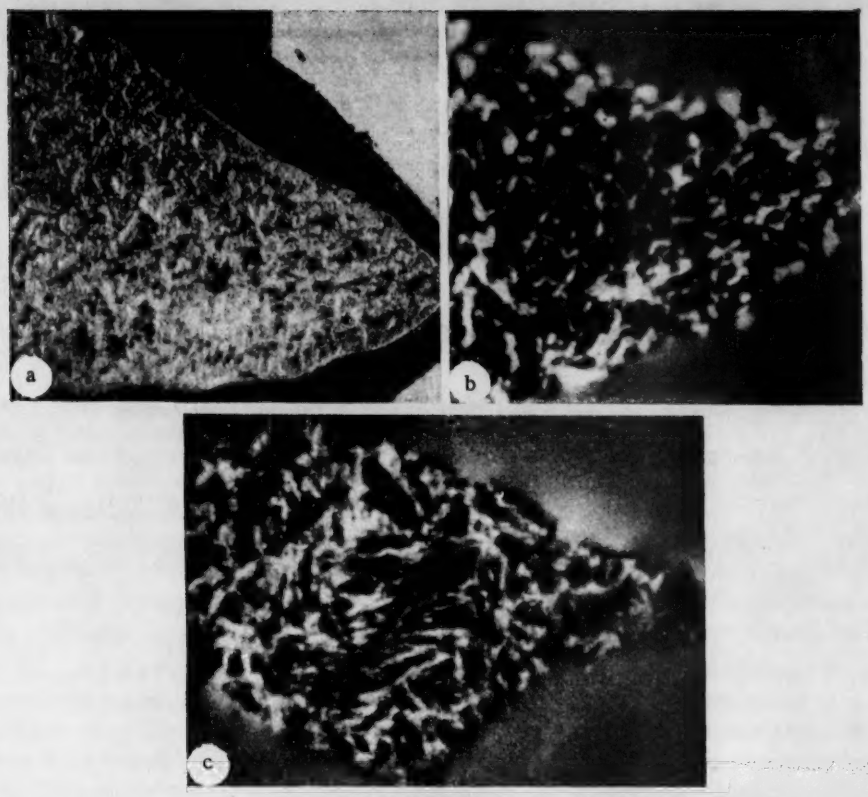

Fig. 2.

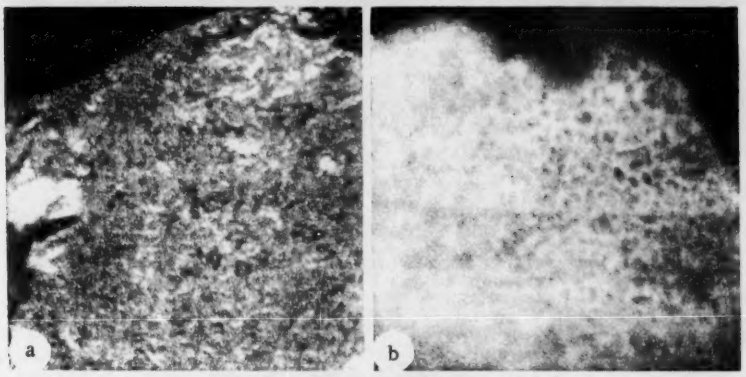

Fig. 3.

The literature contains descriptions of a number of attempts to use surface processes for radiographic purposes. Thus Rabinowicz [5] has described the use of amyl iodide, labeled with I^{131} and adsorbed from solution, for the study of metals and alloys. In this case the process is not one of adsorption but a surface chemical process which spreads into the depth of the grain. Thompson, et al., [6] has used for radiography the compound produced on a surface in the form of characteristic thick layers when gas chemical reactions are carried out with a solid. The authorsregard adsorption as an undesirable additional factor. In our case, supplementary adsorption measurements make it possible to regard the adsorption of CO_2 as a surface process, with no penetration into the

volume of the grain, and this is the chief condition for adsorption gas radiography, whose fundamental idea lies in the use of the peculiar features of physical and chemical adsorption with variations in filling both below the monolayer and in the region of multilayer adsorption and capillary condensation.

LITERATURE CITED

[1] O. Khan, Applied Radiochemistry [in Russian] (1947).

[2] Radiography, A Collection of Articles [Russian translation] (IL, 1952).

[3] The Use of Radioactive Isotopes in Metallurgy, Collection XXXIV, The Stalin Steel Institute [in Russian] (1955).

[4] B. P. Bruk, Radioactive Isotopes in Metallurgy and the Metallography of Welding [in Russian] (1959).

[5] E. Rabinowicz, Nature 170, 1029 (1952)

[6] B. A. Thompson and C. Murphy, Intern. J. Appl. Rad. and Isotop. 1, 37 (1959).

[7] S. Brunauer and P. H. Emmett, J. Am. Chem. Soc. 7, 1732 (1940).

[8] Yu. E. Sinyak, S. Z. Roginskii, and M. I. Yanovskii, Dokl. Akad. Nauk SSSR, 118, 727 (1958). •

•Original Russian pagination. See C. B. Translation.

RADIOCHEMICAL MEASUREMENT OF THE RATE OF CARBON FORMATION DURING THE DECOMPOSITION OF ETHYL ALCOHOL ON A DEHYDROGENATING CATALYST

Academician A. A. Balandin, G. V. Isagulyants, A. P. Rudenko, and G. Stegner

M. V. Lomonosov Moscow State University
N. D. Zelinskii Organic Chemistry Institute, Academy of Sciences, USSR
Translated from Doklady Akademii Nauk SSSR, Vol. 131, No. 4, pp. 861-864, April, 1960
Original article submitted December 26, 1959

Our previous works [1, 2] reported the examination of the mechanisms of tar and carbon formation in the decomposition of ethyl alcohol on catalysts, carried out on the basis of a study of the reaction products and their rates of formation. From these works it follows that, in the decomposition of ethyl alcohol on a dehydrogenating catalyst, several mechanisms are possible, depending on the temperature conditions. At 200-600° a low temperature mechanism is observed, involving the polycondensation of acetaldehyde previously formed from the alcohol; at higher temperatures polycondensation of the original ethyl alcohol with unsaturated condensation products becomes possible, together with polycondensation of various hydrocarbons previously formed from the decomposing alcohol.

Since the processes of carbon formation are complex, involve many stages, and can, in general, be studied only from certain over-all effects and indirect data, it was considered of interest to examine the part played by acetaldehyde and ethyl alcohol as starting material for carbon formation, by measuring the rates of the separate stages of this complex process using the isotopic kinetic method of M. B. Neiman [3, 4]. This method was first applied to heterogeneous catalytic reactions by A. A. Balandin, M. B. Neiman, O. K. Bogdanova, G. V. Isagulyants, A. P. Shcheglova, and E. I. Popov [5].

Radiochemical methods have already been used to examine a number of problems of carbon formation in the decomposition of different organic substances [6-10]. Thus McMahn [7] has established by a radiochemical method that, in the cracking of paraffinic hydrocarbons at low temperatures, the carbon obtained comes from the carbon of the whole original molecule; A. A. Balandin and co-workers [5, 9] have shown that, in the dehydrogenation of a butane–butylene mixture, 90% of the carbon is formed from divinyl and only 1.5% directly from butane; G. M. Zhabrova and B. M. Kadenatsi [10] have found that, under the conditions of the preparation of divinyl from ethyl alcohol, the carbon is formed chiefly from the alcohol, etc.

In the present work two series of experiments were carried out under the same conditions: one using pure ethyl alcohol and the other using a mixture of ethyl alcohol and 3% acetaldehyde labeled with C^{14} (specific activity 11900 counts per mg $BaCO_3$ per min). The experiments were carried out in a flow-through apparatus by the method described earlier [1, 2] at 305 and 485°, with contact time 1-9 seconds, and copper–silica gel catalyst prepared as described in [1]. In the experiments with the labeled acetaldehyde added, measurements were made of the specific activity of the resultant carbonaceous material, acetaldehyde, and alcohol by the method described in [5]. The activity of the alcohol and the carbon were measured in targets of $BaCO_3$ after ignition of the specimens. The activity of the acetaldehyde was determined in targets of 2,4-dinitrophenylhydrazone with appropriate recalculation to the equivalent $BaCO_3$ activity. The carbonaceous material was

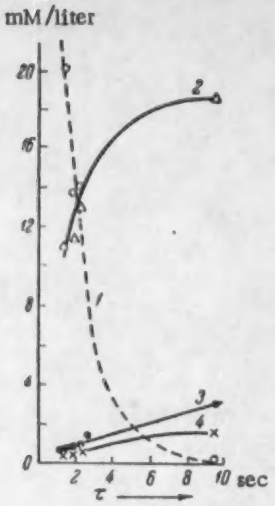

Fig. 1. The influence of the time of contact on the course of the decomposition of ethyl alcohol at a temperature of 305°. 1) Unreacted alcohol, 2) hydrogen, 3) carbonaceous material calculated as free carbon, 4) ethylene (all concentrations are given in millimoles per liter of gaseous products).

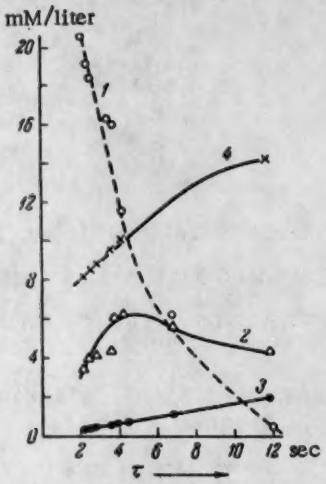

Fig. 2. The influence of the time of contact on the course of the decomposition of ethyl alcohol at a temperature of 485°. 1) Unreacted alcohol, 2) hydrogen, 3) carbonaceous material calculated as free carbon, 4) ethylene (all concentrations are given as millimoles per liter of gaseous products).

ignited at 650° in the apparatus in which the main experiments were carried out, after removal of volatile organic substances.

Preliminary experiments with acetaldehyde and ethylene labeled with C^{14} showed that the rate of formation of carbonaceous material from acetaldehyde is slightly greater than that from ethylene since the percentage transfer of radiocarbon to the carbonaceous material from acetaldehyde is 3 times that in the case of ethylene. On the basis of these data we found it possible to use the scheme illustrated below to determine the separate rates of reaction in the conversion of ethyl alcohol to carbon: the part played by ethylene in the process of carbon formation was neglected

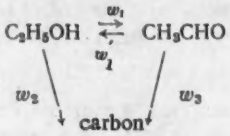

An analogous scheme has been used by A. A. Balandin et al., for the determination of the separate rates of reaction in the dehydration of ethyl alcohol on aluminosilicates [11].

As a result of the reactions taking place according to the scheme indicated, with rates w_1, w_1', w_2, and w_3, the alcohol, acetaldehyde, and carbon will have specific activities equal to α, β, and γ, respectively.

By solving the system of differential equations for the separate reaction rates and the corresponding equations for the changes in radioactivity, as described earlier [11], we obtain the following expressions for the separate rates of the process under study:

$$w_1 = \frac{d\beta}{d\tau}\,\frac{C_2}{\alpha-\beta}, \qquad (1)$$

$$w_1' = \frac{d\alpha}{d\tau}\,\frac{\alpha}{\beta-\alpha}, \qquad (2)$$

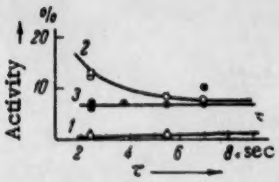

Fig. 3. The influence of the time of contact on the specific activity of the products of the decomposition of ethyl alcohol mixed with 3% of acetaldehyde labeled with C^{14}, at a temperature of 305°. 1) Unreacted alcohol, 2) acetaldehyde, 3) carbonaceous material (all specific activities are given as percentages of the original).

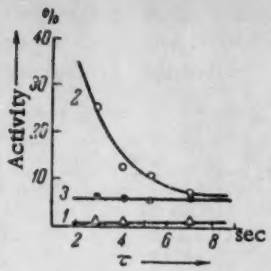

Fig. 4. The influence of the time of contact on the specific activities of the products of the decomposition of ethyl alcohol mixed with 3% of acetaldehyde labeled with C^{14}, at a temperature of 485°. 1) Unreacted alcohol, 2) acetaldehyde, 3) carbonaceous material (all specific activities are given as percentages of the original).

$$w_2 = \frac{dC_3}{d\tau} - w_3, \qquad (3)$$

$$w_3 = \frac{\frac{d\gamma}{dt} + \frac{dC_3}{d\tau}(\gamma - \alpha)}{\beta - \alpha}. \qquad (4)$$

The data for the kinetics of decomposition of ethyl alcohol at 305 and 485° without labeled acetaldehyde added are given in Figs. 1 and 2. In these figures the quantity of substance in millimoles per liter of vapor of the original alcohol is plotted on the y-axis, and an arbitrary contact time, defined as the reciprocal of the volume rate of passage of vapor, plotted on the x-axis. In the calculation of these quantities, account was taken of the change in volume (at N.T.P.) taking place during the reaction (the average of the volumes at the inlet and outlet of the reaction vessel was taken). Graphical differentiation of the data obtained gave the values of C_2 (acetaldehyde concentration) and $\frac{dC_3}{d\tau}$ (the total rate of carbon formation) necessary for the calculations using (1)-(4). The specific activity values necessary for the calculations using (1)-(4) were determined from the corresponding curves (see Figs. 3 and 4) and the derivatives found by graphical differentiation. Table 1 gives the results of the calculations using (1)-(4), expressed as mM/sec per liter of gaseous products. The use of data on the kinetics of decomposition of pure ethyl alcohol for the calculation of the radiochemical quantities obtained in experiments with a mixture of alcohol with 3% acetaldehyde is quite justifiable since we have shown [2] that small additions of acetaldehyde to alcohol do not alter the rate of carbon formation and the effect becomes appreciable only when the quantities added raise the acetaldehyde concentration above the value corresponding to the extent of conversion under the given conditions.

Comparison of the values obtained for the reaction rates for different contact times and two temperatures gave the following results. At 305°, increase in the time of contact by a factor of 4 causes the rate of formation of carbon from acetaldehyde to increase by a factor of 2; at the same time the rate of formation of carbon from alcohol and the rate of formation of acetaldehyde from alcohol decreases by a factor of 10. The ratio of the rates of formation of carbon from acetaldehyde and from alcohol increases from 0.75 to 15, i.e., increases by a factor of 20. At 485°, a similar increase in the time of contact by a factor of 4 leads to an increase in the rate of formation of carbon from acetaldehyde by a factor of 3, with a simultaneous decrease in the rate of formation of carbon from alcohol by a factor of 4 and decrease in the rate of formation of acetaldehyde from alcohol by a factor of 40. The ratio of the rates of formation of carbon from aldehyde and alcohol changes from 0.55 to 4.3, i.e., increases by a factor of 8.

This comparison, which indicates the direction of the changes in the rates of the separate reactions with increase in the time of contact and the temperature, shows that increase in the contact time leads to a decrease in the rate of conversion of alcohol to carbon and of alcohol to acetaldehyde and to an increase in the rate of

Values of the Separate Rates of the Decomposition of Ethyl Alcohol on a Dehydrogenating Catalyst at Different Temperatures and Contact Times, Obtained by the Radiochemical Method

t, sec	305°				485°			
	Rate in mM/sec · liter				Rate in mM/sec · liter			
	w_1	w_1'	w_2	w_3	w_1	w_1'	w_2	w_3
1	—	—	—	—	—	—	—	—
2	3,8	0,05	0,16	0,12	—	—	—	—
3	2,1	0,03	0,11	0,18	3,7	0,07	0,12	0,04
4	1,6	0,02	0,08	0,20	2,8	0,08	0,10	0,06
5	1,2	0,01	0,06	0,23	2,0	0,08	0,08	0,09
6	0,9	0,008	0,045	0,25	1,3	0,08	0,05	0,11
7	0,7	0,005	0,035	0,26	0,7	0,08	0,04	0,12
8	0,5	9,003	0,025	0,27	0,3	0,08	0,03	0,13
9	0,4	0,001	0,020	0,28	0,07	0,08	0,03	0,13

conversion of aldehyde to carbon, i.e., the part played by the aldehyde in the process of carbon formation increases. For example, with a contact time of 9 seconds and a temperature of 305°, 94% of the carbonaceous material is obtained from the acetaldehyde and only 6% from the alcohol. Increase in the temperature, on the other hand, leads to a decrease in the part played by acetaldehyde in the process of carbon formation. For example, at 485°, with a contact time of 9 seconds, only 82% of the carbonaceous material is obtained from acetaldehyde, and the rest is obtained from alcohol.

Thus, the radiochemical method using C^{14} has shown that, in the decomposition of ethyl alcohol on a dehydrogenating catalyst in the temperature range 300-500°, the carbonaceous material is formed chiefly from acetaldehyde. The part played by the ethyl alcohol as starting material in the process of carbon formation, increases with increase in temperature, from 6% at 305° to 18% at 485°, for a contact time of 9 seconds.

The data obtained confirm the theory, put forward by us earlier [1, 2], that acetaldehyde takes an active part in the process of low-temperature formation of carbon from ethyl alcohol, and also confirm the scheme suggested for the process of polycondensation of acetaldehyde to produce the carbonaceous material. In this scheme preliminary dehydrogenation of the alcohol is a necessary condition for the low-temperature mechanism of carbon formation.

The data obtained also confirm the accuracy of the theory that one of the methods by which high-temperature carbon formation takes place in the decomposition of ethyl alcohol is by the direct polycondensation of ethyl alcohol with unsaturated condensation products, leading to the formation of carbonaceous material. The part played by ethyl alcohol as starting material for carbon formation increases considerably with increase in the temperature.

LITERATURE CITED

[1] G. Stegner, A. A. Balandin, and A. P. Rudenko, Izvest. Akad. Nauk SSSR, Otd. Khim. Nauk 11, 1896 (1959). •

[2] G. Stegner, A. A. Balandin, and A. P. Rudenko, Izvest. Akad. Nauk SSSR, Otd. Khim. Nauk, 1, 24 (1960). •

[3] M. B. Neiman, Zhur. Fiz. Khim. 28, 1235 (1954).

[4] M. B. Neiman and A. F. Lukovnikov, Chain Reaction Oxidation of Hydrocarbons in the Gas Phase, Collection [in Russian] (Izd. AN SSSR, 1955).

[5] A. A. Balandin, M. B. Neiman, O. K. Bogdanova, G. V. Isagulyants, A. P. Shcheglova, and E. I. Popov, Izvest. Akad. Nauk SSSR, Otd. Khim. Nauk, 165 (1957). •

•Original Russian pagination. See C. B. Translation.

[6] R. W. Blue and C. J. Engle, Ind. and Eng. Chem. 43, 494 (1951).

[7] R. E. McMahn, Ing. and Eng. Chem. 47, 844 (1955).

[8] M. M. Sakharov, The Study of the Reactions Involved in Catalytic Cracking of Hydrocarbons, Using Radiocarbon C^{14}, Candidates Thesis [in Russian] (Moscow, 1955).

[9] A. A. Balandin, M. B. Neiman, O. K. Bogdanova, G. V. Isagulyants, A. P. Shcheglova, and E. I. Popov, Izv. Akad. Nauk SSSR, Otd. Khim. Nauk 270 (1957).•

[10] G. M. Zhabrova, and B. M. Kadenatsi, Problemy Kinetiki i Kataliza, 9, 187 (1957).

[11] A. A. Balandin, G. V. Isagulyants, et al., Izv. Akad. Nauk SSSR, Otd. Khim. Nauk 2, 233 (1958).•

•Original Russian pagination. See C. B. Translation.

MOLECULAR SIEVES AS ADSORBENTS OF THE 1ST STRUCTURAL TYPE

B. P. Bering, Academician M. M. Dubinin, E. G. Zhukovskaya, and V. V. Serpinskii

Physical Chemistry Institute, Academy of Sciences, USSR
Translated from Doklady Akademii Nauk SSSR, Vol. 131, No. 4, pp. 865-867, April, 1960
Original article submitted December 30, 1959

The porous crystals obtained on removal of water from natural or synthetic zeolites have for long attracted the attention of research workers. An extensive literature is devoted to the study of the adsorptive properties of these crystals. In recent years, interest in these sorbents has grown considerably in connection with their practical application, since the uniform porosity of their molecular dimensions makes it possible to achieve a very sharp separation of mixtures of substances; the mechanism of the separation process is such that it is possible, with complete justification, to call the zeolites molecular sieves. The extensive studies of Barrer and co-workers (see [1], for example) have revealed many features of the adsorptive properties of zeolites and have made it possible to make a classification of molecular sieves, based on their x-ray structural and sorptive properties.

The most important porous sorbents, from the practical viewpoint, can be arranged in order of decreasing pore size, which to a certain extent determines their sorptive properties. In this series (coarsely porous silica gels, active carbons of the second structural type, finely porous silica gels, active carbons of the first structural type, zeolites), the zeolites occupy the place furthest to the right, both as regards the size of the pores (the structural cells) and, particularly, as regards the size of the openings ("channels") leading to these holes.

In spite of the large number of attempts which have been made to carry out a theoretical analysis of adsorption phenomena, there is as yet no single theory which would make it possible to describe quantitatively the adsorption equilibrium for all these types of sorbent. Moreover, even for any individual adsorbent, none of the existing theories makes it possible to calculate beforehand the adsorption equilibrium for a given set of conditions from the known characteristics of the adsorbent and substance being adsorbed. The only exception is the potential theory of adsorption in its improved version [2], since this theory, at any rate for active carbons of the first structural type, makes it possible to solve this problem over a wide range of change in the variables, with an accuracy which is sufficient for most practical purposes.

The equation for the adsorption isotherm, derived on the basis of the potential theory [3], may be written in the following form:

$$\lg a = \lg \frac{W_0}{v} - \frac{0{,}43\ BT^2}{\beta^2} \lg^2 h, \tag{1}$$

which shows a linear relationship between the logarithm of the adsorption a and the square of the logarithm of the relative pressure $h = p/p_s$. This equation accurately describes extensive experimental material on the adsorption of different substances on active carbons of the first structural type and finely porous silicagels [4] and makes it possible to use the constants W_0 and B, determined from the adsorption isotherm for a standard

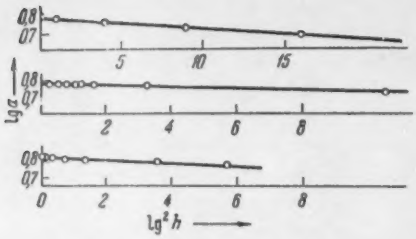

Fig. 1.

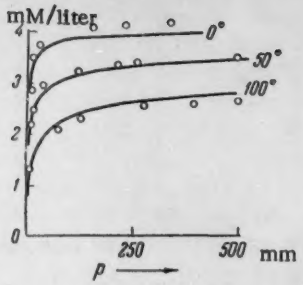

Fig. 2.

substance (for example, nitrogen at -195° or benzene at 20°), to calculate in advance, over a wide temperature range, the adsorption equilibria for other substances on the adsorbent in question from the tabulated values of the molar volume $\underline{v}$, the affinity coefficient of the characteristic curve β, and the saturated vapor pressure p_s for these substances. Since the zeolites may be regarded as the limiting member of this series of porous sorbents, we are led naturally to try to establish the extent to which Eq. (1) is applicable to the quantitative description of adsorption on zeolites. In order to examine this problem, we have represented the experimental data at our disposal (from our own work and from the literature) in the form of graphs with the coordinates of Eq. (1) and have obtained satisfactory linear relationships between log a and $\log^2 h$, as can be seen from Fig. 1. The straight line 1 gives the adsorption isotherm for nitrogen vapor at -195°, measured by the gravimetric method [5], on the molecular sieve, "Linde 5 A," and Graphs 2 and 3 represent the adsorption isotherms for nitrogen and argon, respectively on chabazite at -183°, constructed from the tabulated data given by Barrer and Robins [6]. In all three cases, (1) is obeyed over the whole of the range studied. It should be noted that the adsorption isotherms for argon on natural and calcium chabazite, measured in [7], are described by this equation only over a pressure range of three orders of magnitude (from $h \approx 1 \cdot 10^{-4}$ and above), and considerable deviations from linearity are observed in the range $h < 1 \cdot 10^{-4}$. Although we leave open the reason for these deviations, we would emphasize that in the case of such steep isotherms, the kinetics of the attainment of equilibrium are often considerably drawn-out, so that the measurements of the small equilibrium pressures in the initial section of the isotherm cannot be sufficiently reliable.

Thus, from our point of view it is possible to say that (1) can be satisfactorily applied to the adsorption of the vapor of a substance on zeolites in approximately the same range of relative pressures as in the case of adsorption on active carbons of the first structural type, at any rate for those substances whose adsorption is for the most part determined by dispersion forces. If we use curves 2 and 3 in Fig. 1 to calculate the constants W_0 and B, taking nitrogen as standard substance ($\beta = 1$) and defining β for any other substance as the ratio of the parachor of that substance to the parachor of nitrogen, then the values of W_0 for argon and for nitrogen prove to be equal to 0.192 and 0.217 cm^3/g, respectively, and the values for β, 1.47 and $1.51 \cdot 10^{-6}$, respectively (if benzene is taken as standard substance, then the values of B are 0.160 and $0.165 \cdot 10^{-6}$). In the case of nitrogen, whose critical temperature is close to the temperature of the experiment, the molar volume in the adsorbed state at -183° ($v = 35.7$ cm^3/mole) was estimated by the method described in [8]. The values for B found in this way show good agreement with one another, and the values of W_0 differ from one another by approximately 12%.

In order to judge the extent to which Eq. (1) makes it possible to calculate in advance the adsorption equilibria of other substances on zeolites from the constants W_0 and B characterizing a given W_0 adsorbent and determined from one adsorption isotherm for a standard substance and the tabulated values of the constants of the adsorbed substances, we have calculated the adsorption isotherms for methyl chloride at three temperatures, 0°, 50°, and 100° on chabazite, and have compared the calculated isotherms with the direct measurements of the adsorption of this substance on natural chabazite, given by Barrer and Brook [9]. For these calculations we took the above values $W_0 = 0.217$ cm^3/g and $B = 1.51 \cdot 10^{-6}$ determined from the adsorption isotherm for nitrogen [6], while the necessary values of the molar volume $\underline{v}$ of ethyl chloride in the adsorbed state at these temperatures was estimated by the method suggested in [8], i.e., by linear interpolation between the value of $\underline{v}$ at the boiling point and the value of the Van der Waal's constant $\underline{b}$ at the critical temperature. The affinity coefficient of the characteristic curve β was obtained from the corresponding coefficient for ethyl chloride,

with a correction for the increment in the parachor due to the CH_2-group, and the saturated vapor pressure of CH_3Cl was calculated from the tabulated data [10]. The results of the calculations carried out are shown in Fig. 2; the solid lines give the adsorption isotherms of CH_3Cl on chabazite at temperatures of 0°, 50° and 100°, the equilibrium pressures in milliliters of mercury being plotted on the x-axis, and the values of the adsorption in millimoles per gram being plotted on the y-axis. The small circles on the figure show the experimental points found by Barrer and Brook [9] at the same temperatures. For the isotherm at 50°, very good agreement is shown between the measured and calculated values of the adsorption. The experimental points at 100° lie slightly below, and those at 0°, slightly above the calculated isotherms, but the greatest deviation in either case does not exceed 5%. The agreement between the calculated and experimental values of the adsorption may even be unexpectedly good, if account is taken of the following facts: the calculation of the adsorption of CH_3Cl is made in the range 0-100° from the adsorption isotherm of N_2, measured at -183°; the method used for estimating the molar volume of the material in the adsorbed state can only be approximate; and the adsorbents used in [6, 9] may differ slightly from one another. From what has been said, it may be thought that the affinity coefficients determined from the adsorption isotherms for carbons and expressed in terms of the ratio of the parachors retain their value when applied to adsorption on zeolites.

We would also point out that our calculations of the total heat of adsorption of CH_3Cl on chabazite from the same values of W_0 and B for a = 3 mM/g, using an equation derived on the basis of the potential theory of adsorption [see [11], Eq. (7)], gave the value 11.5 kcal/mole, compared with the value 14.7 found by Barrer and Brook [9] for approximately the same value of the adsorption, using the Clausius–Clapeyron equation.

From our point of view, the results given for the preliminary calculations indicate that (1) may conveniently be applied to the study of adsorption on zeolites (in order to examine the range of their applicability and possible limitations) and also enable us to regard molecular sieves as adsorbents of the first structural type, to which it is possible to apply, to a greater or lesser extent, the methods of calculation of the potential theory developed in recent years in our laboratory.

LITERATURE CITED

[1] R. M. Barrer, The Structure and Properties of Porous Materials, L., 1958, p. 6; British Chemical Engineering 5, 1 (1959).

[2] M. M. Dubinin, Studies on the Adsorption of Gases and Vapors by Carbonaceous Adsorbents [in Russian] (Moscow, 1956).

[3] M. M. Dubinin, E. D. Zaverina, and L. V. Radushkevich, Zhur. Fiz. Khim. 21, 1351 (1947).

[4] M. M. Dubinin and A. G. Zuev, Dokl. Akad. Nauk SSSR 69, 209 (1949).

[5] B. P. Bering, M. M. Dubinin, et al., Zhur. Fiz. Khim. 31, 712 (1957).

[6] R. M. Barrer and A. B. Robins, Trans. Farad. Soc. 49, 929 (1953).

[7] L. Garden, J. Kington, and W. Laing, Trans. Farad. Soc. 51, 1558 (1955).

[8] K. M. Nikolaev and M. M. Dubinin, Izv. Akad. Nauk SSSR, Otd. Khim. Nauk No. 10, 1665 (1958).•

[9] R. M. Barrer and D. W. Brook, Trans. Farad. Soc. 49, 940 (1953).

[10] D. R. Stull, Tables of Vapor Pressures of Individual Substances [Russian translation] (IL, 1949).

[11] B. P. Bering, M. M. Dubinin, and V. V. Serpinskii, Izv. Akad. Nauk SSSR, Otd. Khim. Nauk, No. 6, 981 (1959).•

•Original Russian pagination. See C. B. Translation.

EFFECT OF TEMPERATURE AND CONCENTRATION ON THE FREQUENCY AND INTENSITY OF THE LINES IN THE RAMAN SPECTRUM OF KETONE–CHLOROFORM MIXTURES

Yu. G. Borod'ko and Corresponding Member USSR Academy of Sciences Ya. K. Syrkin

M. V. Lomonosov Moscow Fine Chemical Technology Institute
Translated from Doklady Akademii Nauk SSSR, Vol. 131, No. 4, pp. 868-871, April, 1960
Original article submitted December 30, 1959

Study of the infrared and Raman spectra of the acetone–chloroform system has shown that the frequencies of the valence vibrations of the carbonyl group and C-H group of the chloroform are the same as in the original substances. At the same time the intensity of the corresponding bands increases considerably [1-4]. The increase in intensity in this case is due to the formation of a molecular compound. From this example it can be seen that the formation of a hydrogen bond may have a considerable effect on the intensities and a smaller effect on the frequencies of the vibrations.

In order to examine the nature of the interaction, we have studied the effect of temperature on the frequencies and intensities of the lines in the Raman spectrum in the nonpolar solvent hexane and also in ketone–chloroform mixtures. With decrease in temperature, the interaction is more distinct since the thermal disorientation hindering the formation of molecular compounds is reduced. Experimental data are given below for the effect of concentration and temperature on the Raman lines corresponding to the valence vibrations of the C = O bonds of the ketones and the C-H and C-Cl bonds of the chloroform in the systems and also in the corresponding individual substances.

Tables 1 and 2 give the integral intensities $I = \int I_\nu d\nu$ expressed on an arbitrary scale where the intensity of the Raman line for the individual substance at t = + 30°C, related to one mole, is taken as 100.

The measurements were made on an ISP-51 spectrograph with photoelectric recording of the spectrum. The optical part of the temperature assembly consisted of a thermostatically controlled cell. The necessary temperature was attained by evaporating liquid nitrogen. When measuring the intensities at different temperatures, it was necessary to take account of the change in the ratio n^2/d, where n is the refractive index and d is the density. In our experiments the greatest change in this quantity in the temperature range from + 30° to - 90° amounted to approximately 4%. The error in the measurement of the intensities amounted to 10%, and that in the measurement of the frequencies, to ± 2 cm^{-1}. The temperature between + 30° and - 30° was measured with an error of 1°. The errors in the measurements of lower temperatures did not exceed 3°.

The experiments showed that the intensity of the C = O and C-H lines increases in the ketone + chloroform system and decreases in solutions of these substances in hexane. The intensity of the C-Cl lines in both cases remains practically unchanged (Fig. 1). The fact that the frequency and intensity of the C-Cl lines remain unchanged indicates that the intermolecular interaction affects mainly the C = O bonds of the ketone and the C-H bonds of the chloroform. The picture of hydrogen-bond formation is complicated by the fact that the ketones are extensively associated at room temperature and are apparently partly dimerized. This is confirmed

TABLE 1

Effect of Concentration on the Frequencies and Intensities

Acetone concentration [C], mole/liter	Acetone + chloroform		Acetone + hexane		Acetophenone concentration [C], mole/liter	Acetone + chloroform		Acetone + hexane		Chloroform concentration [C], mole/liter	Chloroform + acetone		Chloroform + acetone		Chloroform + hexane			
	$\Delta\nu_{C=O}$	$I_{C=O}$	$\Delta\nu_{C=O}$	$I_{C=O}$		$\Delta\nu_{C=O}$	$I_{C=O}$	$\Delta\nu_{C=O}$	$I_{C=O}$		$\Delta\nu_{C-H}$	I_{C-H}	$\Delta\nu_{C-Cl}$	I_{C-Cl}	$\Delta\nu_{C-H}$	I_{C-H}	$\Delta\nu_{C-Cl}$	I_{C-Cl}
13.6	1708	100	1708	100	8.5	1682	100	1682	100	12.5	3019	100	667	100	3019	100	667	100
6.8	1709	131	1712	91	4.3	1682	116			6.7					3019	87	668	95
5.5	1711	137	1714	85	4.0			1686	106	6.2	3018	127	667	97				
4.2	1712	155			2.0	1681	139											
2.3	1713	158			1.3			1691	115	4.0	3018	140	667	104				
2.1			1716	74	1.1	1681	149			3.8								
					0.7			1693	118	3.6					3019	78		
					0.3	1680	170			2.7	3017	148	667	103			669	99
										1.9								
										1.8	3016	158	667	101			669	101

TABLE 2

Effect of Temperature on the Frequencies and Intensities

t, °C	Acetone + chloroform				Acetone + hexane		Acetone		Diethyl ketone + chloroform		Acetophenone + chloroform				Acetophenone + hexane		Benzophenone + chloroform		Chloroform	
	acetone 7 mole/liter		chloroform 6.2 mole/liter		acetone 7.5 mole/liter		13.6 mole/liter		diethyl ketone 4.8 mole/liter		acetophenone 2.5 mole/liter		chloroform 9 mole/liter		acetophenone 0.7 mole/liter		benzophenone 3.2 mole/liter		12.5 mole/liter	
	$\Delta\nu_{C=O}$	$I_{C=O}$	$\Delta\nu_{C-H}$	I_{C-H}	$\Delta\nu_{C=O}$	$I_{C=O}$	$\Delta\nu_{C=O}$	$I_{C=O}$	$\Delta\nu_{C=O}$	$I_{C=O}$	$\Delta\nu_{C=O}$	$I_{C=O}$	$\Delta\nu_{C-H}$	I_{C-H}	$\Delta\nu_{C=O}$	$I_{C=O}$	$\Delta\nu_{C=O}$	$I_{C=O}$	$\Delta\nu_{C-H}$	I_{C-H}
+30	1708	133	3019	108	1712	94	1708	100	1711	123	1681	133	3019	120	1693	118	1656	131	3019	100
0		151														123				
−10				123				119				156				128	1655	170	3019	117
−20	1705	172	3016		1709	109	1705	128			1677	157			1691	129				
−30				138				134			1675	166	3015	145			1653	173	3019	123
−40											1674	168								
−50	1703	188	3014	145	1705	125	1703	143	1707	146	1672	185	3013	163			1652	203	3019	130
−60																			3019	140
−70	1700	206	3012	165	1703		1700	154		160							1650	226		
−90	1698	222	3010				1699	167	1703	196										

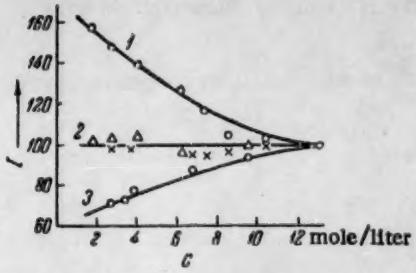

Fig. 1. Effect of concentration on the intensity of the chloroform lines: 1) Intensity of the C-H line (3019 cm^{-1}) in acetone solution; 2) intensity of the C-Cl line (667 cm^{-1}) in solutions of acetone and hexane; 3) intensity of the C-H line (3019 cm^{-1}) in hexane solution.

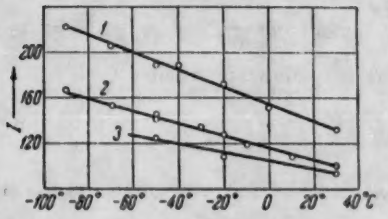

Fig. 2. Effect of temperature on the intensity of the acetone line (1708 cm^{-1}): 1) In chloroform solution (6.5 mole/liter); 2) pure acetone; 3) in hexane solution (7.5 mole/liter).

by the increase in the frequency of vibration of the carbonyl group of the ketones in hexane, with breakdown of the ketone dimers, which are probably associated in the form of quadrupoles

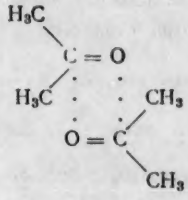

This suggestion agrees with experiments on the dielectric polarization of acetone solutions, which varies from 160 cm^3 in extremely dilute solutions in nonpolar solvents to $\simeq$ 40 cm^3 in pure liquid acetone [5]. In the presence of $CHCl_3$, the frequency of the vibrations of the carbonyl group does not change, in spite of the fact that chloroform leads to breakdown of the dimers. This is possibly explained by the fact that breakdown of the dimers is accompanied by formation of a molecular compound with chloroform, the frequencies of the vibrations of the carbonyl group in the dimers and in the molecular compound being very close. Another reason for the fact that no change takes place in the frequencies is the relatively small concentration of complexes at room temperature Thus, when the temperature is lowered to −90°, the frequency of the vibrations of the C−H bond of the chloroform $\Delta\nu$ = 3019 cm^{-1} in the acetone−chloroform system decreases to 3010 cm^{-1}, whereas in pure chloroform it remains unchanged as far as the freezing point.

The change in the intensity of the lines for the carbonyl group in liquid acetone, in a solution of acetone in hexane, and in a mixture of acetone and chloroform, with change in temperature, is shown in Fig. 2.

The intensity of the lines of the carbonyl bond and the C-H of the chloroform is made up of the intensity of the lines of the isolated molecules (I_m) and molecules associated in the complex (I_c), and $I_c > I_m$. It is possible to estimate the enthalpy of formation (ΔH) of the molecular compound of acetone + chloroform from the change in the integral intensity of the chloroform line of frequency 3019 cm^{-1} with change in temperature. If it is assumed that the intensity of the 3019 cm^{-1} line for chloroform at a given temperature is made up of the intensity of the lines of the monomeric molecules and molecules associated in the complex, which are not separated, then

$$I_t = \left[I_m + (I_c - I_m)\frac{C_c}{C_0^{chl}}\right]\left(\frac{1}{1 - e^{-h\nu/kT}}\right),$$

where I_t is the intensity of the line at a given temperature; I_m is the intensity of the 3019 cm^{-1} line in hexane,

extrapolated to infinite dilution; I_c is the intensity of the 3019 cm^{-1} line in acetone, extrapolated to infinite dilution; C_c is the concentration of the molecular compound; and $C_{0\ chl}$ is the initial chloroform concentration.

The factor $\frac{1}{1-e^{-h\nu/kt}}$ for $\Delta\nu = 3019\ cm^{-1}$ remains practically constant within the temperature range studied. We may therefore, assume that

$$I_t = I_m + (I_c - I_m)\frac{C_c}{C_{0\ chl}}.$$

We have used the experimental data to calculate the equilibrium constants for the reaction

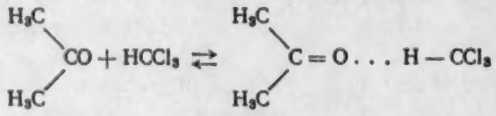

at the temperatures 301, 263, and 243° K and have obtained the values 0.2, 0.44, and 0.75 liter/mole. From these quantities we have found the enthalpy and entropy of the reaction: $\Delta H \simeq -3350$ cal/mole, and $\Delta S = -14.3$ eu. According to Moelwyn-Hughes data from the vapor pressures [6], $\Delta H = -4070$ cal/mole, and according to Pimentel's data obtained from proton magnetic resonance, $\Delta H = -2500$ cal/mole [7]. The values which we have found lie between these values. The standard free energy of formation of the molecular compound is 910 cal/mole. This explains its instability at high temperatures.

LITERATURE CITED

[1] H. W. Thompson and D. J. Jewelle, Sp. Acta 13, 3, 254 (1958).

[2] L. J. Bellamy and R. L. Williams, Trans. Farad. Soc. 55, 1, 16 (1959).

[3] P. P. Shorygin, Zhur. Fiz. Khim. 23, 873 (1949).

[4] V. M. Chulanovskii, Izvest. Akad. Nauk SSSR Ser. Fiz. 22, 9, 1103 (1958).•

[5] Ya. K. Syrkin and A. N. Shidlovskaya, Zhur. Fiz. Khim. 22, 8, 913 (1948).

[6] E. A. Moelwyn-Hughes and A. Sherman, J. Chem. Soc. 101 (1936).

[7] G. C. Pimentel and C. M. Huggins, J. Chem. Phys. 23, 7, 244 (1955).

•Original Russian pagination. See C. B. Translation.

THE EQUILIBRIUM BETWEEN STRONTIUM MOLYBDATE AND HYDROGEN AND THE THERMODYNAMIC CHARACTERISTICS OF $SrMoO_4$

L. A. Zharkova, V. I. Lavrent'ev, Corresponding Member Acad. Sci. USSR Ya. I. Gerasimov, T. N. Rezukhina, and Yu. P. Simanov

M. V. Lomonosov Moscow State University

Translated from Doklady Akademii Nauk SSSR, Vol. 131, No. 4, pp. 872-875, April, 1960
Original article submitted December 17, 1959

The equilibrium for the reduction of strontium molybdate by hydrogen has been studied in the temperature range 950-1392°C. We have used a circulation method, which makes it possible to avoid the effect of thermal diffusion and at the same time to increase the rate at which equilibrium is reached. Two versions of the apparatus were used; the measurements were made in the first up to 1122° and in the second from 1122° upwards. Assemblies analogous to the first version of our apparatus have been described in earlier papers [1-6]. In the second version of our apparatus, we used a small short-circuited molybdenum heater H (Fig. 1) placed inside a quartz vessel P. The outside of the reaction vessel was cooled with water and remained cold during the operation of the heater. The heater was operated using a low voltage current (5-15 v) supplied via brass electrodes E cooled internally with water. The boat was attached to a platinum capillary K_1, through which the H_2 + + H_2O gas mixture passed into the reaction zone. The boat and thermocouple T were introduced into the heater via the ground joint S_1 in the side of the vessel, the hot junction of the thermocouple being kept in contact with the wall of the boat. A semipermeable palladium membrane M was introduced into the heater from the other side via the ground joint S_2 to measure the partial pressure of hydrogen in the heated zone. The membrane consisted of a palladium plate of thickness 0.1 mm forming the foot of a platinum tube K_2, of diameter 3 mm. The membrane was tested beforehand for leaks and the rate of diffusion of hydrogen at t = 1200° K checked. The method of introducing the current leads was borrowed from [7].

The temperature of the heater was kept constant with an accuracy of ± 1-3°. The platinum–platinorhodium thermocouple was calibrated beforehand from the melting points of chemically pure metals and salts. The hydrogen for the reduction was prepared by the electrolysis of 20% NaOH solution using nickel electrodes, purified from oxygen over palladized silicagel, and dried over $CaCl_2$ and P_2O_5. The aqueous vapor pressure in both versions was given by the temperature of a saturator with water, placed in a Dewar vessel with finely ground ice. The equilibrium constant was calculated from the formula

$$K_e = \frac{p_{H_2O}}{p_{H_2}}.$$

The total pressure in the system was measured using a mercury manometer with an accuracy of ± 0.1 mm.

The strontium molybdate was prepared by precipitation from a solution of Na_2MoO_4 with the stoichiometric quantity of $Sr(NO_3)_2$ solution. The original analytically pure salts were purified by recrystallization. The $SrMoO_4$ obtained was washed thoroughly, dried, and ignited at 1000-1100°. The material was analyzed as described by Hillebrand and Lundell [8] with an error of 0.5%; the results confirmed the composition $SrMoO_4$. The gross

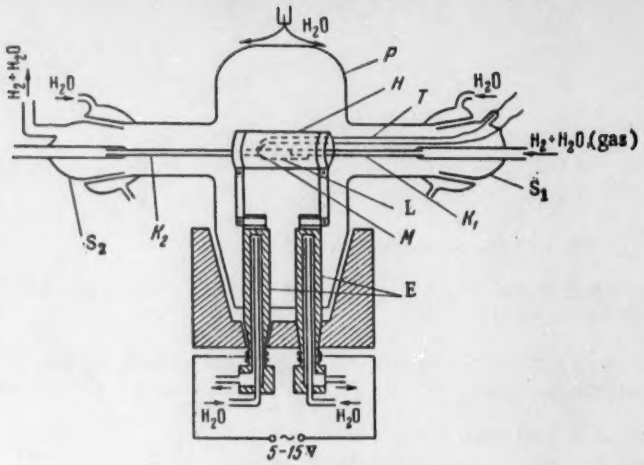

Fig. 1. Diagram of the apparatus.

composition of the reduction products was obtained from the loss in weight of the specimen. The phase composition was determined from an x-ray structural study by the Debye method using a camera with D= 86 mm and a an iron anode.

It should be noted that the high-temperature apparatus described in the present work shows certain improvements compared with the initial version described in [9]. These improvements (the semipermeable membrane and the inlet platinum capillary) were made necessary by the lack of agreement between the data obtained on the first version of the high-temperature apparatus (without input capillary and membrane) and on the apparatus with an ordinary heater. At the same time it has been reported in the literature [10] that, when the heating zone is small and the temperature gradient with the surrounding medium is large, distortion of the results is possible as a consequence of thermal diffusion, in spite of the circulation conditions. If the gas mixture is preheated, the cooling of the boat and contents by a current of colder gas is reduced. Experiments carried out with the semipermeable palladium membrane enabled us to draw the following conclusions. When the inlet platinum capillary is not used, thermal diffusion takes place and the data obtained without the capillary are too high, as can be clearly seen from Fig. 3. The presence of the inlet platinum capillary ensures preheating of the gas mixture and suppresses thermal diffusion completely. The data obtained on the high-temperature apparatus with inlet platinum capillary show good agreement with the data obtained on the ordinary apparatus (up to 1100°).

The reduction of strontium molybdate proceeds in two stages:

$$SrMoO_4 + H_2 = SrMoO_3 + H_2O, \qquad (I)$$

$$^1/_2\,SrMoO_3 + H_2 = {}^1/_2SrO + {}^1/_2Mo + H_2O. \qquad (II)$$

The first stage of the reduction yields a compound of tetravalent molybdenum $SrMoO_3$ with the perovskite structure. We have determined the lattice constant for this compound and obtained the value a = 3.968 A, which is in good agreement with the data of Sholder and Brixner [11]. Table 1 and Fig. 2 show the relationship between the equilibrium constant and the gross composition of the reduction products.

Table 2 and Fig. 3 show the relationship between the equilibrium constant and temperature for the first and second stages of the reduction of $SrMoO_4$.

The following equations were obtained by the method of least squares:

$$\lg K_{pI} = -\frac{3152{,}3}{T} + 1{,}6770\ (\pm 3\%),$$

$$\lg K_{pII} = -\frac{3506{,}5}{T} + 0{,}8762\,(\pm 3\%).$$

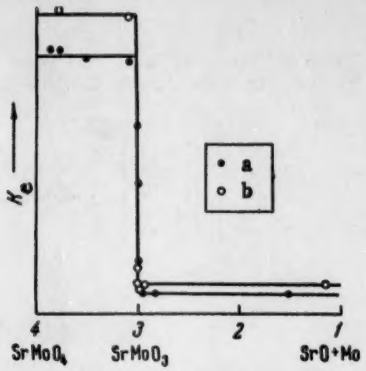

Fig. 2. Isotherms for the reduction of $SrMoO_4$ for the temperatures: a) 994°, b) 1037°.

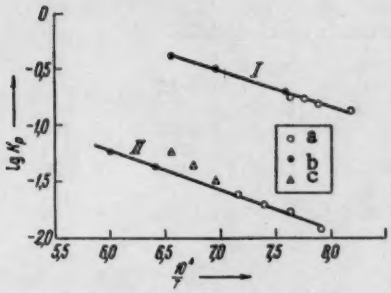

Fig. 3. Polytherms for the reduction of $SrMoO_4$ I) 1st stage of the reduction, II) 2nd stage of the reduction. Experimental points: a) obtained on the ordinary apparatus, b) obtained on the high-temperature apparatus with inlet platinum capillary, c) obtained on the high-temperature apparatus without capillary.

TABLE 1

Gross chemical composition of the specimen	K_p=994°	K_p=1037°	Gross chemical composition of the specimen	K_p=994°	K_p=1037°
$SrMoO_{3,9}$	0,157		$SrMoO_3$	0,0314	
$SrMoO_{3,8}$	0,156	0,180	$SrMoO_{2,95}$	0,0123	0,0168
$SrMoO_{3,5}$	0,148		$SrMoO_{2,9}$	0,0117	
$SrMoO_{3,05}$	0,147	0,175	$SrMoO_{1,5}$	0,0116	
$SrMoO_3$	0,111	0,0279	$SrMoO_{1,1}$		0,0169
$SrMoO_3$	0,0763	0,0186			

By combining these equations, we obtain for the complete reduction of $SrMoO_4$:

$$SrMoO_4 + 3H_2 = SrO + Mo + 3H_2O, \qquad \text{(III)}$$

$$\lg K_{pIII} = \lg K_{pI} + 2\lg K_{pII} = -\frac{10165,3}{T} + 3,4293,$$

from which

$$\Delta Z^0_{III} = 46516 - 15,6925\ T.$$

Using for the reaction of water vapor formation

$$H_2 + {}^1/_2O_2 = H_2O \qquad \text{(IV)}$$

an equation equivalent to the Chipman equation [12] in the temperature range 1000-1600° K

$$\Delta Z^0_{IV} = -59564 + 13,44\ T,$$

TABLE 2

First stage		Second stage	
t, °C	$K_{e\ av}$	t, °C	$K_{e\ av}$
950	0,131		
994	0,150	994	0,0119
1015	0,168		
		1037	0,0169
		1080	0,0194
1037	0,177	1122	0,0236
1164	0,318	1284	0,0423
1248	0,405	1392	0,0575

TABLE 3

Temp., °C	$\Delta Z°_{III}$, cal/mole	$\Delta Z°_{V}$, cal/mole	$\Delta H°_{V}$, cal/mole
1200	27680	158010	225210
1300	26120	152410	
1400	24550	146975	
1500	22980	141190	
1600	21410	135590	

we obtain for the formation of $SrMoO_4$:

$$SrO + Mo + {}^3/_2O = SrMoO_4,$$
$$\Delta Z^0_V = 3\Delta Z^0_{IV} - \Delta Z^0_{III}. \qquad (V)$$

The calculated values of ΔZ^0_{III}, ΔZ^0_V and the average thermal effect of reaction (V) for the temperature of the experiment are given in Table 3. Taking account of the relationship between the heat capacities of the materials taking part in reaction (V) and the temperature

$$C_{pSrMoO_4} = 25{,}2086 + 14{,}3195 \cdot 10^{-3} T \quad [13]$$
$$C_{pSrO} = 10{,}49 + 3{,}2 \cdot 10^{-3} T \quad [14]$$
$$C_{pMo} = 5{,}81 + 1{,}15 \cdot 10^{-3} T - \frac{0{,}347}{T^2} \cdot 10^5 \quad [15]$$
$$C_{pO_2} = 7{,}52 + 0{,}81 \cdot 10^{-3} T - \frac{0{,}9}{T^2} \cdot 10^5 \quad [15]$$

we obtain the following equation for ΔZ°_T, using the method of Temkin and Shvartsman [16]:

$$\Delta Z^0_T = -231138 + 62{,}86\ T - T(M_0\Delta a + M_1\Delta b + M_{-2}\Delta c'),$$

from which $\Delta H^0_{298} = 231.14$ kcal/mole; $\Delta S^0_{298} = -62.86$ cal/mole deg, and $\Delta Z^0_{298} = -212.39$ kcal/mole.

The maximum error in the calculation of ΔZ^0_V does not exceed 0.13% compared with the data in Table 3.

Taking the entropies of the substances taking part in the reaction as SrO: $S^0_{298} = 12.5$ [16]; Mo: $S^0_{298} = 6.83$ [15] $3/2O_2$: S^0_{298} 75.50 [15], and taking ΔH^0_{298} and ΔZ^0_{298} for SrO as -141.1 kcal/mole and -133.8 kcal/mole respectively [18], we obtain for $SrMoO_4$ $S^0_{298} = 29.97$ cal/mole · deg, $\Delta Z^0_{298} = -346.2$ kcal mole and $\Delta H^0_{298} = -372.2$ kcal mole. In view of the absence of heat capacity data for $SrMoO_3$, we have had to restrict ourselves to the calculation of the thermodynamic characteristics of $SrMoO_3$ at 1273° K: $\Delta Z^0_{1273} = -211.8$ kcal/mole $\Delta H^0_{1273} = -279.6$ kcal mole, and $S^\circ_{1273} = 72.65$ cal mole · deg.

LITERATURE CITED

[1] T. N. Rezukhina, Ya. I. Gerasimov, and Yu. P. Simanov, Vestnik Moskovsk. Univ. 6, 103 (1949).

[2] T. N. Rezukhina, Ya. I. Gerasimov, and V. A. Morozova, Zhur. Fiz. Khim. 25, 93 (1951).

[3] T. N. Rezukhina, Yu. P. Simanov, and Ya. I. Gerasimov, Zhur. Fiz. Khim. 25, 305 (1951).

[4] I. A. Vasil'eva, Ya. I. Gerasimov, and Yu. P. Simanov, Zhur. Fiz. Khim. 31, 682 (1957).

[5] I. A. Vasil'eva, Ya. I. Gerasimov, et al., Zhur. Fiz. Khim. 31, 825 (1957).

[6] T. N. Rezukhina, T. M. Dugacheva, and Yu. P. Simanov, Zhur. Fiz. Khim. 31, 2206 (1957).

[7] E. I. Smagina, V. S. Kutsev, and B. F. Ormont, Zavodskaya Laboratoriya, 22, 1249 (1956).

[8] W. Hillebrand and G. Lundell, Applied Inorganic Analysis [Russian translation] (Moscow, 1957).

[9] Ya. I. Gerasimov, T. N. Rezukhina, et al., Vestnik Moskovsk. Univ. 4, 185 (1957).

[10] J. Chipman and M. G. Fontana, J. Am. Chem. Soc., 56, 2011 (1934).

[11] R. Sholder, and L. Brixner, Zs. Naturforsch. 106, 3, 178 (1955).

[12] J. Chipman, Trans. Am. Soc. Metals. 22, 385 (1934).

[13] L A. Zharkova and T. N. Rezukhina, Zhur. Fiz. Khim. 32, 2233 (1958).

[14] H. Wartenberg and B. Schütte, Zs. anorg. Chem. 211, 1569 (1946).

[15] K. P. Mishchenko and A. A. Ravdel' (Editors) Short Hand Book of Physicochemical Quantities [in Russian] (Leningrad, 1957).

[16] M. I. Temkin and L. A. Shvartsman, Uspekhi Khimii 17, 259 (1948).

[17] O. Kubashewski, Trans. Farad. Soc. 45, 931 (1949).

[18] Selected Values of Chemical Thermodynamic Properties, Circ. NBS, 500, 1952.

THE THEORY OF FLAME PROPAGATION IN SYSTEMS WITH BRANCHED CHAIN REACTIONS

L. A. Lovachev

Chemical Physics Institute, Academy of Sciences, USSR
(Presented by Academician V. N. Kondrat'ev, December 14, 1959)
Translated from Doklady Akademii Nauk SSSR, Vol. 131, No. 4, pp. 876-879, April, 1960
Original article submitted December 8, 1959

Giddings and Hirschfelder [1] have carried out a numerical integration of a system of differential equations describing the process of propagation of a laminar flame during a branched chain reaction, which was represented by a model reaction with one active center and included two processes: $2P \rightarrow A$ (quadratic chain rupture) and $P + A \rightarrow C + 2P$ (the process of chain growth and branching).

A general solution of the problem of flame propagation for the case of a one-center model reaction has been given in [2], where relatively simple formulas for determining the rate of propagation of the flame, taking account of the effect of branching and the quadratic rupture of the chains, were derived for reactions of the degenerately branched type. According to the data given in [2], it is possible to obtain an approximate formula corresponding to the reaction scheme assumed in [1] and to determine the discrepancy between the value of the rate of flame propagation given by this formula and the results obtained by numerical integration [1], as has been done for cases with nonbranched reactions [3-5].

The reaction scheme in which A is the original substance, P the active center, and C the reaction product is written, in accordance with [2], in the form

$A \rightarrow 2P$ (initiation	$Q_R = h_R R(T')$;
$P + A \rightarrow 2C + P$ (growth)	$Qn = hFn = hK(T')\, n_A n$;
$P + A \rightarrow C + 2P$ (branching)	$Q_V n = hVn = h_V K_V(T')\, n_A n$;
($P \rightarrow$ linear rupture)	
$2P \rightarrow A$ (quadratic rupture)	$Q_W n^2 = h_W W(T')\, n^2$ *;

Expressions for the rates of evolution (or absorption) of heat are given on the right. Here h_i is the thermal effect of the reaction (cal/mole); K_i and W the rate constants of the reactions ($g^2/cm^3 \cdot$ mole $\cdot$ sec); R the rate of chain initiation 3 (mole/$cm^3 \cdot$ sec); $\underline{n}$ the concentration of P (mole/g mixture); n_A is the concentration of A (mole/g mixture); and T the temperature (°K). It is assumed, in accordance with [2-5], that $R = R(T')$ and $F = F(T')$.

The rate of propagation of the flame u_0, according to [2], will be defined by the relationship

$$u_0 = \frac{1}{\rho_0}\eta\rho_*,$$

*W is the rate constant of the consumption of P.

where $\underset{\cdot}{p}$ is found from the equation

$$p_{\cdot}^{6}\eta A_1 - p_{\cdot}^{4}(\eta^2 A_2 + \eta A_3 + A_5) - p_{\cdot}^{2}(\eta A_4 - A_6 - \eta A_7 + A_8) + A_9 = 0, \tag{2}$$

whose coefficients are calculated from the formulas:

$$A_1 = 4cD_m^2 h_W, \tag{3}$$
$$A_2 = (c + lh_W)^2 r^2 W_m, \tag{4}$$
$$A_3 = 2D_m r\,[(c - lh_W)\,Q_{\Sigma m} + 2cV_m h_W - t\,(c + lh_W)\,Q_{Wm}], \tag{5}$$
$$A_4 = r^2\,[lQ_{\Sigma m}^2 - V_m\,(c - lh_W)\,Q_{\Sigma m} - cV_m h_W], \tag{6}$$
$$A_5 = 4D_m^2\,(t^2 Q_{Wm} + Q_{Rm} + tQ_{\Sigma m})\,h_W, \tag{7}$$
$$A_6 = 2D_m tr\,(Q_{\Sigma m} + V_m h_W)\,Q_{\Sigma m}, \tag{8}$$
$$A_7 = 2r^2\,(c + lh_W)\,(R_m h_W + Q_{Rm})\,W_m, \tag{9}$$
$$A_8 = 2D_m r\,[(R_m h_W - Q_{Rm})\,Q_{\Sigma m} + 2t\,(R_m h_W + Q_{Rm})\,Q_{Wm} - 2V_m h_W Q_{Rm}], \tag{10}$$
$$A_9 = r^2\,[(Q_{\Sigma m} R_m + V_m h_W R_m - V_m Q_{Rm})\,Q_{\Sigma m} - Q_{Rm}^2 W_m - (V_m^2 Q_{Rm} + 2W_m R_m Q_{Rm} + Q_{Wm} R_m^2)\,h_W]. \tag{11}$$

In (1)-(11) the following symbols are used: ρ is the density (g/cm^3); c the heat capacity (cal/g · deg C); D_p the diffusion coefficient of the active center P (cm^2/sec); λ the thermal conductivity of the mixture (cal/cm · sec · deg C); $D = \rho D_p$; $T = T' - T_0'$; $t = T_m\,(T_c - T_m)$; $T_m = 0.5\,T_c$; $Q_\Sigma = Q + Q_V$; $l = \frac{n_c - n_0}{T_c}$; $t = n_0 + l\,T_m$ and $\eta = \frac{4\lambda_0}{c_0 T_m}$. The subscript 0 refers to the initial state of the fresh mixture ($T' = 0$), the subscript c to the state at the combustion temperature ($T' = T_c'$), and the subscript m to the state corresponding to the maximum value of the temperature gradient ($T' = T_m'$).

In [2] the rate of quadratic chain rupture was assumed to be given by the expression $W(n^2 - n_t^2)$, which became zero when $T' = T_c'$. This was unnecessary, since it was there assumed, on the basis of the scheme previously accepted [3], that $R(T_c') = 0$. Here it is assumed that $R(T_c') = W(T_c')n_c^2$, so that there is no need in this notation for the rate of quadratic rupture of the chains.

For systems with branched reactions, the relations (1)-(11) may be simplified if it is assumed that the initial and final concentrations of the active center are zero ($n_0 \cong n_c \cong 0$, i.e., $l \cong t \cong 0$). Even in this form, however, the expressions for A_i remain complex. It has previously been shown [3-5] that, for ordinary rates of chain initiation, their influence on the value of the rate of propagation of the flame is small. The same conclusions may be reached on the basis of the relationships derived in [2, 6]. Thus assuming that $R_m \cong 0$ (so that $Q_{Rm} \cong 0$), we obtain instead of (2)-(11) the new formulas ($A'_5 = A'_6 = A'_7 = A'_8 = A'_9 = 0$):

$$p_{\cdot}^{4}A_1' - p_{\cdot}^{2}\,(\eta A_2' + A_3') - A_4' = 0, \tag{2'}$$

where

$$A_1' = 4D_m^2 h_W,$$
$$A_2' = cr^2 W_m,$$
$$A_3' = 2D_m r\,(Q_{\Sigma m} + 2V_m h_W),$$
$$A_4' = -r^2\,(Q_{\Sigma m} + V_m h_W)\,V_m.$$

From (2') we obtain an expression for the determination of p_*:

$$p_*^2 = \frac{(\eta A_2' + A_3')}{2A_1'}\left[1 - \sqrt{1 + \frac{4A_1'A_4'}{(\eta A_2' + A_3')^2}}\right]. \tag{12}$$

The fraction under the root in (12) is always less than unity (this condition is also observed when $W_m = 0$). By expanding the root in (12) into a series and retaining the first two terms, we find an approximate value of p_*, and substitution of this value in (1) gives an expression for determining the rate of propagation of the flame with the condition that $n_0 = n_c = R_m = 0$:

$$u_0 = \eta \frac{1}{\rho_0} \sqrt{\frac{r(Q_{\Sigma m} + V_m h_W) V_m}{\eta c_m r W_m + 2D_m (Q_{\Sigma m} + 2V_m h_W)}}. \tag{13}$$

If in (13) we put $F_m = 0$, i.e., if it is assumed that a completely branched reaction is taking place, then we obtain the expression

$$u_0 = \frac{4\lambda_0}{\rho_0 c_0} \sqrt{\frac{c_0 (h_V + h_W) V_m^2}{2\lambda_0 c_m T_G W_m + 2c_0 D_m (h_V + 2h_W) V_m}}, \tag{14}$$

which corresponds to the simplification of the reaction scheme adopted in [1], consisting of only two processes: $2P \rightarrow A$ and $P + A \rightarrow C + 2P$.

The expression (14) was used to calculate the values of the rates of flame propagation for three cases, for which in [1] the values of u_0 were determined by numerical integration of the corresponding system of equations. The calculations were carried out using starting data taken from [1]. The results of the calculations are given in Table 1.

The data given in the Table illustrate the good agreement between the values of the rate of flame propagation, calculated from the approximate relationship (14), and the values obtained by numerical integration [1].

Rates of Flame Propagation (cm/sec)

	$k = C_0 P_0 D_{p0} / \lambda_0$		
	1	2	3
Numerical integration [1]	55.1	54.8	58.3
From expression (14)	59.7	58.5	60.9

This confirms the accuracy of the expression (14) and makes it possible to use it for the determination of the experimental values of the rate constants of the unit processes for branched chain reactions from the relationship between the rate of propagation of the flame and the temperature.

An approximate expression has been obtained in [6] for the determination of the rate of flame propagation in the combustion of hydrogen by a branched chain reaction involving three forms of active center:

$$u_0 = \frac{4\lambda_0}{\rho_0 c_0} \sqrt{\frac{K_{2m}^0 n_{Bm} \rho_m}{D_{p2m}}}, \tag{15}$$

where K_2^0 (cm^3/mole · sec) is the rate constant of the process $H + O_2 \rightarrow OH + O$; n_B (mole/g mixture) the concentration of O_2; and D_{p2} (cm^2/sec) the diffusion coefficient of the hydrogen atoms.

If in Eq. (14) we put $W_m \cong 0$ and $h_w \cong 0$, we obtain a relationship corresponding to Eq. (15), which was obtained in [6] for the condition that $W_m = 0$. With a solution of Eq. (14) for the model reaction scheme, but taking account of quadratic chain rupture, it is possible to estimate the influence of quadratic chain rupture using Eq. (15).

It has been pointed out [2] that (15) was not confirmed by comparison with data obtained by numerical integration. The data given in Table 1 can be used for this comparison and make it possible to use (15) to determine the experimental value of K_2^0 given in [2].

It has been established in [1] (Table) that a marked change in the diffusion coefficient of the active center, other conditions being equal, does not lead to an appreciable change in the rate of flame propagation, while the latter decreases as D_p increases. The relationship (14) makes it possible to explain this change in u_0. In the numerical integration [1] an extremely high value was taken for the rate constant of quadratic chain rupture, for which the first term in the denominator of expression (14) is approximately 10-20 times the second. The calculated value of u_0 is therefore almost independent of D_p.

The authors of [2], using data from [7], gave the experimental ratio of the rates of flame propagation for two mixtures ($0.21H_2+0.11O_2$), one of which contained 0.68 A and the other 0.68 He. This ratio $(u_0)_{He}/(u_0)A = 2.40$. The same ratio calculated using the expression (15) was found to be equal to 2.85. From (14) it follows that if the first term in the denominator under the root is much greater than the second, then u_0 is proportional to the square root of the thermal conductivity, $u_0 \sim \sqrt{\lambda_0}$, and is practically independent of the quantity D_{Pm}. In this case, when argon is replaced by helium, we should have $(u_0)_{He}/(u_0)_A = \sqrt{\lambda_{He}/\lambda_A} = 1.94$. The experimental ratio lies between 1.94 and 2.85. From this it apparently follows that in this case, quadratic chain rupture plays a significant part, and it is possible to solve the opposite problem—to determine the experimental value of the rate constant for quadratic chain rupture from the ratio 2.40. If the denominator under the root in (14) is written in the form $(C_1\lambda_0 + C_2D_{Pm})$, where C_1 and C_2 are independent of λ_0 and D_{Pm} and equal in magnitude for the mixture with argon and the mixture with helium, then when $\lambda_{He}/\lambda_A = 3.76$, $(D_p)_{He}/(D_p)_A = 1.74$ and $(u_0)_{He}/(u_0)_A = 2.40$ [7], the ratio $(C_1\lambda_0/C_2D_{Pm})_A$ for the mixture with argon, calculated using (14), is equal to 0.52. This also shows that the influence of quadratic chain rupture is considerable.

In order to find C_1 and C_2 and calculate the rate constant for quadratic chain rupture with ternary collisions $K_{Wm} = W_m\mu_m/\rho_m^3$, it is necessary to know all the quantities present in (14). When $(C_1\lambda_0/C_2D_{Pm})_A = 0.52$, however, the calculation of K_{Wm} can only be roughly approximate. For $C_1\lambda_0 > C_2D_{Pm}$, such calculation would be much more accurate, but for this it would be necessary to determine $(u_0)_{He}/(u_0)_A$ at a lower temperatures, at which the effect of quadratic chain rupture should be much more marked than at temperatures of 2200-2400°K.

Since the estimation of the quantity K_{Wm} is approximate, its calculation for the above mixtures was carried out without calculating the combustion temperature and all the other parameters. All the quantities necessary for the calculation were taken from the data given in [6] for a mixture containing $0.43H_2 + 0.57$ air. It was found that $K_{Wm} \cong 10^{17}$ cm^6/mole^2 · sec.

LITERATURE CITED

[1] J. C. Giddings and J. O. Hirschfelder, Sixth Symposium on Combustion (N. Y., 1956), p. 199.

[2] L. A. Lovachev, Dokl. Akad. Nauk SSSR 123, No. 3, 501 (1958).•

[3] L. A. Lovachev, Dokl. Akad. Nauk SSSR 120, No. 6, 1287 (1958).•

[4] L. A. Lovachev, Dokl. Akad. Nauk SSSR 124, No. 6, 1271 (1959).•

[5] L. A. Lovachev, Ddkl. Akad. Nauk SSSR 125, No. 1, 129 (1959).•

[6] L. A. Lovachev, Dokl. Akad. Nauk SSSR 128, No. 5, 995 (1959).•

[7] C. E. Mellish and J. W. Linnett, Fourth Symposium on Combustion (Baltimore, 1953) p. 407.

• Original Russian pagination. See C. B. Translation.

THE MECHANISM OF CHAIN BRANCHING IN THE OXIDATION OF n-DECANE

Z. K. Maizus, I. P. Skibida, and Corresponding Member
Acad. Sci. USSR N. M. Émanuél'

Chemical Physics Institute, Academy of Sciences, USSR
Translated from Doklady Akademii Nauk SSSR, Vol. 131, No. 4, pp. 880-882,
April, 1960
Original article submitted January 3, 1960

In the majority of papers devoted to the study of the mechanism of hydrocarbon oxidation, it is assumed that the degenerate branching of the chains results from the formation of free radicals from molecules of intermediate hydroperoxides [1].

Direct experimental proof of this view has been given only recently [2].

The rate of chain branching in the oxidation of n-decane was measured by the inhibitor method, and it was shown that the rate increases linearly with increase in the concentration of hydroperoxides in the system. In other words, the hydroperoxides are the chief branching agents.

This conclusion has also been confirmed by the results of the work on the study of the kinetics of n-decyl hydroperoxide decomposition in the presence of α-naphthol [3]. It was shown that the rate constant for the decomposition of the hydroperoxide molecule to form radicals is of familiar magnitude to the rate constant for chain branching measured by the inhibitor method. The mechanism of the chain branching reaction, however, is not yet clear. Most authors consider that the primary decomposition of the hydroperoxide takes place according to the scheme

$$ROOH \rightarrow RO\cdot + OH\cdot. \qquad (1)$$

At the same time N. N. Semenov [4] and a number of other authors point out that the formation of free radicals in a reaction between two saturated molecules may be energetically more favorable than simple monomolecular decomposition to form radicals. This takes place in cases where at least one of the bonds being broken is not very strong, and the bond being formed has a high dissociation energy. From this point of view, it might be expected that the formation of free radicals from hydroperoxides—degenerate branching—also takes place by bimolecular interaction between two saturated molecules according to the scheme

$$2ROOH \rightarrow RO_2\cdot + RO\cdot + H_2O \qquad (2)$$

or

$$ROOH + RH \rightarrow R\cdot + RO\cdot + H_2O, \qquad (3)$$

since the energy of the R-H and RO-OH bonds being broken is less than the energy of formation of the H-O bond in water. Evidence in support of reaction (2) is provided, for example, by the fact that a linear relationship is

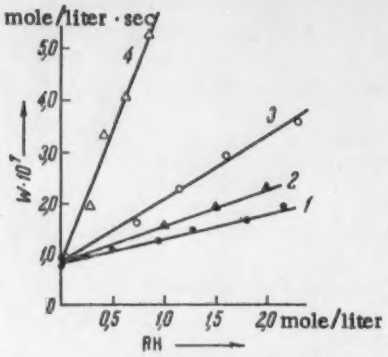

Fig. 1. Relationship between the rate of branching and the concentration of hydrocarbon in the solutions. Chlorobenzene–decane (1); chlorobenzene–isodecane (2); chlorobenzene–ethylbenzene (3); and chlorobenzene–methyl oleate (4). Concentration of hydroperoxides 0.03 mole/liter. Temperature 130°.

observed, as a rule, between the rate of the oxidation reaction and the hydroperoxide concentration. If the branching were due to monomolecular decomposition of hydroperoxide according to reaction (1), then in this case the reaction rate should be proportional to the square root of the hydroperoxide concentration.

It has already been suggested in the literature that, when the concentration of hydroperoxide is not too low, its decomposition proceeds according to reaction (2) [5]. The thermal effect of the bimolecular decomposition of the hydroperoxides Q = -9 kcal, i.e., it is 26 kcal more exothermic than the reaction ROOH → RO. + OH·, for which the thermal effect is Q = -35 kcal.

It appears more probable that degenerate branching takes place as a result of interaction between hydroperoxides and solvent. The thermal effect of this reaction is dependent on the strength of the R-H bond in the hydrocarbon molecule, and, in a number of cases, reaction (3) may prove to be more favorable than the bimolecular interaction between two hydroperoxide molecules (especially since, in the medium of the hydrocarbon being oxidized, the hydrocarbon concentration is much greater than the hydroperoxide concentration). Thus, even in the case of n-decane, in which the strength of the C-H bond amounts to 92 kcal, the thermal effect of the reaction

$$Q = Q_{H-OH} - Q_{RO-OH} - Q_{R-H} = 116 - 35 - 92 = -11 \text{ kcal}$$

i.e., reaction (3), is 24 kcal more exothermic than reaction (1). In the case of hydrocarbons with a bond strength less than 81 kcal, however, this reaction should take place with a positive thermal effect.

Some papers contain indirect reports of the possibility of a bimolecular reaction between hydroperoxide and hydrocarbon. In [2] it was shown that the chain branching reaction in the oxidation of n-decane is of first order with respect to hydroperoxide, with a rate constant of $k = 6.8 \cdot 10^8 \exp -24{,}800/RT$. The value of the preexponential factor is much less than that expected for monomolecular decomposition of the hydroperoxides. The suggestion that the primary decomposition of the hydroperoxide takes place by a bimolecular mechanism was also made in a recently published paper devoted to a study of the influence of solvent on the rate constant of the elementary reaction in the decomposition of tetralin hydroperoxide [6].

The aim of the present work was to examine the mechanism of the chain branching reaction in the oxidation of n-decane.

Since the difference between reactions (1) and (3) is that a hydrocarbon takes part in one of them, the rate of hydroperoxide decomposition should be found to be dependent on the hydrocarbon concentration in the case where branching takes place according to reaction (3).

Experiments were carried out to measure the rate of branching in solutions of n-decyl hydroperoxides in chlorobenzene, chosen as inert solvent, and in mixtures of chlorobenzene and n-decane. In the preparation of the solutions of the hydroperoxides in chlorobenzene, the hydroperoxides, obtained by oxidation of n-decane were converted to the sodium salts, which were then decomposed with sulfuric acid and extracted from the aqueous layer with chlorobenzene.

The rate of chain branching was measured by the inhibitor method described in [2], from the slope of the straight line for the α-naphthol consumption.

The concentration of α-naphthol in the solution was determined spectrophotometrically. The α-naphthol in the sample was extracted twice with 1 N NaOH and coupled with benzenediazonium sulphate; the intensity of the color of the latter was measured with a SF-4 spectrophotometer at the maximum absorption of the azo compound, 520 mμ.

It was established that decomposition of the hydroperoxides takes place even in pure chlorobenzene (apparently by the reaction ROOH $\rightarrow$ · RO + OH ·).

With increase in the concentration of n-decane in the chlorobenzene, the rate of decomposition of the hydroperoxides (branching) increases linearly (Fig. 1, 1), which indicates that the reaction is of first order with respect to the hydrocarbon.

We thus come to the conclusion that the chain branching in the oxidation of n-decane takes place by two parallel routes (according to mono- and bimolecular laws).

The rate constant for the monomolecular decomposition, determined from experiments on the decomposition of n-decyl hydroperoxide in pure chlorobenzene, is $k_1 = 0.28 \cdot 10^{-5}$ sec^{-1}. The rate constant for the bimolecular reaction between the hydroperoxides and n-decane is given by the slope of the straight line 1 and is found to be $k_2 = 1.65 \cdot 10^{-6}$ mole$^{-1} \cdot$ sec$^{-1} \cdot$ liter.

Thus the rate constant for the branching reaction measured in [2] is the effective constant and may be represented as the sum of the constants k_1 and k_2, using the equation $k_{eff} = k_1 + k_2$ [RH].

Assuming that in the oxidized n-decane [RH] = 5.2 mole/liter, and substituting the values of the rate constants obtained in the present work, we find for the effective rate constant for the branching reaction

$$k_{eff} = 1{,}1 \cdot 10^{-5}\ \text{sec}^{-1}.$$

This value shows satisfactory agreement with the value for the rate constant for the branching reaction measured in [2], $k = 1.9 \cdot 10^{-5}$ sec^{-1}.

In order to study the way in which the rate of branching depends on the solvent, experiments were carried out to measure the rate of decomposition of hydroperoxides in solutions of chlorobenzene with different quantities of isodecane, ethylbenzene, and methyl oleate.

The slopes of the straight lines 1, 2, 3, and 4 (Fig. 1) gave the following rate constants for the bimolecular branching reactions:

	$k_2\ 10^6$ mole$^{-1} \cdot$ sec$^{-1} \cdot$ liter
Chlorobenzene–decane	1.65
Chlorobenzene–isodecane	2.40
Chlorobenzene–ethylbenzene	4.10
Chlorobenzene–methyl oleate	16.6

The value of the rate constant for the branching reaction is evidently greater, the more readily the given hydrocarbon is oxidized, i.e., the lower the strength of the CH bond in the hydrocarbon (decane 92 kcal, isodecane 88 kcal, and ethylbenzene 77 kcal).

LITERATURE CITED

[1] D. G. Knorre, Z. K. Maizus, L. K. Obukhova, and N. M. Émanuél', Uspekhi Khim. 26, No. 4, 416 (1957).

[2] D. G. Knorre, Z. K. Maizus, and N. M. Émanuél', Dokl. Akad. Nauk SSSR 123, No. 1, 123 (1958).•

[3] Z. K. Maizus, N. M. Émanuél', and V. N. Yakovleva, Dokl. Akad. Nauk. SSSR, 131, No. 2 (1960).••

[4] N. N. Semenov, Some Problems in Chemical Kinetics [in Russian] (Izd. Akad. Nauk SSSR, 1958), p. 391.

[5] J. Bateman, Quart. Rev. 8, 147 (1954).

[6] J. R. Thomas and O. L. Harle, J. Phys. Chem. 63, 1027 (1959).

•Original Russian pagination. See C. B. Translation.

••See C. B. Translation.

THE THERMODYNAMICS OF THE EXTRACTION EQUILIBRIA FOR STRONG ELECTROLYTES DISSOCIATED IN THE ORGANIC PHASE

A. M. Rozen, L. M. Gindin, and I. F. Kopp

A. P. Zavenyagin Noril'sk Hydrometallurgical Combine

(Presented by Academician A. N. Frumkin, July 2, 1959)
Translated from Doklady Akademii Nauk SSSR, Vol. 131, No. 5, pp. 883-886, April, 1960
Original article submitted March 27, 1959

A number of extraction equilibria for electrolytes are characterized by the fact that the salt is dissociated in the aqueous phase, but in the organic phase is not dissociated, i.e., behaves as a nonelectrolyte. A detailed examination of these equilibria has been given in a paper by one of the present authors [1]. When solvents with a high dielectric constant are used, however (for example, in the extraction of chlorides with alcohols), this explanation is clearly incorrect, as follows from the comparatively high electrical conductivity of the organic phase (see Table 1).

Comp. of aqueous phase	x_{CaCl_2}, g/liter	—	—	—	—	—	—	120	240
	x_{HCl}, mole/liter	—	2,6	3,9	5,5	6,3	6,6	1,2	1,75
Comp. of the organic phase, (isoamyl alcohol)	y_{HCl}, mole/liter	0,01	0,75	1,16	2,34	3,3	3,9	1,3	5,5
Electrical conductivity	$\varkappa \cdot 10^3$, ohm^{-1} · cm^{-1}	10^{-3}	0,53	1,06	2,6	5,0	8,5	0,6	0,8
Viscosity, cp		3,5	5,0	5,9	6,3	6,6	6,1	7,5	12,0

The table shows that the solution of HCl in alcohol obtained in the extraction has an electrical conductivity typical of that for electrolyte solutions, i.e., dissociation of the HCl takes place in the organic phase. Let us examine how this affects the extraction equilibria. Using the distribution law

$$a_o / a_w = k;\ a_o = k a_w, \tag{1}$$

where a_w and a are the activities of the substance being extracted in the aqueous and organic phases, and k is the distribution constant. For hydrochloric acid, $a_w = (H^+)_o \cdot (Cl^-)_w \gamma^2_{\pm\, w}$, where $\gamma_{\pm\, w}$ is the mean activity coefficient, the brackets denoting molal concentrations. In the organic phase when no dissociation takes place, $a_w = (HCl)_o \gamma_o$; when dissociation takes place, $a_o = (H^+)_o (Cl^-)_o \gamma^2_{\pm o}$. If the extraction is accompanied by hydration by m molecules of water and solvation by n molecules of solvent S, then when no dissociation takes place, $a_o' = a_o / S^n a^m_{H_2O}$, and when dissociation takes place, $a_o' = a_o / a^m_{H_2O}$. Substituting in Eq. (1), putting $(HCl)_w = x$ and $(HCl)_o = y$, and taking account of the fact that in the absence of salting-out agents, $(H^+)_w = (Cl^-)_w = x$ and $(H^+)_o = (Cl^-)_o = y$, we find that when dissociation takes place in the organic phase,

$$(H^+)_o (Cl^-)_o = k (H^+)_w (Cl^-)_w \gamma^2_{\pm w} a^m_{H_2O} / \gamma^2_{\pm o};\quad y = \sqrt{k} x \gamma_{\pm}\, a^{m/2}_{H_2O} / \gamma_{\pm o}. \tag{2}$$

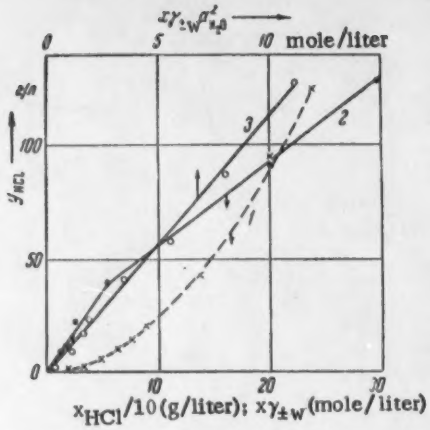

Fig. 1. Distribution of hydrochloric acid between water and isoamyl alcohol. 1) Relationship between y and x; 2) relationship between y and $x\gamma_{\pm w}$; 3) relationship between y and $x\gamma_{\pm w}a^2_{H_2O}$.

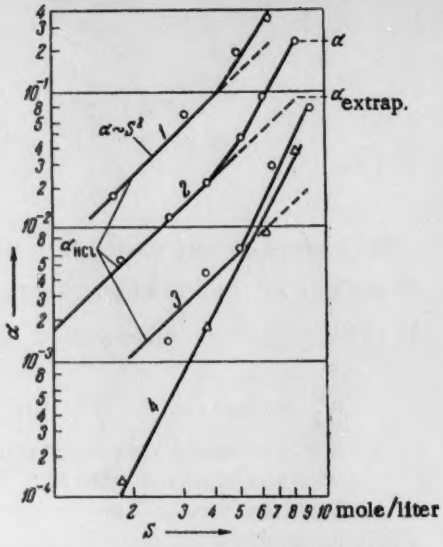

Fig. 2. Relationship between the distribution coefficients of HCl (1, 2 and 3) and $CaCl_2$ (4) and the concentration of isoamyl alcohol S with dilution by benzene. 1) x_{HCl} = 4.2 mole/liter; 2) 2.6 mole/liter; 3) 0.75 mole/liter. $S = S_0 - 2y_{HCl}$ or $S = S_0 - 4yCa$; S_0 = mole/liter (as in the Russian original).

When no dissociation takes place in the organic phase,

$$(HCl)_o = k(H^+)_w(Cl^-)_w\gamma^2_{\pm w}S^n a^m_{H_2O}/\gamma_{o\,w}$$

$$y = kx^2\gamma^2_{\pm w}S^n a^m_{H_2O}/\gamma_o. \qquad (3)$$

Let us compare (2) with experiment [2]. The activity coefficient $\gamma_{\pm o}$ for the solution of HCl in isoamyl alcohol, according to [4], decreases sharply in the concentration range 0-0.1 mole/liter, but when $x > 0.2$ mole/liter the change is slight, so that we may take $\gamma_{\pm o} = 0.05 = \text{const}$. Then if no hydration takes place, $m = 0$, and Eq. 2 predicts a linear relationship between $x\gamma_{\pm w}$, and y, which does not agree with experiment (Fig. 1, 2; $\gamma_{\pm w}$ and a_{H_2O} are taken from [3]). If account is taken of hydration, however, and if it is assumed that $m = 4$ (from the change in volume of the phases, $m = 4$, and from Fischer titration, $m = 3.5$), then (2) shows good agreement with the experimental data (Fig. 1, 3); when $\gamma_{\pm o} = 0.05$ and x is expressed in moles per kg, we find that $k = 2.5 \cdot 10^{-4}$.* Thus the extraction equilibria for hydrochloric acid are satisfactorily explained on the assumption that the acid is dissociated in the organic phase and that 4 molecules of water are extracted simultaneously ($m = 4$).

Even (3), which is based on the assumption that the nondissociated acid is extracted, may be made to agree approximately with the experimental data if it is assumed that the HCl molecule is solvated by 2 molecules of alcohol. A direct check of the way in which the distribution coefficient α_{HCl} depends on the concentration of free alcohol, carried out by the method involving dilution with benzene (Fig. 2), has shown that at high dilution, $\alpha \sim S^2$ (for $CaCl_2$, $\alpha \sim S^4$, $n = 4$). Thus the chief objection to this mechanism is the high electrical conductivity of the organic phase. At high dilutions, however, this is no longer the case, since k decreases

*This value should be compared with that calculated for zero activity coefficient for the ions γ_o [4], bringing the nonaqueous solution to the same standard state as the aqueous solution, so that $a_o\gamma^2_o = a_w$ and $k = 1/\gamma^2_o$. We find that $\log k = -3.6$, instead of $-2 \log \gamma_o = -6$ according to [4]. The difference is probably related to the simultaneous extraction of HCl and water and the decrease in $\Delta G_{solvation}$ [Eq. (6)].

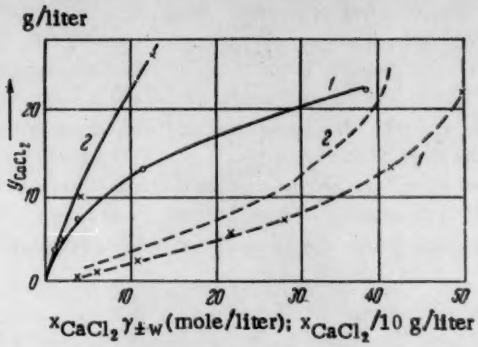

Fig. 3. Distribution of $CaCl_2$ between water and alcohols. Broken lines) relationship between y and x; solid lines) relationship between y and $x\gamma_{\pm w}$; 1) isoamyl alcohol; 2) butyl alcohol

sharply with dilution (at x_{HCl} = 150 g/liter and alcohol contents of 100, 70, 40, and 30%, we obtain $k \cdot 10^2$ = 1.34, 0.27, 0.016 and 0.008 $ohm^{-1} \cdot cm^{-1}$, respectively). Thus, when the dilution of the alcohol by benzene (dielectric constant $\approx$ 2) is sufficiently high, the dielectric constant decreases, and the undissociated acid is extracted. This mechanism is also possible in the extraction by pure alcohol [if the fraction of HCl extracted as undissociated molecules is estimated roughly by extrapolating the distribution coefficients obtained at high dilutions to high alcohol concentrations, we find that this fraction is $\sim \alpha_{extrap}$ α ($\approx$ 20-25%), but in (2) it is taken into account automatically by the activity coefficients $\gamma_{\pm o}$].

The distribution of calcium, cobalt, and nickel chlorides can also be interpreted assuming dissociation in the organic phase, i.e., assuming $\{M^{2+} + 2Cl^-\}_w \rightleftharpoons \{M^{2+} + 2Cl^-\}_o$.

$$(Me^{2+})_o (Cl^-)_o^2 \gamma_{\pm o}^3 = k_{Me} (Me^{2+})_w (Cl^-)_w^2 \gamma_{\pm w}^3 \qquad (4)$$

If only one salt is being distributed, with concentration x in the aqueous phase and y in the organic phase, then $(M^{2+})_o = (Cl^-)_o = y$ and

$$y = k'_{Me} x \gamma_{\pm w}/\gamma_{\pm o}; \quad \alpha = y/x = k'_{Me} \gamma_{\pm w}/\gamma_{\pm o}. \qquad (5)$$

Equation (5) was checked for calcium chloride using the data from [2], and the result is shown in Fig 3. Fig. 3 shows that considerable deviation from (5) takes place; possibly a reducing coefficient should be introduced into the equation to take account of the hydration (it is sufficient to assume m = 6). Fig. 3 also gives data for the extraction of $CaCl_2$ by butyl alcohol. Comparison of the curves shows that butyl alcohol, which has a high ratio of oxygen to carbon and a high dielectric constant, is a more efficient extracting agent. This follows from the theoretical equation for the electrolyte–electrolyte equilibrium constant, which can be derived using the calculation of the hydration energy according to [5] •

$$RT \ln k = -\Delta G_{hydr} \approx 0{,}5\, e^2 N (1/D_{H_2O} - 1/D_{alc}) \sum z_i^2/r_i + \Delta G_{solv.} \qquad (6)$$

where D is the dielectric constant, and z_i and r_i are the charge and radius of the solvated ions. For the two alcohols, $\ln k_{but}/\ln k_{amyl} \sim (1/D_{amyl} - 1/D_{but}) > 0$, and $k_{amyl} < k_{but}$. On going to higher alcohols, the dielectric constant, and hence k_{alc}, decreases, and the extraction properties become less satisfactory.

•$G_{solvation}$ is the free energy of formation of the solvate sheath [$\Delta G_{solvation} \approx$ zeN $(n_{alc}\mu_{alc} - n_{H_2O}\mu_{H_2O}/r^2)$ $-T\Delta S_{solvation}$:

Let us now check (5) for the case of cobalt and nickel. According to the data given in [6] (for the extraction of $CoCl_2$ and $NiCl_2$ by capryl alcohol), $\log \alpha_{Co,Ni} = ax-b$, where a = 0.088, b = 5.8, and x is expressed in weight percentages. It can be shown that, for $CoCl_2$ and $NiCl_2$ at high concentration, the logarithm of the activity coefficient is linearly dependent on the concentration, $\log \gamma_{\pm w} = a_1x-b_1$, and from (5) it follows that $\log \alpha = a_1x-b_1 + \log k^{1/3}/\gamma_o$, which shows qualitative agreement with the data given in [6]. The quantitative agreement, however, is unsatisfactory (the slope of the $\log \gamma_{NiCl_2} = f(x)$ curve gives $a_1 = 0.04$ instead of $a_1 = 0.088$). It is possible that in view of the low dielectric constant of capryl alcohol, the $CoCl_2$ is dissociated only to $CoCl^+$ and Cl^-, so that $a_o = y^2\gamma^2_{\pm o}$ eff. In this case $y = k^{1/2}(x\gamma_{\pm w})^{3/2}/\gamma_o$, and $\log \alpha = (1.5\, a_1x + 0.5 \log x) + \log k^{1/2}\gamma_o - 1.5\, b_1$. When x > 20%, the term in brackets ≈ 0.08 x, i.e., a = 0.08, which is close to the result obtained in [6].

In the extraction of HCl with isoamyl alcohol in the presence of large quantities of $CaCl_2$, it has been found [2] that $y_{HCl} = k_1\sqrt{x_{HCl}}$ We can show that this follows from (2). We take account of the fact that the $CaCl_2$ is extracted to a much smaller extent than HCl, and it may be assumed that the concentration of Cl ion in the organic phase is determined only by the extraction of the HCl, i.e., $(H^+)_o = (Cl^-)_o = y_{HCl}$. In the aqueous phase, however, $(H^+)_w = x_{HCl}$, and $(Cl^-)_w = x_{HCl} + 2x_{Ca}$. Substituting the values for the ion concentrations in (2), we obtain

$$y_{HCl} = \sqrt{k}\,(\sqrt{x_{HCl} + 2x_{Ca}}\,\gamma_{\pm w}\, a^{m/2}_{H_2O}/\gamma_{\pm o})\sqrt{x_{HCl}} = \sqrt{k}B\sqrt{x_{HCl}} \approx k_1\sqrt{x_{HCl}}, \qquad (7)$$

since x_{Ca} = const $\approx$ 5 mole/liter $\gg x_{HCl}$, so that B $\approx$ const. In the case of the distribution of cobalt chloride in the presence of $CaCl_2$, it is necessary to solve simultaneously the distribution equations (4) for Co and Ca; dividing the first by the second, we obtain

$$\beta_{Co/Ca} = \alpha_{Co}/\alpha_{Ca} = k_{Co}/k_{Ca} = \text{const}. \qquad (8)$$

We have already shown [7] that $\beta_{Co/Ca} = 5$ = const. This result can now be very simply explained, for $k_{Co} = 5\, k_{Ca}$ ($k_{Co} > k_{Ca}$, probably because $r_{Co} > r_{Ca}$). In the case of the extraction of $CoCl_2$ from an aqueous phase containing HCl, it is necessary to solve (4) and (2) simultaneously. Dividing the first by the square of the second, we find•

$$k^2_{HCl}/k_{Co}\gamma_o = \alpha^2_{HCl}/\alpha_{Co}\gamma_{\pm w} = a^{2m}_{H_2O} = A = \text{const}. \qquad (9)$$

Examination has shown that, when x_{HCl} = 0.16-7 mole/liter and x_{Co} = 19-50 g/liter, A = 20 ± 2 = const.

The considerable increase in the distribution coefficient of cobalt and in the separation coefficient $\beta_{Co/Ni}$ when HCl and $CaCl_2$ are added simultaneously [7] may be explained by a change to the extraction of the anionic complex $CoCl^{2-}_4$, which gives the solution its blue color. At low dielectric constants, dissociation in the organic phase is impossible since $k_{ass} \sim D^{-3}$.

The authors wish to thank A. P. Ilozhev and T. A. Slepyan for measuring the electrical conductivity and the relationship between the distribution and the alcohol concentration.

LITERATURE CITED

[1] A. M. Rozen, Atomnaya Energiya, 2, No. 5, 445 (1957). ••

[2] L. M. Gindin, A. M. Rozen, et al., Zhur. Neorg. Khim. No. 1 (1960).

[3] R. Robinson and R. Stokes, Electrolyte Solutions (London, 1956).

[4] N. A. Izmailov, Zhur. Fiz. Khim. 30, 2164 (1956); 31, 2169 (1957).

•Expressions (8) and (9) are also obtained when dissociation does not take place or is incomplete.

••Original Russian pagination. See C. B. Translation.

[5] J. Bernal and R. Fowler, Uspekhi Fiz. Nauk, 14 , 586 (1934).

[6] L. Garwin and A. Hixon, Ind. Eng. Che. 41, 2298 (1949).

[7] L. M. Hindin, I. F. Kopp, et al., Zhur. Neorg. Khim. No. 1 (1960).

THE RELATION BETWEEN ACTIVATION ENERGY AND RELATIVE ADSORPTION COEFFICIENT

A. E. Agronomov, Academician A. A. Balandin, and Yu. S. Mardashev

The M. V. Lomonosov Moscow State University.
The N. D. Zelinskii Institute of Organic Chemistry, Academy of Sciences, USSR
Translated from Doklady Akademii Nauk SSSR, Vol. 131, No. 5, pp.1120-1122,
April, 1960
Original article submitted December 28, 1959

We have investigated the activity over a wide temperature range of a series of nickel catalysts (identical proportions by weight of nickel were deposited on different carriers)* on the dehydrogenation of cyclohexane.

As can be seen from Table 1, the apparent activation energy Q for the dehydrogenation of cyclohexane, calculated by the Arrhenius equation, as well as the relative adsorption coefficient of benzene z_2, determined by the formula derived in [3] and from adsorption data [1], depend basically on the nature of the carrier used. It has also been shown that z_2 is independent of the temperature, and that the relative adsorption coefficient of hydrogen z_3 is practically zero, i.e., hydrogen does not inhibit this reaction [4].

TABLE 1

Nos.	Catalyst	Q, kcal/mole	z_2	E, kcal/mole	No.	Catalyst	Q, kcal/mole	z_2	E, kcal/mole
1	Ni/Al_2O_3	9,8	4,0	12,8	4	Ni/ Ni black	11,0	2,1	13,7
2	Ni/silica gel	4,8	7,3	14,0	5	Ni/Al_2O_3	10,8	2,05	13,0
3	Ni/Al_2O_3	10,0	2,1	13,0	6	kieselguhr	7,0	6,0	—

To compare the results given in Table 1, we determined the following relation between the apparent activation energy Q and the relative adsorption coefficient of benzene z_2:

$$Q = E - k \lg z_2, \tag{1}$$

where E and k are constants. A graph of this relationship is given in Fig. 1.

A common kinetic equation (which we derived [5]) for unimolecular heterogeneous catalytic reactions in a flow system can, taking into consideration the fact that the % conversion m was < 30 and that the reaction rate was independent of pressure, be simplified [6] to give the following:

$$m = \frac{KA_1}{\Sigma z_r A_r + K/2}, \tag{2}$$

where K is the rate constant, A_r is the number of moles of r-th substance introduced into the reactor and z_r is the relative adsorption coefficient of the corresponding substance.

*The catalysts were prepared by a method similar to that in [1]; nickel black similar to that in [2].

TABLE 2

Dependence of z_2 on the Composition of the C_6H_6–C_6H_{12} Mixture for Catalyst 2

C_6H_6, %	C_6H_{12}, %	z_2
10.1	89.9	6.0
17.4	82.6	7.5
34.5	65.5	8.0
56.9	43.1	20.0
70.2	29.8	>> 100

For absolute activation energy E shown in Table 1 was calculated from the temperature dependence of the reaction rate constant determined from Eq. (2). The values of E were effectively the same for all the samples investigated. As can be seen from Fig. 1, the value E gives a straight line near the axis of ordinates. Thus the constant E in Eq. (1) is the absolute activation energy.

For most of our investigations on catalysts the difference between E and Q was not great and remained around 3 kcal/mole, the exception being catalyst 2, nickel on silica gel, for which the apparent activation energy is only one third the absolute energy. It should be noted that the value of z_2 is at a maximum for this type of catalyst, and such a large difference between E and Q would follow from Eq. (1).

Obviously the apparent activation energy will be equal to the absolute energy when $z_2 = 1$; this was also brought out by one of the authors [7] during a kinetic study of the dehydrogenation of cyclohexane and its homologs.

We also derived a relation for catalyst 2 between z_2 and the amount of benzene in the initial mixture according to which z_2 increases with increasing percentage of benzene (as can be seen from Table 2). The dependence of z_2 on the amount of benzene in the initial mixture is shown graphically in Fig. 2. In Table 1 we have quoted z_2 for mixtures containing a small quantity of benzene for this catalyst.

The value of the relative adsorption coefficient is determined by the relative lifetime of molecules of reaction product on the catalyst surface compared with molecules of the reacting substance [3]. For catalyst 2 the benzene molecules remain on the catalyst surface 6-7 times as long as the cyclohexane molecules. It was shown in [8] that catalytic activity must take place on sites of average adsorption strength.

If it is assumed that the benzene obtained as a result of the reaction is adsorbed initially on the most active adsorption sites, only slight inhibition by benzene will occur. Thus we should obtain the absolute activation energy from the temperature dependence of $\underline{m}$. However, as the percentage conversion $\underline{m}$ increases, and the amount of benzene in the bulk phase and on the surface increases, more and more benzene will accumulate on sites of average adsorption strength. At this point inhibition by benzene occurs in the dehydrogenation of cyclohexane, as has been observed by a number of authors [4]. This inhibition shows that even under flow system conditions the catalyst for the reaction will not be that part of the nickel surface which catalyzed the reaction initially, but that part of the nickel surface which is partially covered by benzene. Taking into account the ability of the π-electrons of benzene to interact with the d-electrons of nickel [9], this effect must lead to a relation of the type $z_2 = f(m)$. This relation will have greater effect on that catalyst having a larger value of z_2, since in this case the benzene molecules will remain relatively longer on the catalyst surface. To determine the value of z_2 by a kinetic method in this case, a mixture containing a low percentage of benzene should be taken, as we did for catalyst 2. This effect must result in a deviation in the value of Q. There is indirect evidence in the literature which indicates the existence of this effect. One of us with Yur'ev investigated Q in relation to the percentage of xylene in a xylene–dimethylcyclohexane mixture in dehydrogenation over Ni/Al_2O_3. It was shown that in a mixture containing up to 90% of the aromatic component, Q does not depend on the composition of the mixture (in this case $z_2 = 1$ [7]). In addition to this, for the dehydrogenation of cyclohexane on a nickel/pumice catalyst, we obtained $Q < 5$ kcal/mole (unstable catalyst) and $z_2 \sim 20$ even for mixtures containing 10% benzene.

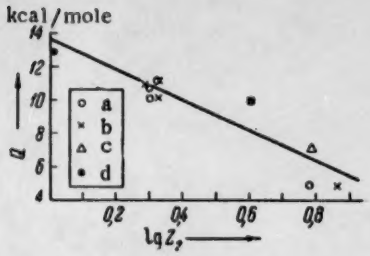

Fig. 1. Dependence of Q on log z_2 for nickel catalysts: a) From kinetics, b) from adsorption, c) for nickel black, d) from the data of Balandin and Herbo [7, 11].

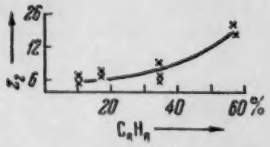

Fig. 2. Dependence of relative adsorption coefficient of C_6H_6 on the composition of the C_6H_6–C_6H_{12} mixture.

Thus the essential points of the observed effects can be summarized as follows: as long as the dehydrogenation of cyclohexane by nickel catalysts proceeds on activated sites of average adsorption strength, which are not covered to any significant degree by benzene molecules, there is no inhibition and z_2 does not depend on m.

Only as the covering of the sites of average adsorption strength becomes significant does inhibition by benzene begin, leading to the relation $z_2 = f(m)$, which is particularly significant for catalysts with large z_2 values.

Here it is necessary to investigate this relation in order to determine the activation energy for the given case. The value of E obtained in this way for catalyst 2 agrees well with the value of E determined for the other catalysts (see Table 1). Another possible solution is to use a graph of Eq. (1), from which it is possible to obtain E for $z_2 = 1$.

It is interesting to note that Eq. (1) can be used to represent the data obtained by one of us for a series of dehydrogenation reactions of cyclohexane derivatives on Ni/Al_2O_3 [7], and also for the data of Herbo for Ni/BeO [11] obtained by the use of some other methods and equations (Fig. 1). It is noteworthy that a value of E ≈ 14.0 kcal/mole was obtained in our laboratory [12] for certain other nickel catalysts on carriers.

LITERATURE CITED

[1] A. E. Agronomov, A. A. Balandin, and Yu. S. Mardashev, Dokl. Akad. Nauk SSSR 127, 325 (1959).•

[2] A. E. Agronomov and Yu. S. Mardashev, Vestn. Moskovsk. Univ. 3, 83 (1955).

[3] A. A. Balandin, Zhur. Org. Khim. 12, 160 (1942).

[4] R. M. Flid and M. Ya. Kogan, Zhur. Fiz. Khim. 24, 1409 (1950); C. Herbo, J. Chim. Phys. 47, 445 (1950).

[5] A. A. Balandin, Zhur. Org. Khim. 12, 150 (1942).

[6] A. A. Balandin, Vestn. Moskovsk. Univ. 4, 137 (1957).

[7] A. A. Balandin, Zhur. Fiz. Khim. 31, 745 (1957).

[8] A. A. Balandin, Uch zap. Moskovsk. Univ. B175, 104 (1956).

[9] P. W. Selwood, J. Am. Chem. Soc. 79, 4637 (1957).

[10] A. A. Balandin and Yu. K. Yur'ev, Zhur. Fiz. Khim. 5, 393 (1934).

[11] C. Herbo, Bull. soc. chim. Belg. 54, 203 (1945).

[12] A. A. Balandin, Usp. Khimii 4, 1004 (1935).

•Original Russian pagination. See C. B. Translation.

THE DIFFERENCES BETWEEN THE TIMES OF COMPLETION OF HYDRATION AND ATTAINMENT OF MAXIMUM HARDNESS OF CRYSTAL STRUCTURE IN PLASTER OF PARIS SUSPENSIONS

E. A. Amelina, E. E. Segalova, and Academician P. A. Rebinder

Physical Chemistry Institute, Academy of Sciences, USSR and
M. V. Lomonosov Moscow State University
Translated from Doklady Akademii Nauk SSSR, Vol. 131, No. 5, pp. 1123-1125,
April, 1960
Original article submitted December 28, 1959

It is often assumed [1] that, during the setting of mineral cements, hydration must be completed before the attainment of maximum hardness in the setting material. This would follow from the views of A. A. Baikov on the setting process, according to which the development of the concreted material occurs through the crystallization of a gel into apolycrystalline concretion. However, comparative measurements of the kinetics of hardening and of hydration for various specimens of plaster of Paris, carried out by O. V. Kuntsevich, Ya. L. Zabezhinskii, V. B. Ratinov, and other [2-4], and by P. A. Rebinder and his collaborators [5-6], have shown that these processes are completed practically simultaneously, and the continued hardening of the calcium sulphate specimens subsequently is believed to be due to increase in the completeness of crystalline structure as a result of drying out.

We have carried out a more detailed examination of this problem on suspensions of α- and β-calcium sulphate half-hydrate of various degrees of dispersion and with different values of the water-solid ratio (W/S) and have been able to show that, in general, increase in hardness is completed before the completion of hydration, while the difference between the times of hydration and of hardening depends on the conditions of the experiment. Investigations have been made on suspensions whose solid phase consisted of 30% plaster of Paris and 70% finely ground quartz sand having a specific surface in conventional units, determined in the Tovarov apparatus, of 3600 cm^2/g.

The kinetics of the structure formation have been followed by means of a conical plastometer [7]. The kinetics of the hydration of the same specimens has been studied in a calorimeter with automatically controlled adiabatic sheath [8].

An example of the experimental results is shown in Fig. 1, which refers to α-calcium sulphate half-hydrate of two different degrees of dispersion. It appears from the figure that the maximum hardness of the crystal structure is attained appreciably earlier than the completion of the hydration of the half-hydrate. At this point, increase in hardness (which is associated with the crystallization of the bulk of the half-hydrate) ceases, and no further increase in hardness occurs (Fig. 1 A), but, for a high degree of dispersion of the initial half-hydrate, a reduction of hardness then takes place even during the completion of hydration (Fig. 1 B).

The discrepancy between the time of completion of hydration and the time of structure formation is represented by the appreciably shorter time required for the attainment of maximum hardness τ_m, compared with that for the completion of hydration τ_H, and can be denoted $h = (\tau_H - \tau_m)/\tau_H$. The greater the value of h, which has the form of a fraction of the time required for full hydration, the earlier in the course of crystallizing out the new structure does the increase in hardness cease; it may then even be replaced by a falling off in hardness. In this connection it should be observed that the sudden appearance of a reduction of hardness in the course of crystallization of a new structure is also observed in quicklime suspensions undergoing hydration-hardening [9].

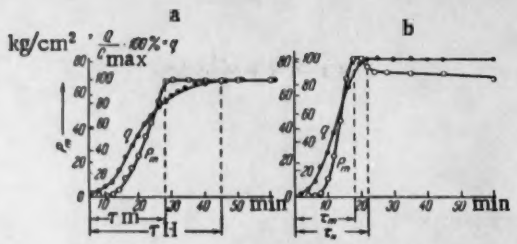

Fig. 1. The kinetics of structure formation (P_m) and of hydration (q) as determined by heat evolution, for suspensions of α-calcium sulphate half-hydrate, when W/S = 0.4; t = 18°C. Conventional specific surface of the initial half-hydrate: A) 3000 cm²/g; B) 9700 cm²/g.

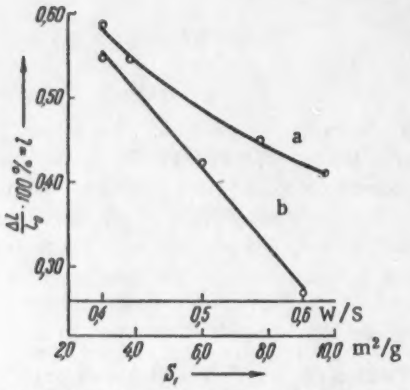

Fig. 2. Relationship between the relative linear expansions of specimens of α-calcium sulphate half-hydrate and: A) the degree of dispersion of the initial half-hydrate (W/S = = 0.4); B) the value of W/S (S_1 = 3900 cm²/g) at t = 22°C. Composition of solid phase of suspension: 30% calcium sulphate half-hydrate and 70% ground quartz sand.

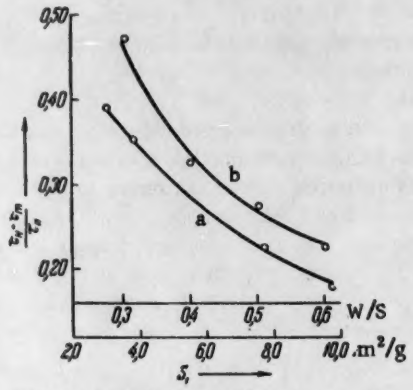

Fig. 3. Relationship of $h = (\tau_H - \tau_m)/\tau_H$ for suspensions of α-calcium sulphate half-hydrate to: A) Degree of dispersion of initial half-hydrate (W/S = 0.4); and B) the value of W/S (S_1 = 3900 cm²/ g); t = 18°C.

These phenomena may be explained by the partial destruction of the crystalline structure at its weakest points, under the influence of the tension produced during the directional growth of the crystals, which become linked with one another through stable contacts, causing the development of the skeleton of a crystal structure [10, 11]. Further growth superimposed on this skeleton leads, on the one hand, to a hardening of the structure through increase in the size of the crystallites of which it is made up, and, on the other, to the development of an internal stretching tension which causes destruction of the structure and reduction of its hardness. These two processes of hardening and destruction proceed simultaneously, and are superimposed on one another. Depending on which of the processes predominates, we may account for either the continuous increase of hardening up to the completion of hydration, which occurs in the cases discussed in the papers mentioned above [2-4], or the cessation of growth shown in Fig. 1 A, or even its reduction while hydration is being completed (Fig. 1B).

Since the internal tensions arise from the growth of the crystals which make up the structure of the solid, they would be expected to be stronger and arise sooner, the lower the degree of dispersion of the initial half-hydrate, for in this case the high supersaturations which provide for the formation of the crystalline skeleton are

S_1, cm²/g	$\frac{(P_m)_H - (P_m)_s}{(P_m)_H}$	
	W/S = 0.4	W/S = 0.6
3000	0.09	0.31
3900	0.12	0.37
7700	0.13	0.44
9700	0.14	0.46

maintained in the system for a relatively shorter time and are set up more slowly. Thus, very favorable conditions are created for the growth of the crystals which make up this skeleton. We should expect, therefore, that these stretching tensions would arise more abruptly in initial cements of lower dispersion. A similar effect on the magnitude of the tension should also be produced by the quantity W/S, since reduction of W/S also reduces the porosity of the structure and creates great difficulties in the way of growth of the crystals. The external result of the internal tension developed in the structure during its formation is expansion, which always occur to a greater or lesser extent during the hardening of the cements. The expansion increases with increase in the internal tension and should, therefore, be increased with reduction in the initial specific surface of the cement and in the value of W/S. Actually the investigations which we have made on the linear expansion of samples α-calcium sulphate half-hydrate, with different specific surfaces of the initial half-hydrate and different values of W/S, have shown that the relative values of these expansions show an inverse relationship to the quantities named (Fig. 2).

The observed discrepancies between the time of completion of hydration and the time when the structure attains its greatest solidity seem also to be the result of the effect of the stretching tension. Hence the value of h, which represents this discrepancy, ought, like that of the expansion, to depend on the specific surface of the initial material and on the value of W/S. This is confirmed by the data given in Fig. 3.

It is important to distinguish the cessation of hardness-increase, or its diminution, which occurs during the crystallizing out of the new structure from the reduction in hardness which occurs after the completion of hydration on account of recrystallization (which leads to the breaking of the thermodynamically non-equilibrium crystal contacts). In the specimens we have studied, such reduction of hardness through rupture of these contacts, does take place, but is shown only during the more protracted investigations of the hardness of samples preserved under moist conditions. In contrast with the phenomena considered earlier, reduction in hardness owing to rupture of the crystal contacts proceeds more strongly, the greater the degree of dispersion of the initial cement and the greater the value of W/S (Table 1), which agrees with earlier published results [10, 12].

LITERATURE CITED

[1] A. A. Baikov, Collected Works 5 [in Russian] (Academy of Sciences of USSR Press, 1948).

[2] O. V. Kuntsevich, Tr. soveshch. po khimii tsementa (Transactions of the Council on the Chemistry of Cement) [in Russian] (Moscow, 1956).

[3] O. V. Kuntsevich, P. E. Aleksandrov, et al., Dokl. Akad. Nauk SSSR 104, 4 (1955).

[4] V. B. Ratinov, Ya. L. Zabezhinskii, and T. I. Rozenberg, (Collected Transactions of the All-Union Scientific and Research Institute of Ferroconcrete) [in Russian] 1, (3) (1957).

[5] V. N. Izmailova, E. E. Segalova, and P. A. Rebinder, Dokl. Akad. Nauk SSSR 107, 3 (1956).*

[6] Z. N. Markina and Ezhi Stoklosa, Koll. Zhur. 21, No. 6 (1959).*

*See C. B. Translation.

[7] E. E. Segalova, P. A. Rebinder, and O. I. Luk'yanova, Vestn. Moskovsk. Univ. (Moscow University Herald) [in Russian] No. 2 (1954).

[8] V. F. Kiselev, (Transactions of the Council on the Chemistry of Cement) [in Russian] (Moscow, 1956); O. I. Luk'yanova, E. E. Segalova, and P. A. Rebinder, Koll. Zhur. 19, 4 (1957).•

[9] E. E. Segalova, S. I. Kontorovich, and P. A. Rebinder, Dokl. Akad. Nauk SSSR 129, 6 (1959).•

[10] E. S. Solov'eva and E. E. Segalova, Koll. Zhur. 20, 5 (1958).•

[11] E. E. Segalova, S. I. Kontorovich, and P. A. Rebinder, Koll. Zhur. 22, 1 (1960).•

[12] V. N. Izmailova, E. E. Segalova, and P. A. Rebinder, Dokl. Akad. Nauk SSSR 110, 5 (1956).•

•See C. B. Translation.

WORK FUNCTION AND CATALYTIC ACTIVITY OF IRON CONTACTS IN THE SYNTHESIS OF AMMONIA

É. Kh. Enikeev, A. V. Krylova, L. D. Kuznetsov, S. S. Lachinov, and Corresponding Member of the Academy of Sciences of USSR S. Z. Roginskii

Physical Chemistry Institute of the Academy of Sciences of USSR

Translated from Doklady Akademii Nauk SSSR, Vol. 131, No. 5, pp. 1126-1129, April, 1960
Original article submitted December 21, 1959

The industrial production of ammonia is based on the use of iron catalysts into which potassium and aluminum oxides have been introduced so as to increase their activity and stability. In spite of numerous studies, the chemical structure and the mechanism of the effect of the additive on the operation of the contact remains up to now practically unexplained. This is true to an even greater extent of other additives (CaO, SiO_2), by means of which significant improvements in ammonia catalysts have recently been effected [1]. In a series of theoretical studies [2], the catalytic activity and adsorptive power of semiconductors and metals have been connected with the electronic work function. É. Kh. Enikeev, L. Ya. Margolis, and S. Z. Roginskii [3] have established for NiO and ZnO a direct connection between the change in the work function and the change in the energy of activation of catalysis and of chemisorption, produced by the introduction of various modifying additions. For metallic catalysts practically no similar work has been done. It has therefore become a matter of interest to compare the change in the work function with the catalytic activity of modified iron catalysis in the synthesis of ammonia.

The electronic work function was determined from the contact potential difference measured by the vibrational condenser method [3] with an accuracy of 0.01 eV. The reproducibility of measurements in different experiments was $\pm$ 0.05 eV. To obtain the connection between $\Delta\varphi$ and the catalytic activity, it is desirable to carry out the measurements under the conditions of catalysis, but the very strict conditions for the ammonia synthesis (high temperature and pressure) make this at present very difficult to achieve. For the determination of the work function, passivated samples were taken after the determination of their catalytic activity in the column. The catalysts were ground to fine powders in an atmosphere of nitrogen. Training was carried out by heating in a vacuum or in an atmosphere of hydrogen at a temperature of 320-340° in the cell described earlier [3]. The construction of the apparatus guaranteed that the conditions of training would be identical, and reduced to a minimum the influence of variation in the reference electrode on the measured quantity. The work function of all passivated catalysts in air was the same, and differences between the specimens arose only after training; this gives reason to suppose that the oxygen was removed from the major part of the surface. Table 1 gives values for the magnitude of the contact potential difference V_c (that is, the difference between the work function of the electrode under consideration and a standard gold electrode); the table also gives the values of $\Delta\varphi$ (that is, the change in the work function for various promoted catalysts in comparison with the work function for nonpromoted catalyst).

The specimens of the catalysts were prepared under production conditions by the method of oxidative fusion of the iron with the introduction of various additives. The chemical composition of the catalysts studied before reduction is given in the left-hand portion of the Table. The activity of the samples was determined by a flow

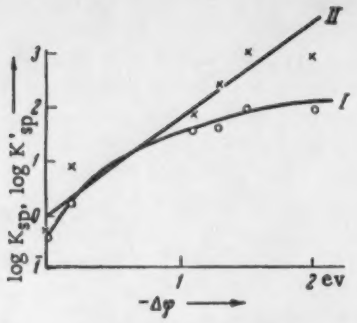

Fig. 1. Relationship between the specific catalytic activities K (I) and K' (II) and change in the initial work function.

method in a five-channel column at high pressure [4], into which was fed 1-2 ml of each sample of catalyst of grain size 2-3 mm. Before determination of the activity, reduction of the catalysts was carried out under a pressure of 100 atm of a hydrogen-nitrogen mixture of stoichiometric composition (volume rate 30,000 $hour^{-1}$) by the method of stepwise temperature rise. The reduction was completed by a two-hour exposure of the catalyst to a temperature of 550°. The usual duration of the reduction was 32 hours. The determination of the percentage of ammonia in the gas mixture was performed at a pressure of 300 atm, a temperature of 350-550° and a volume rate of 15,000-30,000 $hour^{-1}$. After determination of activity, the samples of the catalysts were passivated in a current of nitrogen containing 0.1% oxygen at room temperature. The over-all surface of the passivated samples (S_{ov})• was determined by the BET method by the low temperature adsorption of nitrogen. From the chemisorption of carbon monoxide at -78° [5], the conventional size of that part of the surface free from promotor was determined (S_{Fe} in the Table).•

Catalytic Activity and Electronic Work Function for Promoted Iron Catalysts•

No. of specimen	Chemical composition in % before reduction••						Volume rate, $hour^{-1}$•••	NH_3, %•••	Over-all surface S, m^2/g	Conventional surface of free iron, S_{Fe}, m^2/g	Specific rate constant, $atm_2^{0.5} \cdot hr^{-1}$, m^{-2}		Contact potential difference, V	Change in work function on introducing additive, Δφ, eV
	FeO	Fe_2O_3	Al_2O_3	K_2O	CaO	SiO_2					$K_{sp}=\frac{K}{S}$	$K_{sp}=\frac{K}{S_{Fe}}$		
1	25,2	74,1	0,2 (Impurity)	—	—	—	14500	0,25	0,5	0,325••••	$2,8 \cdot 10^{-1}$	$4,3 \cdot 10^{-1}$	−0,5	0
2	37,2	52,1	10,2	—	—	—	14800	3,6	17	3,9	1,8	7,95	−0,3	0,2
3	22,1	75,1	0,3 (Impurity)	2,0	—	—	15000	3,5	0,7	0,35	$4,3 \cdot 10$	$8,6 \cdot 10$	+0,6	1,1
4	25,0	66,95	4,8	2,3	0,3 (Impurity)	0,15 (Impurity)	30000	11,0	11,0	2,2	$5,5 \cdot 10$	$2,7 \cdot 10^{1}$	+0,8	1,3
5	30,8	59,7	3,2	0,9	4,0	0,9	29600	16,4	13,0	1,04	$1,1 \cdot 10^{3}$	$1,3 \cdot 10^{3}$	+1,0	1,5
6	39,3	54,4	3,1	0,7	2,0	—	30000	17,8	12,0	1,44	$1,3 \cdot 10^{3}$	$1,1 \cdot 10^{3}$	+1,5	2,0

•We have also studied the catalytic activity and work function of Armco iron. A strip of Armco of over-all surface 1 m^2 at 550° and 300 atm, and volume rate of 15,000 $hour^{-1}$ possessed practically no catalytic activity; this specimen possessed the greatest value of the work function.

••About 0.5% of each specimen consisted of various impurities: MgO, MnO, P_2O_5, SO_3, Cr_2O_3, NiO and others.

•••Conditions of test: P = 300 atm, T = 400°.

••••The quantity S_{Fe} was not determined for this sample. The table gives the value of S_{Fe} obtained from data in the literature for a sample of closely similar chemical composition.

• Such an interpretation of S_{Fe}, calculated from the limit of adsorption CO_{chem}, is conventional, but it gives some representation of the capacity of the surface for chemisorption of N_2. The measurement of the surface was carried out by V. N. Shishkova, to whom the authors wish to express their thanks.

The catalytic activity of the specimens is shown in Table 1, in the form of rate constants for the reaction, calculated from the percentage of ammonia on exit from the column by means of the Temkin equation [6], and referred to unit over-all surface, $K_{sp} = K/S_{ov}$, and to unit conventional surface of iron free from promotor, $K'_{sp} = K/S_{Fe}$. It can be seen from the Table that the introduction of 10% of aluminium oxide, which had formerly been thought of only as a stabilizing additive (specimen 2) causes some increase in the specific catalytic activity K_{sp} in comparison with the unpromoted catalyst (specimen 1). This change in activity corresponds to an insignificant reduction in the work function (0.2 eV). Addition of 2% potassium oxide (specimen 3) increased the catalytic activity 150-fold. The work function for this was reduced by 1.1 eV. The activity of the doubly promoted catalyst (specimen 4), containing 2.3% K_2O and 4.8% Al_2O_3 increased 200-fold, and the work function was reduced by 1.3 eV. Addition of CaO (specimen 6), or CaO + SiO_2 (specimen 5) still further increased the catalytic activity and diminished the work function.

Figure 1 shows the large, regular increase of log K_{sp} with reduction in the electronic work function (I). The extreme samples differ by 2 eV in their work function and by a factor of 450 in their specific catalytic activity. In view of the fact that the capacity for chemisorption of nitrogen per cm^2 of catalyst surface is diminished by promotion, it is of interest to compare the work function with the specific catalytic activity referred to unit conventional surface of iron. Curve II in the same figure shows the change in the quantity log K'_{sp}, on change of $\Delta\varphi$ and reveals that the relationship obtained may be represented by a straight line.*

At constant values of temperature and K_0, the Arrhenius equation relates the change in catalytic activity of different specimens to change in the activation energy by the relationship:

$$j\Delta \lg K'_{sp} = \Delta E. \tag{1}$$

From the experimental data

$$j\Delta \lg K'_{sp} = \alpha\Delta\varphi, \tag{2}$$

from which it may be concluded that

$$\Delta E = \alpha\Delta\varphi. \tag{3}$$

The most reliable values for the activation energies are those known for catalysts numbered 1 and 4 (Table 1) E changes from 65 ± 4 kcal/mole (specimen 1) to 40 ± 2 kcal/mole (specimen 4); that is, $\Delta E_{kin_{1.4}} \sim 25$ kcal/mole. The change in the work function, $\Delta\varphi = \varphi_4 - \varphi_1 = 1.3$ eV. By converting electron volts into kilocalories per mole, we obtain ΔE_{el} around 30 kcal/mole, which is close to $\Delta E_{kin_{1.4}}$, that is, α in equation (3) is close to unity. Thus the change in the energy of activation with change in work function is larger than the effects predicted by the theory of Budar for metals, and corresponds to the effects predicted theoretically for semiconductors [8].

The magnitude of the coefficient α obtained from the slope of the straight line II on Fig. 1 is considerably less than 1 ($\alpha' = 0.26$) which may be accounted for by the presence of some compensating effect, or by insufficient accuracy in the values of E_{kin_1} and E_{kin_4} which have been used. For a more thorough understanding of the connection between catalytic activity and work function it is necessary to study a larger number of catalysts, and to carry out the measurement of φ under catalytic conditions. Quantitative comparison of ΔE_{kin} and ΔE_{el} and estimation of the size of the compensation effect, more careful measurements of the activation energy are needed.

In spite of the defects which have been mentioned, the data in this work show a nearly exponential increase of the rate constant of the ammonia synthesis, calculated on the basis of unit conventional iron surface, with the reduction in the work function on promoted iron catalysts:

$$K'_{sp.prom.} = K'_{sp.unprom.} \exp(-\alpha\Delta\varphi).$$

* For a definite conclusion as to the nature of the dependence of log K' on $-\Delta\varphi$ it would be necessary to investigate a larger number of catalysts, and this we are at present engaged in doing.

Apparently the reduction of φ affects in the first instance the E of the reaction, reducing its value. This points to an electronic mechanism for the effect of the additive, and explains the reason for the superiority of 3- and 4-component catalysts.

Any more detailed review of the mechanism of the effect of additives would lie outside the scope of the present communication.

LITERATURE CITED

[1] S. S. Lachinov, L. D. Kuznetsov, et al., (Problems of Kinetics and Catalysis) [in Russian] 10 (1960); A. Nielsen and H. Bohlbro, J. Am. Chem. Soc. 74, 965 (1952).

[2] M. Boudart, J. Am. Chem. Soc. 74, 3556 (1952); J. H. de Boer, Adv. in Catalysis 8 (1956).

[3] É. Kh. Enikeev, L. Ya. Margolis, and S. Z. Roginskii, Dokl. Akad. Nauk SSSR 130, 4 (1960). •

[4] L. D. Kuznetsov and S. S. Lachinov, Zhur. fiz. Khim. 33, 11 (1959).

[5] S. Brunauer and P. H. Emmett, J. Am. Chem. Soc. 62, 1732 (1940).

[6] M. I. Temkin, Khim. Nauka i prom. (Chemical Science and Industry) 2, 219 (1957).

[7] Catalysis, ed. P. H. Emmett 3, 1955, p. 283.

[8] S. Z. Roginskii, Dokl. Akad. Nauk SSSR 126, 4, 817 (1959).••

•See C. B. Translation.

••Original Russian pagination. See C. B. Translation.

EQUILIBRIUM IN THE REACTION BETWEEN LEAD TUNGSTATE AND HYDROGEN, AND THE THERMODYNAMIC CHARACTERISTICS OF $PbWO_4$

L. A. Zharkova, Corresponding Member of the Academy of Sciences of USSR Ya. I. Gerasimov, T. N. Rezykhina, and Yu. P. Simanov

M.V. Lomonosov Moscow State University
Translated from Doklady Akademii Nauk SSSR, Vol. 131, No. 5, pp. 1130-1133, April, 1960
Original article submitted December 22, 1959

The equilibrium of lead tungstate has been studied by means of the circulation method described in detail in the literature [1-6].

The lead tungstate was prepared by precipitating a solution of potassium tungstate by a solution of lead acetate, using stoichiometric proportions. The starting salts were of Ch. D. A. (Pure for Analysis) standard, and were purified by recrystallization. The precipitate of lead tungstate was carefully washed, dried and roasted at 800-900°C. Analysis of the product by the method of Hillebrand and Lundell [7], established within an accuracy of 0.5% that the structure corresponded to the formula $PbWO_4$. Hydrogen for reduction was obtained by the electrolysis of a 20% sodium hydroxide solution.

A definite weight of lead tungstate in a porcelain boat was placed in the quartz reactor. The reactor was itself contained in a tube furnace, the temperature of which could be maintained constant to within ± 1°. The temperature was measured by means of a platinum-platinorhodium thermocouple, previously calibrated at the melting points of chemically pure metals and salts.

The water vapor pressure was given at the saturation temperature, using doubly distilled water placed in an ultrathermostat. The temperature of the ultrathermostat was held constant to within 0.05°. The total pressure was measured by means of a mercury manometer with an accuracy of ± 0.1 mm. The equilibrium constant was expressed by the formula $K_p = P_{H_2O}/P_{H_2}$. The gross composition of the products of the reduction was determined by the decrease in weight of the product (the solid lead tungstate), or by the volume of hydrogen used up. The determination of the gas composition was carried out by means of x-ray investigation of the reduction products by the Debye method, using a chamber of diameter 57 mm at the copper anode.

The reduction of lead tungstate proceeds in four stages:

$$10\ PbWO_4 + H_2 = 10\ PbWO_{3.9} + H_2O; \quad \text{(I)}$$

$$^{50}/_{59}\ PbWO_{3.9} + H_2 = {}^{50}/_{59}\ Pb + {}^{50}/_{59}\ WO_{2.72} + H_2O; \quad \text{(II)}$$

$$^{50}/_{36}\ WO_{2.72} + H_2 = {}^{50}/_{36}\ WO_2 + H_2O; \quad \text{(III)}$$

$$^{1}/_{2}\ WO_2 + H_2 = {}^{1}/_{2}\ W + H_2O. \quad \text{(IV)}$$

It should be said that the reduction of $PbWO_4$ to $PbWO_{3.9}$ is considered simply as a formal stage, since we take into account the corresponding portion of the isotherm in calculating the thermodynamic characteristics of $PbWO_4$. We have actually not been able to observe any change in the structure of the material corresponding

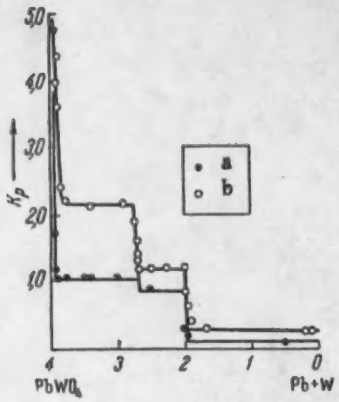

Fig. 1. Isotherms of the reduction of lead tungstate. Temperatures: a) 675°; b) 825°.

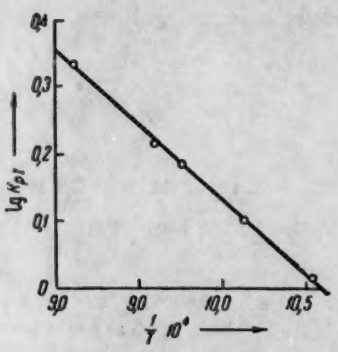

Fig. 2. Relationship between log K_p and 1/T for the second stage in the reduction of lead tungstate.

to the loss of about 0.1 atom of oxygen per molecule. In addition to this, the equilibrium constants for this stage are quite high, and suddenly diminish with composition, which creates considerable difficulties in their measurement. This part of the isotherm has not, therefore, been considered as thoroughly as the others.

For the calculation of the thermodynamic characteristics of completely reduced $PbWO_4$, the first stage must be taken account of by integrating log K_{pI} against the number of oxygen atoms, n, from n = 4 to n = 3.9:

$$\frac{\Delta Z_1^0}{4{,}576T} = -\int_{3{,}9}^{} \lg K_{pI}\, dn.$$

The low accuracy of the high values of the equilibrium constant obtained by us for this interval of n makes it possible to carry out the integration as a straight line function, or, what comes to the same thing, to use a value of K_p obtained by interpolation of the straight line for the mean value of n, and to substitute the slope of the line at the equivalent stage. If we take the values of log K_{pI} for n = 3.95 on the straight line log $K_{pI} = f$ (n) obtained by a graphical approximation, we have, for T = 825°, log K_{pI} = 0.763; and for T = 675°, log K_{pI} = 0.672.

The equation of the straight line through the two points has the form:

$$\lg K_{pI} = -633{,}6\, T^{-1} + 1{,}3404. \qquad (1)$$

In the second stage of the reduction, metallic lead and the tungsten oxide $WO_{2.72}$ are produced, while in the third and fourth stages the oxides of tungsten are reduced. Table 1 gives the relationship between the equilibrium constant and the gross composition of the products of reduction. The same relationship is depicted in Fig. 1.

Table 2 and Fig. 2 give the relationship between the equilibrium constant and the temperature for the second stage of reduction of the lead tungstate. The data of Table 2 are represented with an accuracy of ± 0.5% by the equation:

$$\lg K_{pII} = -2227{,}5\, T^{-1} + 2{,}3635. \qquad (2)$$

For the third and fourth stages we have used the equations provided by I. A. Vasil'eva and her collaborators [6], since our data on the reduction, and the results of x-ray analysis agree with the data of Vasil'eva within the limits of experimental error.

$$\lg K_{pIII} = \lg p_{H_2O}/p_{H_2} = -904{,}83\, T^{-1} + 0{,}90642; \qquad (3)$$

$$\lg K_{pIV} = \lg p_{H_2O} / p_{H_2} = -2325\,T^{-1} + 1{,}650. \quad (4)$$

By combining equations I, II, III and IV we obtain, for the complete reduction reaction of lead tungstate:

$$\begin{gathered} PbWO_4 + 4H_2 = Pb_l + W + 4H_2O; \\ \lg K_{pV} = 0{,}1 \lg K_{pI} + 1{,}18 \lg K_{pII} + 0{,}72 \lg K_{pIII} + 2 \lg K_{pIV}; \\ \lg K_{pV} = -8054\,T^{-1} + 6{,}8756, \end{gathered} \quad (5)$$

hence,

$$\Delta Z^0_V = 36568 - 31{,}4558\,T.$$

TABLE 1

Gross composition of the solid	K_p at 825°	K_p at 675°	Gross composition of the solid	K_p at 825°	K_p at 675°
$PbWO_{3,98}$	10,2	9,9	$PbWO_{2,72}$	1,38	
$PbWO_{3,96}$	8,9	8,8	$PbWO_{2,72}$	1,34	
$PbWO_{3,95}$	6,5	4,7	$PbWO_{2,72}$	1,218	
$PbWO_{3,95}$	5,2	4,77	$PbWO_{2,5}$	1,211	
$PbWO_{3,93}$	4,4	1,76	$PbWO_{2,25}$	1,209	
$PbWO_{3,92}$	3,98	1,25	$PbWO_{2,0}$	1,201	0,3520
$PbWO_{3,90}$	3,6	1,06	$PbWO_{2,0}$	0,7611	0,293
$PbWO_{3,8}$	2,2	1,04	$PbWO_{2,0}$	0,6365	0,242
$PbWO_{3,5}$	2,1	1,03	$PbWO_{2,0}$	0,4448	0,216
$PbWO_{2,9}$	2,2	1,03	$PbWO_{1,7}$	0,3345	0,1790
$PbWO_{2,75}$	1,91	0,898	$PbWO_{0,5}$		0,1558
$PbWO_{2,73}$	1,88	0,87	$PbWO_{0,13}$	0,3394	
$PbWO_{2,73}$	1,63		$PbWO_{0,1}$	0,3402	

By combining reaction (5) with that for the production of water vapor:

$$H_2 + {}^1/_2O_2 = H_2O, \quad (6)$$

We obtain, for the reaction of formation of lead tungstate from its elements:

$$\begin{gathered} Pb_l + W + 2O_2 = PbWO_4, \\ \Delta Z^0_{VII} = 4\Delta Z^0_{VI} - \Delta Z^0_V. \end{gathered} \quad (7)$$

For the formation of water vapor we use the equation of Chipman [8]:

$$\Delta Z^0_T = -59251 + 0{,}871\,T \ln T - 7{,}5 \cdot 10^{-5} T^2 + 408000\,T^{-1} + 6{,}8085\,T.$$

Table 3 gives the calculated values of ΔZ^0_V, ΔZ^0_{VII} and the mean heat of reaction (7) for the temperatures of the experiment.

To calculate the thermodynamic characteristics under standard conditions of the reaction:

$$Pb_{Th} + W + 2O_2 = PbWO_4, \quad (8)$$

we proceed in the following way. By calculating the relationship between the heat capacity and the temperature

TABLE 2

Temp °C	K_p mean	K_p calc.
825	2.16	2.16
770	1.64	1.68
751	1.53	1.53
713	1.28	1.275
675	1.04	1.035

TABLE 3

Temp. °C	ΔZ^0_V, cal/mole	ΔZ^0_{VII}, cal/mole	ΔH^0_{VII}, cal/mole
973	+5962	−191762	−273770
1023	+4388	−187648	
1073	+2816	−182616	
1123	+1243	−179123	

for liquid lead (Pb_{liq}) and all the remaining participating species, we may calculate the thermodynamic functions of reaction (7) for the melting point of lead, T = 600.6°K:

$$c_{pPb\,l} = 7{,}7633 - 0{,}73714 \cdot 10^{-3}T \quad [12]$$

$$c_{pPbWO_4} = 28{,}505 + 9{,}412 \cdot 10^{-3}T \quad [9]$$

$$c_{pO_2} = 7{,}52 + 0{,}81 \cdot 10^{-3}T - 0{,}9 \cdot 10^{5}T^{-2} \quad [10]$$

$$c_{pW} = 5{,}74 + 0{,}76 \cdot 10^{-3}T \quad [11]$$

For ΔC_p we have: $\Delta C_p = -0.038 + 7.769 \cdot 10^{-3} T + 1.8 \cdot 10^{5} T^{-2}$.

Hence: $\Delta H^0_T = \Delta H_0 - 0.038\ T + 3.884 \cdot 10^{-3}T^2 - 1.8 \cdot 10^{5}T^{-1}$.

Substituting the experimental value ΔH^0_T = -273,770 cal for the mean experimental temperature T = 1048°K, we obtain ΔH_0 = - 277,824. Further, we may write the equation for ΔZ^0_T:

$$\Delta Z^0_T = -277824 + 0{,}038\ T \ln T - 3{,}884 \cdot 10^{-3}T^2 - 0{,}9 \cdot 10^{5}T^{-1} + IT,$$

where I is an integration constant, which is evaluated by inserting some experimental value of ΔZ^0_T. The value obtained is I_{mean} = 92.12.

Thus, for reaction (7) at T = 600.6°K, we obtain: $\Delta Z^0_{600.6}$ = - 223,734 cal/mole; $\Delta H^0_{600.6}$ = - 276,746 cal/mole; $\Delta S^0_{600.6}$ = - 88.26 cal/mole · deg.

Converting to solid lead (Pb_{sol}), and taking ΔH for the fusion from [11] to be 1200 cal/mole, and ΔS to be 2.03 cal/mole · deg, we obtain for reaction (8) at 600.6°K the following values: $\Delta H^0_{600.6}$ = - 275,526 cal/mole; $\Delta S^0_{600.6}$ = − 86.23 cal/mole · grad; $\Delta Z^0_{600.6}$ = − 223734 cal/mole.

We now convert to a temperature of 298°K. The heat capacity for each of the participants in the reaction, remains the same except for Pb_{sol}. For this we take:

$$C_{pPbsol} = 5.640 + 2.30 \cdot 10^{-3}T \ [12].$$

Subsequent calculations follow the plan outlined above. As a result, we obtain for $PbWO_4$: ΔZ^0_{298} = -250.0 kcal/mole; ΔH^0_{298} = - 277.0 cal/mole; ΔS^0_{298} = - 89.48 cal/mole · deg.

Taking the entropies of the constituents of the reaction as Pb_{sol}: S^0_{298} = 15.51 [10]; W: S^0_{298} = 8.00 [10]; O_2: S^0_{298} = 49.00 [10], we then obtain $PbWO_4$: S^0_{298} = 32.03 cal/mole · deg.

LITERATURE CITED

[1] T. N. Rezukhina, Ya. I. Gerasimov, and Yu. P. Simanov, Vestn. Moskovsk. Univ. (Moscow University Herald), 6, 103 (1949).

[2] T. N. Rezukhina, Ya. I. Gerasimov, and V. A. Morozova, Zhur. Fiz. Khim. 25, 93 (1951).

[3] T. N. Rezukhina, Yu. P. Simanov, and Ya. I. Gerasimov, Zhur. fiz. Khim. 25, 305 (1951).

[4] T. N Rezukhina, T. M. Dugacheva, and Yu. P. Simanov, Zhur. fiz. Khim. 31, 2206 (1957).

[5] I. A. Vasil'eva, Ya. I. Gerasimov, et al., Zhur. fiz. Khim. 31, 825 (1957).

[6] I. A. Vasil'eva, Ya. I. Gerasimov, and Yu. P. Simanov, Zhur. fiz. Khim. 31, 682 (1957).

[7] V. Hillebrand and G. Lundell, (Practical Handbook of Inorganic Analysis)[in Russian] (Leningrad, 1957).

[8] J. Chipman, Trans. Am. Soc. Metals, 22, 385 (1934).

[9] L. A. Zharkova and T. N. Rezukhina, Zhur. fiz. Khim. 31, 2278 (1957).

[10] Short Reference Book of Physicochemical Quantities, edited by K. P. Mishchenko and A. A. Ravdelya [in Russian] (Leningrad, 1957).

[11] Selected Values of Chemical Thermodynamic Properties, Circ. N. B. S. 500 (1952).

[12] T. B. Douglas and J. L. Dever, J. Am. Chem. Soc. 76, 4824 (1954).

STATISTICAL THEORY OF THE DOUBLE LAYER AT THE METAL-SOLUTION SURFACE

Corresponding Member of the Academy of Sciences of USSR
V. G. Levich and V. A. Kir'yanov

Institute of Electrochemistry of the Academy of Sciences of USSR
Translated from Doklady Akademii Nauk SSR, Vol. 131, No. 5, pp. 1134-1136, April, 1960
Original article submitted January 4, 1960

The double electrical layer at the surface of a metal and a solution plays a most important part in electrochemical and colloidal processes. The basic theoretical ideas concerning the structure of the diffuse double layer were formulated in the works of Gouy, Chapman and Stern [1]. In papers [2-4] attempts have been made to improve the theory of the double layer by taking into account a number of factors left out of consideration in the works just mentioned.

Although the Gouy-Stern theory describes the properties of the double layer over quite a wide range of potentials and concentrations, the neglect of interionic interactions which is characteristic of this theory leads in a number of cases to a divergence between theory and experiment [5-8]. This is especially true of those experimental data which concern nonequilibrium processes taking place in the double layer.

One of the possible causes leading to this divergence between theory and experiment is that which was emphasized by A. N. Frumkin [9], namely, the neglect of the discrete nature of the ionic layers. Efforts to develop theoretically the idea of the discrete structure of the charge in the double layer have been reported in the works of Esin and Shikhov, of Érshler and of Grahame [2-4].

It is also very important to take account of successive-statistical considerations of other aspects of the problem of taking account of the interionic interaction in the theory of the double layer. At the basis of the theory of the diffuse double layer lies the assumption of the finite nature of the layer. This would mean that the potential of the field in the double electrical layer may be calculated on the basis simply of the distance from the surface of the metal. It is clear, however, that in reality the interionic interaction ought to lead to some regularity in the spatial disposition of the ions in planes parallel to the surface of the metal electrode. On the other hand, The Gouy-Stern theory is found to be applicable to solution concentrations at which, it would seem, the assumptions on which it is based can hardly be justified. Finally, it must be noted that the absence of a positive adsorption effect of ions on the metal surface near the point of zero charge cannot be interpreted on the standpoint of the Gouy theory.

Thus, although the theory of the double layer is widely and generally applied in electrochemistry and colloid chemistry, its statistical basis and the limits of its applicability cannot be regarded as having been essentially elucidated.

In this paper we describe an attempt to construct a successive-statistical theory of the double layer at the metal-electrolyte surface.

At the basis of the generalization of the theory lies the correlated function method worked out by Bogolyubov [10, 11], and by Born and Green [12]. In describing the boundary between two phases it is necessary to generalize this method for the case when an external field is present. For high concentrations of the solution,

the calculation of the thermodynamic characteristics of the diffuse double layer may in principle be carried on[10] the basis of "successive approximations". The mathematical difficulties are, however, very considerable.

Therefore, a consistent representation of the theory of the double electrical layer is possible if the values in the starting equation are low. When the volume concentrations of the solution are not too great, it is found possible to use as the relaxation parameter the nondimensional quantity $\epsilon = v/r_d^3$, where $\underline{v}$ is the specific volume, and r_d is a characteristic length depending on the temperature and concentration of the solution. By the configurational space method [10, 11] have been found unary and binary functions for the distribution of the first and second approximations of the parameter ϵ.

It is not possible to present here the complicated procedure [12], and therefore we set out only the summary of the results.

The first approximation leads to the general Gouy theory of the double layer. In the second approximation (the approximation of self-consistent field) the centers of the ions located in the external field are independent of one another, and the mean field does not depend on their mutual position in the planes parallel to the boundary

This approximation is obtained from the Gibbs distribution on the basis of two conditions: that the concentrations of these solutions is so small that $N \ll N_0$, where N_0 is the number of molecules of the solvent; and the absence of correlation between the positions of the ions.

These conditions permit a unique solution of the problems of the self-consistency of the Poisson-Boltzmann equation in the theory of the double layer. This, in contrast with the similar equation of Gronwall, la Mer and Sandwed for a bulk solution [13], does in fact appear to be self-consistent. The physical premises underlying the approximation under discussion make it possible at the same time to point out the limits of applicability of the ordinary theory of the diffuse double layer.

The development of the ordinary theory of the double layer into the successive-statistical theory, makes it possible also, in principle, to estimate the effect of correlation of the ions, on the basis of any arbitrarily chosen law of interaction between them. This effect is described by the second and subsequent approximations by the parameter δ.

At charges close to zero, the calculations are greatly simplified on account of the low value of this second parameter, $\delta = e\varphi_0/kT$ (where φ_0 is the electrode potential).

Calculation taking account of the correlation between the positions of the ions gives a basic value in the immediate neighborhood of the electrode surface (that is, where $x \ll 1/\chi$, where $1/\chi$ is the effective thickness of of the double layer). In order to calculate the correlation, it is necessary to take into account the requirement of equipotentiality of the metal surface, as by the introduction of image forces. It is necessary also to take into account the finite size of the ions when considering their closeness to the surface of the metal. To simplify the calculation we assume that both kinds of ions have the same radius. The separation of the correlation functions of the first and second order in a series according to the values of the small parameters of the theory— ϵ and δ —has made it possible to calculate the correlation functions which determine the probabilities of the mutual position of the ions, the distribution of the mean concentrations and the mean charge densities, and the potential of the self-consistent field in the double layer at the second approximation (that is, to calculate the correction to the Gouy theory of the electrical double layer). In this connection it has been shown that the correction to the characteristics of the double layer determined directly by experiment is practically nil. In an unsymmetrical electrolyte it differs from zero, but is very small. This calculation makes it possible to understand why the theory of Gouy agrees with experiment to a considerable degree of accuracy, even though the concentration in the double layer is not as low as the development of this theory assumes.

We also calculated in the course of this work the adsorption of ions on the electrode near the point of zero charge. In the Gouy approximation no positive adsorption effect is allowed for, since the number of ions undergoing attraction and repulsion at the metal surface is, on the average, the same.

In the subsequent approximations it is necessary to take the image forces into consideration. It has been shown that these in such a case play a very important role, in preventing the accumulation near the metal surface of ions of any one sign.

As a result of the calculations, it has been shown that for the second approximation, also, the numbers of attracting and repelling ions are equivalent. Hence the effect of located adsorption on account of the electrical forces, when these are near to the zero point, appears to be extremely small. The small effect of negative adsorption which is observed experimentally is apparently due to forces of a nonelectrical character.

LITERATURE CITED

[1] Collected Papers: The Coagulation of Colloids [in Russian] (Moscow, 1936).

[2] I. A. Esin and V. S. Shikhov, Zhur. fiz. Khim. 17, 236 (1943).

[3] B. V. Érshler, Zhur. fiz. Khim. 20, 678 (1946).

[4] D. C. Grahame, Chem. Rev. 41, 441 (1947); J. Am. Chem. Soc. 63, 1207 (1941); 68, 301 (1946); 71, 2975 (1949); J. Chem. Phys. 18, 903 (1950).

[5] I. A. Esin and B. A. Markov, Zhur. fiz. Khim. 13, 318 (1939).

[6] Z. A. Iofa and A. N. Frumkin, Zhur. fiz. Khim. 18, 268 (1944).

[7] Graxford, Trans. Farad. Soc. 34, 85 (1940).

[8] Z. A. Iofa, B. Ustinskii, and F. Élman, Zhur. fiz. Khim. 13, 934 (1939).

[9] A. N. Frumkin, Zhur. fiz. Khim. 17, 308 (1943); Phys. Zeits. Sowietunion 4, 256 (1933).

[10] N. N. Bogolyubov, Problems of Dynamical Theory in Statistical Physics [in Russian] (Moscow, 1946).

[11] N. N. Bogolyubov, Vestn. Moskovsk. Univ. (Moscow University Herald), 4-5, 115 (1955).

[12] M. Born, H. S. Green, Proc. Roy. Soc. A 188, 10 (1946); Proc. Roy. Soc. A. 189, 455 (1947).

[13] Gronwall, La Mer Sandwed, Phys. Zs. 22 (1928); A. N. Frumkin, The proceedings of the second international congress of surface activity 3, 1958. D. P. Benton and Fulton, The proceedings of the second international congress of surface activity 3 (1958). R. Parsons, Trans. Faraday Soc. 51, 1518 (1955).

THE PLASTICITY OF THE HIGH-TEMPERATURE MODIFICATIONS OF POLYMORPHIC METALS

E. M. Savitskii and Ch. V. Kopetskii

A. A. Baikov Metallurgy Institute, Academy of Sciences, USSR
(Presented by Academician I. P. Bardin, December 10, 1959)
Translated from Doklady Akademii Nauk SSSR, Vol. 131, No. 5, pp. 1137-1139, April, 1960
Original article submitted December 1, 1959

In 1950, on the basis of a detailed examination of experimental data on polymorphic metals, one of us established a rule [1] according to which the form of a polymorphic metal corresponding to the highest temperature is the one with the highest plasticity, i.e., it should have the cubic crystal structure, predominantly face-centered, which favors plastic deformation. From this rule, a number of important theoretical and practical conclusions were drawn. Since then the rule has been confirmed by a number of papers devoted to the study of new and rare metals [2, 3].

The rule is illustrated by the data in the table, which lists polymorphic metals, together with their crystal structures and the temperatures of the changes from one modification to another (an exception is tin, whose high-temperature modification has a complex tetragonal lattice). The appearance of plastic high-temperature modifications is apparently explained by the fact that in all phase changes, the crystal structures most stable at the higher temperatures are those which are simplest and most symmetrical, since these have the lowest free energy and greatest entropy.

It may be assumed that the existence of different polymorphic forms of a substance is due to a change in the electronic structure of the combined atoms and to the corresponding qualitative changes in the interatomic bonds, with change in temperature [4]. Increase in temperature apparently leads to an increase in the proportion of metallic bonding. The electronic state of the combined atoms of a metal and the number of free electrons per atom, or electron concentration, are apparently affected by temperature changes. Different polymorphic modifications correspond to different electronic states and different electron concentrations.

According to the zone theory of metals, the number of free electrons per atom of a given polymorphic modification, or electron concentration, determined the degree of filling of the Brillouin energy zones, which in turn determines the crystal structure shown by the polymorphic modification in question.

According to the theory of Jones [5] and Hume-Rothery [6-9], the limiting electron concentration corresponding to the point where the Fermi surface touches the first Brillouin energy zone [point of inflection on the N(E) = f(E) curve] has the value 1.36 for the face-centered cubic structure, 1.48 for the body-centered cubic structure, 1.41 for a structure of the β-Mn type, and 1.75 for the close-packed hexagonal structure.

The table shows that for polymorphic metals, with the exception of calcium, strontium and tin, the polymorphic changes accompanying decrease in temperature take place with a definite sequence of crystal structure changes: C12 (C8) $\rightarrow$ H12 (complex).

Decrease in temperature leads to the appearance of the close-packed hexagonal structure, or a complex structure, in place of face or body-centered cubic structures. The H12 structure is stable at higher temperatures than the C12 structure only in the case of calcium and stronium ; in ten cases out of 12, however (scandium,

Metal	M. p., °C	Crystal structure of modifications					Temp. of change, °C
		α	β	γ	δ	ε	
Calcium	851	C 12	H 12	C 8	—	—	350, 450
Strontium	770	C 12	H 12	C 8	—	—	248, 614
Scandium	1205	H 12	C 12	—	—	—	?
Lanthanum	920	H 12	C 12	—	—	—	260, 868
Cerium	805	H 12	C 12	—	—	—	754
Praseodymium	935	H 12	C 12	—	—	—	798
Neodymium	1020	H 12	C 12	—	—	—	868
Samarium	1050	Rhombo-hedral	Close to C 12	—	—	—	917
Titanium	1680	H 12	C 8	—	—	—	885
Zirconium	1857	H 12	C 8	—	—	—	862
Hafnium	2230	H 12	C 8		—	—	1310
Uranium	1133	Rhombic	Complex tetragonal	C 8	—	—	660, 760
Neptunium	640	Rhombic	Ditto	C 8	—	—	278, 540
Manganese	1244	Complex cubic	Complex cubic	C12	C 8	—	727,1090,1134
Iron	1530	C 8	C 8	C12	C 8	—	910, 1405
Cobalt	1490	H 12	C 12	—	—	—	350—470
Thallium	303	H 12	C 12	—	—	—	230
Tin	232	Complex cubic (diamond type)	Tetragonal (complex)	—	—	—	13—18
Rhodium	1960	C 8	C 12	—	—		1030
Plutonium	637	Monoclinic	Complex unknown	Rhombic	C 12 (face-centered tetragonal	C8	122,203,317, 453, 477
Thorium	1750	C 12	C 8	—		—	1400

Note: C12 = face-centered cube, H12 = close-packed hexagonal lattice, C8 = body-centered cube.

lanthanum, cerium, praseodymium, neodymium, titanium, zirconium, hafnium, cobalt, and thallium), the H12 structure is stable at lower temperatures than the C12 or C8 structures. In the remaining cases, complex structures (β -Mn, α-Mn, rhombic, etc.) are stable at low temperatures and the C12 or C8 structures are stable at high temperatures.

From this it follows that with decrease in temperature the crystal structure of the polymorphic modifications changes in such a way as to lead to stepwise increase in the limiting electron concentrations (an exception is the stepwise nature of the change in the crystal structures of the polymorphic modifications observed for calcium and strontium). At low temperatures the stable crystal structures are those with higher limiting electron concentration, while the high-temperature modifications have lower limiting electron concentration. From the step-wise nature of the change in the crystal structures of the polymorphic modifications of metals it may be concluded that with decrease in temperature, a polymorphic substance passes through a succession of states characterized by a definite electron concentration. This electron concentration increases constantly as the temperature decreases, and leads to the step-wise change in crystal structures. It may also be concluded that the number of free electrons per atom in polymorphic metals increases with decrease in temperature.

In some cases (manganese, iron, plutonium and thorium), this sequence is broken– with increase in temperature, the modification corresponding to the highest temperature, with C8 structure and limiting electron concentration 1.48, is converted to a modification with C12 structure (limiting electron concentration 1 36). This discrepancy becomes understandable if it is assumed that at these temperatures (close to the melting point) the electron concentration in the polymorphic metal is less than 1.36 and close to 1.0. At electron concentrations close to 1.0, the face-centered and body-centered cubic lattices have identical stabilities [6-8]. The face-centered cubic lattice is preferred in the presence of forces produced by overlap of the electron clouds of the ions. In the absence of overlap, the body-centered cubic structure is favored. For these metals, the conditions leading to overlap of the electron clouds apparently changes significantly with change in temperature.

Thus the rule concerning the plasticity of the high-temperature modifications of polymorphic metals has a deep physical significance. It apparently indicates a close relationship between the polymorphism and the change in the electronic structure of the atoms of the polymorphic metals with change in temperature.

LITERATURE CITED

[1] E. M. Savitskii, Dokl. Akad. Nauk SSSR 73, 5 (1950).

[2] W. H. Zachariasen, Acta Crystallogr. 5, 5 (1952).

[3] E. M. Savitskii, The Influence of Temperature on the Mechanical Properties of Metals and Alloys [in Russian] (Acad. Sci. USSR Press, 1957).

[4] E. S. Makarov, The Crystal Chemistry of Simple Compounds of Uranium, Thorium, Plutonium, and Neptunium [in Russian] (Acad. Sci. USSR Press, 1958).

[5] H. Jones, Proc. Phys. Soc. 49, 250 (1937).

[6] W. Hume-Rothery, Electrons and Metals [Russian translation] (Moscow, 1949).

[7] W. Hume-Rothery, Atomic Theory for Metallurgists [Russian translation] (Moscow, 1955).

[8] W. Hume-Rothery and G. V. Raynor, The Structure of Metals and Alloys [Russian translation] (Moscow, 1959).

[9] Ya. S. Umanskii, B. N. Finkelshtein, et al., Physical Metallography [in Russian] (Moscow, 1955).

THE REACTION OF THE ISOPROPYL RADICAL WITH THE OXYGEN MOLECULE

L. I. Avramenko and R. V. Kolesnikova

Chemical Physics Institute of the Academy of Sciences of USSR
(Presented by Academician V. M. Kondrat'ev, October 26, 1959)
Translated from Doklady Akademii Nauk SSSR, Vol. 131, No. 6, pp. 1370-1372, April, 1960
Original article submitted October 20, 1959

There seems to be no evidence in the literature of any experimental work devoted to the investigation of the direct interaction of isopropyl radicals with molecular oxygen. Works devoted to the study of the photochemical oxidation of hydrocarbons in no way contribute to an understanding of those in which the direct interaction of aliphatic radicals and oxygen is considered, since the effect of the light is exerted not only on the hydrocarbons, but also on the oxygen [1], as well as on the products of oxidation themselves, so that new radicals, and such atoms as H and O, are formed by this process. Because of this, it is not possible, by the photochemical method, to distinguish between primary, secondary and repetitive* reaction products, etc., therefore it is difficult by this method to draw unequivocal conclusions as to the reaction mechanism. This is especially true in mercury-sensitized reactions.

We have decided to investigate the problem of determining the reaction products of the interaction of isopropyl radicals and oxygen molecules, using strictly regulated conditions in which the effect of light on the reaction products, such as occurs in photochemical experiments, would be eliminated. For this purpose we have used the method which we have presented previously [2, 3] in connection with the investigation of the reaction of the ethyl radical with the oxygen molecule.

EXPERIMENTAL WORK AND DISCUSSION OF RESULTS

The isopropyl radicals were obtained by us by means of the reaction of hydrogen atoms, produced in a stream of gas by an electrical discharge through hydrogen, on propylene. A conical connection between the discharge and reaction vessels made it possible to separate the region in which the hydrogen atoms were produced from that in which the reaction: $H + C_3H_6 \rightarrow$ iso-C_3H_7 took place. The surface of the reaction vessel was coated with potassium chloride. The work of Bradley, Melville and Robb [4] has shown that the reaction between H and C_3H_6 produces preferentially the isopropyl radical. In order to avoid any possibility of the subsequent reaction: $H + C_3H_7 \rightarrow CH_3 + C_2H_5$, the propylene in the reaction zone was used at pressures of from 0.3 to 0.5 mm of mercury, which exceed the hydrogen atom concentration by more than an order of magnitude. It has been shown, by means of special experiments carried out in plate-glass vessels coated with carbon black, that at such propylene concentrations, no hydrogen atoms can be detected even as close as 2 cm from the place

* Translator's note: "kvadratichnyi" presumably means, in this context, products due to a reaction already considered, the reactants for which have been produced by a secondary or later reaction: that is, the reaction may be primary or secondary in itself, but the materials taking part in it are not wholly those originally introduced, but are, at least partly, those produced by later processes.

TABLE 1

Rate of oxygen supply, 1×10^{-17} mol/sec	Rate of formation of peroxide, 1×10^{-16} mol/sec	Rate of formation of acetone, $1 \times \times 10^{-16}$ mol/sec	Formation of aldehydes
5.48	0.31	0.1	Not detected.
6.4	0.36	0.1	Not detected.
8.2	0.29	0.1	Not detected

of mixing, which is an obvious indication of the rapidity of their reaction with the propylene. If we are to obtain reliable evidence concerning the reaction of aliphatic radicals with oxygen molecules, it is of the first importance that H-atoms shall be absent at the point where the radicals and the oxygen molecules are mixed.

For this reason, the oxygen molecules were in this work introduced into the reaction zone at distances of 2 cm or more from the coupling. The introduction of the oxygen at this distance ensured that there would be no interaction between H atoms and O_2 molecules. It should be noted, however, that it is only possible to ensure this if no back diffusion of the oxygen occurs. This will depend on the rate of the stream of the carrying gas and on the concentration of the oxygen. It is important that H atoms should be absent from the diffusion zone, for, as the authors have shown [5], under the flow conditions and the low temperatures and pressures, there would otherwise take place on the walls of the vessel a reaction leading to the formation of oxygen atoms: $H + O_2 \rightarrow OH + O$, which would then participate in the reaction and contribute to the reaction products.

If there were to occur simultaneously reaction of oxygen atoms with the hydrocarbons, and of oxygen molecules with the aliphatic radicals, it would be impossible to draw unequivocal conclusions either about the reaction products or about the reaction mechanism.

Amongst the oxygen-containing products of the reaction of the isopropyl radical with oxygen molecules, there might be expected hydrogen peroxide, acetone, acetaldehyde and formaldehyde and isopropyl alcohol. The reaction products, together with the propylene, were collected in a trap cooled with liquid nitrogen, and subsequently analyzed. The peroxide was determined polarographically and by titration of the iodine liberated on acidification and addition of potassium iodide. In our experiments no hydrogen peroxide was found. Acetone was determined by the furfural method. Analysis of the aldehydes was carried out by a polarographic method, and in addition the formaldehyde was determined by means of a sensitive color reaction (a solution of phenylhydrazine hydrochloride + potassium ferricyanide + HCl was the reagent used). The isopropyl alcohol was detected qualitatively by means of its reaction with m-nitrobenzaldehyde.

The results of analyzing the reaction products in certain experiments are set out in Table 1. The experiments were conducted at an over-allpressure $P_{tot} = 8$ mm, and a temperature of 150°. The rate of propylene supply was 4.15×10^{18} mol/sec. Oxygen was introduced at a distance of 3 cm from the point where the H-atoms were mixed with the propylene. Under these experimental conditions, the products detected from the reaction of the isopropyl radicals were: peroxide, acetone and isopropyl alcohol. Careful search for aldehydes (formaldehyde and acetaldehyde) was made, but with negative results. Since peroxide was detected among the reaction products, there can be no doubt as to the formation of the peroxidic radicals iso-$C_3H_7O_2$. If isomerization of the peroxidic radical takes place, we should expect to find that the CH_3O radical and acetaldehyde were formed, but under the conditions of our experiments no aldehydes are formed. It can be supposed that the reason for the absence of aldehydes is that the temperature is not sufficiently high to bring about the decomposition of the iso-$C_3H_7O_2$ radical. In order, therefore, to study the behaviour of the isopropylperoxide radical at temperatures higher than 150°, a new temperature arrangement was provided for the apparatus. In the first place, for a distance of 9 cm from the coupling, a temperature of 150° was maintained in the reaction vessel (so that under these conditions the iso-$C_3H_7O_2$ would be formed, a fact confirmed by the detection of peroxide in the reaction products); and then for a distance of 25 cm, the temperature of the reaction vessel was maintained at 350°.

TABLE 2

Rate of oxygen supply, 1 × × 10^{-17} mol/sec	Rate of formation of peroxide, 1 × × 10^{-16} mol/sec	Rate of formation of acetone, 1 × × 10^{-16} mol/sec	Formation of aldehydes	Formation of isopropyl alcohol
5.5	0.03	0.08	Not observed.	Not observed.
6.5	0.03	–	Not observed.	Not observed.
5.5	–	0.08	Not observed.	Not observed.

It was assumed that the peroxide radical formed at a temperature of 150° in the first zone would only be decomposed when it attained a temperature of 350° in the subsequent zone, and that corresponding changes would be observed in the reaction products. Such changes in reaction products were actually observed experimentally, but the results were by no means those which we expected. The experimental results under the new temperature conditions are shown in Table 2. The experiments were carried out at P_{tot} = 8 mm mercury. The rate of propylene supply, and the point at which oxygen molecules were introduced were the same as in the experiments described in Table 1.

It is seen from Table 2 that increase in temperature led to a reduction in the peroxide yield by a factor of 10. The yield of acetone was only slightly reduced; and at the same time it was impossible to observe any aldehyde production, in spite of very careful search and in spite of our expectations. Since increase in temperature to 350° led to decomposition of the iso-$C_3H_7O_2$ radical (with an abrupt reduction in the peroxide yield as the result), without any production of aldehydes, then it might have been expected that an increase in the of isopropyl alcohol or of acetone would occur. But, although isopropyl alcohol is observed at 150°, at this temperature it does not occur at all, and the acetone yield is actually reduced. This experimental fact leads to the conclusion that at comparatively low temperatures (150°), the isopropyl peroxide reaction undergoes simultaneous reactions, the one giving rise to the peroxide, and the other to the alcohol. It can reasonably be supposed that the formation of these products occurs according to the following scheme:

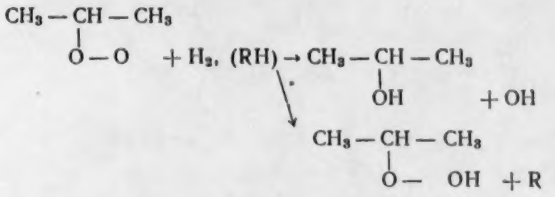

Decomposition of the isopropyl peroxide radical is accompanied by the disappearance of the peroxide and the alcohol as reaction products (in the reaction at 350°). And since there is no formation of aldehydes under these conditions either, it must be supposed that the decomposition of the peroxide radical leads back to the isopropyl radical and molecular oxygen.

$$\text{iso-}C_3H_7O_2 \rightarrow \text{iso-}C_3H_7 + O_2.$$

It is not possible to explain the disappearance of peroxide from the reaction products at 350° by the decomposition of this peroxide itself, since if this occurred it should not be accompanied by the disappearance of the isopropyl alcohol.

The formation of acetone under our experimental conditions is assumed to take place on the surface, in a manner similar to that in which acetaldehyde is formed by the interaction of ethyl radicals with oxygen [2, 6]. But since we have been able to explain the formation of acetaldehyde on a potassium chloride surface from C_2H_5 and O_2 on the basis of the assumption that modification of the reaction vessel and coating with potassium

chloride gives only the one hydroperoxide as reaction product, it follows in the reaction involving iso-$C_3H_7O_2$ that coating of the vessel with potassium chloride will not cause acetone to disappear from the reaction products. The absence of acetaldehyde formation in the reaction of iso-C_3H_7 with oxygen molecules, and the decomposition of iso-$C_3H_7O_2$ radical at the increased temperature without the formation of aldehydes and isopropyl alcohol gives reason to suppose that, if the iso-$C_3H_7O_2$ radicals are formed, their subsequent transformation must involve either the formation of the hydroperoxide, or decomposition without the formation of aldehydes or alcohols.

LITERATURE CITED

[1] R. H. Burgess and J. C. Robb, Trans. Farad. Soc. 54, 1015 (1958).

[2] L. I. Avramenko and R. V. Kolesnikova, Izv. Akad. Nauk SSSR, Otd. Khim. Nauk 1192 (1958).*

[3] L. I. Avramenko, R. V. Kolesnikova and L. M. Postinkov, Izv. Akad. Nauk SSSR, Otd. Khim. Nauk 277 (1958).*

[4] J. N. Bradley, H. W. Melville, and J. C. Robb, Proc. Roy. Soc. 236, 339 (1956).

[5] L. I. Avramenko and R. V. Kolesnikova, Zhur. fiz. Khim. 32, 2780 (1958).

[6] L. I. Avramenko and R. V. Kolesnikova, Izv. Akad. Nauk SSSR (in the press).

*Original Russian pagination. See C. B. Translation.

THE ORIENTATION OF THE π-ELECTRON ORBITAL IN THE CYCLOPROPANE RING

V. T. Aleksanyan and Kh. E. Sterin

Spectroscopy Commission of the Division of
Physico-Mathematical Sciences of the Academy of Sciences of USSR
(Presented by Academician B. A. Kazanskii, January 4, 1960)
Translated from Doklady Akademii Nauk SSSR, Vol. 131, No. 6, pp. 1373-1375,
April, 1960
Original article submitted December 25, 1959

During the investigation of the Raman spectra hydrocarbons, in which a three-membered ring occurs together with a series of double bonds or a phenyl nucleus, we have discovered the occurrence of anomalous intensification of some of the lines corresponding to the three-membered ring and to the double bonds, or to both rings, when compared with the same lines for alkylcyclopropanes, alkylbenzenes, or alkenes; that is, for compounds containing only one of the structures under consideration [1]. A similar effect, more clearly revealed, is well-known in conjugated systems, and therefore the observed phenomenon has been ascribed to the conjugation of the three-membered ring with the double bonds (whether simple or aromatic).

It is well known that the conjugation effect of π-bonds is a maximum if their π-electron orbitals are parallel, and the greater the deviation from parallel alignment, the weaker is the conjugation effect. We have investigated the Raman spectra of the stereoisomers of 1,2-diphenyl-2-cyclopropylcyclopropane [2]. Calculation has shown that with the cis-isomers the common orientation of the cyclopropyl and phenyl rings, which is the most favorable for conjugation, may not be realized because of steric hindrance. With the trans-isomers, on the other hand, such orientations are permissible. Comparison of the spectra of each pair of isomers has shown distinctly in which cases the conjugation is the stronger, and on this basis the cis-configuration has been ascribed to the lower-boiling isomer, and the trans-configuration to the higher-boiling isomer.*

The investigation of the stereoisomeric 1-phenyl-2-cyclopropylcyclopropane gives results of great interest. The conjugation effect is practically absent from the spectrum of the cis-isomer; but in the case of the trans-isomer the magnitude of the effect is the same as in the case of phenylcyclopropane. A consideration of the configuration of the cis-isomer has shown that the steric hindrance is a minimum when the phenyl and cyclopropane rings take up the mutual positions shown in A (Fig. 1); in this case, according to theory [5, 6], conjugation would not be expected to take place.**

*The effect of the stereochemical factor on the conjugation conditions for three-membered rings with substituents has also been investigated by Cromwell and his colleagues [3, 4] for some derivatives of ethylene imine. These authors draw their conclusions about the existence of conjugation from the existence of an absorption band in the near ultra-violet region, and of an absorption band corresponding to C = O in the infrared spectrum. We consider that the most convenient and reliable spectra for this purpose are the Raman spectra (cf. [2]).

**Theory suggests that the π-electron "octet" of the cyclopropane molecule is situated in the plate of the ring, perpendicular to the plane of the CH_2 groups [5].

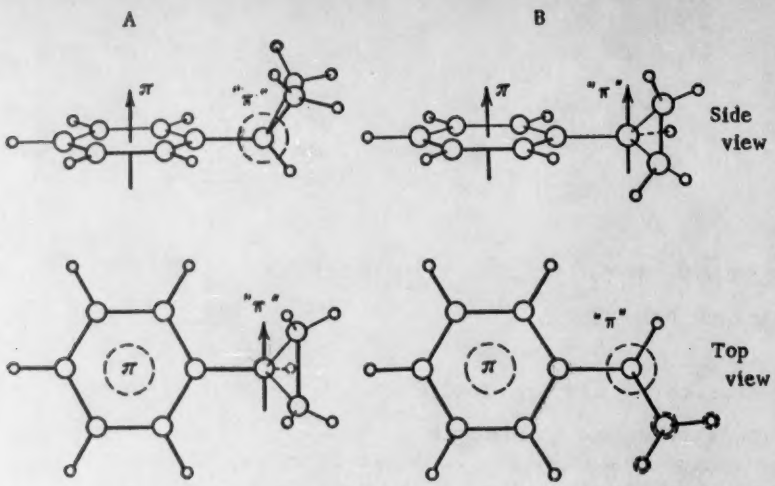

Fig. 1.

Thus the facts adduced show the utility of the present ideas on the structure of the three-membered ring. This conclusion, however, cannot be regarded as definitely established, since the difference between the most favorable configuration A, from a steric point of view, of cis-1-phenyl-2-cyclopropylcyclopropane, and other possible but sterically less favorable configurations (amongst which must be considered those in which the phenyl ring occupies the position B in relation to the cyclopropane ring), is not great. Therefore, in order to provide more convincing evidence about the structure of the three-membered ring, it was judged necessary to study a compound in which, because of the steric peculiarities, one or the other of the configuration A and B is more stably fixed.

For this investigation the compound chosen was 1-1-diphenylcyclopropane, in which it would be expected that each of the phenyl rings would, because of its steric peculiarities, occupy position A in relation to the cyclopropane ring. The method of measuring the frequencies and intensities of lines at the maximum has been described earlier [7]. The integral intensity was determined by direct measurement from the coauthors of the lines at each 1-1.2 cm^{-1}.

1,1-diphenylcyclopropane

$\Delta\nu$ (cm^{-1}): 150(60,b)•• 211 (49), 220(50), 263 (14), 285(6), 302(34), 325(3), 336(3), 375(12), 402(45), 451(8), 479(5), 499(2), 537(14), 551(7, g)•• 563(13), 582(26), 621(90, s), 655(6), 670(6), 692(125, s), 708(3), 724(4), 738(3), 763(23), 773(12, g), 808(5), 825(10, b), 842(17, b), 875(32), 935(60), 989(15, s), 1002(540, s), 1026(40), 1032(140), 1053(3), 1085(6), 1129(41), 1157(47), 1179(20), 1192(19), 1265(50), 1280(88), 1298(80), 1313(20), 1328(35), 1342(10), 1359, (5, b), 1404(2), 1426(12), 1444(10), 1460(27), 1476(3, b), 1496(12), 1580(34), 1601(250, b), 1634••(3), 1684••(3, b), 2426 (15, g), 2449(5, b, g), 2495(20, b), 2524(10, b), 2560(20, b), 2842 (5, g), 288(110, g)••• 2909(15, g), 2931(10, g), 2978(50), 3005(190, b), 3064(470), 3084(70), 7315(30), 3200(20).

DISCUSSION OF RESULTS

The table gives the results of measurements of the integral intensities of the line around 1600 cm^{-1} in the spectrum of 1,1-diphenylcyclopropane, as well as in the spectra of 1-phenyl-2-cyclopropyl- and 1,2-diphenylcyclopropanes which have been studied earlier. It can be seen that the intensity of the line around 1600 cm^{-1} of 1,1-diphenylcyclopropane is much less than those of the stereoisomeric 1,2-diphenylcyclopropanes. The intensity of this line for 1,1-diphenylcyclopropane in relation to one phenyl group is only twice as great as for the different alkylbenzenes, and is practically the same as that for the cis-isomer of 1-phenyl-2-cyclopropylcyclopropane. Since the orientation of each of the phenyl rings in relation to the cyclopropyl ring in the molecule

•Symbols: b = broad; s = sharp; g = background.

••It is not impossible that these lines may be due to impurities.

•••As in the original Russian.

Integral Intensities of the line I_{ω} around 1600 cm^{-1} for some Aromatic Compounds

Compounds	I_{ω}	I_{ω} related to a single phenyl ring
Toluene	290	290
Isopropylbenzene	330	330
Phenylcyclopropane	1150	1150
Cis-1,2-diphenylcyclopropane	2200	1100
Trans-1,2-diphenylcyclopropane	4100	2050
Cis-1-phenyl-2-cyclopropylcyclopropane	600	600
Trans-1-phenyl-2-cyclopropylcyclopropane	1100	1100
1,1-diphenylcyclopropane	1300	650

of 1,1-diphenylcyclopropane may be calculated to be satisfactorily described by configuration A, it is easy to conclude that in this case the phenyl and cyclopropyl rings are only weakly conjugated with each other. As we have shown above, this is in agreement with the conclusions of the theory which proposes that the π-electron orbital is located in the plane of the three-membered ring, and also, evidently, supports the creditability of the premise from which this conclusion was drawn. It should be noted that the relatively weak conjugation between the cyclopropane and phenyl rings in 1,1-diphenylcyclopropane is also confirmed by chemical evidence: of all the diphenylcyclopropanes investigated, the compound here considered has the lowest rate of hydrogenation leading to the rupture of the C-C bond of the three-membered ring [8].

In conclusion, we should observe that in the spectrum of 1,1-diphenylcyclopropane there is present a line very characteristic for the cyclopropane ring: that is, the line for the valency oscillations of the C-H bonds at around 3005 cm^{-1} [1].

LITERATURE CITED

[1] V. T. Aleksanyan, Kh. E. Sterin, et al., Proceedings of the 10th All-Union Conference on Spectroscopy (L'vov, 1956); [in Russian]: Physical Symposium of L'vov, 1956); [in Russian] 3, (8) (1957).

[2] V. T. Aleksanyan, Kh. E. Sterin-et al., Optika i spektroskopiya 7, 178 (1959).

[3] N. H. Cromwell and M. A. Graff, J. Org. Chem. 17, 414 (1952).

[4] N. H. Cromwell and G. V. Hudson, J. Am. Chem. Soc. 75, 872 (1953).

[5] A. D. Walsch, Trans. Farad. Soc. 45, 179 (1949).

[6] C. A. Coulson and W. E. Moffit, Phil. Mag. 40, 1 (1949).

[7] V. T. Aleksanyan and Kh. E. Sterin, Optika i spectroskopiya 3, 562 (1957).

[8] B. A. Kazanskii, M. Yu. Lukina, and I. L. Safonova, Dokl. Akad. Nauk SSSR 130, 2 (1960).*

*See C. B. Translation.

THE COMPOSITION OF THE PRODUCTS, AND THE MECHANISM OF INITIATED CRACKING OF GASEOUS ALKANES

E. M. Gamus-Chernyavskaya, S. Sh. Reznikova, and A. D. Stepukhovich

N. G. Chernyshevskii Saratov State University

(Presented by Academician V. N. Kondrat'ev, December 7, 1959)
Translated from Doklady Akademii Nauk SSSR, Vol. 131, No. 6, pp. 1376-1379, April, 1960
Original article submitted November 30, 1959

Practically no investigations have been made on the composition of the products obtained during the initiated cracking of alkanes by the addition of azomethane. Although the study of the kinetics of initiated cracking by means of measurements of Δ_p against time for the decomposition of the initiating substance makes it possible to establish the reality of the initiation [1-3], it is still desirable to have it directly demonstrated by an investigation of the composition of the products of decomposition of the mixture of alkane and initiating substance. A study of the products of the initiated cracking is also necessary for the elucidation of the mechanism of initiated cracking and of the ways in which it differs from the ordinary decomposition of the alkanes.

In the present work there has been studied first of all, in detail, the composition of the products obtained from the cracking of propane and butanes, initiated by addition of azomethane, using the method of gas chromothermography. This gives clear evidence that initiation of the decomposition of the alkanes proceeds to a considerable extent, which is, perhaps, a most weighty reason in support of a radical-chain mechanism of thermal cracking. The same data provide confirmation of the reality of initiation previously proved on the basis of purely kinetic data not free from objection. In addition to this, the study leads to new conclusions about the mechanism of this process.

The elaborate vacuum plant which has been erected for this complicated investigation of initiated cracking of alkanes has been described by us in an earlier publication [4].

The results of analyzing the products of the initiated cracking of propane and the butanes on a chromothermographic column are given in the table. They show that neither propane (364°, 80 mm, cracking time 10 min) nor butane (355°, 70-76 mm, cracking time 10 min) decomposes by itself, even under conditions when the initiating substance decomposes. However, the introduction of small quantities of azomethane (1-3%) produces cracking of the alkanes to a considerable extent. In the initiated cracking of propane, both dehydration and demethanation may occur. In comparison with ordinary cracking, the introduction of even this small amount (1-3%) of azomethane causes dehydrogenation to exceed demethanation by a factor of three, while thermal cracking under approximately the same conditions with respect to pressure and amount of cracking gives dehydrogenation and demethanation to the same extent, or slightly in favor of the demethanation. In addition to this, the methane yield with the same starting mixture is about twice as great as that of ethylene. With ordinary cracking the yields of methane and ethylene remain about equal up to very high degrees of decomposition. Small additions of the initiator produce high yields of ethane, which are due not only to the decomposition of the azomethane, but also to the enhancing, under the conditions of the initiated reaction, of the recombination reaction between methyl radicals.

Composition of the Products of the Cracking of Propane and the Butane, Initiated by Azomethane (in volume percent)

P of alkane, mm	P of azomethane, mm	N_2	H_2	CH_4	C_2H_4	C_2H_6	C_3H_6	C_3H_8	C_4H_8	C_4H_{10}
Propane (364°, 10 min)										
80,0	—	—	—	—	—	—	—	—	—	100
77,6	2,4 (3%)	3,3	1,5	0,75	0,44	1,65	1,79	90,5	—	—
74,4	5,6 (7%)	4,16	2,6	4,4	2,8	3,51	2,8	79,5	—	
72,0	8,0 (10%)	7,18	3,1	5,63	3,36	4,2	3,24	73,4	—	—
—	2,2 in a medium of CO_2 (70 mm)	50,0	—	—	—	5,0	—	—	—	—
Butane (355°, 10 min)										
70,0	—	0	0	0	0	0	—	0	0	100
70,0	2,1 (3%)	2,59	0,97	7,46	2,39	2,33	9,72	0,77	1,1	72,64
70,0	2,1 (3%)	2,59	0,97	7,79	2,27	2,33	9,67	0,84	1,1	72,72
—	2,1 in a medium of CO_2 (70 mm)	50,0	—	—	—	50,0	—	—	—	—
Isobutane (355°, 10 mm)										
76,0	—	0	0	0	0	0	0	0	0	100
76,0	0,76 (1%)	1,2	1,47	4,44	0,48	0,7	2,2	0,9	1,47	87,63
76,0	2,4 (3%)	2,8	1,6	7,48	0,5	0,75	4,1	1,13	1,5	80,1
76,0	3,8 (5%)	5,2	1,75	8,52	0,7	0,85	6,3	1,1	1,63	72,75
76,0	5,3 (7%)	6,0	1,8	10,76	0,7	1,1	6,35	~1,0	1,64	70,56
76,0	7,6 (10%)	5,9	1,86	11,45	0,7	1,24	6,5	~1,1	1,65	68,72

Increase in the concentration of the added azomethane to 7-10% also increases the extent of initiated cracking, although at a slower rate than with low additions, and the demethanation reaction becomes increasingly predominant. Increase in the concentration of the additive from 3 to 10% causes a 7.5-fold increase in the ethylene yield, while at the same time the yield of C_3H_6 is only increased 2-fold. The methane yield, as before, is considerably greater than the ethylene yield, while the ethane yield amounts to slightly more than half that of nitrogen.

These results show not only the initiating effect of the methyl radical on the decomposition of propane, but also reveal, even more clearly than in the ordinary cracking previously studied by us [4], the enhancing of the demethanation reaction. Increase in the azomethane concentration in the range 3-10% causes the ratio $C_2H_4 : C_3H_6$ to increase from 0.25 to 1, or roughly proportionally to the concentration of the azomethane. The shift in the direction of demethanation is probably to be explained by the isomerization of the isopropyl radicals, formed preferentially at the lower temperatures, into propyl radicals. It is less probable that the increase in the yield of $CH_3CH_2-\dot{C}H_2$ radicals is due to increase in the concentration of CH_3 radicals.

The increase in the yield of CH_4 in comparison with that of C_2H_4 shows that the CH_3 radicals are distributed between the azomethane and the propane. In the decomposition of pure azomethane there undoubtedly also occurs a reaction between CH_3 and azomethane to give methane. It follows that in azomethane the double bond, N = N, weakens the C-H bond in the β-position, in the same way as C=C weakens the C-H bond in the methyl group of propylene. On the other hand, the C-H bond in azomethane is less stable than the secondary C-H bond in propane. In the light of these facts, the decomposition of azomethane cannot be considered as a simple unimolecular reaction, as we also observed in our study of the kinetics of the decomposition of azomethane.

It is possible that the increased yield of ethane is due to an addition reaction of the CH_3 to the azomethane: $CH_3 + CH_3N = NCH_3 \rightarrow (CH_3)_2N\text{-}\dot{N}CH_3$, with subsequent regeneration of the azomethane according to the reaction:

$$\dot{C}H_3 + (CH_3)_2N - \dot{N}CH_3 \rightarrow C_2H_6 + CH_3N = NCH_3.$$

This is equivalent to a recombination in the bulk phase through the intermediate reaction with a molecule of azomethane, not on the walls. The decomposition of azomethane in a medium of carbon dioxide produces

nitrogen and ethane exclusively. In the alkane medium the decomposition must proceed in a different way, which is of interest in connection with the development of the initiated cracking process.

In the initiated cracking of butane, the same trends are observed, and approximately the same ratio between the products as in ordinary cracking. The two products are obtained in equalyields (with a slightly larger amount of C_3H_6 than of CH_4). The ratio $C_3H_6 : C_2H_4 : H_2$ in the initiated cracking (355, 70 mm, 10 min) is equal to $1^0 : 2.5 : 1$, whereas in ordinary cracking (548°, 180 mm, 6 min) the values are $9 : 3.5 : 1$ [4]. Thus, in the initiated cracking of butane, demethanation gains further ground in comparison with the splitting off of ethane. This is explained by recognizing that reduction of temperature is more favorable to the decomposition of $CH_3CHCH_2CH_3$ radicals (heat of decomposition 27.7 kcal) than to that of $CH_3CH_2CH_2CH_2^{\cdot}$ radicals (heat of decomposition 31 kcal), and as a result there is a partial conversion of the latter into the former.

In the ordinary cracking of isobutane, as is well known, the dehydrogenation process predominates over the reaction in which decomposition occurs to CH_4 and C_3H_6. The ratio iso-$C_4H_8 : C_3H_6 : C_2H_4$ at 548° and 180 mm after 6 minutes is equal to 7 : 3 : 1 [4], which is determined by the preferential formation of the tertiary isobutyl radicals, $(CH_3)_3C^{\cdot}$, and their subsequent decomposition.

In the initiated cracking of isobutane (at 355.76°, 76 mm, and 10 min), even from the start, with low additions of the initiator (3%), the demethanization reaction predominates, and the ratio given above amounts now to 2 : 6 : 1. The ratio of iso-C_4H_8 to C_3H_6 is changed from the value of 2.4 which it has in ordinary cracking, to 0.26 in the initiated process, or by a factor of 10. This shift in the decomposition tendency is explained by the fact that, notwithstanding the preferential formation of tertiary isobutyl radicals (through attack of the isobutane molecule by CH_3 radicals), these latter decompose less readily under the conditions which obtain during initiated cracking, and are partially isomerized into primary isobutyl radicals: -

$$(CH_3)_3\dot{C} + (CH_3)_3CH \rightleftarrows (CH_3)_3CH + \dot{C}H_2CH(CH_3)_2.$$

The isomerization reaction requires a much smaller energy of isomerization (around 25 kcal), and the decomposition of the primary isobutyl radicals proceeds very easily (energy of decomposition is 3.5 kcal).

As in the case of the induced cracking of propane, increased yield of CH_4 is observed, which is due to the sharing of the CH_3 radicals obtained from the initiator between the alkane molecules and those of the added initiator, according to the concurrent reactions:

$$\dot{C}H_3 + (CH_3)_3CH \rightleftarrows CH_4 + (CH_3)_3\dot{C} \text{ (activation energy 7.9 kcal)}$$
$$CH_3 + CH_3N = NCH_3 \rightleftarrows CH_4 + \dot{C}H_2N = NCH_3 \text{ (activation energy 6.4 kcal).}$$

With an increase in the azomethane concentration (1-3%), the initiating effect at first increases rapidly, but further increase in the additive (5-7%) only produces small increase in the extent of decomposition, and the initiated cracking approaches a limit of initiator effect, as had earlier been predicted by us [5]. This demonstrates the effectiveness of initiation by small quantities of the initiator. The limit of effectiveness is due to the fact that the initiator can act not only as a donor but also as an acceptor of radicals.

On the other hand, with an increase in the extent of the initiated cracking, a retarding effect of the products of cracking begins to arise [5]. The experimental data on the initiated cracking of propane and the butanes are well represented by the Dinzes and Frost equation for autoretarded reactions. Comparison of the initiated cracking of butanes shows that butane is initiated more effectively than isobutane, which is due to the easier decomposition of the primary and secondary butyl radicals compared with tertiary isobutyl radicals. The fact should be mentioned that the extent of the initiated cracking of alkanes, arrived at after a somewhat longer time, corresponds to the extent of ordinary cracking, which may prove to be of some practical consequence, especially in the search for new ways of effecting chemical transformation of well-head petroleum gases, waste gases from cracking processes, and alkanes of high molecular weight.

It is difficult to explain at present the formation of propane in the initiated cracking of isobutane since it is not clear how propyl (or ethyl) radicals can arise in the absence of primary decomposition of the isobutane. It is possible that they are formed by the addition of CH_3 radicals to ethylene. More careful investigation of the kinetics of the initiated cracking of propane and isobutane has shown that the curves for their initiated decomposition are similar (percentage decomposition plotted against time) and, in particular, that the curves for propane do not have the S-shape. In other respects the previous results have been confirmed [1].

The rate of the initiated cracking of propane and isobutane with constant addition of azomethane diminishes with increase in time according to a curve similar to that obtained for the relationship between rate and time for autoretarded cracking, with the single difference that the curve for the rate of initiated cracking approaches the axis of abscissas.

Consideration of the results presented above leads to the conclusion that it might be advantageous to carry out experiments on the application of initiated cracking under industrial conditions, with a view to gathering information about its suitability as a new technological process.

In conclusion we wish to express our thanks to R. V. Kosyreva for helping with the analyses.

LITERATURE CITED

[1] A. D. Stepukhovich and V. V. Tatarintsev, Dokl. Akad. Nauk SSSR 94, 1049 (1954).

[2] A. D. Stepukhovich and E. G. Kaplan, Zhur. fiz. Khim. 30, 929 (1956).

[3] A. D. Stepukhovich and E. E. Nikitin, Zhur. fiz. Khim. 30, 1291 (1956).

[4] A. D. Stepukhovich, Dissertation [in Russian] (Moscow, 1958).

[5] A. D. Stepukhovich, Zhur. fiz. Khim. 30, 556 (1956).

CALCULATION OF PRODUCT YIELDS IN THE RADIOLYSIS OF ALKANES

Yu. A. Kolbanovskii and B. A. Smirnov

Institute of Petroleum-Chemical Synthesis, Academy of Sciences of USSR
(Presented by Academician A. V. Topchiev, November 6, 1959)
Translated from Doklady Akademii Nauk SSSR, Vol. 131, No. 6, pp. 1380-1382, April, 1960
Original article submitted November 6, 1959

The object of the present work was to arrive at an equation for the balance of the products of radiolysis of alkanes, so as to permit the determination of the various fractions from a limited number of experimental data. For this purpose the calculation of the yield of the heavy residue, which is most difficult to obtain from experimental determinations, is very important. To illustrate the relationships arrived at, a calculation is given of the balance of the products of radiolysis of n-heptane in the linear and nonlinear regions.

The basic products of the radiolysis of alkanes are hydrogen, monoolefins and also alkanes of normal and isomeric structure and of different molecular weight, having $\underline{x}$ carbon atoms in the molecule, where $\underline{x}$ may be greater than, equal to or less than $\underline{n}$, the number of carbon atoms in the initial hydrocarbon. When the number of molecules after irradiation, N_K, is connected with the initial number of molecules of the starting alkane, N_0, we have the relationship:

$$N_к = N_0 + N'', \tag{1}$$

where N'' is the number of molecules of monoolefins obtained by radiolysis. In addition, we may write another equation for N_k:

$$N_к = N_n + N_L + N_L'' + N_т + N_x'', \tag{2}$$

when N_n is the number of molecules of the original alkane left after radiolysis; N_L'' is the number of molecules of hydrogen and of alkanes with $\underline{x}$ less than $\underline{n}$; N_L'' is the number of molecules of monoolefins with $\underline{x}$ less than $\underline{n}$; N_x'' is the number of molecules of monoolefins with $x \geq n$; and N_T is the number of molecules of alkanes with $\underline{x}$ greater than $\underline{n}$.

It follows from (1) and (2) that

$$N_n = N_0 - (N_L + N_т) \tag{3}$$

or,

$$N_т + N_n = N_0 - N_L'. \tag{3'}$$

For practical purposes we arrive at the useful relationships:

$$N_x = N_n + N_T + N_x^{''} \tag{4}$$

or, taking into account (1) and (2),

$$N_x = N_0 + N_x^{''} - N_L, \tag{5}$$

where N_X is the total number of molecules having $x \geq n$. Equations (1)-(5) are the exact equations of balance.

The subsequent considerations are concerned with the linear and nonlinear regions of radiolysis separately. By the linear region we mean the initial part of the radiolysis, in which there take place no secondary reactions between the final products. Then for the linear region, if the length of the reaction chain is close to unity, two limiting equations for the calculation of N_T may be written:

$$N_{T_1} = N_L - N''. \tag{6'}$$
$$N_{T_2} = N_L - N_x^{*}. \tag{6''}$$

Equation (6') will be exact if the destruction of free radicals only occurs through their recombination. But if disproportionation takes place, equation (6') will give results which are too low. Thus in the general case equation (6') gives the lower limit of the yield of the saturated part of the heavy residue, and the corresponding upper limit of the molecular weight of alkanes for which $x > n$.

Equation (6") will be exact if the decrease in free radicals owing to recombination is equal to, or greater than, their removal by disproportionation. If the majority of the free radicals are removed by disproportionation, than (6") will give results which are too high. Therefore, in the general case equation (6") gives the upper limit of N_T, and, correspondingly, the lower limit of the molecular weight of alkanes for which $x > n$. We should note in addition that in the linear region the inequality below ought to be strictly fulfilled:

$$N_{H_2} < N_x^{''} + N_T. \tag{7}$$

In the nonlinear region, when there will have occurred considerable polymerization of unsaturated hydrocarbons with $x > n$, the inequality (7) may not be true.

To evaluate the balance of the products of the radiolysis of n-heptane in the linear region, we take the following values for the radiation-chemical yields (in molecules per 100 eV of absorbed energy): $G(H_2) = 4.9$; G (saturated products of decomposition) $\approx$ G (unsaturated products of decomposition) = 0.7; G (monoolefins with $x > n$) = 2.0. Then by the use of (6') and (6") we get the corresponding lower and upper limits of the yield of the saturated part of the heavy residue: $G_1(T) = 2.9$; and $G_2(T) = 3.6$. But the value of G_1 (T) does not satisfy the inequality (7), and so we shall use the value $G_2(T)$.

Then for 1 ml of the initial n-heptane at a dosage of 10^{19} eV/ml, for example, we should have: $N_0 = 683.8 \times 10^{-5}$ mole; $N_x^{''} = 0.033 \times 10^{-5}$ mole; $N_L = 0.093 \times 10^{-5}$ mole; $N_L^{''} = 0.012 \times 10^{-5}$ mole; $N_T = 0.06$ mole. According to (3), $N_n = 683.65 \times 10^{-5}$ mole, and the degree of conversion of the initial n-heptane is: $y = 100\,(N_0 - N_n)/N_0 = 0.022$ mol. %. Table 1 gives the yield of radiolysis products per 100 molecules of n-heptane converted.

If we now use the equations we have derived to calculate the balance of the products of radiolysis of n-heptane in the nonlinear region, the initial data for the calculation [1, 2] are set out in Table 2.

According to equation (6") we obtain the number of moles $N_T = 39.62 \times 10^{-5}$, and according to equation (3), $N_n = 542.66 \times 10^{-5}$ mole/ml (with the number of g-atoms of carbon given by $N_C = 3798.62 \times 10^{-5}$, and the number of g-atoms of hydrogen by $N_H = 8682.52 \times 10^{-5}$). We consider now the elementary composition, and the mean molecular weight of alkanes in which $x > n$. The calculation gives the mean formula $C_{11.35}H_{24.7}$, and the mean molecular weight M = 161, which, as we have said earlier, represents the lower limits of the values of $\underline{x}$ and M. The degree of conversion of the original n-heptane in this case is 20.8 mol.%. Table 1 gives the yields of the basic products of radiolysis in molecules per 100 molecules of converted n-heptane in the nonlinear region with a dose of 650 Mrad (without reconversion to the n-heptane basis).

TABLE 1

Yield of the Major Products of the Radiolysis of n-Heptane per 100 Molecules of the Original Substance Converted.

Converted n-heptane	Hydrogen	Hydrocarbons in which x < n	Hydrocarbons with C_7	Hydrocarbons in which x > n	Total
		In the linear region			
100	53	15	22	39	129
		In the nonlinear region			
100	55	18	44	28	145

TABLE 2

Components	mole/ml × 10^5	g · atoms of C × 10^5	g atoms of H × 10^5
H_2	77,77	—	155,54
N_L	101,52	94,79	392,6
N_L	2,02	8,81	17,52
N_x	61,9	433,3	866,6
N_0	683,8	4786,6	10940,8

Comparison and analysis of the results obtained shows that increase of the dose causes the yield of hydrogen to increase at a rate falling below linear increase. With respect to the other components the nonlinearity is very evident: the yield of the saturated part of the heavy residue diminishes, while that of the unsaturated hydrocarbons with $x \geq n$ increases abruptly. This points to the considerable degree of unsaturation in the heavy residue in the nonlinear region. With increase in the dose, the total number of molecules formed from each 100 molecules of the starting substance continues to increase. This shows that in the course of radiolysis the mean molecular weight of the products must be diminished.

The authors express their thanks to G. D. Gal'perna for valuable comments during the discussion of the work.

LITERATURE CITED

[1] A. M. Brodskii, Yu. A. Kolbanovskii, et al., Dokl. Akad. Nauk SSSR, 122, 1035 (1958).•

[2] B. A. Smirnov, Optics and Spectroscopy 4 (1960).

•Original Russian pagination. See C. B. Translation.

MEASUREMENT OF THE VAPOR PRESSURE OF SOLID CHROMIUM BY MEANS OF RADIOACTIVE INDICATORS

An. N. Nesmeyanov and De Dyk Man

M. N. Lomonosov State University of Moscow
(Presented by Academician V. I. Spitsyn, January 3, 1960)
Translated from Doklady Akademii Nauk SSSR, Vol. 131, No. 6, pp. 1383-85, April, 1960
Original article submitted December 23, 1959

The vapor pressure of liquid chromium was measured by the boiling-point method [1, 2]. Because of the poor reliability of the methods used in carrying out the measurements and of the poor purity of the metal, these data were not very good. The measurements of the vapor pressure of solid chromium were carried out by the method of evaporation from an open surface [3-5].

The data of [3] and [4] agree satisfactorily with each other. The somewhat lower values of [4] can be explained by the condensation of the metal on the suspension wire during its evaporation. Results of [5] were appreciably higher. It is difficult to comment about their difference from [3, 4]. It may have been the result either of a systematic error of measurement, or of a higher purity of the metal used in [5]. The data concerning the vapor pressure of chrome require a verification.

We have measured the vapor pressure of solid chrome by an integral variant of the effusion method of Knudsen using the radioactive isotope of chrome Cr^{51} for determining the amounts of condensate. Chromium 99.99% pure, previously melted in the vacuum, was used in our work. The chrome was exposed in sealed ampoules to neutrons in a nuclear reactor. Its radio-chemical purity was demonstrated by the disintegration curve, which showed the absence both of long-lived and short-lived radioactive impurities.

The apparatus on which the measurements were carried out and the method used were similar to those described previously [6].

Cuttings of radioactive chrome were loaded in a molybdenum effusion camera with a molybdenum diaphragm, whose opening varied from experiment to experiment from $9.847 \cdot 10^{-3}$ to $7.740 \cdot 10^{-4}$ cm^2. The internal diameter of the camera was 0.9 cm. The camera was heated in the apparatus by means of the high frequency field of an external-inductor furnace MVP-3M. The temperature measurements were carried out by a Pt-PtRh thermal couple by a compensation method with a PPTN-1 potentiometer and an M21/4 galvanometer as a zero indicator. The thermal couple was graduated in the experimental conditions directly in the effusion camera by the melting points of copper, gold and nickel of high purity.

The chrome from the vapor container was washed in three portions by fuming sulfuric acid. The acid was eliminated by evaporation to dryness. The residue was dissolved in diluted acid. The first step consisted in precipitating chrome hydroxide from the solution, and in separating it out on a Buchner funnel. The filter with the dried precipitate was used as the sample for the measurements. The second procedure consisted in evaporating the solution from miniature glass beakers to dryness, and in measuring after this the activity of the dry residue. The activity was measured on the unit B with the γ - counter AMM-4. The two procedures gave identical results.

The individual activity of the metals was measured from an aliquot part of the solution by weighing the chrome, in the same way as the activity from the solution of the condensate.

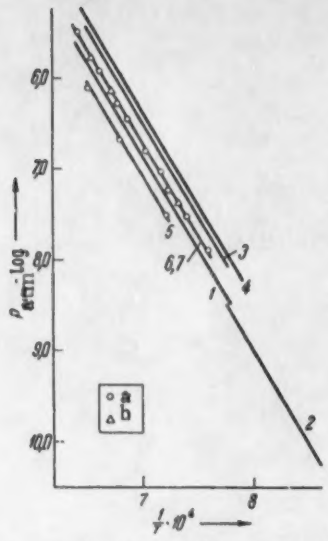

Fig. 1. Dependence of the vapor pressure of solid chrome upon the temperature; 1) According to ref. [3]; 2) according to ref. [4]; 3) according to ref. [5] (chrome condensed from its vapor); 4) according to ref. [5] (chrome melted in the vacuum); 5) experimental data for a slit opening of $9.847 \cdot 10^{-3}$ cm^2; 6) experimental data for openings of $1.384 \cdot 10^{-3}$ cm^2 (a), and of $7.74 \cdot 10^{-4}$ cm^2 (b).

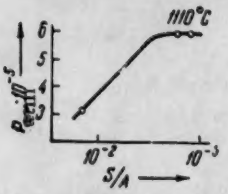

Fig. 2. Dependence of the vapor pressure of chrome upon the ratio of the area of the effusion opening and of the camera section.

The vapor pressure was measured according to the formula:

$$P = \frac{I}{I_0 atK}\sqrt{\frac{T}{M}}\ \text{mm},$$

Where I is the activity of the condensate, I_0 is the partial activity, a is the area of the effusion opening, t the exposure time, T is the absolute temperature, N is the molecular weight of the vapor, K is the Clausius coefficient.

The results obtained are shown in Table 1 and in in Fig. 1. Table 1 and Fig. 1 indicate that the effusion rate increases when the area of effusion opening decreases. However, for opening areas of $1.384 \cdot 10^{-3}$ and $7.74 \cdot 10^{-4}$ cm^2, the evaporation rates practically coincided, i.e., for these values of the opening areas a saturation was reached in the camera, and the results corresponded to the saturated vapor pressure. This can be immediately seen from Fig. 2. Using the values of the evaporation rate for different opening areas of the effusion camera, we calculated Langmuir's coefficient for solid chrome ($\alpha = 0.5$) by a method described before [7]. The saturated vapor pressure obtained from the

Vapor Pressure and Heat of Sublimation of Chrome

Temp., °C	t, sec	Wt. of the condensate $1 \cdot 10^6$ g	$a \cdot 10^3$, cm^2	K	Evaporation rate, $\frac{1}{t} \cdot 10^6$, g/cm^2	$P \cdot 10^4$, mm	$\Delta\Phi°$, cal/deg·g-at	$\Delta H_0°$, cal/g-at
1114	3082	8,15	9,847	0,965	0,269	0,246	—	—
1198	691	11,8	9,847	0,965	1,74	1,63	—	—
1262	302	18,4	9,847	0,965	6,20	5,98	—	—
1044	14401	2,52	1,384	0,924	0,0928	0,100	34,54	92962
1078	10825	3,69	1,384	0,924	0,246	0,227	34,50	93123
1110	3612	2,33	1,384	0,924	0,466	0,445	34,47	93436
1120	5412	5,82	1,384	0,924	0,778	0,723	34,46	92758
1149	3602	6,21	1,384	0,924	1,25	1,21	34,43	93193
1181	1504	5,82	1,384	0,924	2,80	2,74	34,40	92880
1201	911	5,05	1,384	0,924	4,03	3,92	34,38	93078
1236	596	7,38	1,384	0,924	8,94	8,83	34,34	92797
1285	305	10,5	1,384	0,924	24,8	25,2	34,29	92489
1092	7262	1,94	0,774	0,923	0,345	0,328	34,49	93078
1213	1237	5,24	0,774	0,923	5,47	5,44	34,37	92855
1254	897	8,74	0,774	0,923	12,6	12,6	34,37	92784

data of [3], and the values of α differed only by 15% from the vapor pressure values obtained by us with the smallest effusion openings. A still lower difference was obtained by using the data of [4].

Thus, the fact that Langmuir's coefficient is different from unity for solid chrome in evaporation conditions can be considered as established. It follows from this that the vapor pressures calculated from the evaporation rates from an open surface are not reliable.

On the basis of the preceding considerations we took as equilibrium vapor pressures those obtained for areas of effusion openings of $1.384 \cdot 10^{-3}$ and $7.74 \cdot 10^{-4}$ cm^2, and using them, we found, by the least square method, the equation:

$$\log P_{\text{mm}} = 10{,}807 - \frac{20907}{T}.$$

From the equilibrium vapor pressures obtained by us and from the values of the thermal dynamic potentials for the solid phase and the gas phase, calculated from the data of [8], we found the sublimation heat of chrome at 0°K (ΔH°_0) according to the formula

$$\Delta H^\circ_0 = T(\Delta\Phi^\circ - R \ln P_{\text{atm}}), \quad \text{for} \quad \Delta\Phi^\circ = \Phi^\circ_{\text{gas}} - \Phi^\circ_{\text{cond}}$$

where Φ°_{gas} and Φ°_{cond} are the thermodynamic potentials of the vapor and of the solid matter.

The data obtained are presented in the table. The mean value of the heat of sublimation is 92952 ± 184 cal/g-at.

LITERATURE CITED

[1] H. C. Greenwood, M. S. B. Pellow, Proc. Roy. Soc. A 82, 396 (1909); A 83, 483 (1910).

[2] E. Baur and K. Brunner, Helv. Chim. Acta 17, 958 (1934).

[3] R. Speiser, H. L. Johnston, and P. B. Bleakburn, J. Am. Chem. Soc. 72, 4142 (1950).

[4] E. A. Gulbransen, and K. F. Andrew, J. Electrochem. Soc. 99, 402 (1952).

[5] V. D. Burlakov, Fiz. Metallov i Metalloved 5, 90 (1957).

[6] An. N. Nesmeyanov, L. A. Smakhtin, and V. I. Lebedev, Dokl. Akad. Nauk SSSR 112, 700 (1957).•

[7] An. N. Nesmeyanov and De Dyk Man, Dokl. Akad. Nauk SSSR 123, 6 (1958).••

[8] D. K. Stull and G. C. Sinke, Thermodynamic Properties of the Elements, (Washington, 1956).

•Original Russian pagination. See C. B. Translation.

••See C. B. Translation.

MAGNETIC PROPERTIES OF $Cr_2O_3 - Al_2O_3$ CATALYSTS

A. M. Rubinshtein and A. A. Slinkin

N. D. Zelinskii Institute of Organic Chemistry, Academy of Sciences USSR
(Presented by Academician B. A. Kazanskii, January 5, 1959)
Translated from Doklady Akademii Nauk SSSR, Vol. 131, No. 6, pp. 1386-1389, April, 1960
Original article submitted January 2, 1960

The magnetic properties of $Cr_2O_3-Al_2O_3$ catalysts prepared by saturating γ-Al_2O_3 with chromic acid and by a subsequent reduction by H_2 at 360° and containing 0.1-40% in weight of Cr_2O_3 were studied by Selwood and co-workers [1]. They found that the magnetic moment for small concentrations of Cr_2O_3 is ~ 3.7 μ_B, and from $\sim$ 5% to 40% Cr_2O_3 in weight it is equal to 3.2 μ_B; the authors relate this fact to the presence of Cr^{6+} ions. A sharp discontinuity was observed in the behavior of the susceptibility (χ) curve for $\sim 8\%$ Cr_2O_3. A fast increase for χ when the concentration of Cr_2O_3 decreased was also observed. On the curve representing the dependence of Veiss* constants (Δ) upon the composition in the same point there was a discontinuity and Δ dropped to zero when the concentration of Cr_2O_3 decreased. These changes in the behavior of the concentration dependence of χ and Δ were correlated by the authors with the character of the distribution of Cr_2O_3 on the surface of γ-Al_2O_3.

A study of the oxidation process of layer catalysts of the type $Cr_2O_3-Al_2O_3$ and Cr_2O_3-ZnO by oxygen by constructing the curves representing the dependence of magnetic susceptibility upon the oxidation depth was carried out by Matsunaga [2, 3]. He succeeded in proving that the process of oxidation of Cr^{3+} ions to Cr^{6+} ions take place most intensively in the initial concentration region of Cr_2O_3 (roughly up to 10% in weight), after which the oxidation becomes more and more difficult when the carrier surface decreases. Similar results were obtained by the same author in a magnetochemical study of the process of thermal decomposition of CrO_3 added to γ-Al_2O_3 [4], and in reference [5] in a study of CrO_3-SiO_2 catalysts.

We were interested in carrying out a study of the oxidation processes of Cr^{3+} ions to Cr^{6+} ions for catalysts jointly deposited in a large range of concentrations of Cr_2O_3, and to explain how the content of Cr^{6+} ions would change in the catalysts during a catalytical reaction carried out with them, depending upon the concentration of Cr_2O_3. In addition we intended to obtain a rough picture of the distribution of Cr_2O_3 in the mass of Al_2O_3 by means of a detailed magnetic analysis of this system.

Catalysts of the $Cr_2O_3-Al_2O_3$ type with contents of 0; 1.48; 4.4; 7.28; 14.2; 20.8; 33.2; 60.0; 80.0; 93.2 and 100% Cr_2O_3 in weight were prepared by precipitating together Al and Cr hydroxides from mixtures of 10% solution of NH_4OH. Two series of catalyst preparation were obtained by treating thermally in the air for 6 hours at 450 and 600° the precipitates washed and dried at 110°. The catalytic activities of the preparations thus obtained were studied in the decomposition reaction of iso-C_3H_7OH in the temperature range 275-320°. We carried out a magnetochemical investigation of the catalysts of both series before and after the catalytical experiments, and also additional measurement of χ of fresh catalysts subjected to agglutination by heating in the air at 1000° for 6 hours.

Figure 1 shows the variation of the magnetic susceptibility referred to 1 g of Cr ($\chi_{Cr} \cdot 10^6$) with the concentration of Cr_2O_3 in the catalysts heated to 450° before and after the work. One can see immediately the sharp difference in the values of χ_{Cr} of treated and non-treated catalysts for concentrations of Cr_2O_3 up to $\sim$ 40% in weight. It is interesting that the concentration interval of Cr_2O_3 in which the sharp decrease of χ_{Cr} is observed

* Transliteration of Russian – Probably the name is Weiss.

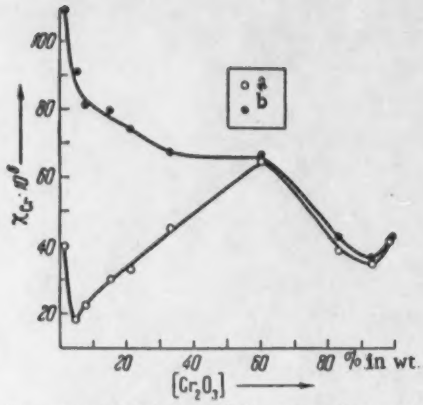

Fig. 1. Dependence of χ_{Cr} upon the composition of catalysts heated at 450°. a) Before use; b) after use.

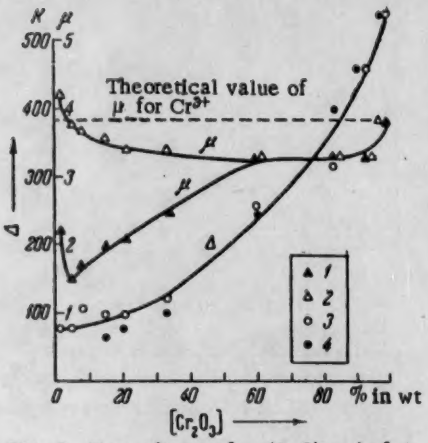

Fig. 2. Dependence of μ (1, 2) and of Δ (3, 4) upon the composition of catalysts calcined at 450°. 1, 3) Before use; 2, 4) after use.

for non-treated catalysts with respect to catalysts reduced during the reaction is much greater in the case we are considering of oxides precipitated together, than in the case of impregnation catalysts. This is apparently related to the higher degree of dispersion of Cr_2O_3 in coprecipitated catalysts with respect to impregnated catalysts. Also, as can be seen from Fig. 1, χ_{Cr} for catalysts before and after the alcohol decomposition reaction is practically the same, starting with ~ 60% Cr_2O_3 in weight. This, however, does not mean that in this region of Cr_2O_3 concentrations there are no Cr^{6+} ions. We calculated the magnetic moments (μ) of the catalysts before and after use on the basis of the temperature dependence χ_{Cr}. The corresponding data are reported in Fig. 2. Catalysts that have not been used and containing up to 40% in weight of Cr_2O_3 had a lower μ than after use; this depended upon the presence in the former of an appreciable quantity of Cr^{6+} ions. The magnetic moments of catalysts with 60, 80, and 93.2% in weight of Cr_2O_3 were the same ($3.3\mu_B$) both before and after use, and were lower than the theoretical value of μ for the Cr^{3+} ion. Apparently also in these catalysts there are Cr^{6+} ions (as was revealed by qualitative chemical analysis) which are not restored during the reaction. The percent of Cr^{6+} ions in the series of catalysts calcined at 450°, as calculated from the values of μ, is given in Fig. 3.

Analogous data were obtained for the catalysts calcined at 600° but in this case the maximum content of Cr_2O_3, for which catalysts that had not been used showed an appreciable concentration of Cr^{6+} ions, was lowered to 20% in weight, and the concentration of Cr^{6+} ions in the catalysts calcined at 600° was approximately 1.5 times less than in the corresponding preparations calcined at 450°. Also in this series the value of χ_{Cr} for contents of Cr_2O_3 of 60% in weight and higher was identical for used and nonused catalysts, i.e., the Cr^{6+} ions did not appear to be reduced during the work of the catalysts upon the dehydrogenation–dehydration of alcohol.

In order to clarify the causes which may produce such a behavior of preparations containing 60% in weight or more Cr_2O_3, we examine the possible phase composition of Cr_2O_3–Al_2O_3 catalysts on the basis of magnetic data. Let us revert to Fig. 1. We can see that χ_{Cr} does not decrease smoothly when the concentration of Cr_2O_3 is decreased, but for 60% in weight of Cr_2O_3 χ_{Cr} is equal to χ_{Cr} for 33% in weight of Cr_2O_3 (this corresponds to a maximum of the susceptibility for 1 g of catalysts). The same fact can be observed for catalysts calcined at 600°. Between 33% and 60% in weight of Cr_2O_3 a sharp increase of Δ from 125 to 250° (Fig. 2) is also observed. The increase of Δ between 33 and 60% Cr_2O_3 takes place also for catalysts calcined at 600 and 1000°: Δ increases, respectively, from 125 to 300° and from 130 to 460°. However, χ_{Cr} does not increase when the composition goes from 33 to 60% in weight of Cr_2O_3 for catalysts calcined at 1000°.

The way Δ varied for all three series of catalysts in the interval 1.5-33% in weight of Cr_2O_3 was characteristic. For catalysts calcined at 450°, Δ changed from 75 to 100° in the interval 1.5-14% Cr_2O_3, from 100 to 130° in the interval 14-33% Cr_2O_3 (Fig. 2). The catalysts calcined at 600° were characterized by a Δ changing

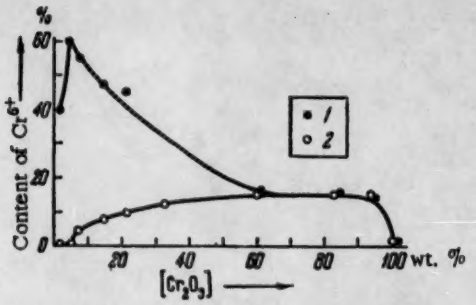

Fig. 3. Dependence of the ion content upon the composition for catalysts calcined at 450°. 1) Before use; 2) after use.

from 30 to 70° in the interval 1.5-14% Cr_2O_3 in weight, and by a Δ changing from 70 to 130° in the interval 14-33% Cr_2O_3. In the catalysts calcined at 1000° Δ was close to zero in the interval 1.5-14% Cr_2O_3, and changed from 100 to 130° in the interval 14-33% Cr_2O_3.

We had thus three regions of concentrations of Cr_2O_3 in which Δ changed in a completely different way according to the calcination temperature: 1) the region 1.5-14% Cr_2O_3 where Δ dropped approximately to 0° when the calcination temperature of the catalysts is increased; 2) the region 14-33% Cr_2O_3, where Δ remained practically constant when the calcination temperature is increased, its value being around 100-130°; 3) the region of concentration $\geq$ 60% Cr_2O_3, where Δ increased rapidly when the calcination temperature is increased. The latter region of concentrations of Cr_2O_3 was also interesting because the catalyst with 93% of Cr_2O_3 calcined at 600° was antiferromagnetic, whereas pure Cr_2O_3 prepared in the same way was paramagnetic. When the calcination temperature was 1000° the catalysts containing from 93 to 100% Cr_2O_3 became antiferromagnetic.

On the basis of the above considerations the following rough picture of the distribution of Cr_2O_3 in Al_2O_3 for the catalysts under investigation can be given. In the interval 0-14% Cr_2O_3 in weight one is dealing with a solid solution of Cr_2O_3 in Al_2O_3, which becomes more ordered with an increase in the calcination temperature, thus leading to a decrease of Δ. In the interval 14-33% Cr_2O_3 there is a mixture of different phases. In addition to the solid solution of Cr_2O_3 in Al_2O_3 there are apparently also solid replacement solutions of Al_2O_3 in Cr_2O_3, i.e., there are phases rich and poor in Cr_2O_3. In some of them Δ may decrease when the calcination temperature is increased; in others it may increase. The combination of these two processes may lead to a constant value of Δ. In the concentration interval 60-93% Cr_2O_3 appears first a phase of free Cr_2O_3; in catalysts calcined at 450 and 600° this phase is in a sufficiently dispersed stage and its appearance (at 60% Cr_2O_3) corresponds to an increase of X. In addition, in this region of concentrations of Cr_2O_3 an intrusion solution of Al_2O_3 in Cr_2O_3 is apparently formed: the appearance of antiferromagnetism in catalysts with a high content of Cr_2O_3 calcined at 600 and 1000° is connected with this.

Probably, when they form a solid intrusion solution, the Al^{3+} ions cause local displacements of the O^{2-} ions in the lattice, and therefore give rise to favorable conditions for indirect exchange between the Cr^{3+} ions as a result of the fact that the valence angle $Cr^{3+}—O^{2-}—Cr^{3+}$ approaches 180°.

In the light of the above considerations, the absence of marked differences in the magnetic properties of fresh and used catalysts containing more than 60% in Cr_2O_3 in weight can be explained by the fact that the amount of surface Cr^{6+} ions is very small in comparison with the amount of them contained in the volume of the catalyst crystals. The surface Cr^{6+} ions are easily reduced, whereas those situated in the mass of the crystal are not reduced in the conditions (T, time) under consideration because of the absence of immediate contact with the gas phase and of the slowness of the diffusion of vapors and gasses supplied inside the crystals.

Besides the $Cr_2O_3—Al_2O_3$ catalysts described above, we carried out a number of measurements for $Cr_2O_3—SiO_2$ catalysts obtained* by depositing CrO_3 on SiO_2 with a subsequent thermal treatment. The treatment of $CrO_3—SiO_2$ was carried out in two ways: 1) by ethyl alcohol at room temperature, and then by H_2 at 515° for one hour; 2) treatment by H_2 or air also at 515° for one hour. These two groups of catalysts were sharply different in their magnetic and crystallographic properties. The first group were paramagnetic with $\mu = 3.2\ \mu_B$ and amorphous to the x-rays. The second group were antiferromagnetic and their x-ray photographs showed clear lines of crystalline Cr_2O_3. We think that it is possible that this difference in magnetic behavior of the two groups of catalysts finds an explanation in the formation of chrome silicates taking place when $CrO_3—SiO_2$ was treated by alcohol at the expense of the high heat production during the oxidation-reduction percent. More detailed information about these catalysts will be published together with characteristics of their catalytic activity in one of our next communications.

*Together with M. I. Rozengart.

LITERATURE CITED

[1] R. P. Elschens and P. W. Selwood, J. Am. Chem. Soc. 69, 2698 (1947).

[2] Y. Matsunaga, Bull. Chem. Soc., Japan, 30, 868, 984 (1957).

[3] Y. Matsunaga, Bull. Chem. Soc. Japan 31, 58 (1958).

[4] Y. Matsunaga, Bull. Chem. Soc. Japan 31, 745 (1958).]

[5] R. Mihail, P. Corlateanu, and A. G. Ionesco, J. Chim. Phys. 56, 568 (1959).

THE TIME OF ESTABLISHMENT OF SORPTION EQUILIBRIUM

D. P. Timofeev

Institute of Physical Chemistry, Academy of Sciences, USSR
(Presented by Academician M. M. Dubinin, December 25, 1959)
Translated from Doklady Akademii Nauk Vol. 131, No. 6, pp. 1390-1392, April, 1960
Original article submitted December 22, 1959

When the sorption isotherms are measured, the equilibrium is often reached exceptionally slowly. For instance, in Kuadzhe's experiments [1] in a region near to saturation, the readings of the values of the sorption of benzene vapors on natural substrates (clays) were taken after 1-2 days. Kaganer [2] observed a small sorption rate at low pressures. According to the author's data, the equilibrium values of nitrogen sorption on coals, silica gels and other substrates for pressures below 10^{-3} mm/Hg, were reached after 15-25 hours. The slow sorption of water vapor on activated coals in the region of the steep ascent of the sorption isotherm is well known. Many other examples of slow sorption of gases and vapors, when the process is not complicated by chemical interaction or by absorption, can be found in the literature [3-5].

On the other hand, the measurement of gas and vapor sorption in the central region of the isotherm in many cases does not present any difficulty in connection with time, since the equilibrium is reached quite rapidly (in a few minutes). The causes of such wide variations in time when different points of the sorption isotherm are measured were not clarified sufficiently in the literature, and we considered it appropriate to discuss briefly the main causes upon which the time required for reaching the sorption equilibrium depends. By "sorption" we mean in the present paper adsorption and capillary condensation.

If the sorption process is not complicated by chemical interactions, the sorption rate is determined by the rate of molecule transfer from the gas phase to the adsorption centers of the substrate. The transfer of matter to the porous substrate will take place by different mechanisms, but since all known forms of transfer have the same dependence upon the pressure gradient, the rate of the over-all process can be described formally by a diffusion equation with some "effective" (or "fictitious") diffusion coefficient, which we shall simply call diffusion coefficient for the sake of conciseness.

The diffusion equation of the adsorbed gas in an isotropic porous medium can be written in the form

$$\frac{\partial c}{\partial t} = \frac{D}{1 + f'(c)} \nabla^2 c, \qquad (1)$$

where D is the diffusion coefficient, f' (c) is the derivative of the concentration function determined from the equation of the sorption isotherm, a is the value of the sorption, ∇^2 is Laplace's operator, t is the time.

The integration of equation (1) presents serious mathematical difficulties if the function f (c) is nonlinear. But since in practice this is a most common case, then, sacrificing somewhat the accuracy of the calculations, one can take f' (c) = Γ_c = const and also D = D_c = const in a concentration interval more or less wide,* because

*The condition "in a more or less wide concentration interval" is automatically fulfilled if the sorption isotherm is measured with not too small numbers of experimental points.

in general D changes with the filling [6-8].

The final conclusions do not change if we carry out our further discussion on a most simple case, taking a piece of substrate having the form of a sphere. The solution of equation (1) for a sphere of radius R under the additional conditions

$$c(x, 0) = c_н, \quad c(0, t) = c_0, \quad \frac{\partial c(R, t)}{\partial x} = 0$$

by integration over the volume and substitution of c by a has the form

$$\frac{a - a_н}{a_0 - a_н} = 1 - \frac{6}{\pi^2} \sum_{n=1}^{\infty} \frac{1}{n^2} \exp\left[-n^2\pi^2 \frac{D_c t}{\Gamma_c R^2}\right]. \tag{2}$$

where a is the value of the adsorption at the instant t, a_H is the initial value of the adsorption for t = 0, a_0 is the equilibrium value of the adsorption ($t \to \infty$), n = 1, 2, 3. . . The unity in the expression 1 + f' (c) has been left out, because usually $1 \ll f'(c)$.

According to equation (2), for $a = a_0$, $t = \infty$, i.e., the time required for the establishment of the sorption equilibrium is equal to infinity. On the other hand, as is well known, experiments are completed after a finite interval of time. This apparent disagreement between theory and experiment arises from the fact that after some time after the beginning of an experiment the difference between the true equilibrium value of the sorption and the observed one becomes smaller than experimental error and the experiment is terminated, since the further growth of the sorption cannot be detected. If the absolute error of measurement is equal to ξ, then the attainment of equilibrium will be recorded when the value of the sorption reaches the value $a_\xi = a_0 - \xi$ (the variant $a_\xi = a_0 + \xi$ has no meaning because it does not satisfy equation (2).

Thus, the time needed to reach the sorption equilibrium is determined by the equation

$$\frac{a_\xi - a_н}{a_0 - a_н} = 1 - \frac{6}{\pi^2} \sum_{n=1}^{\infty} \frac{1}{n^2} \exp\left[-n^2\pi^2 \frac{D_c t_\xi}{\Gamma_c R^2}\right] = N, \tag{3}$$

where N is a constant for a given interval of concentration, but can change in other regions of the isotherm, since it depends both upon the error of measurement, and upon the difference $a_0 - a_H$.

From equation (3) it follows that

$$\frac{D_c t_\xi}{\Gamma_c R^2} = k_\xi, \tag{4}$$

where k_ξ is a constant uniquely depending upon N.

Solving equation (4) with respect to t_ξ, we find

$$t_\xi = k_\xi \frac{\Gamma_c R^2}{D_c}. \tag{5}$$

Equation (5) is valid for substrate pieces having the form of spheres. If the substrate pieces have another shape, one must introduce a correction factor (form factor) k_g. The value of R in this case represents the radius of a sphere having the same volume. Thus,

$$t_\xi = k_g k_\xi \frac{\Gamma_c R^2}{D_c}. \tag{6}$$

Equation (6) gives the dependence of the time required to reach the sorption equilibrium upon the basic factors, the experimental accuracy, the sorption power of the material, the dimensions of the pieces, the diffusion coefficient and the shape of the pieces.

For a given substrate the ratio of the times t''_ξ and t'_ξ in the different regions of the sorption isotherm will be expressed by the equation

$$\frac{t''_\xi}{t'_\xi} = \frac{\Gamma''_c}{\Gamma'_c} \frac{D'_c}{D''_c}. \quad (7)$$

When $D''_C \approx D'_C$ the time for the establishment of the sorption equilibrium is approximately proportional to the sorption coefficient Γ_C. In connection with this it is interesting to mention Herbst's observation [9], that the equilibrium is reached more slowly for the more active coals. However, one should remember that, according to equation (6) t_ξ depends upon a number of other factors.

Equation (1), as well as all the subsequent consequences of it, is true only when the quantity of adsorbed gas is small in comparison with its over-all amount in the volume of the apparatus, i.e., when the limit condition $c(0,t) = c_0$ is fulfilled. If during the sorption process the pressure in the apparatus changes and $c(0, t) \neq \text{const}$, as, for instance, in the volume method for the measurement of the sorption isotherm, the solution of the differential equation (1) is different from (2). We shall not report the solutions of the equation and the subsequent transformations for this case, since they are completely similar to those given above, and shall confine ourselves to the final equation, which has the form

$$t_\xi = k_r k_g k_\xi \frac{\Gamma_c R^2}{D_c}, \quad (8)$$

where k_r is a coefficient depending upon the ratio of the value of the sorption to the amount of gas in the apparatus.

Equation (8) differs from (6) only for the presence of the coefficient k_r. For an infinite volume of the system $k_r = 1$ and equation (8) becomes identical to (6). When the volume of the system decreases, or the quantity of the substrate increases, k_r becomes smaller and the sorption equilibrium is reached more quickly. However, the use of small volumes and of large quantities of substrate involves the risk of deviations of the results of the experiment in the region of hysteresis, since, when the pressure is decreased after sorption at a high pressure, a desorption process starts in the surface layers of the pieces. Consequently, the measured value of the sorption will result from the values of the sorption in the surface layers of the pieces relative to the desorption branch, and from the values of the sorption in the central parts of the pieces, relative to the sorption branch. This undesirable effect increases when the hysteresis loop, the dimensions of the substrate and the difference between the equilibrium and initial concentrations when the gas is introduced into the system become larger.

LITERATURE CITED

[1] M. I. Kuadzhe, Zhur. Prikl. Khim. 31, 1001 (1958).*

[2] M. G. Kaganer, Dokl. Akad. Nauk SSSR 122, 416 (1957).*

[3] J. R. Decey and D. G. Thomas, Trans. Farad. Soc. 50, 740 (1954).

[4] H. W. Habgood, Canad. G. Chem. 36, 1384 (1958).

[5] P. Cannon, J. Phys. Chem. 63, 160 (1959).

[6] R. M. Barrer and D. W. Brook, Trans. Farad. Soc. 49, 1049 (1953).

[7] P. C. Carman and F. A. Raal, Trans. Farad. Soc. 50, 842 (1954).

[8] D. P. Timofeev and I. T. Erashko, Dokl. Akad. Nauk SSSR 132, 1 (1960).*

[9] H. Herbst, Kolloidch Beih. 21, 1 (1925).

*See C. B. Translation.

A NEW CAVITATION METHOD FOR EMULSION POLYMERIZATION•

S. S. Urazovskii

(Presented by Academician P. A. Rebinder, December 21, 1959)
Translated from Doklady Akademii Nauk, Vol. 131, No. 6, pp. 1393-1395, April, 1960
Original article submitted December 21, 1959

Polymerization in dispersion, as is well known, has a number of important advantages, leading to a significant increase in the speed of the process (by 2-3 orders of magnitude) and to the possibility of increasing the mol. wt. of the polymer. In addition, favorable steric conditions for obtaining more homogeneous and ordered structures exist in this type of process.

However, all these advantages, due to the use of impurities (the emulsifiers), are balanced to a large extent as a consequence of the disturbance of those optimal topochemical characteristics of the process which must be present for the polymer to be formed in emulsions [1]. The use of emulsifiers is also particularly bad because of the difficulty of eliminating them when polymers with high insulation properties are required.

In connection with these remarks it is interesting to study the emulsification paths of the monomers without the use of special emulsifiers, both in order to investigate the mechanism of dispersion polymerization in pure form, and for the technology of polymer production.

It is well known that, under the action of ultrasonic vibrations, very highly dispersed emulsions can be obtained without emulsifiers, since stabilizing factors arise under the influence of cavitation. However, the complexity and inefficiency of big apparatuses for obtaining sufficiently powerful sources of acoustic energy make an extensive use of them in industry impractical. An analysis of the dispersing action of ultrasonic vibrations leads to the conclusion that the solution of the problem of building a powerful and at the same time practical source of acoustic energy must be sought in the elaboration of a simple method for producing cavitation. A most simple and sufficiently effective method appeared to be the use of the energy produced by the disappearance of cavitations produced when an overheated vapor is condensed in the liquid phase.

Earlier we elaborated and applied successfully [2, 3] a method using cavitationphenomena for exciting acoustic vibrations, and this method appeared to be very effective for obtaining the most varied highly dispersed systems. Recently this method was used also by other investigators [4].

If an overheated vapor is made to pass through a capillary tube under a small pressure (2-3 atm) into a liquid phase, the consequence of the sudden condensation of the arriving vapor is that the region (at the immediate end of the capillary tube) occupied for a moment by an element of volume of the vapor phase, decreases sharply to almost vanishing dimensions, and the mechanical shock arising because of this (collapse of the cavity) must create in the neighboring layers a strong compression reaching very high values. The vapor condensation and the phenomena connected with it in given experimental conditions—a sufficient difference in temperature between the liquid phase and the vapor—take place so rapidly that even in the immediate vicinity

•Presented May 8, 1959, at the Technical-Scientific Conference of the Polytechnic Institute of Khar'kov.

of the opening , it is already difficult to detect disturbances of the continuity of the vapor phase. The elementary act of disturbance of the continuity of the liquid phase by some volume element of the vapor and the subsequent disappearance of these disturbances due to the condensation, is nothing else than the process of formation and destruction of an individual cavity; the totality of such elementary facts gives a typical cavitation phenomenon.

The calculation reported below of the frequencies of the shock wave leads to values of the order of tens of kilocycles per second, and this corresponds to the region of audible high tones just below ultrasonic vibrations.

Let us assume that the initial radius of the collapsing cavity (r) does not differ too much from the length of the free path of the vapor molecules (of the order 10^{-3} cm), and that consequently the condensation time of the vapor inside the cavity will be shorter than the time it takes to collapse; then the conditions for a typical cavitation phenomenon will be present, i.e., the formation and collapse of cavities free from vapor. Then the collapse time of a single cavity (τ) is determined from the acceleration of some layer of the liquid freely moving towards its center under the action of the unidirectional force F.

Taking into account the capillary pressure, let us express the motive force acting on the unit of surface of the collapsing cavity by the following equation

$$F_s = P_0 + 2\sigma/r,$$

where P_0 is the atmospheric pressure.

The mass of a moving layer having an area of 1 cm^2 and a thickness v_τ, where $\underline{v}$ is the propagation velocity of the elastic wave $m_s = \rho v \tau$, where ρ is the density of the liquid.

Then the acceleration $\underline{a}$ can be found from the equation

$$a = \frac{P_0 + 2\sigma/r}{\rho v \tau}.$$

Now, since the radius of the cavity is the distance covered by a layer of the liquid during the time required for the cavity to collapse

$$\tau = \sqrt{2r/a}.$$

Substituting the corresponding value of $\underline{a}$, we find

$$\tau = \frac{2r\rho v}{P_0 + 2\sigma/r}.$$

If we substitute in the latter equation the orders of magnitude of the numerical values of the quantities appearing in it, we obtain for τ a value of about 10^{-4}, which corresponds to frequencies of the order of tens of kilocycles per second. This shows that the process under consideration gives rise to high-frequency acoustical vibrations.

The dispersing action of the cavitations produced by the method described is very effective. The formation of stable and concentrated emulsions of the oil-water type when a capillary tube is introduced near the separation boundary lasts for 5-10 sec for nonmiscible phases. In this way we succeeded in obtaining dispersions of different types of oils: vaseline oil, almond oil, castor oil, camphor oil (with an increased content of camphor), paraffin, phenol, cresol, liquid fractions of the cracking of naphtha, and also sulphamide preparations scarcely soluble in water, iodine and other medicinal substances [2, 3].

The method described for producing cavitations appears to be sufficiently effective and very promising for the polymerization in dispersion. We tested successfully this method in applications to the polymerization processes of styrene, methyl, methacrylate, acrylonitrile, and also of various combinations of these monomers with each other. We established that under the influence of cavitations both stages of the emulsion polymerization process (both the emulsification and especially the polymerization) took place more effectively than with

the usual procedure. In order to obtain 100 g of emulsion (1 : 5) a few seconds are usually required, and high-dispersion emulsoids with a mean diameter of the order of 10^{-4} cm are formed.

The polymerization process, which is usually carried out at high temperatures, reaches an appreciable rate already during the emulsification in the conditions provided by the cavitation method. Under the influence of the heat of condensation of the overheated vapor, which increases the temperature of the emulsion to 40-60°, and under the immediate action of the cavitations, which provide favorable microkinetics and topochemical conditions for the process, the formation of the polymer is terminated in most cases already after a few minutes after emulsification without any additional heating. For such polymers as acrylonitrile or mixtures of it with styrene or methyl methacrylate, the polymerization proceeds rapidly even at room temperature. In this case, i.e., in the case of polymerization at low temperatures, polymers are obtained which have a higher thermal stability than those obtained by the customary methods.

Thus, for instance, the copolymer of acrylonitrile with styrene (in a ratio 1 : 1) obtained by a cavitation polymerization softens at 140°, and the copolymer of acrylonitrile with methyl methacrylate (in a ratio 70 : 30) softens at 120°, i.e., 30° higher than that obtained by the usual methods.

The immediate mechanical effect of cavitations on the energetic state of the polymer molecules is particularly interesting. Due to the development of high pressures and temperatures when a cavity collapses the molecules of the adjacent layers of monomer may undergo a process of cracking, with formation of free radicals. This is supported by our observation that some monomers, like acrylonitrile, polymerize without the influence of initiators, and also that some monomers, like cyclopentadiene, polymerize partially only in the presence of catalysts according to an ionic mechanism

An important domain of application of the cavitation method can be found also, in our opinion, in the production of graft- and block-copolymers, and also for such processes of construction of complex high-polymer systems, where the destruction and reconstruction processes of polymer chains play a decisive role.

LITERATURE CITED

[1] P. M. Khomikovskii, Usp. Khim. 27, 9, 1025 (1958); 28, 5, 547 (1959).

[2] S. S. Urazovskii, Tr. Khar'kovsk. Khim.-Tekhnol. Inst. 4, 10 (1942-44).

[3] S. S. Urazovskii, I. G. Polotskii, Dokl. Akad. Nauk SSSR Sec. Phys. Chem., Math., Sci. 11, 146 (1944).

[4] B. B. Kudryavtsev, Koll. Zhur. 21, 1, 58 (1959).•

•Original Russian pagination. See C. B. Translation.

SIGNIFICANCE OF ABBREVIATIONS MOST FREQUENTLY ENCOUNTERED IN SOVIET PERIODICALS

FIAN	Phys. Inst. Acad. Sci. USSR.
GDI	Water Power Inst.
GITI	State Sci.-Tech. Press
GITTL	State Tech. and Theor. Lit. Press
GONTI	State United Sci.-Tech. Press
Gosenergoizdat	State Power Press
Goskhimizdat	State Chem. Press
GOST	All-Union State Standard
GTTI	State Tech. and Theor. Lit. Press
IL	Foreign Lit. Press
ISN (Izd. Sov. Nauk)	Soviet Science Press
Izd. AN SSSR	Acad. Sci. USSR Press
Izd. MGU	Moscow State Univ. Press
LEIIZhT	Leningrad Power Inst. of Railroad Engineering
LET	Leningrad Elec. Engr. School
LETI	Leningrad Electrotechnical Inst.
LETIIZhT	Leningrad Electrical Engineering Research Inst. of Railroad Engr.
Mashgiz	State Sci.-Tech. Press for Machine Construction Lit.
MEP	Ministry of Electrical Industry
MES	Ministry of Electrical Power Plants
MESEP	Ministry of Electrical Power Plants and the Electrical Industry
MGU	Moscow State Univ.
MKhTI	Moscow Inst. Chem. Tech.
MOPI	Moscow Regional Pedagogical Inst.
MSP	Ministry of Industrial Construction
NII ZVUKSZAPIOI	Scientific Research Inst. of Sound Recording
NIKFI	Sci. Inst. of Modern Motion Picture Photography
ONTI	United Sci.-Tech. Press
OTI	Division of Technical Information
OTN	Div. Tech. Sci.
Stroiizdat	Construction Press
TOE	Association of Power Engineers
TsKTI	Central Research Inst. for Boilers and Turbines
TsNIEL	Central Scientific Research Elec. Engr. Lab.
TsNIEL-MES	Central Scientific Research Elec. Engr. Lab.–Ministry of Electric Power Plants
TsVTI	Central Office of Economic Information
UF	Ural Branch
VIESKh	All-Union Inst. of Rural Elec. Power Stations
VNIIM	All-Union Scientific Research Inst. of Metrology
VNIIZhDT	All-Union Scientific Research Inst. of Railroad Engineering
VTI	All-Union Thermotech. Inst.
VZEI	All-Union Power Correspondence Inst.

Note: Abbreviations not on this list and not explained in the translation have been transliterated, no further information about their significance being available to us. – Publisher.